CYCLOTRON HARMONIC EMISSION IN A PENNING DISCHARGE

Thesis by

John B. Wilgen

In partial fulfillment of the requirements

for the degree of

Doctor of Philosophy

California Institute of Technology

Pasadena, California

1975

(Submitted April 9, 1975)

ACKNOWLEDGMENT

I would like to express my gratitude for the assistance I have received throughout the course of this work. Professor Robert Harp suggested the problem and provided guidance at the beginning of the work. For his advice and counsel throughout the remainder of the work and for his critical reading of the manuscript, I would like to thank Professor Roy Gould.

I wish to thank my associates with whom various aspects of this work have been discussed. In particular I would like to express my gratitude to Dr. Charles Moeller, Dr. Richard Smith, Dr. Fritz Leuterer and Dr. Keith Burrell for their assistance, encouragement and useful suggestions.

Assistance with the preparation of the manuscript from my wife, Dianne, Ruth Stratton, and Dian Rapchak is especially appreciated.

The support of the Office of Naval Research in carrying out this work is gratefully acknowledged.

ABSTRACT

Microwave noise emission at the harmonics of the electron cyclotron frequency from the magnetized plasma column of a Penning discharge is investigated experimentally. The harmonic emission spectrum is observed using oxygen gas in a variety of discharge configurations. It is found that grid stabilization of the plasma column has very little effect on the emission spectrum. Measurements of the shape and location of the harmonic emission lines are described in detail. On the basis of a microwave interferometer measurement of the electron density, it is concluded that the existence of a hybrid layer somewhere on the plasma column is a necessary condition for the observation of harmonic emission. The relaxation time and the cathode voltage dependence of the harmonic emission are investigated using a pulse modulation technique. It is found that the emission intensity increases rapidly with the magnitude of the cathode voltage and that the relaxation time decreases with increasing neutral gas pressure. High intensity nonharmonic radiation is observed and identified as resulting from a beam-plasma wave instability thereby eliminating the same instability as a possible source of the harmonic emission. It is found that the collective experimental results are in reasonable agreement with the single particle electrostatic radiation theory of Canobbio and Croci.

TABLE OF CONTENTS

CHAPTER I

INTRODUCTION

1.1 Historical Background and the Significance of the Problem

Microwave radiation at the harmonics of the electron cyclotron frequency has been observed in a wide variety of plasma experiments [1-3]. Of these, Landauer's observations are of particular interest [4]. He discovered that the Penning discharge is very effective in exciting radiation at a large number of the higher harmonics of the electron cyclotron frequency, all having roughly the same amplitude.

Harmonic radiation was initially observed from hot plasmas produced in controlled fusion experiments. In 1959, Wharton [5] reported observations of radiation at the fundamental and the first several cyclotron harmonics from a plasma in a magnetic mirror device. In 1961, Landauer reported observing approximately 20 harmonics in a Penning discharge [6]. Subsequently, many investigators observed harmonic emission in positive column discharges [7-9] and in beam-produced plasmas [10-12]. In addition, Tetenbaum [13] has investigated harmonic emission in an electrodeless r-f discharge.

These observations of harmonic emission were not expected and can not be explained on the basis of synchrotron radiation. For weakly relativistic electrons, $\beta^2 = kT/mc^2 \ll 1$, synchrotron radiation occurs primarily at the fundamental electron cyclotron frequency. The power radiated into the n^{th} harmonic is reduced by a factor of $\beta^{2(n-1)}$. In contrast, Landauer observed harmonics of nearly equal intensity, but emission at the fundamental cyclotron frequency was found to be almost

nonexistent.

The experimental results stimulated considerable theoretical interest, partly because of relevance to thermonuclear research. The greatest importance of the phenomenon lies in the understanding of many fundamental properties of the plasma. It appears likely that a better understanding of harmonic emission could lead to applications for diagnostic purposes.

An impressive number of distinctly different theories have appeared as a result of many independent attempts to explain the harmonic emission observed in the experiments. While many of the theories involve the excitation of slow electrostatic plasma waves, several mechanisms have been identified which result in direct excitation of electromagnetic radiation. In the case of the electrostatic waves, it is necessary to consider the coupling of the electrostatic wave energy to the electromagnetic signals which are detected in the experiments.

It is usually assumed that the harmonic emission results from the presence of nonmaxwellian electrons in the laboratory-produced plasma. In the single particle radiation theories, it is assumed that these source electrons radiate independently. In another class of theories the electrons interact coherently in the form of a wave instability which might result from either a nonmaxwellian electron velocity distribution or a beam-plasma interaction. In either case, the excited radiation might be either electrostatic or electromagnetic. The theories of harmonic emission will be reviewed in greater detail in Chapter IV.

Although several attempts to relate theoretical results with experiments have shown qualitative agreement, detailed quantitative comparisons are often prohibitively complex because of the basic difficulty of accurately modeling a nonuniform and sometimes turbulent experimental plasma with a calculable theoretical model. Nevertheless, the qualitative agreement of these comparisons indicates that several of the radiation mechanisms described by the theoretical models have been detected experimentally. Although the gross properties of the harmonic emission observed in various plasma sources are similar, the details differ greatly, indicating that perhaps the emission mechanism is not the same in every case.

It has been pointed out that the various experimental investigations can be distinguished according to the nature of the wave-plasma interaction which takes place [13]. In the experiments of Landauer and Tetenbaum, the dimension of the plasma is significantly greater than the free space wavelength. In the experiments which employed a positive column or a beam-generated plasma, the column diameter is typically much less than the radiation wavelength. This geometrical factor affects the nature of the interaction between the electromagnetic radiation and the plasma column and may account for major differences in the harmonic emission observed in the two cases.

For example, Landauer and Tetenbaum observed that within experimental error the harmonic emission maxima were located at the harmonics of the electron cyclotron frequency. However, the emission maxima observed in positive columns and beam-generated plasmas of small diameter are often found to shift from the harmonic locations when the

plasma density is varied [8-10,12]. This might be due to the geometrical difference or it might indicate that the radiation mechanism is not the same in each case.

To avoid such complications, it is expedient to restrict a discussion or investigation of harmonic emission to a single plasma source, and that is what has been done in the present investigation. The Penning discharge has been chosen for the investigation principally because it has been found to be highly effective in producing harmonic emission. Experimental results obtained using other types of plasma sources will rarely be mentioned in this report because they could easily prove to be misleading with respect to what is happening in the Penning discharge.

The purpose of this investigation is to develop additional experimental data and to explore the areas of agreement between the qualitative predictions of the theoretical models and experimental results of the Penning discharge. It is hoped that the results of this investigation will eventually contribute to the positive identification of the radiation mechanism in the Penning discharge and a better understanding of the plasma phenomena which are involved.

1.2 Previous Investigations of Harmonic Emission in the Penning Discharge

Having decided to investigate the harmonic emission of the Penning discharge, it is appropriate to review in greater detail the history of the experimental investigation of Landauer radiation in the Penning discharge.

As previously mentioned, Landauer first reported his observation of 20 harmonics in 1961. In subsequent work, Landauer observed emission up to the 45th harmonic of the electron cyclotron frequency [14]. A sketch of Landauer's experiment is given in Figure 1.1a and the harmonic emission spectrum is displayed in Figure 1.1b. It is essential to realize that the emission spectrum of the Penning discharge is obtained by sweeping the magnetic field. Varying the magnetic field involves major changes in the density, the density profile, the electron temperature and the stability of the plasma. The spectrum might instead be obtained by varying the receiver frequency at a constant magnetic field, but this procedure is more difficult and can only be used to obtain a fraction of the entire emission spectrum in a single sweep.

The emission spectrum of Figure 1.1b shows very prominent, well defined harmonic emission lines. In contrast with the harmonic emission spectra typically observed in other plasma sources, these emission lines are relatively narrow and large in amplitude. Careful calibration of the magnetic field revealed that the emission lines occurred at magnetic field values which satisfy the relation $\omega = n\omega_c$ to within experimental accuracy. The amplitude of the harmonics falls off slowly with harmonic number and the largest amplitude harmonic ($m = 5$) corresponds to an equivalent black body radiation temperature of between $50{,}000^{o}K$ and $100{,}000^{o}K$ (or roughly 4.5 to 9 eV). Although the displayed spectrum was obtained using a receiver frequency of 34 GHz, similar measurements were also carried out at 10 GHz. Landauer found that the harmonic amplitude decreases rapidly with increasing helium gas

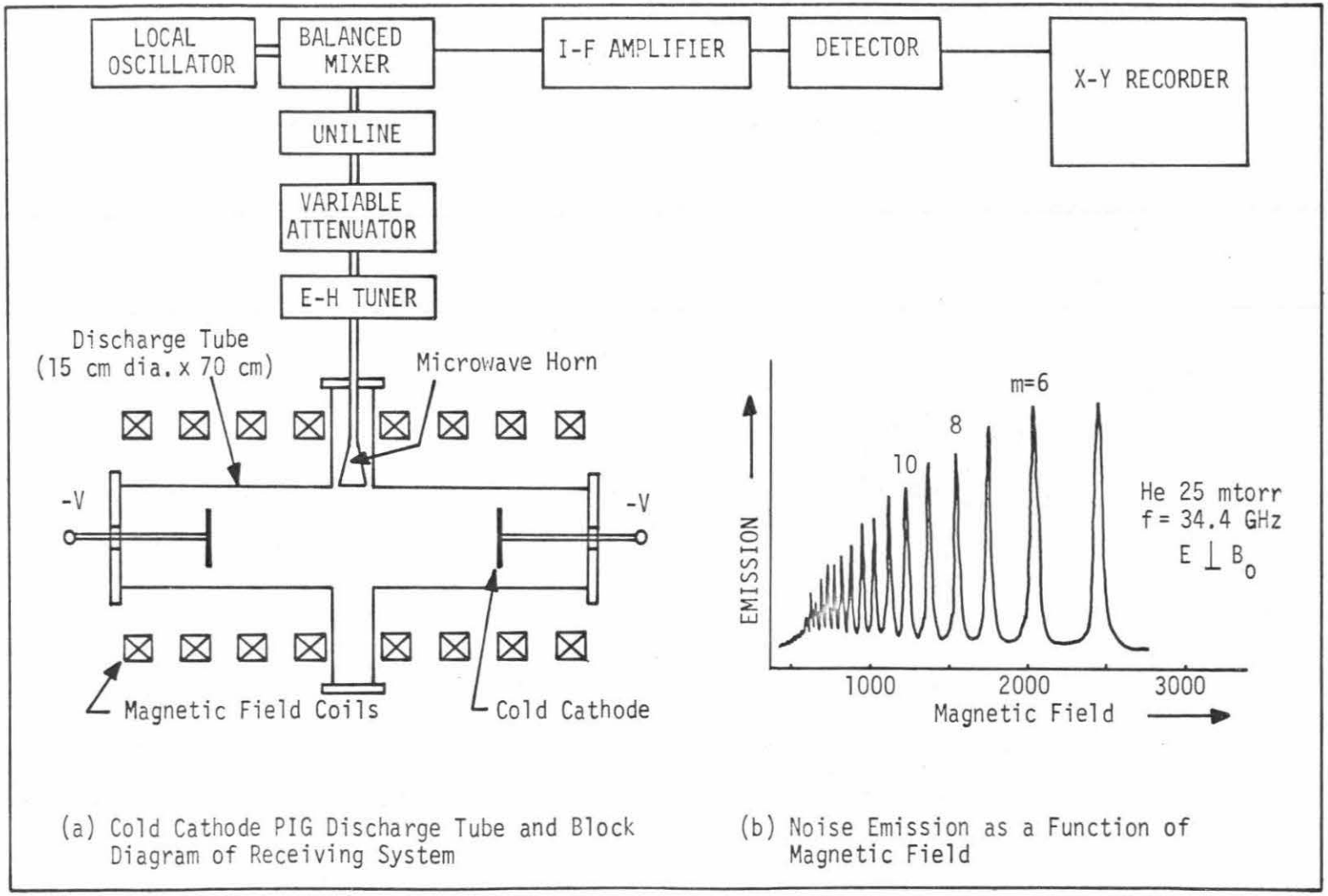

(a) Cold Cathode PIG Discharge Tube and Block Diagram of Receiving System

(b) Noise Emission as a Function of Magnetic Field

Figure 1.1 Landauer's Investigation of Harmonic Emission in a PIG Discharge

pressure and that the harmonics were not detected by his receiver when the pressure was greater than 40 mtorr. When the current of the discharge tube was increased, it was found that the harmonics appeared suddenly at a discharge current of 0.5 to 1.0 amperes. At larger currents, the emission remained at a nearly constant level. The intensity of the extraordinary wave polarization of the emission ($E \perp B_0$) was found to be considerably stronger than the ordinary wave polarization ($E \parallel B_0$). However, the other features of the emission spectrum were found to be independent of the polarization.

In order to display the details of the emission spectrum in greater detail, an emission spectrum from the present investigation (obtained using oxygen gas) has been included for inspection in Figure 1.2. The intensity of the harmonic emission is somewhat greater than in the helium discharge, but generally the spectrum is very similar. The emission intensity typically reaches a maximum at the $m = 4$ or $m = 5$ harmonic. The harmonic emission lines are nearly symmetrical in shape and the normalized line width at half maximum, $\Delta f/f$, is essentially independent of the harmonic number.

The behavior of the harmonic emission spectrum discovered by Landauer was subsequently verified by Dreicer, using a helium gas Penning discharge of virtually the same dimensions [15]. Dreicer utilized microwave receivers of greater sensitivity at frequencies of 18 GHz and 36 GHz and extended the pressure range of the measurements to 2-200 mtorr [16].

The agreement between the observations of Landauer and Dreicer is noteworthy. Dreicer observed harmonic emission of virtually the

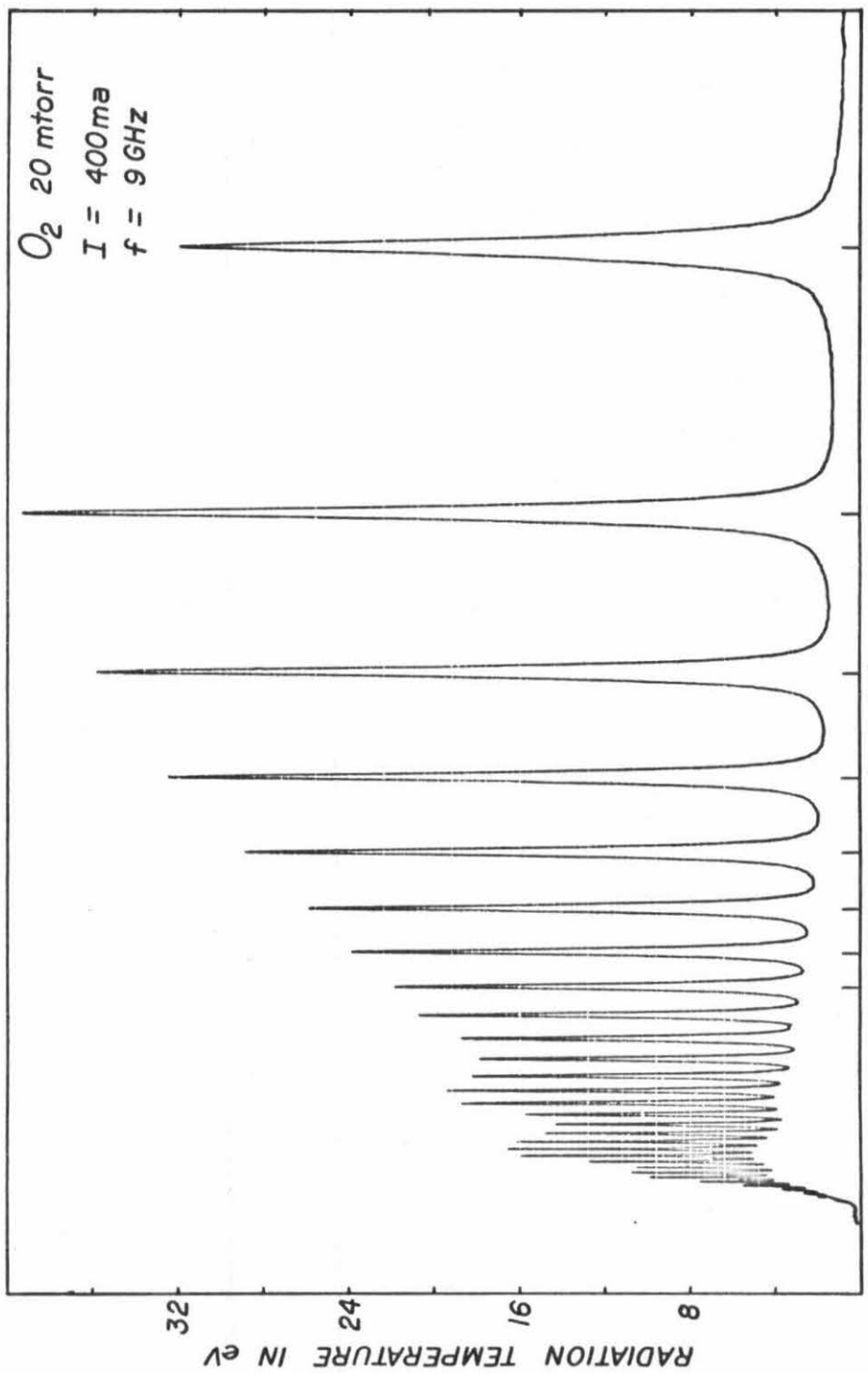

Figure 1.2 The Harmonic Emission Spectrum in Greater Detail. This spectrum was obtained in the present investigation using the oxygen gas Penning discharge.

same intensity, observed the onset of harmonic emission with increasing discharge current, and verified that the harmonic amplitude decreased with increasing neutral gas pressure. However, Dreicer carried out additional measurements which led to several important conclusions.

In addition to observing harmonic emission from the plasma column, Dreicer also measured the transmission and reflection properties of the plasma column. The purpose of these measurements was to detect the existence of a hybrid layer on the density profile of the plasma column by observing its properties directly. Dreicer showed that a large transmission loss was a direct indication of the existence of a hybrid layer and presented evidence of a direct correlation between strong harmonic emission and large transmission loss. With the aid of simultaneous emission measurements at 18 GHz and 36 GHz, Dreicer was able to establish a definite relationship between the harmonic emission and the existence of a hybrid layer. Basically, the existence of a hybrid layer on the plasma column is a necessary condition for the observation of harmonic emission.

Dreicer observed radiation in the vicinity of the fundamental electron cyclotron frequency and explored it in detail. He pointed out that the evidence suggests that the physical mechanism which is responsible for emission at the fundamental and possibly also the $m = 2$ harmonic is only indirectly related to the emission process at the higher harmonics. This point is well taken and the present investigation concentrates mainly on the higher harmonics, although phenomena at the $m = 2$ harmonic will be mentioned occasionally.

Dreicer also reported the results of an investigation of the

line shape of the harmonic emission lines [17]. In the same investigation, the emission lines were found to be located at the cyclotron harmonics to within an experimental accuracy of 0.5%.

Many developments in the theory of harmonic emission were inspired by the experimental work of Landauer and Dreicer. Unfortunately, it appears that the emission spectra and the other experimental evidence described up to this point are not sufficient to distinguish between the proposed mechanisms. In Dreicer's opinion, "no experiments capable of definitely identifying a specifically proposed mechanism have as yet been performed" [15].

Investigations of Landauer emission in the Penning discharge have since been continued by other investigators, but further experimental development has proved to be difficult. Pavlichenko [18] observed harmonic emission in a helium gas Penning discharge but found that the emission spectrum was often dominated by a different type of high intensity radiation. Using the same experimental apparatus, additional investigations of microwave radiation were carried out in hydrogen gas [19-21]. However, the harmonic emission spectra obtained in these investigations are not very well defined, partly due to the complication of an inhomogeneous magnetic field. Dushin [22] verified the hybrid layer condition for the existence of harmonic emission and measured the location of the emission lines with an accuracy of 1%. But for the most part, these investigations were oriented toward the exploration of other types of higher intensity radiation which the investigators discovered in their Penning discharge.

Contrary to the results obtained by Dreicer and Dushin et al., Hanisch and Stetson observed harmonic emission even when the plasma density of their helium discharge, as measured by a microwave interferometer, was well below that needed for the existence of a hybrid layer on the plasma column [23]. In another helium gas Penning discharge, Klan [24] observed amplitude modulation of the harmonic emission by a low frequency rotational instability.

1.3 Definition and Discussion of the Present Investigation

The review of previous experimental work indicates several points which require experimental clarification. Due to the results of Hanisch and Stetson, there appears to be some doubt concerning the role of the hybrid layer in the harmonic emission process. A microwave density measurement will be undertaken in the present investigation to provide an independent determination of whether the existence of a hybrid layer on the plasma column is a necessary condition for the harmonic emission. In addition, the importance of low frequency drift instabilities and turbulence to the harmonic emission process will be examined in detail. However, there are additional considerations of greater importance which need to be explored.

In view of the multiplicity of harmonic emission theories, it appears that the greatest need is for additional experimental work which is capable of pointing the direction for future theoretical development. In this regard, it is important to determine whether the harmonic radiation can be explained on the basis of a single particle radiation theory or is the result of a wave instability induced by a

nonmaxwellian velocity distribution or beam-plasma interaction. Does the emission result from direct excitation of electromagnetic radiation, or are electrostatic waves involved? In addition, it would be very useful to determine which particular group of the nonmaxwellian electrons present in the Penning discharge is responsible for the harmonic emission. It is questions such as these which the present investigation will seek to answer.

Although many of the measurements which are described in this report are similar to what has been done in previous investigations, virtually all of the results are new in some respect. In fact, the similarities which exist with previous experiments are essential to provide continuity in order that the results which are original to this investigation might be related to previous work in the Penning discharge.

Unlike the previous investigations of harmonic emission in the Penning discharge, the present investigation does not use helium or hydrogen for the neutral gas. Instead, argon was used in the initial stages of the investigation, but oxygen gas is used throughout most of the work. The unconventional choice of oxygen for the neutral gas proved to be beneficial. As noted earlier in the introduction, the harmonic emission which is produced in this discharge is exceptionally intense.

Another feature of this investigation is the use of grid stabilization of the plasma column of the Penning discharge. Such a plasma column represents a considerable improvement in the experimental conditions. Typically, the plasma column produced in an argon or oxygen

Penning discharge is extremely turbulent and exhibits large amplitude fluctuations of the density and potential. In the grid-stabilized discharge, the fluctuation level is reduced by several orders of magnitude. Certainly the quiet plasma of the grid-stabilized discharge is a more desirable environment in which to investigate a phenomenon whose origin is not well understood. And the fact that harmonic emission has been observed under such contrastingly different conditions should not be overlooked.

The use of a Penning discharge tube with a pyrex vacuum wall differs from the more conventional practice of enclosing the plasma column in a metal chamber. In the present investigation, harmonic emission is observed in both types of discharge tubes. The use of a pyrex vacuum wall makes it easier to estimate the total emission from the plasma column because the complication of strong reabsorption of emission by the plasma column, which occurs in the metal cavity discharge tube, is avoided.

Although it is Chapter V which contains much of the work which is unique to the present investigation, this does not degrade the importance of the more conventional measurements contained in Chapter III. The experimental approach and the results described in Chapter V are quite unlike anything done in previous experiments. Therefore it is the more conventional measurements of Chapter III which demonstrate that the harmonic emission observed in the present investigation is indeed of the same nature as that observed previously by Dreicer and Landauer in the helium gas Penning discharge.

It is appropriate to end the introduction with a brief outline of the content of each of the remaining chapters of this report.

In Chapter II, the equipment and the instrumentation employed in the investigation are described. The construction and operation of two Penning discharge tubes is discussed in detail, and grid stabilization of these discharge tubes is described. The use of oxygen as the neutral gas is discussed, including both the advantages of its use and the complications which arise. Chapter II concludes with an analysis of the Penning discharge and the energetic electrons which it contains. Using cross sections for inelastic electron-neutral collisions, a rough quantitative picture of the number density and energy distribution of the energetic electrons is obtained.

Chapter III is a collection of many measurements which are carried out to explore specific features of harmonic emission, principally in the oxygen gas Penning discharge. Measurements of the shape, location, and polarization of the emission lines are described. Harmonic emission is reported from a grid-stabilized discharge and measurements of the transmission and reflection properties of the plasma column are presented. A polar microwave interferometer measurement of the electron density is described and implications concerning the presence of a hybrid layer on the plasma column when harmonic emission is detected are discussed.

In Chapter IV, the various theories of harmonic emission are reviewed and compared with the experimental results described in Chapter III. Several promising theoretical possibilities emerge from the analysis, but most of the theories are not found to be relevant to

the Penning discharge. Motivation for additional experimental work of a basically different nature is given in terms of questions which can not be answered on the basis of the experimental results presented in Chapter III.

The development and the results of a new experimental approach to the investigation of harmonic emission in the Penning discharge are described in Chapter V. The technique used to pulse modulate the cathode voltage of the Penning discharge is described. High intensity radiation which is observed in the emission spectrum, principally between the cyclotron harmonics, is documented and is identified as resulting from a beam-plasma interaction.

Data are presented which demonstrate the effects of pulse modulation on the harmonic emission. The rise time of the harmonic emission is measured by using a wideband I-F system. It is demonstrated that the intensity and the width of the emission lines depend strongly on the cathode voltage. The experimental results are evaluated and it is shown that the evidence favors the concept of single particle radiation. The evidence also indicates that the harmonic emission results principally from fast electrons of intermediate energy, roughly $15\ \text{eV} < E < 100\ \text{eV}$.

Chapter VI provides a summary of the important results and conclusions, as well as suggestions for further work.

CHAPTER II

THE EXPERIMENTAL APPARATUS AND THE PLASMA

2.1 Introduction

This chapter contains a description of the experimental apparatus and the plasma. It begins with a basic description of the magnetic field, the vacuum system, and the microwave receiver. Then the design and characteristics of a specialized wideband I-F system are discussed in detail. A direct reading microwave interferometer is described and its accuracy is evaluated.

In Section 2.3 the mechanism of the Penning discharge and several variations of the electrode geometry are discussed. The construction of a brass Penning discharge chamber is specified and many modifications of the device are noted. The use of oxygen gas is discussed, including both the advantages of its use and the complications which arise. Details of the construction of a Penning discharge tube with a pyrex vacuum wall are given. Grid stabilization of both of the Penning discharge tubes is described and typical voltages and radial profiles are presented.

An analysis of the energetic electrons ($E > 15$ eV) which are present in the Penning discharge is given in Section 2.4. The number density and the energy distribution function of the energetic electrons are computed. The time dependence of the energy of a fast electron is calculated from the cross sections for inelastic electron-neutral collisions.

2.2 Equipment and Instrumentation

2.2.1 Magnetic Field and Vacuum System

The magnetic field which is necessary for the operation of the Penning discharge is produced by an air core solenoid. The solenoid has an inside diameter of 12 inches and consists of 16 individual coils (see Figure 3.18). The coils are spaced so as to maximize the homogeneity of the magnetic field. Within an 18 inch length along the axis of the solenoid, the magnetic field variation is less than 0.15% from minimum to maximum. This upper bound for the spatial variation was obtained from NMR probe measurements and also from the computer computations which determined the optimum spacing of the coils. The volume occupied by the plasma can be approximated by a right circular cylinder 18 inches long and roughly 4 inches in diameter. The field variation within this volume is less than 0.4% from minimum to maximum.

The solenoid is powered by a transformerless SCR power supply with a constant current stability of 0.1% for the time periods involved in the experiments. An L-C filter reduces the current ripple in the solenoid below 0.04% rms for the magnetic fields typically used in the experiments. The system produced magnetic fields up to 3.2 kilogauss, which corresponds to an electron cyclotron frequency of 9 GHz. A remote control sweep unit allows the current output of the power supply to be swept automatically at any rate which is desired.

Although argon gas was tried initially, oxygen gas is employed in most of the experiments. The neutral gas pressure is measured with a Hastings DV-5M thermocouple tube (0.2-100 mtorr). Readings are

corrected for the thermal conductivity of the gas using the nomogram supplied with the tube.

At the conclusion of the experiments the linearity of the Hastings thermocouple measurement was tested by comparison with a Schulz-Phelps high pressure ionization gauge tube and a CVC thermocouple tube. From the consistency of the three measurements, it was concluded that good linearity with pressure was obtained in the pressure range of 5-100 mtorr. The agreement between the Hastings and CVC thermocouples was better than 10%, however a factor of two in the absolute calibration of the Schulz-Phelps ion gauge control unit was not resolved.

The vacuum system consists of a 4" diffusion pump and a mechanical backing pump. A refrigerated cold trap is located at the inlet of the diffusion pump. Using silicone diffusion pump oil, the system has a base pressure of $2X10^{-7}$ torr. The pressure at the inlet to the vacuum station is monitored with a NRC 831 ionization gauge control unit.

2.2.2 Microwave Receiver

The radiometer employed to study the microwave emission of the plasma is a calibrated superheterodyne receiver. A block diagram of the receiver is given in Figure 2.1. The receiver is calibrated by replacing the microwave horn with a standard noise source. A calibrated variable attenuator greatly extends the operating range of the radiometer and allows accurate comparison of emission levels which differ by many orders of magnitude.

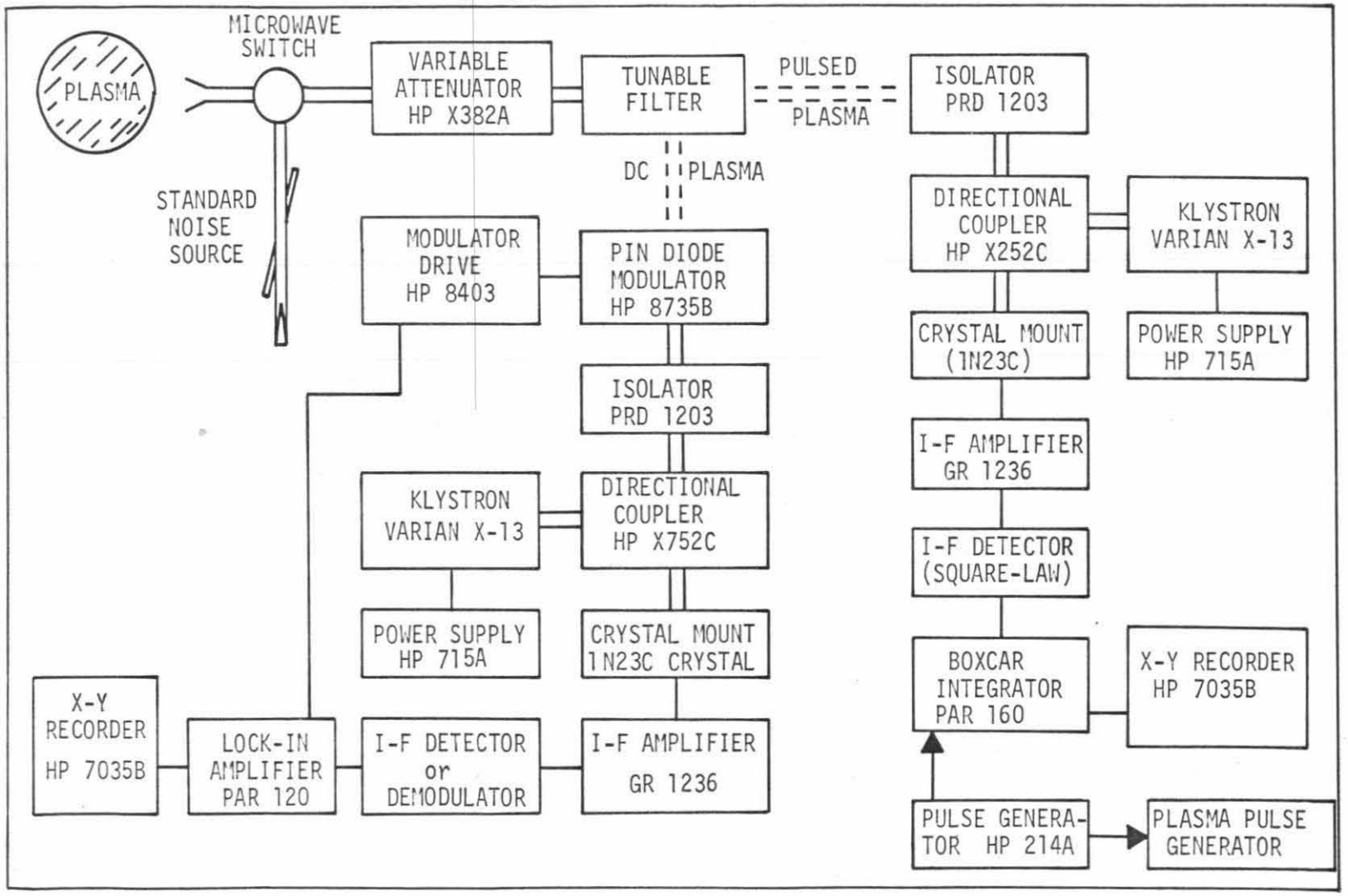

Figure 2.1 Block Diagram of Microwave Receiver

The tunable microwave filter consists of a shunt tee, a length of waveguide and a movable short. This arrangement exhibits a tunable narrow stopband which is effective in rejecting one image frequency of the superheterodyne receiver without attenuating the other image frequency.

All of the microwave components are broadband and as a result the receiver works well over the entire frequency range of 7-12 GHz. When using a 1N23C mixer crystal, the receiver has a noise figure of 9.5 db at 9.0 GHz. Away from the center frequency the noise figure deteriorates somewhat. This is especially noticeable at lower frequencies near 7.0 GHz.

The receiver takes on a different configuration depending on whether the plasma is operated continuously or on a pulsed basis. When the plasma is operated from a dc power supply, the PAR lock-in amplifier is usually used. In this case the demodulation output feature of the I-F amplifier unit is employed as the I-F detector. The response of the demodulation output is close to square law if the signal levels are kept small. The 30 MHz I-F amplifier has a bandwidth of 4 MHz and a noise figure of 2 db. Differences in plasma emission as small as $100^{o}K$ (equivalent radiation temperature) can easily be distinguished when a 1 second time constant filter is used.

The plasma emission level is usually sufficiently large that synchronous detection is not essential. Therefore the emission spectra were occasionally recorded directly from the output of an I-F detector, using an appropriate filter. However, the spectra obtained in this way are somewhat noisy.

The frequency range of the Varian X-13 klystron is 8.2 - 12.4 GHz. Whenever it became necessary to use a lower frequency for the local oscillator, the klystron was replaced by either a test oscillator or a sweep oscillator, both of which operate down to 7.0 GHz.

Although a double balanced mixer was used initially, it is not essential and does not possess the broadband characteristics of the single crystal mount.

Because some of the local oscillator signal is reflected by the mixer, an isolator is needed to prevent this signal from being modulated by the pin diode modulator and appearing again as a false signal in the mixer.

The discharge is frequently operated on a pulsed basis in order to achieve higher plasma densities and to carry out experiments in the afterglow plasma. In this mode of operation the pulse repetition rate is controlled by the HP 214A pulse generator which triggers both the boxcar integrator and the pulse generator which generates the plasma.

The output of the I-F detector is sampled by the PAR 160 boxcar integrator. A HP 420A crystal detector is used together with an appropriate terminating resistor to provide a square-law I-F detector. A square-law detector is desirable because it produces an output which is proportional to the emission power received from the plasma. When fluctuations are present in the emission, the time averaged output of the detector then indicates the time averaged power emitted by the plasma.

The Y axis of the recorder is driven from the output of either the lock-in amplifier or the boxcar integrator. When sweeping the magnetic field to obtain the emission spectrum, the X axis of the recorder is

driven by a current shunt which monitors the current flowing in the magnetic field coils. Because of the transformerless nature of the field coil power supply, the voltages at the current shunt contain a very large common mode 180 Hz voltage waveform. This waveform is almost entirely removed using a dual two-stage L-C filter. The filtered voltage from the current shunt is then applied to the floating inputs of the X axis of the recorder.

During pulsed plasma experiments, the plasma emission can also be recorded as a function of the time during the pulsed discharge by using the automatic scan feature of the boxcar integrator. In this case the X axis of the recorder is controlled by the boxcar integrator.

2.2.3 Wideband I-F System

The response time of the microwave receiver for pulsed operation is limited by the 4 MHz bandwidth of the I-F amplifier. This bandwidth corresponds to a rise time of 180 nsec, assuming that the rise time of the I-F detector can be neglected. The pulse modulation experiment of Chapter V requires a considerably faster response time. For this purpose, the I-F system displayed in Figure 2.2 was developed.

The crystal mixer is coupled to the I-F preamplifier by a double tuned circuit [25]. An inductive T-network is utilized to obtain a large fractional bandwidth [26]. The coupling network determines the shape and width of the I-F bandpass. Because the frequency response of the preamplifier is not flat, an attenuator was designed to compensate for the frequency dependence of the gain. The combination of the preamplifier and attenuator gives a flat frequency response over the

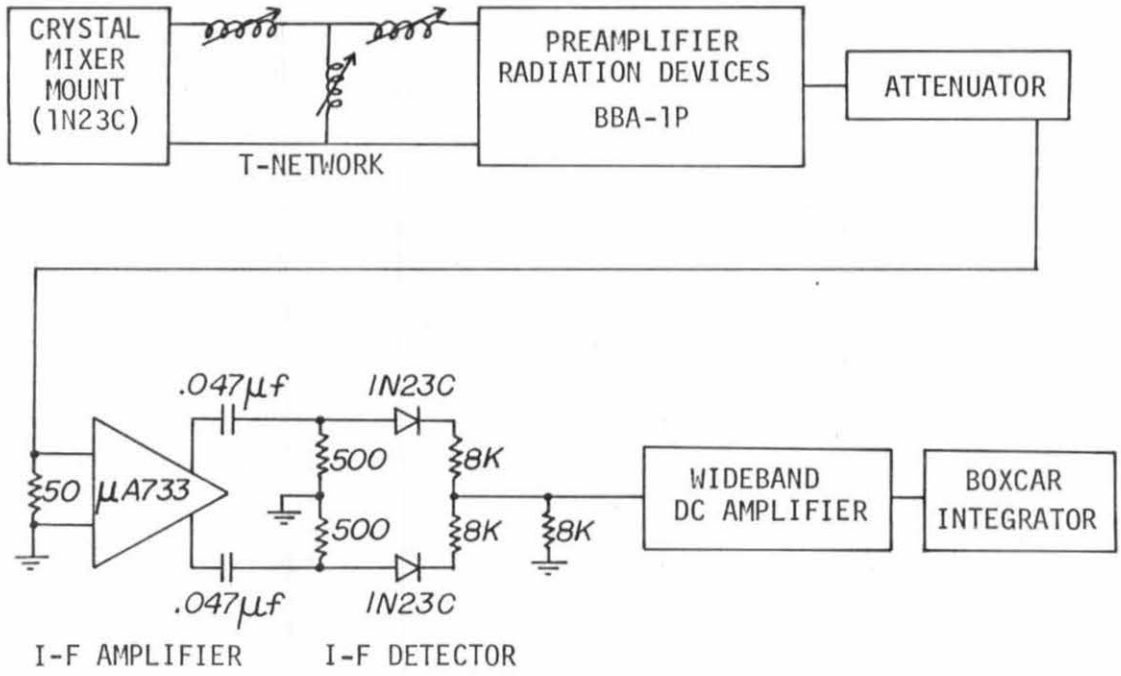

Figure 2.2a Block Diagram of Wideband I-F System

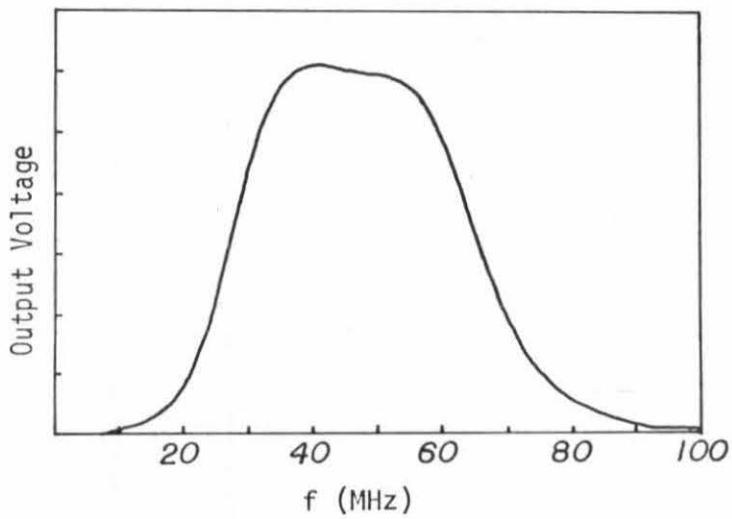

Figure 2.2b Frequency Response of I-F System

bandwidth determined by coupling network and provides a signal gain of 38 db. The noise figure of the preamplifier is less than 3 db.

The I-F signal is then amplified by a broadband amplifier (90 MHz) and rectified by an I-F detector. The amplifier is a linear integrated circuit video differential amplifier. The amplifier gain is set at 32 db by means of an external resistor. This gain provides the desired signal level for the I-F detector.

When the differential output of the video amplifier is full wave rectified by a pair of matched diodes, the resulting waveform includes a ripple at twice the I-F frequency. However, the ripple is at a sufficiently high frequency that it can easily be removed by a low pass filter without compromising the response time of the system.

Although various diodes were tried for the I-F detector, only the point contact mixer diode proved to be satisfactory. Minimum junction capacitance and fast recovery time provide very flat frequency response below 100 MHz and excellent pulse response. In addition, these diodes are capable of providing square-law behavior over a sizable dynamic range. Unfortunately, this requires a large diode load impedance which is somewhat incompatible with fast response. Deviation of crystal response from square law was found to be minimized by using a load impedance of about 15 KΩ . Even when this impedance is distributed as indicated in Figure 2.2a, a stray capacitance of only 2 pf results in a 15 nsec time constant.

In order to maintain both fast pulse response and square-law behavior, the output of the I-F detector must be followed by a wideband dc amplifier which has a very low input capacitance and a large

input resistance. The amplifier must also be capable of driving the 50Ω line which leads to the boxcar integrator. These requirements were satisfied by using another μA733 video amplifier and an emitter follower transistor. This combination does result in noticeable output drift but the system is usable. The output amplifier provides a signal gain of 32 db for the small output voltages of the I-F detector.

Figure 2.2b shows the frequency response of the wideband I-F system. The I-F center frequency and bandwidth are 45 MHz and 40 MHz, respectively. The pulse response of the system is slightly asymmetric. Although the rise time is noticeably faster than the fall time, in both cases the 10%-90% response time is roughly 25 nsec.. The propagation delay time of the system is less than 40 nsec. The system exhibits square-law behavior over a usable dynamic range of more than 20 db.

When the wideband I-F system is used with the microwave receiver, the receiver has a 10.5 db noise figure. In order to shield the receiver from transient pickup, the entire system from the waveguide mixer to the wideband dc amplifier is housed in a metal box. When the wideband I-F system is used, the aperture time of the boxcar integrator is operated close to the minimum value of 10 nsec.

2.2.4 Microwave Interferometer

This section describes the polar microwave interferometer which is used to measure the absolute plasma density, together with an analysis of the accuracy of the density measurement. A block diagram of

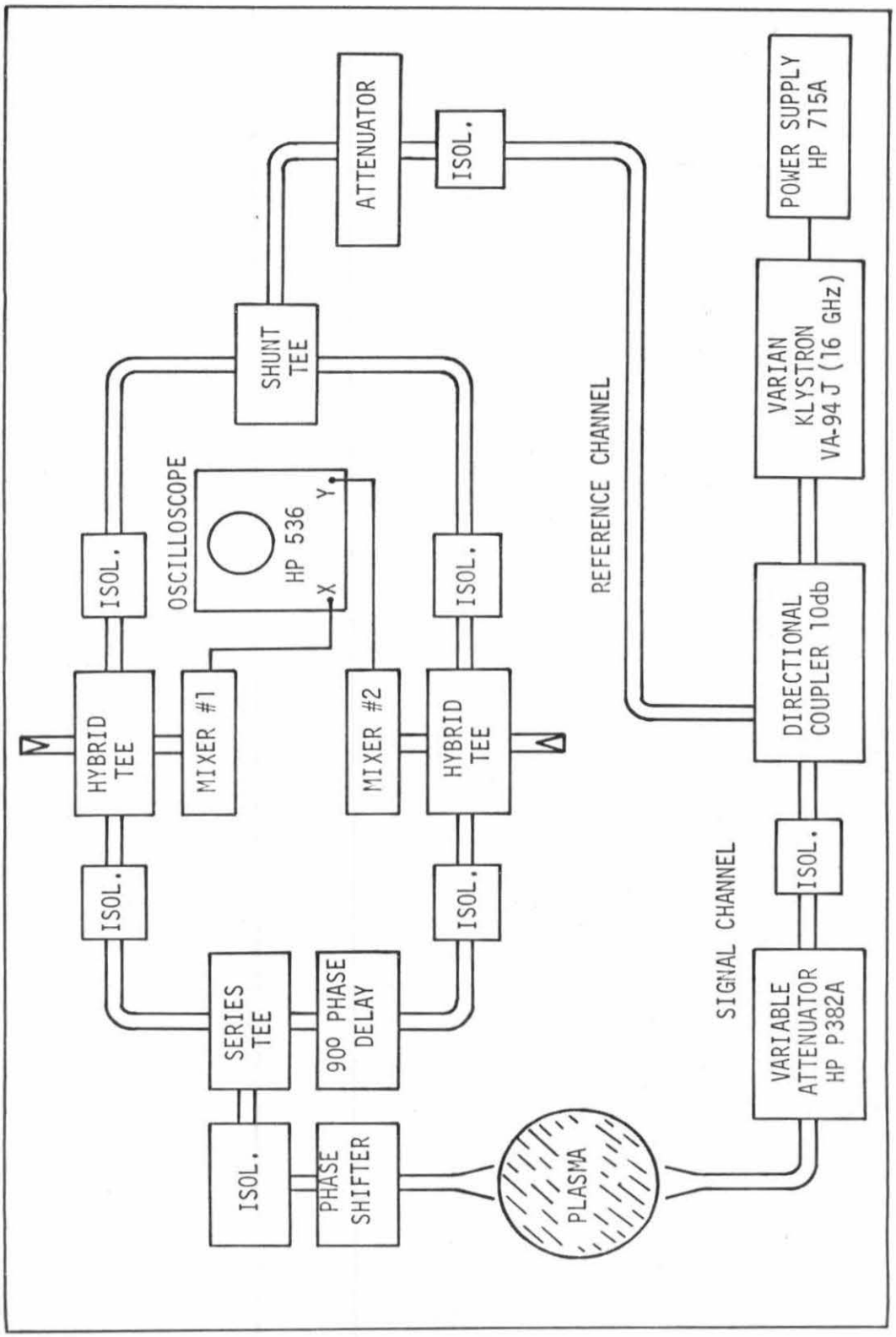

Figure 2.3 Block Diagram of Microwave Polar Interferometer

the polar interferometer is given in Figure 2.3. A more detailed cross-sectional view of the plasma, microwave horns, and surrounding environment is given in Figure 2.5.

The polar interferometer consists of a test channel which intercepts the plasma column and a reference channel. The reference and test signals are compared at two crystal mixers. A 90^{o} phase delay is added in the test channel of mixer #2. Except for this 90^{o} phase shift, the path lengths to the two crystal mixers are identical.

The microwave crystals are operated in the square-law domain. The resulting crystal output voltages are given by

$$V_1 = \beta_1[A_R^2 + A_T^2 + 2A_RA_T \cos \phi]$$

$$V_2 = \beta_2[A_R^2 + A_T^2 + 2A_RA_T \sin \phi]$$

where A_R and A_T are the amplitudes of the test and reference microwave signals, ϕ indicates the difference in path length between the reference and test channels, and β_1 and β_2 indicate the microwave crystal sensitivites. The crystal mixer output voltages, V_1 and V_2, are applied to the X and Y inputs of an oscilloscope.

When the phase difference, ϕ , is varied by 2π , the voltage vector $V_1 + V_2$ describes an ellipse on the oscilloscope as indicated in Figure 2.4. When $\beta_1 = \beta_2$, the ellipse becomes a circle. The radius of the circle in volts is equal to $2\beta A_RA_T$, where $\beta = \beta_1 = \beta_2$. When the circle is centered on the scope face and a polar graticule is used, the phase difference can be read directly off the oscilloscope. This is how the interferometer is operated for the plasma density measurements.

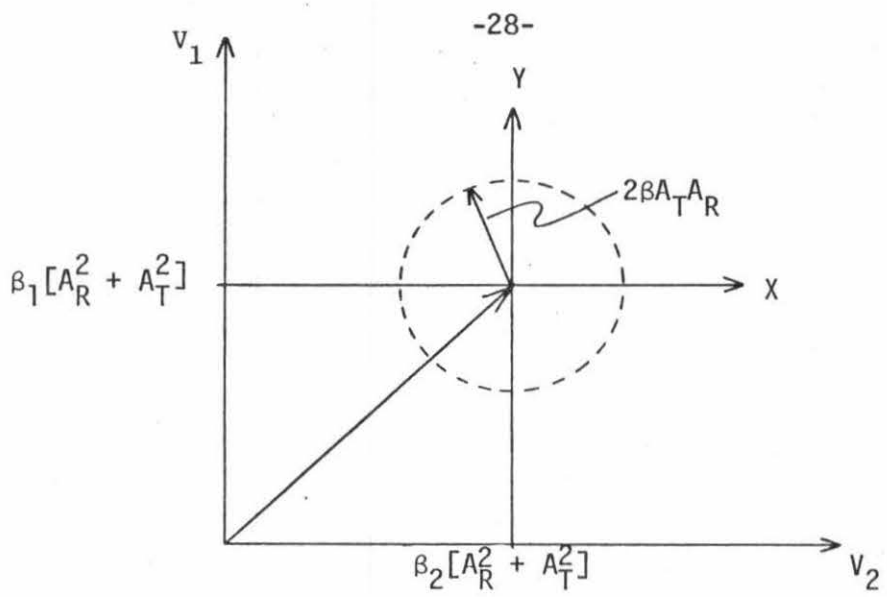

Figure 2.4 Displaying the Interferometer Phase Difference on an Oscilloscope.

There are several adjustments which must be made before the direct reading polar interferometer will operate satisfactorily. When there is no plasma present in the test channel, the phase shifter in that channel is adjusted to give $\phi = 0$ on the oscilloscope graticule.

It has already been noted that an ellipse is obtained when the crystal sensitivities are not equal, $\beta_1 \neq \beta_2$. This situation is corrected by appropriate adjustment of the gain of the oscilloscope input amplifiers. Although it is still possible to determine the phase angle, ϕ, even when the voltage vectors describe an ellipse, direct reading of the phase then requires an appropriate elliptical graticule for the oscilloscope.

An ellipse is also obtained if the phase delay in the test channel of mixer #2 deviates from 90^o. Careful adjustment of the phase shift is essential because an error of ε degrees in the phase delay

results in a maximum error of ϵ degrees in the interferometer phase measurements.

Finally, sizable errors can result if the response of the 1N78 point-contact mixer diodes is not square law. The crystal response is found to be optimal when the crystals are terminated with a 20KΩ load resistor. The crystal response is then approximately square law for output voltages up to 60 mV. Without the terminating resistors, square-law behavior is limited to output voltages which are too small to be compatible with the 1 mV/cm sensitivity of the oscilloscope.

The interferometer accuracy is found to be improved by limiting the amplitude of the microwave signal in the test channel to a level which is 15 db below the reference channel. This also reduces the shift of the polar display which occurs when the test channel amplitude is decreased by plasma effects. Oscilloscope drift is minimized by utilizing the largest crystal output voltage compatible with the requirement of square-law response.

After adjustments are made to minimize each of the above sources of error, the voltage vectors trace out a nearly perfect circle on the oscilloscope when ϕ is varied by 2π. And when the phase measurement read directly from the graticule is plotted versus the actual phase shift ϕ as determined by a phase shifter, the error is usually less than $\pm 3^{o}$. This represents an error of approximately 3% for most of the plasma density measurements.

There is one additional source of error of undetermined magnitude. It is assumed that the microwave signal propagates across the plasma column from the transmitting horn to the receiving horn in a narrow

beam which only samples the plasma density profile along a well defined line. This assumption is not fully realized in the present situation. The plasma diameter, D , at the 50% points on the density profile is typically between 6.0 and 6.4 cm, and the free space wavelength of the interferometer signal source is 1.9 cm. A value of $D/\lambda = 3.3$ indicates that the beam width is a significant fraction of the column diameter. An informative discussion of many aspects of this problem, including the significance of the value of the parameter D/λ , is presented by Heald and Wharton [27].

The standard gain horns used with the interferometer have a gain of 10.5 db at the interferometer frequency. Therefore the horns are not highly directional. As a result, the receiving horn will pick up microwave signal which has been scattered by the surrounding environment, principally the magnetic field coils. To reduce this problem, the field coils in the vicinity of the interferometer horns are lined with microwave absorber as indicated in Figure 2.5.

Microwave signal can also be scattered by the six support rods of the discharge structure and by the pyrex vacuum wall surrounding the plasma. The support rods were initially covered with absorber. However, this material had to be removed to facilitate cooling of the pyrex tube, which was heated excessively by the discharge.

Reflection from the pyrex tube was not as severe as might be expected. At the interferometer frequency, 15.8 GHz, the vacuum wall is slightly more than one-half wavelength in thickness. This significantly reduced the potentially troublesome reflections of the microwave signal.

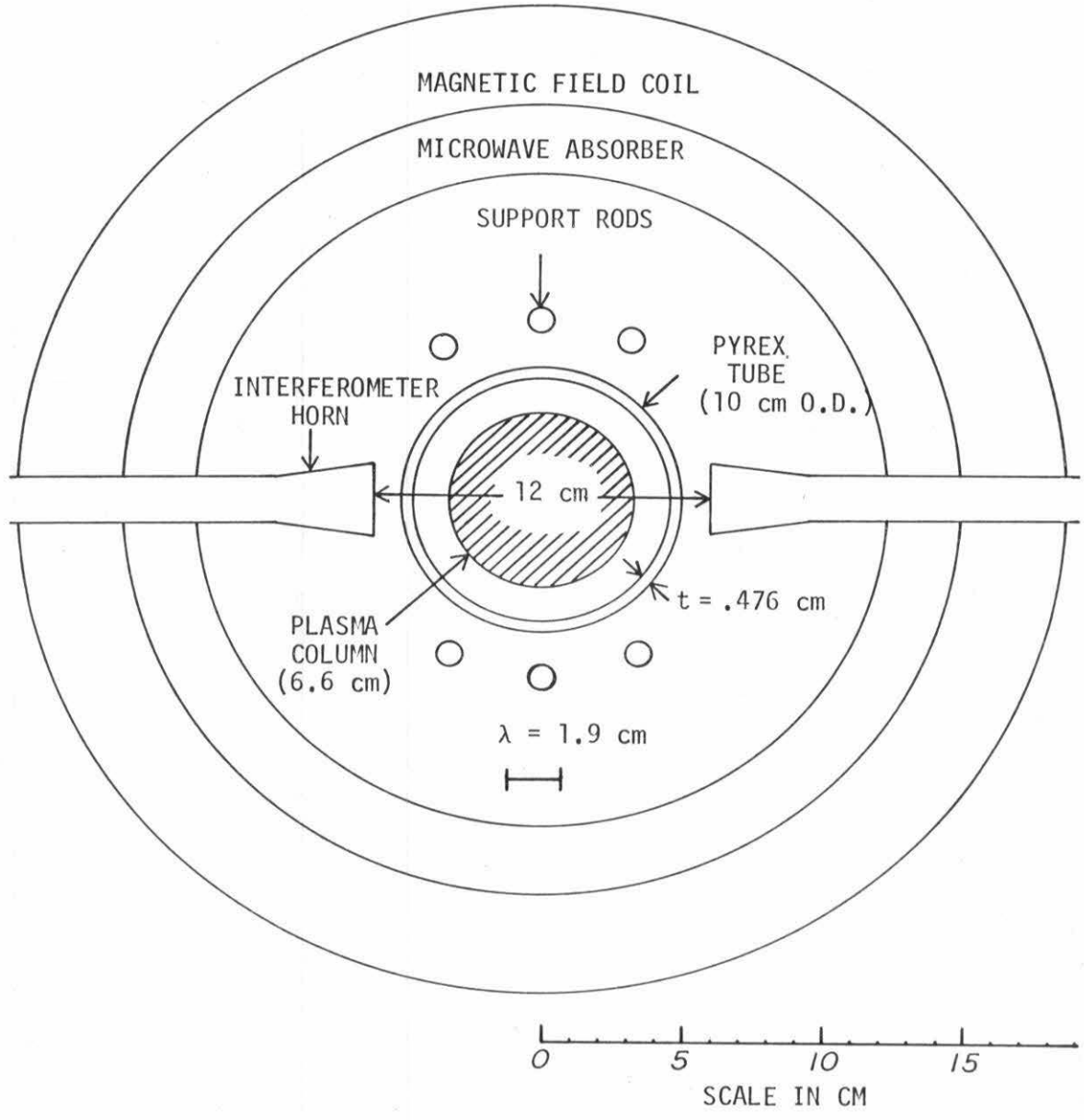

Figure 2.5 The Environment for the Microwave Density Measurement

Although reflection for normal incidence vanishes for a lossless half-wave plate, reflection for arbitrary angles of incidence is minimized by maintaining a slightly larger value of t/λ, where t is the thickness of the plate [28]. In the present situation, the limited frequency range of the klystron dictates a minimum value of $\sqrt{\varepsilon}t/\lambda = 0.565$ which is 13% thicker than a half-wave plate. For the above computation the dielectric constant of No. 7740 pyrex is taken to be $\varepsilon = 5.1$ [29].

However, a rough measurement of the dielectric constant of the pyrex tube (using the polar interferometer) indicates a slightly smaller value of $\varepsilon \simeq 4.7$ at 16 GHz. In this case, $\sqrt{\varepsilon}t/\lambda = .54$. Although this thickness does not entirely eliminate reflection for normal incidence, it is nearly optimal for minimizing microwave scattering for arbitrary angles of incidence.

Considerable care was taken to insure that the available microwave equipment would produce results with maximum accuracy. Although the magnitude of the errors resulting from $D/\lambda = 3.3$ and scattered microwave signal are difficult to estimate, phase measurements carried out by inserting slabs of dielectric materials of known dielectric constant into the pyrex tube indicate that the error is within the estimated accuracy of 5-10%.

2.3 The Penning Discharge

2.3.1 The Mechanism of the Discharge

The electrode configuration herein referred to as the Penning discharge was first investigated in a magnetic field by F. M. Penning [30]. It is also commonly known as the PIG (Philips ionization gauge)

discharge [31,32], named after a pressure measuring device developed by Penning using this electrode configuration [33,34]. Several variations of the discharge configuration are indicated in Figure 2.6.

The configuration is essentially a cold cathode glow discharge of complicated geometry capable of operating at low pressures. Electrons are produced at each cathode as a result of secondary emission by ion bombardment. Most of the voltage drop between the cathode and anode occurs in the immediate vicinity of the cathode. Hence, the secondary electrons are accelerated to a high energy by the cathode sheath, but are constrained by the magnetic field to follow a helical path parallel to the magnetic field. If an electron loses some of its initial energy on the first transit of the discharge, it will be reflected by the opposite cathode. It subsequently oscillates between the cathodes many times while migrating across the magnetic field to the cylindrical anode.

As the energetic electron oscillates between the cathodes, it ionizes neutral gas molecules and thereby loses its energy. The ions and electrons so produced migrate to the cathodes and anodes, respectively. The ions are accelerated to high energies by the cathode sheath, and produce new secondary electrons which continue the process of sustaining the plasma. Because of the reflex action of the cathodes, the discharge operates well even at low pressures where the ionization mean free path is orders of magnitude larger than the anode-cathode electrode separation.

The discharge is capable of operating in many distinct modes such that the discharge exhibits qualitatively different behavior for

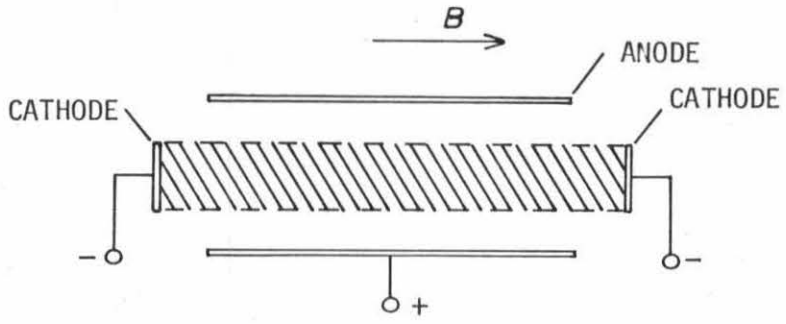

(a) Philips Ionization Gauge Type Discharge (PIG)

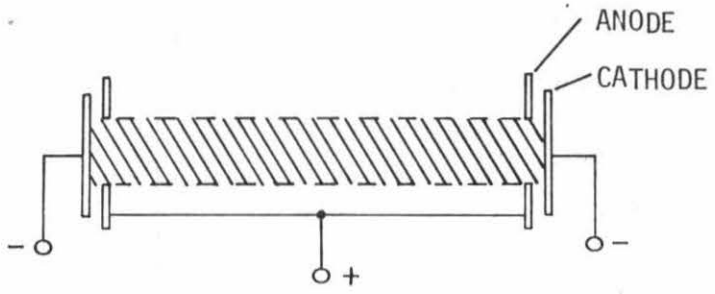

(b) Klan's Q-PIG (Q = Quiescent)

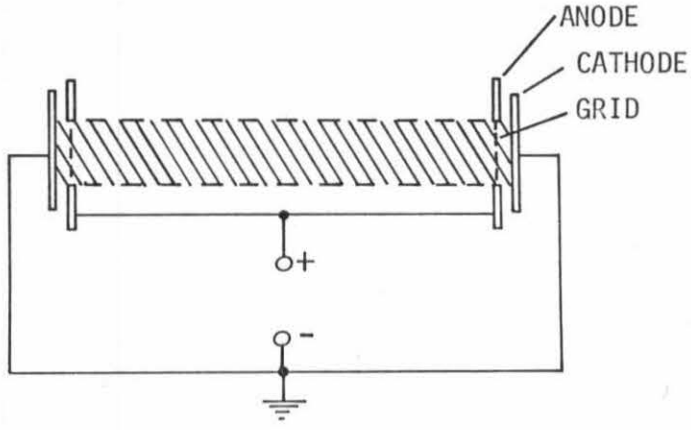

(c) Grid Stabilized Discharge

Figure 2.6 Common Variations of the Penning Discharge

different values of the pressure, magnetic field, discharge current, and voltage. Hooper has completed a review which covers many investigations of the Penning discharge [35]. The discharge has numerous complicating features including plasma instabilities, nonmaxwellian particle distributions, secondary emission processes at the cathode surfaces, large radial electric fields, and ionization phenomena in the neutral gas. It is fair to say that many effects characteristic of the discharge are not well understood.

2.3.2 Variations of the Penning Discharge

Each of the three Penning discharge variations sketched in Figure 2.6 were tried. They were found to exhibit different behavior, indicating that the electrode geometry has a significant effect on the operation of the discharge. The major difference involves radial currents, radial electric fields, instabilities, turbulence, and anomalous diffusion.

In the first variation, Figure 2.6a, the hashed area indicates the region in which ionization by fast electron inelastic collisions occurs. The anode current is driven across a region in which there is no plasma generation. When the magnetic field is large, electron diffusion is greatly inhibited and strong radial electric fields appear on the column. This electric field drives instabilities which eventually lead to a turbulent plasma and anomalous diffusion.

This discharge configuration is found to be turbulent except for a special set of operating parameters. At low magnetic fields, a stable plasma could often be obtained for a particular combination of the discharge current and neutral gas pressure.

In the second variation, Figure 2.6b, the radial flow of current is changed significantly. This configuration is very stable at low magnetic fields. Klan [36] referred to it as the Q-PIG (Q = quiescent) discharge. However, when the magnetic field is increased, there is a critical magnetic field above which the discharge again exhibits low frequency instabilities and anomalous diffusion. The onset of instability and turbulence is marked by the appearance of large amplitude fluctuations in the cathode potential. In addition, probe measurements indicate the presence of large amplitude fluctuations in the floating potential and ion saturation current.

Finally, in the third variation, Figure 2.6c, radial currents and electric fields are greatly reduced by placing a grid across the plasma column. The grid is attached to the anode structure and collects much of the anode current. The resulting plasma is found to be stable for all values of the magnetic field used in the experiment.

Allen [41] has previously observed that low frequency oscillations in the Penning discharge can be suppressed by placing a grid across the discharge column. In addition, the plasma has likewise been stabilized by operating the discharge in a magnetic well created by Ioffe bars [42,43]. With both instability suppression techniques it is found, as expected, that the instability returns if the magnetic field is again increased sufficiently. This behavior is not observed in the present experiment, probably because sufficiently large magnetic fields can not be produced.

The behavior described above suggests that the instability responsible for the turbulence might be what Lehnert [37] and Hooper [38]

call the neutral drag instability. Physical descriptions of the instability are given by Simon [39] and Hoh [40]. The instability is driven by a combination of radial electric field and density gradient.

Many of the experiments which are described in this report were performed using both the Q-PIG configuration of Figure 2.6b and the grid-stabilized configuration of Figure 2.6c. Hereafter, these configurations will be referred to as the nonstabilized and the grid-stabilized discharge, respectively. The grid-stabilized discharge was not available until the later stages of the investigation.

2.3.3 Brass Discharge Chamber and Modifications

The brass Penning discharge chamber is sketched in Figure 2.7. The anode, a 6" ID brass cylinder, is electrically isolated from the brass end plates by a gasket cut from 1/16" viton sheet. The viton provides both the electrical isolation and the vacuum seal. A periodic structure in the region of the vacuum seal prevents microwave radiation from leaking out, thereby maximizing the Q of the overmoded microwave cavity. The water cooled brass end plates provide a heat sink and electrical contact for the aluminum cathodes which are mounted thereon. Nylon bolts are used to clamp the end plates to the anode structure.

Aluminum anode rings determine the diameter of the plasma by defining the region in which ionization by energetic electrons takes place. The aluminum rings have an ID of 4 inches and are rigidly attached to the brass cylinder by set screws.

Two fabricated X-band microwave horns are brazed to the brass cylinder at the midplane location, separated by 90^{o} in azimuth around

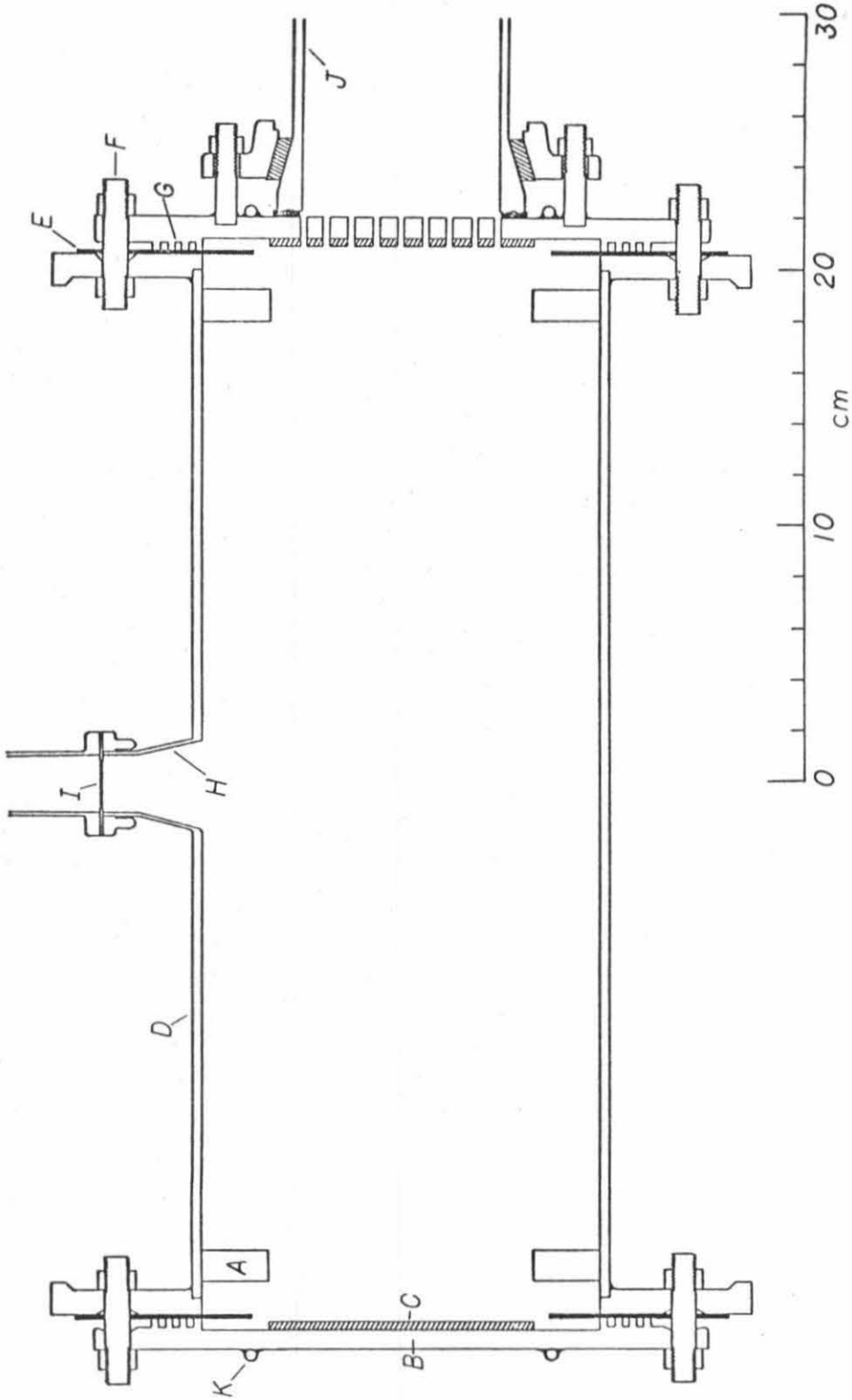

Figure 2.7 Scale Drawing of the Brass Discharge Chamber

A - aluminum anode rings, B - brass endplate, C - aluminum cathodes, D - brass cylinder (6" ID), E - viton gasket, F - nylon bolt, G - periodic structure, H - microwave horn, I - vacuum iris, J - conical pyrex pipe (3" ID), K - water cooling coil

the cylinder. Resonant microwave vacuum irises provide the vacuum interface inside of the waveguide. One of the horns is connected directly by continuous waveguide to the microwave receiver which monitors the plasma emission.

The discharge chamber is centered inside of the magnetic field solenoid which was described earlier. One end of the chamber is connected to the 3" ID conical pyrex pipe of the vacuum system. There are many small holes in the cathode and end plate. The working gas flows through these holes to the vacuum pump; it is fed directly into the discharge chamber and flows continuously during the experiment. During operation of the discharge, plasma streams out of the holes along the magnetic field lines.

Argon gas was used in the initial experiments. Significant sputtering of the aluminum cathodes by the argon ions was observed. After many hours of operation, the viton insulator obtained such a thick coating of aluminum that a sporadic cathode-anode short developed. Arcing occurred around the viton sheet. It was then necessary to disassemble the entire system and remove the sputtered aluminum. The interior of the discharge chamber was found to be completely coated with a thick layer of aluminum metal and significant wear was noticed at the aluminum cathodes.

It was determined that aluminum is only deposited on surfaces which are exposed by a direct line of sight path to the plasma. In other words, surfaces which are in the shadows of other objects are not coated. When the surface of the insulating material between the cathode and anode structures is properly contoured so that part of the

surface is protected from sputtered aluminum, then the arcing problem does not occur.

The discharge chamber was not always operated as indicated in Figure 2.7. The diagrammed discharge chamber is the result of many modifications, and numerous subsequent changes were also made. For example, the discharge diameter was initially limited by pyrex rings instead of aluminum anode rings. This situation corresponds to the highly turbulent configuration of Figure 2.6a, at least until the insulating rings become coated with a conductive layer of sputtered aluminum.

Later modifications include removal of the periodic structure and replacement of the viton sheet with a 1/2" thick teflon O-ring gasket. The exposed surface of the gasket is shaped so as to minimize the sputtering problem. The teflon gasket reduces the capacitance between the cathode end plate and the anode flange so that voltage pulses with very fast rise times can be applied to the cathodes. These modifications are indicated in Figure 5.2.

In addition, the perforated cathode was modified to allow the neutral gas to flow around the cathode instead of through it. The modified cathode construction is also used in the pyrex discharge tube, Figure 2.8.

The brass discharge tube is operated in two ways. A continuous discharge can be maintained at low currents in the range of 100-600 ma. In order to achieve very high plasma densities, the discharge is pulsed at a repetition rate of 100 Hz with discharge currents as large as 75 amps. Pulse lengths range from several hundred microseconds to several

milliseconds.

The continuous discharge is powered by a voltage-regulated 1000V - 500 ma power supply. The anode of the discharge tube is at ground potential and the cathodes, which are connected together by a low inductance copper strap, are fed through a series resistor. The discharge operates best when the voltage drop across the series resistor is at least as large as the discharge voltage. When larger currents and voltages are needed, the regulation system of the power supply is bypassed. Currents up to 700 ma are then available at a variable voltage of 800-1600 V . In this situation an additional filter stage is added to the power supply to reduce 120 Hz ripple.

2.3.4 Use of Oxygen as the Neutral Gas

The problem of sputtered aluminum depositing as a conductive layer on insulator surfaces can easily be solved by using oxygen as the working gas. The deposited material then consists of nonconducting oxides of aluminum. To test this idea, the discharge was operated in oxygen. After about ten hours of operation, visual inspection of the inside of the chamber revealed no trace of sputtered aluminum metal. The discharge does indeed burn. Operation for a corresponding period of time in argon results in a thick peeling layer of aluminum on all exposed surfaces.

The behavior of the oxygen gas discharge differs considerably from that of the argon discharge used previously. The discharge always starts very readily, operates at a lower discharge voltage, and works over a much larger pressure range. The behavior is also much more reproducible. This change in the nature of the discharge is attributed

to cathode surface conditions.

The argon discharge did not operate below a minimum pressure of about 10^{-3}torr. If the pressure was suddenly lowered below the minimum value, the discharge would continue to function but the discharge voltage would rise slowly. The discharge eventually stops operating when the discharge voltage exceeds the power supply voltage. If the pressure is again raised, the discharge at first operates at a very high voltage with a small discharge current. The discharge voltage decreases slowly and finally returns to the original level after many minutes of operation.

This effect has been observed previously by Backus [44]. When he tested cathodes of various materials, he observed that only Be and Al exhibit a low discharge voltage of about 300 volts. Other cathode materials such as Mo, Cu, Zn, and Ni operate at voltages exceeding 2 kilovolts. The low operating voltage is attributed to a surface layer of oxide.

When the neutral gas pressure is lowered, the oxide is eventually sputtered off the cathode surface and the discharge voltage rises to roughly 3 kilovolts. When the neutral pressure is increased, the oxide layer returns very slowly because only minute quantities of oxygen are present.

However, if oxygen gas is supplied as the working medium oxygen ion bombardment of the aluminum cathodes regenerates the oxide layer as rapidly as it is sputtered away, even at very low pressures. The oxygen gas discharge operates well at pressures as low as 10^{-5}torr.

Although oxygen gas improves some of the operating characteristics of the discharge and eliminates the deposition of sputtered aluminum on insulator surfaces, it also creates several problems. After operating the discharge in oxygen for a long period of time, the anode becomes coated with a thick layer of nonconducting oxides of aluminum. This greatly inhibits the operation of the discharge.

Probe measurements are also complicated by this same condition. Not only does the probe become covered with a nonconducting layer, but in addition the surface layer supports strong secondary emission processes.

The cathodes of the discharge have a strong tendency to oscillate due to a negative resistance effect associated with secondary electron emission by electron bombardment. The coefficient of secondary emission by electron bombardment can be greater than unity, apparently because of the presence of the oxide layer. Whenever a potential difference exists between the cathodes, electron bombardment occurs at the most positive cathode. That cathode experiences a negative resistance if the coefficient of secondary emission is greater than unity. Electron bombardment of the cathodes also occurs under other circumstances which are discussed in Appendix B. Appendix B also describes a rough measurement of the coefficient of secondary emission by electron bombardment.

Despite some of the complications of the aluminum oxides, oxygen presents an added bonus which is difficult to overlook. The oxygen discharge produces much more microwave emission at the harmonics of the electron cyclotron frequency, and is therefore very attractive for this

investigation.

There is one additional change in the operating characteristics of the oxygen gas discharge which eventually led to a reduction of the plasma column diameter from 10.2 cm to 6.6 cm. It was observed that a larger discharge current is needed to obtain the same plasma density in the oxygen discharge that was previously obtained in the argon discharge.

Observe that the cathodes collect an ion saturation current at each end of the plasma column. Since the relationship between the ion saturation current and the plasma density depends on the square root of the ion mass, a 60% larger current is needed to obtain the same density in the oxygen discharge, assuming that the temperature does not change. This is approximately what is observed.

When the stabilizing grid was introduced, it was observed that even larger discharge currents were needed. This can be partially understood on the basis of changes in the radial density profile of the discharge column. The radial density profile for the stabilized discharge is relatively flat, whereas the profile for the non-stabilized discharge is peaked at the center of the column. In addition, the non-stabilized discharge exhibits large density fluctuations. As a result, the peak plasma density of the non-stabilized discharge is significantly larger than that of the grid-stabilized discharge, provided both are operated at the same discharge current.

In any case, the increased current requirements of the grid-stabilized oxygen gas discharge exceed the current capability of the available dc power supply. This problem was overcome by reducing the

diameter of the anode ring from 10.2 cm to 6.6 cm. This reduces the effective cathode area and therefore the cathode current at constant plasma density by a factor of 2.37. Such a reduction in the current requirement of a 6.6 cm diameter discharge column was verified experimentally.

Unfortunately, the reduction in the diameter of the plasma column was accompanied by 100-150 V increase in the operating voltage of the discharge. The voltage of the regulated power supply was then barely sufficient to operate the discharge satisfactorily. Therefore the power supply was operated unregulated with an additional filter stage.

2.3.5 Pyrex Discharge Tube

Because the plasma density is a very important parameter in the investigation of cyclotron harmonic emission, it is essential to have an accurate microwave interferometer density measurement. Sufficient Ku-band microwave hardware was available to construct a polar interferometer at 16.0 GHz. Unfortunately, the brass discharge chamber is not a very satisfactory environment in which to perform the measurement. The phase measurement is strongly affected by standing waves and by coupling to resonances of the discharge cavity. This problem can be partially resolved by lining the discharge cavity with a microwave absorber. However, it is difficult to construct an absorber which has minimal reflection and does not outgas when heated by the Penning discharge.

The plasma density measurement was finally carried out in a specially constructed discharge tube with a pyrex vacuum wall. Because

the wall of the pyrex tube is one-half wavelength in thickness at 16 GHz, reflection by the pyrex tube is minimized. Therefore construction of the discharge tube is simplified by locating the microwave interferometer horns outside the vacuum wall. Conventional microwave absorbing materials are then used to minimize microwave scattering by the surrounding environment, principally the magnetic field coils.

A scale drawing of the pyrex discharge tube is presented in Figure 2.8. The important dimensions are identical with the construction of the 6.6 cm diameter column in the brass discharge chamber. The cathode and anode diameters are 6.6 cm and the distance between the cathodes is 43 cm. The same grid structure is used to stabilize both discharge tubes. Actually, the only major change is that the pyrex tube has a 3.7" ID, whereas the brass chamber has a 6" ID. Only oxygen gas can be used in the pyrex discharge tube because of the sputtering problem. Deposition of sputtered aluminum metal on the pyrex tube would quickly result in severe reflection of the microwave interferometer signal.

Both ends of the discharge assembly are attached to sections of 3" OD pyrex conical pipe. Oxygen gas flows in one end of the device and out the other end to the diffusion pump. The gas flows around and behind the cathode and through holes in the brass end plate. A teflon O-ring gasket provides the necessary spacing between the cathode and the anode (4-5 mm). The grid support structure is an integral part of the anode. Parallel wire grids at opposite ends of the discharge tube are rotated 90^{o} with respect to each other in an effort to minimize the spatial density variation associated with the grids.

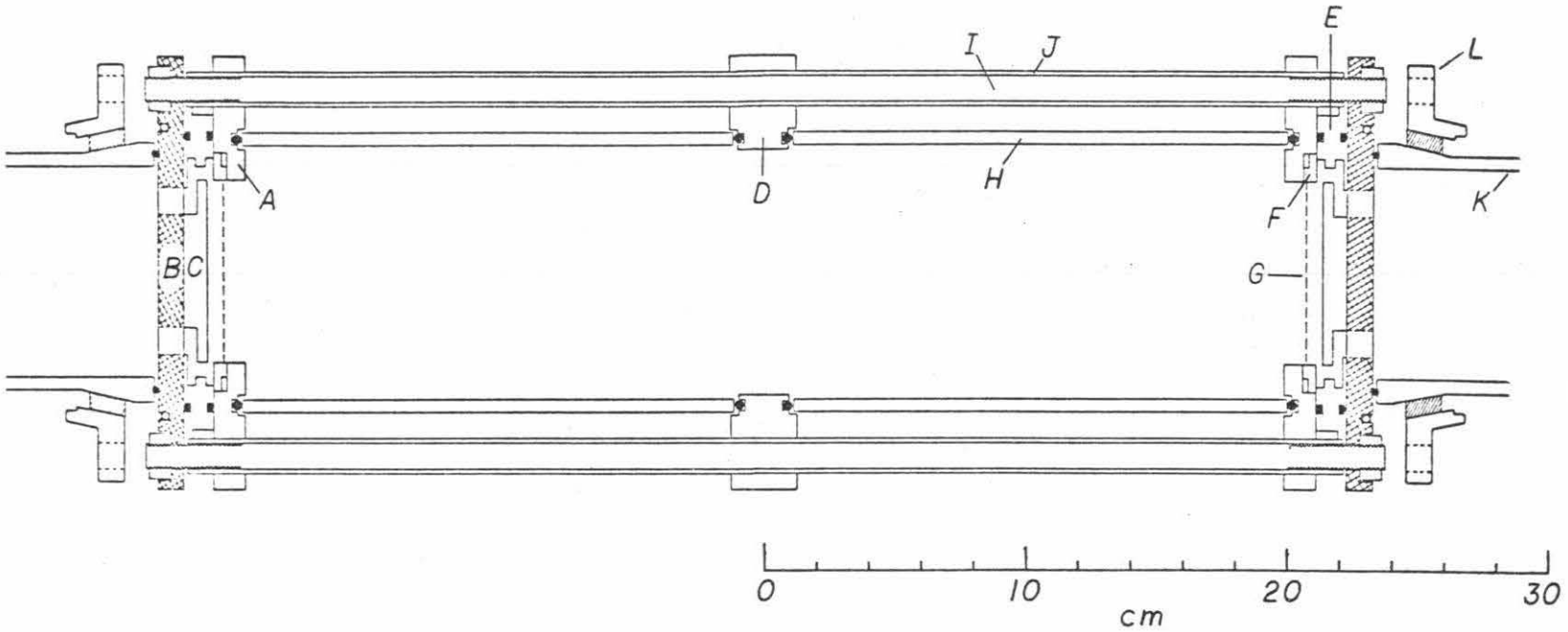

Figure 2.8 Scale Drawing of the Pyrex Discharge Tube

A - aluminum anode, B - brass endplate, C - aluminum cathode, D - aluminum ring insert, E - teflon O-ring gasket, F - grid support structure, G - tungsten parallel wire grid, H - pyrex tube (4" OD), I - brass rod, J - lucite tube, K - conical pyrex pipe (3" ID), L - standard flange for conical pipe, M - O-rings.

An aluminum ring at the midplane of the device provides access to the plasma. A probe assembly is mounted thereon to obtain radial profiles of the ion saturation current. In order to obtain an accurate indication of the neutral gas pressure inside the discharge tube, a thermocouple gauge tube is also attached at this location.

The entire assembly is held together by six threaded rods. Two brass rods, which also serve as a low inductance electrical connection between the cathodes, are shown in the scale drawing. These rods are insulated from the anodes by covering the rod with lucite tubing. In addition, there are four stainless steel rods (actually threaded stainless steel tubing) which are not shown because they are located at a different angular position than the cross section which is drawn (see Figure 2.5). They provide most of the tension which compresses the O-rings and in general keeps everything together, including the pyrex conical pipe at each end.

The stainless steel tubing is in direct contact with the anodes and the aluminum ring insert, but is electrically insulated from the cathodes. Cold water flows through the tubes; thus they provide cooling and also serve as an electrical interconnection for the anodes and the ring insert. Water cooling is also provided for the cathodes and forced air cooling is provided for the pyrex tube.

2.3.6 Grid Stabilization of the Plasma Column

Several grid configurations were tried and it was determined that they all worked equally well. One of the first configurations consisted of two orthogonal layers of parallel tungsten wires. The

7.5 mil wires were spaced at 0.200 inch intervals, giving a transparency of 92.5% for the two layers. The grid was attached at the midplane position of the brass discharge tube. The grid was found to be extremely effective in eliminating fluctuations in the cathode voltage, floating potential, and ion saturation current.

Probe measurements carried out on the turbulent plasma of the nonstabilized discharge display chaotic fluctuations of the ion saturation current and the floating probe potential. The ion current received by the probe is very spiky in appearance. The fluctuations are several times larger than the average value of the ion saturation current. Fluctuations in the floating potential of the probe frequently exceed 100 volts peak to peak.

In comparison, ion saturation current fluctuations for the grid-stabilized plasma are less than 1% and fluctuations in the floating potential are reduced by three orders of magnitude. Because the stabilizing grid can easily be installed or removed, it is relatively simple to determine what effects, if any, the plasma turbulence has on the experimental results.

When one layer of wires is removed from the grid, the effectiveness of the grid does not change. Thus, a parallel wire grid is equally as effective, but much more transparent. The grids which are used for the 2.6 inch diameter plasma column consist of .010 inch tungsten wires spaced at .100 inch intervals. Two such parallel wire grids are used, attached to the anode structures at each end of the discharge structure, as in Figure 2.8.

The grids have an important effect on the plasma density profile. Radial profiles of the ion saturation current indicate a periodic spatial variation in the plasma density. The periodicity corresponds to the spacing of the grid wires. The magnitude of the variation increases with magnetic field and decreases with neutral gas density. Hence, the grid wires cast shadows in the plasma along the magnetic field and the plasma is maintained in these shadow regions by diffusion from the surrounding plasma. The plasma generation rate in the shadow regions is greatly reduced because energetic electrons are collected by the grid.

The grids, as designed, have an additional defect. The grid support structure does not compensate for expansion of the tungsten wires upon heating by the plasma. As a result, the wires warp and the spacing of the grid wires becomes nonuniform. This results in a larger scale density variation which changes with the plasma density.

The severe heating of the grids by the high density plasma presents yet another problem. The hot tungsten wires oxidize excessively. As the oxide layer grows, the transparency of the grids decreases and the discharge voltage becomes excessive.

2.3.7 Typical Voltages and Radial Profiles

The description of the plasma will be concluded with a synopsis of the operating characteristics of the discharge. Each of the many variations of the Penning discharge exhibit somewhat different macroscopic parameters. However, the differences are mainly quantitative, such as a change in the operating voltage. The most important

qualitative changes are associated with the presence of the stabilizing grid.

The probe used to obtain radial profiles of the floating potential and ion saturation current and fluctuations in these parameters consists of a .030" diameter platinum wire sheathed by a thin glass tube. The probe is directly attached to a linear potentiometer. Ion saturation current profiles were plotted on the X-Y recorder by using the linear potentiometer to drive the X axis and the ion current to drive the Y axis. Profiles of the floating potential were obtained in a similar fashion.

Figure 2.9 displays the I-V characteristics of the 2.6" diameter column for several values of the oxygen gas pressure. Note the changes in both the cathode voltage, V_c , and the floating potential, V_f , when the stabilizing grid is present. The I-V characteristic of the discharge changes somewhat with magnetic field but remains qualitatively the same. The cathode voltage of the 4.0" column, if shown, would be considerably smaller than that of the 2.6" discharge column. Also, when argon is used as the working gas, the magnitudes of V_c and V_f change noticeably. The qualitative behavior, however, is similar.

Because the harmonic emission spectrum is obtained at a fixed microwave receiver frequency by sweeping the magnetic field, it is of interest to know how the discharge characteristics change with the field. This is indicated in Figure 2.10. The cathode and floating potentials are indicated for several values of the oxygen gas pressure and the same parameters are noted for the grid stabilized discharge. Again, these curves describe the 2.6" diameter column. Because the

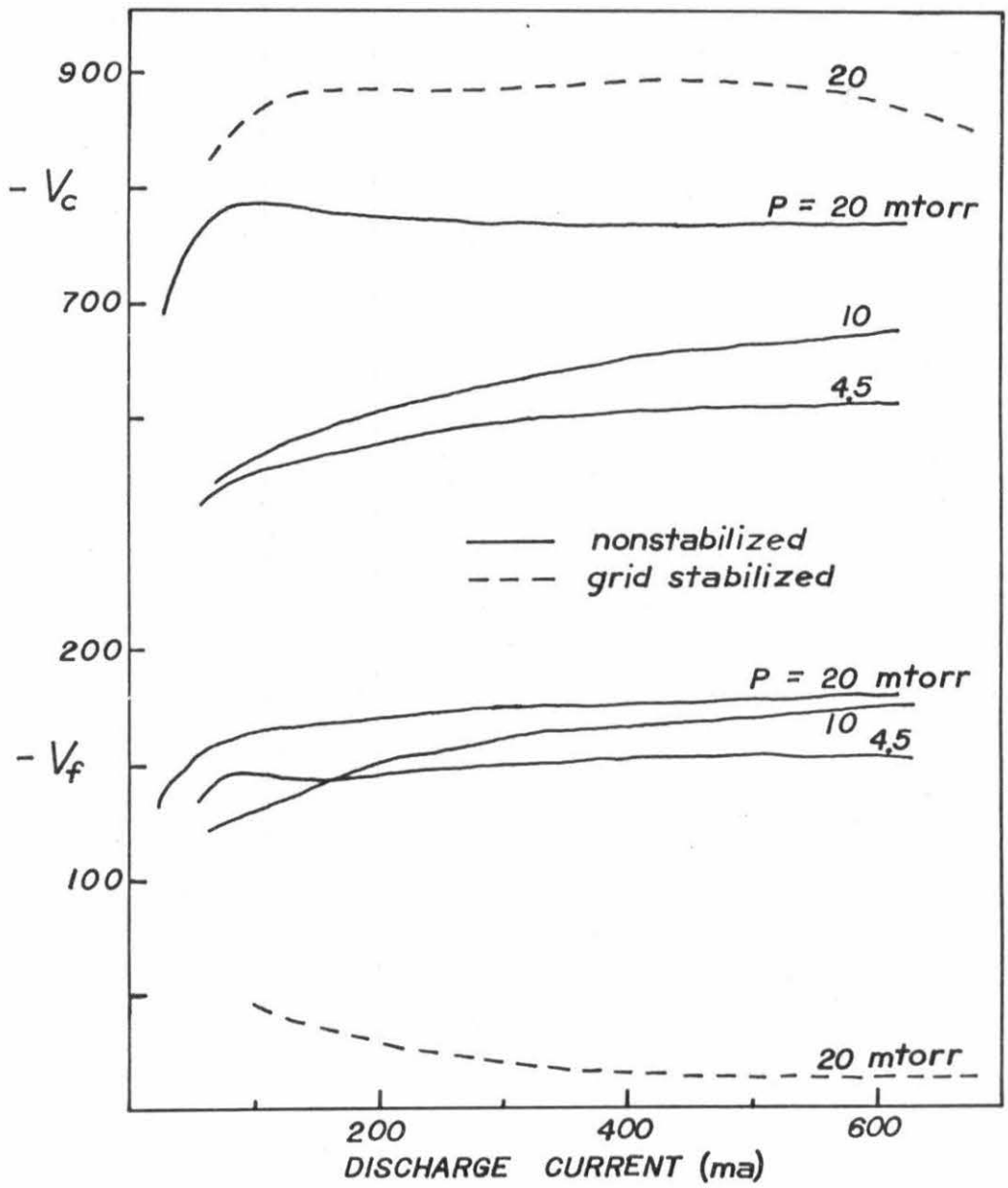

Figure 2.9 Variation of the Cathode Voltage V_c and the Floating Probe Potential V_f with the Discharge Current of the Oxygen Gas Penning Discharge (B = 1.0 Kilogauss).

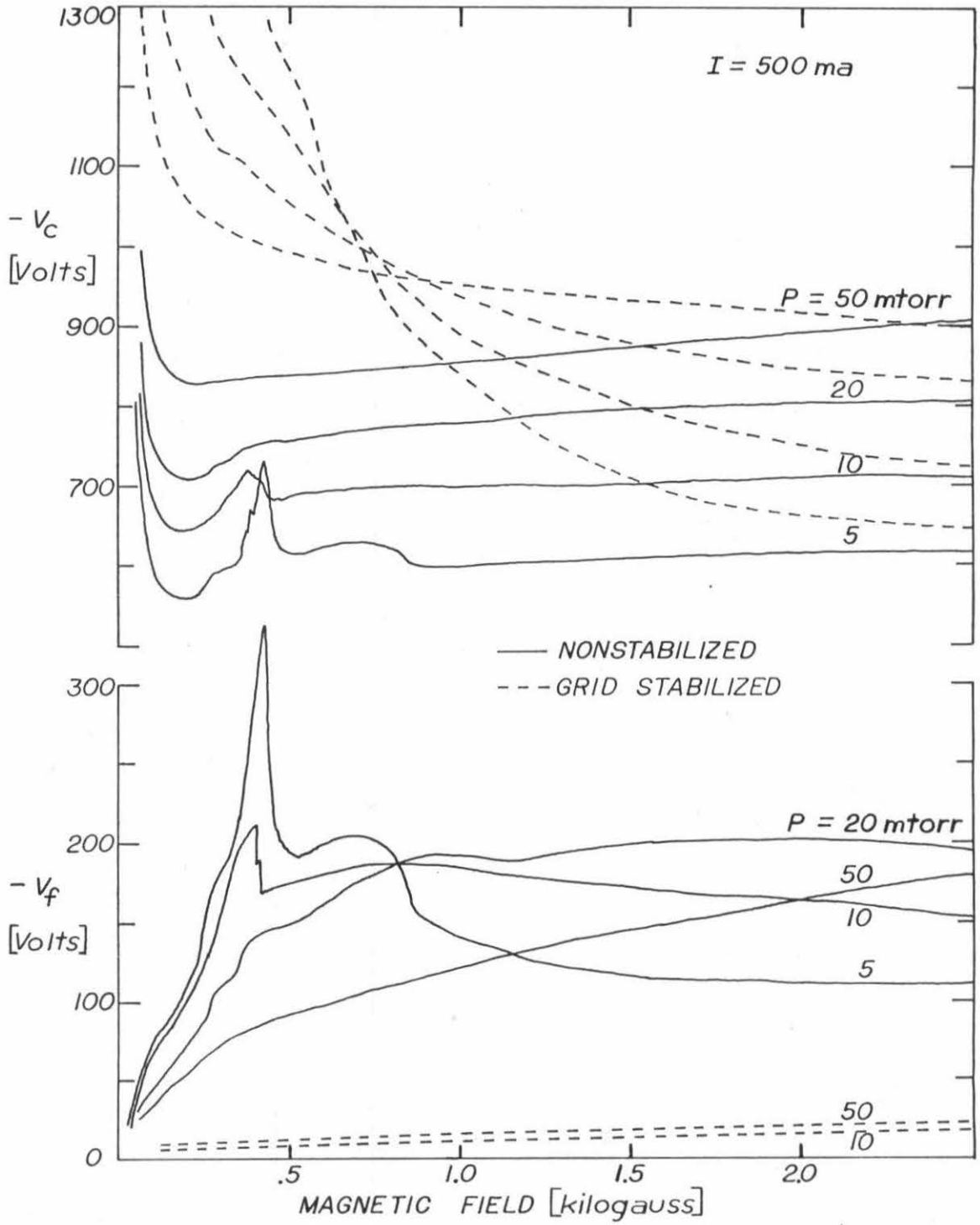

Figure 2.10 Variation of the Cathode Voltage V_c and the Floating Probe Potential V_f with the Magnetic Field of the Oxygen Gas Penning Discharge (I = 500 ma).

parameters of the non-stabilized discharge exhibit large amplitude fluctuations, the corresponding curves indicate time averaged values.

Again, the first thing to be noted from these curves is the effect of the stabilizing grid on the cathode and floating potentials. The floating potential is greatly reduced by the presence of the grid. The cathode voltage increases markedly at low magnetic fields, especially when the neutral gas pressure is low. This latter effect results from the fact that the grids intercept some of the energetic electrons which sustain the discharge. Balance between the plasma generation and loss rates then takes place at a larger voltage. At higher pressures a smaller fraction of the energetic electrons are lost because they pass through the grids fewer times. At high magnetic fields the grid produces only a small change in the cathode voltage.

Note the behavior of V_c and V_f in the nonstabilized discharge when the neutral gas pressure is low. When the magnetic field is about 0.5 Kgauss, these parameters change rapidly. This behavior coincides with the onset of gross instability on the plasma column. Naturally, this effect does not appear in the grid-stabilized discharge.

Finally, radial profiles of the nonstabilized and grid stabilized plasma columns are presented in Figures 2.11a and 2.11b, respectively. These profiles of the floating potential and ion saturation current were obtained from the 2.6" diameter column of the pyrex discharge tube. The ion saturation current profiles are found to depend strongly on the magnetic field when the field is less than

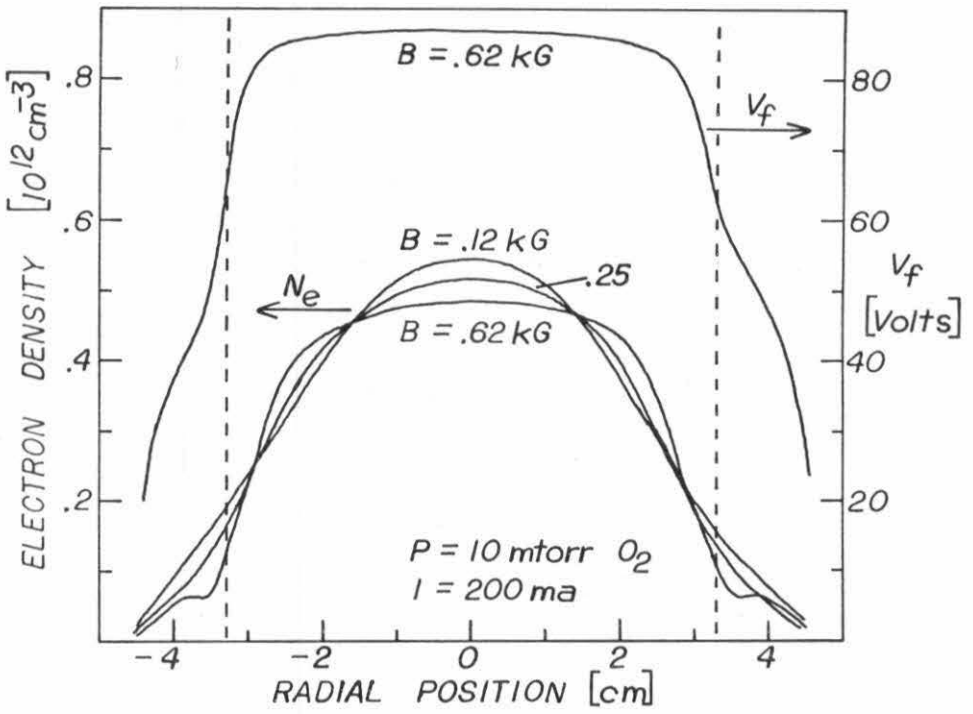

Figure 2.11a Radial Profiles of the Density and Floating Potential of the Nonstabilized Plasma Column

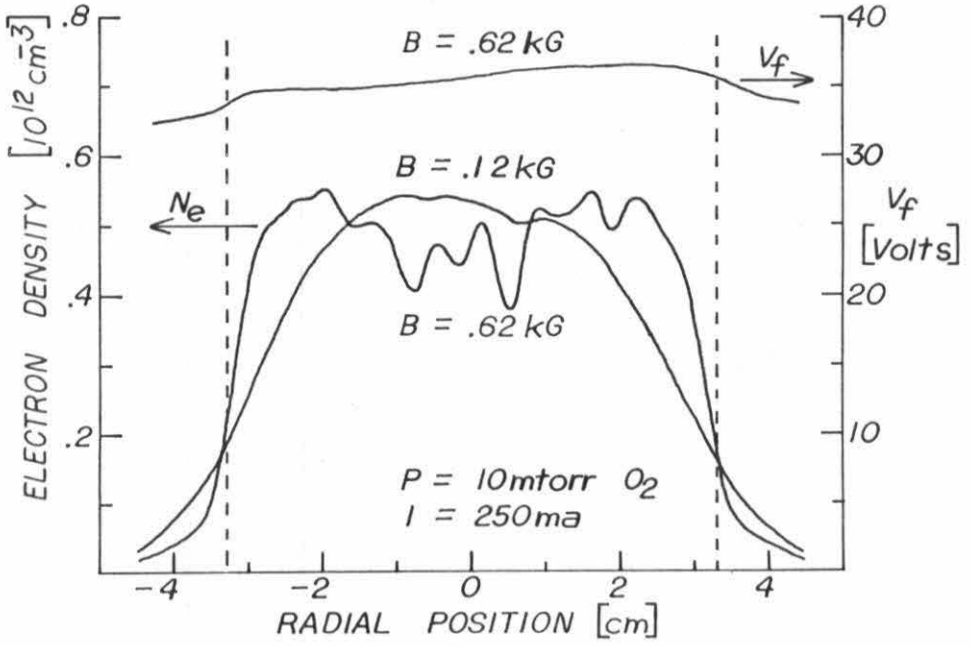

Figure 2.11b Radial Profiles of the Density and Floating Potential of the Grid-Stabilized Plasma Column

1 kilogauss. The corresponding changes in the potential profile are not as great. The effect of the grid on the magnitude of the radial electric field is particularly noticeable. Also displayed are the spatial density variations associated with the stabilizing grid. Again, the profiles obtained from the nonstabilized discharge represent the time averaged values over large amplitude fluctuations.

Microwave interferometer density measurements of the 2.6" plasma column indicate that when the magnetic field is swept and the discharge is operated at constant current, the average plasma density remains nearly constant. The density decreases noticeably only when the field drops below 0.2 kilogauss. However, as noted above, the density profile does change significantly.

2.4 Analysis of Energetic Electrons

As already indicated, the Penning discharge is sustained by the presence of a significant number of high energy electrons ($E > 15$ eV). Since these electrons appear to be the source of nonthermal harmonic emission, it is of interest to know such parameters as the generation rate, number density, and energy distribution of these electrons. For the neutral gas pressure range used in the experiments, the energy loss of the energetic electrons is dominated by inelastic electron-neutral collisions. Therefore, an indication of the energy distribution of electrons with energies greater than 20 eV can be obtained from the probabilities of ionization and excitation.

As noted earlier, the high energy electrons in the Penning discharge are produced as a result of ion bombardment of the cold aluminum

cathodes. The ions strike the surface with an energy equal to the difference between the plasma potential and the cathode potential, typically 400-800 eV. Secondary electrons result by either kinetic or potential ejection. For a clean metal surface and ions of these energies, the only important process is Auger excitation of conduction band electrons [45]. If J_i is the incident ion saturation current, then the secondary electron emission current, J_e, is given by

$$J_e = \gamma_i J_i \tag{1}$$

where γ_i is the coefficient of secondary emission by ion bombardment. The presence of an oxide layer on the cathode surface has been discussed in Section 2.3.4, and a measurement of γ_i for the oxide covered cathodes is described in Appendix A.

The secondary electrons are accelerated into the plasma column by the cathode sheath, acquiring an energy, E_o, corresponding to the difference between the cathode potential and the plasma potential. The secondary electrons have nearly identical energies and constitute a diffuse, low temperature electron beam. At every point on the radial profile of the plasma column, the electron beam density is a constant fraction of the plasma density. That fraction is determined mainly by the value of γ_i. The electron beam density, n_b, is given by

$$n_b(r) = \frac{\gamma_i J_i(r)}{e v_b}$$

where v_b is the injection velocity of the beam ($= \sqrt{2E_o/m}$), and $J_i(r)$ is the ion saturation current profile.

The total discharge current is equal to the surface integral of the total current density, $J_i + J_e$, at each cathode,

$$I = 2 \int_0^R (J_i + J_e)\, r\,dr\,d\theta$$

$$= 4\pi(1 + \gamma_i) \int_0^R J_i(r)\, r\,dr$$

Therefore the spatially averaged ion saturation current, secondary electron current, and electron beam densities are given by the following equations:

$$J_{io} = \frac{I}{(1 + \gamma_i)2\pi R^2} \tag{2}$$

$$J_{eo} = \frac{\gamma_i}{1 + \gamma_i} \frac{I}{2\pi R^2} \tag{3}$$

$$n_{bo} = \frac{J_{eo}}{e\, v_b} \tag{4}$$

The equivalent generation rate, G, of fast electrons per unit volume of the discharge is given by

$$G = \frac{2J_{eo}}{e\, L} \tag{5}$$

where L is the length of the plasma column.

For the oxygen gas pressures used in the experiment, nearly all of the secondary electrons are repeatedly reflected by the cathodes until most of their energy has been expended by inelastic ionization and excitation collisions. The electrons retain some energy because the cross sections for the inelastic processes vanish at energies below 10-15 eV.

The energy loss rate for the energetic electrons can be expressed in the form

$$\frac{dE}{dt} = -\nu_i \langle \Delta E \rangle \tag{6}$$

where ν_i is the ionization collision frequency and $\langle \Delta E \rangle$ is the average energy loss per ionization time. Energy loss by excitation collisions can thereby be included by assuming that the probability of excitation has the same energy dependence as the probability of ionization. From Brown [46], the ionization collision frequency ν_i is given by

$$\nu_i = \frac{273^o}{T} \; p(mm) \; P_i \; v_E \tag{7}$$

where T is the temperature of the neutral gas, p is the neutral gas pressure in millimeters of Hg, P_i is the probability of ionization, and v_E is the electron velocity (cm/sec). If $T = 300^oK$, then equations (6) and (7) give

$$\frac{dE}{dt} \left(\frac{eV}{sec}\right) = -1.62 \times 10^9 \sqrt{E(eV)} \; p(mm) \; P_i(E) \tag{8}$$

where $E = \frac{1}{2} m v_E^2$.

Figure 2.12 displays the energy dependence of P_i for O_2 gas [47], and also the energy loss rate, dE/dt, for several values of the oxygen gas pressure. Also indicated for comparison is the energy loss rate to the thermal plasma electrons via Coulomb collisions.

As the beam electrons move through the plasma, they give up energy and acquire an energy spread. For high neutral gas pressures,

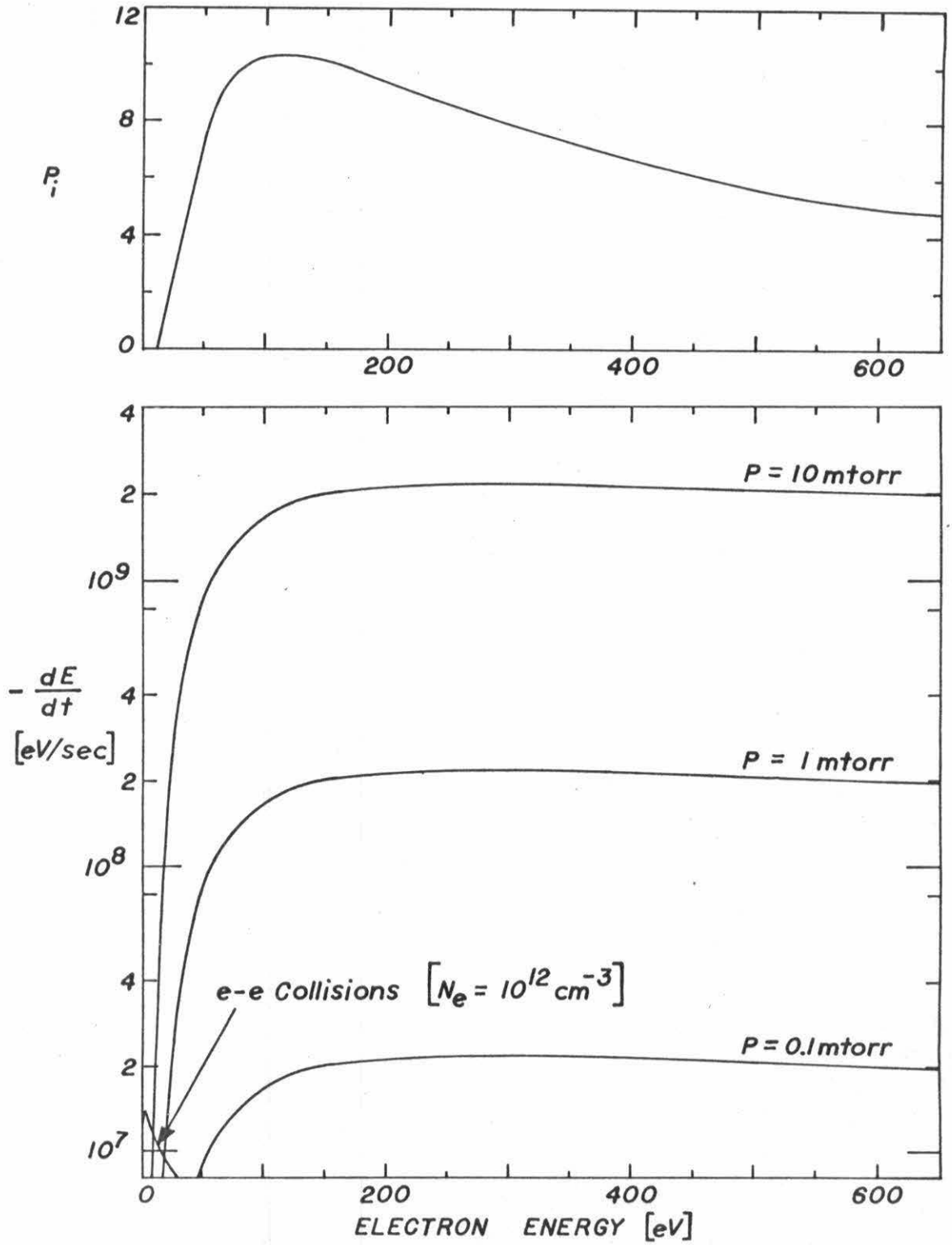

Figure 2.12 The Probability of Ionization P_i and the Computed Inelastic Energy Loss Rate dE/dt for Electrons in Oxygen Gas.

the energy distribution function of the beam changes rapidly as a function of distance from the cathode. Moreover, there is very little overlap of the beams injected on successive transits of the discharge.

At lower pressures such that the ionization length is much longer than the discharge dimension, electrons emitted on successive transits of the discharge have nearly the same energy. In this case, the energy distribution function is nearly independent of position and there is no well defined beam of electrons. Rather, there is almost a continuum of high energy electrons.

The neutral gas pressures used in the experiment lie between the extremes indicated above. There is a well defined electron beam in the vicinity of the cathode but after several inelastic collisions, the energetic electrons form a continuum.

A good estimate of the energy distribution function, $f(E)$, for the continuum of energetic electrons can be obtained from the energy dependence of the inelastic loss rate. In energy space, there is a source of electrons at E_o, the energy at which beam electrons are injected into both ends of the discharge. If the only electron sink is located at $E < 20$ eV, then the continuity equation in energy space,

$$\frac{df}{dt} + \frac{d(f \frac{dE}{dt})}{dE} = 0 \qquad (9)$$

is valid for $20 \text{ eV} < E < E_o$.

For steady state operation of the discharge ($df/dt = 0$), the flux of electrons in energy space is independent of E and is given

by

$$f(E)\,\frac{dE}{dt} = G \tag{10}$$

The energy distribution of the energetic electrons is then given by

$$f(E) = \frac{G}{dE/dt} \tag{11}$$

where dE/dt is given by equation (8) and G is given by equation (5). Thus, the full expression for $f(E)$ is

$$f(E) = \frac{\gamma_i}{1+\gamma_i}\,\frac{T}{273^o}\,\frac{I}{e\pi R^2 LP_i\; p(mm)\langle\Delta E\rangle v_E} \tag{12}$$

The speed distribution, $g(u)$, of the energetic electrons can be obtained from the relationship

$$g(u) = f(E)\,\frac{dE}{du} \tag{13}$$

The expression for $g(u)$ is then

$$g(u) = \frac{\gamma_i}{1+\gamma_i}\,\frac{T}{273^o}\,\frac{m}{e}\,\frac{I}{\pi R^2 LP_i\; p(mm)\langle\Delta E\rangle} \tag{14}$$

Substitution of appropriate parameters into the above equations yields a quantitative picture of the high energy electrons. Table 2.1 presents a summary of the results obtained on substitution of the listed parameters into the indicated equations. For simplicity, the computations are based on a plasma density of $10^{12}/cm^3$. See Appendix A for a measurement of γ_i .

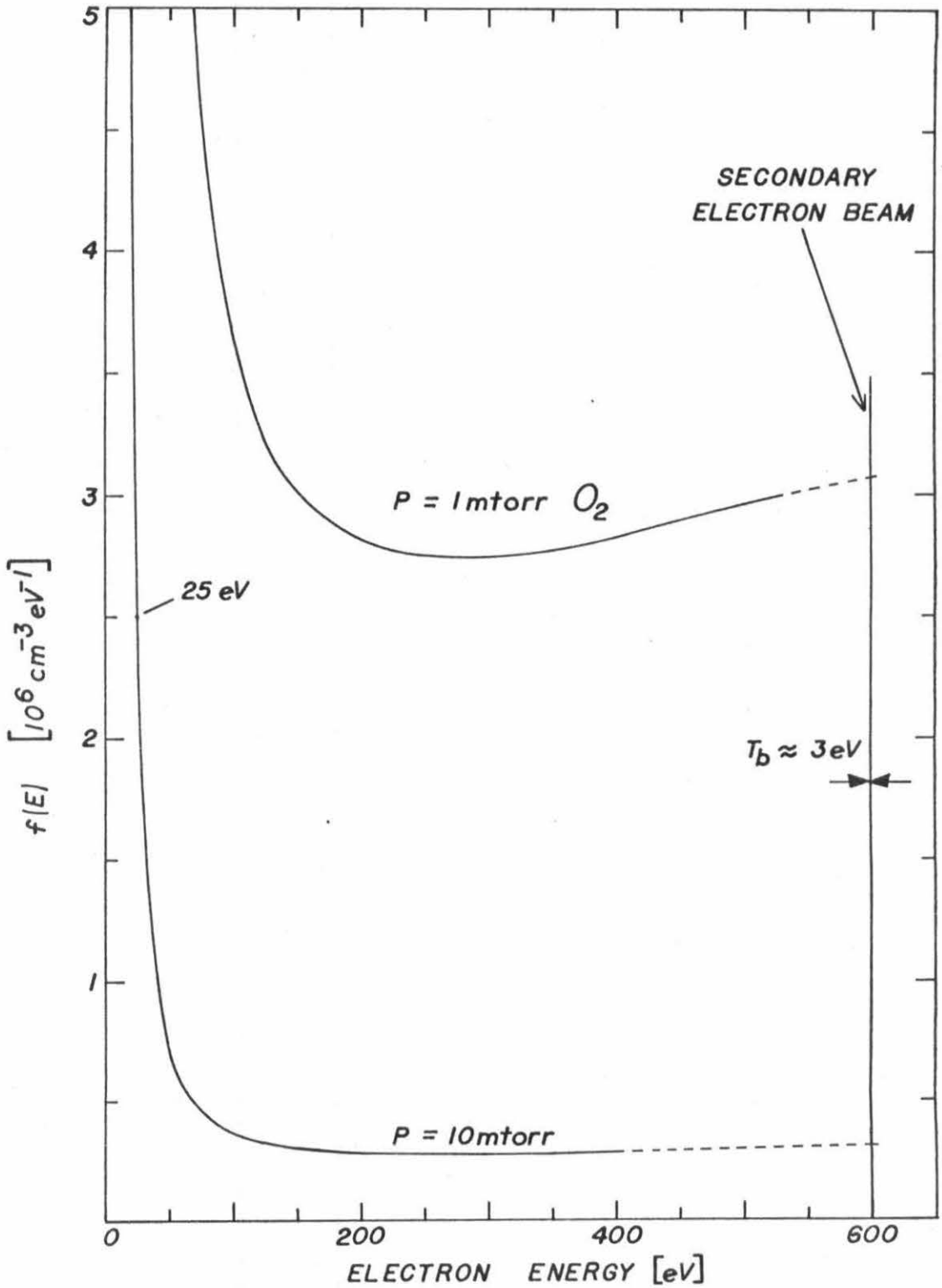

Figure 2.13 The Computed Energy Distribution Function f(E) of the Fast Electrons (E > 20 eV) in the Oxygen Gas Penning Discharge

TABLE 2.1

Parameters	Equation	Results
$n_e = 10^{12}/cm^3$	(2)	$J_{io} \simeq 5.2$ ma/cm^2
$I = 500$ ma	(3)	$J_{eo} \simeq 2.1$ ma/cm^2
$R = 3.3$ cm	(4)	$n_{bo} \simeq 1.0 \times 10^7 cm^{-3}$
$L = 43$ cm	(5)	$G \simeq 6.0 \times 10^{14} cm^{-3} sec^{-1}$
$\gamma_i = 0.4$	(8)	$\frac{dE}{dt} \simeq -1.62 \times 10^7 \sqrt{E}\, P_i(E) eV\ sec^{-1}$
$v_b(600eV) = 1.45 \times 10^9 cm/sec$	(12)	$f(E) \simeq \frac{3.75 \times 10^7}{\sqrt{E(eV)}\, P_i(E)}\ cm^{-3} eV^{-1}$
$\langle \Delta E \rangle = 30$ eV		
$p = 10$ mtorr O_2	(14)	$g(u) \simeq \frac{1.26}{P_i(u)}\ cm^{-4} sec$

The results of the computations are illuminating. The electron beam is indeed diffuse, having a density which is five orders of magnitude less than the plasma density. The energy distribution, $f(E)$, is graphed in Figure 2.13 for several values of the oxygen gas pressure. Also indicated is the energy distribution of the secondary electron beam, $f_b(E)$. Close to the cathode, $f_b(E) = n_b/T_b$, where T_b is the energy spread (or temperature) of the beam. The dashed line indicates a transition region wherein $f(E)$ may have some structure as the electron beams injected on successive transits of the discharge acquire energy spread and blend together to form a continuum of energetic electrons. There are very few electrons such that $E > E_o$, where E_o is the beam energy, simply because electrons for which $E_{||} > E_o$ are not reflected by the cathodes.

The total number of energetic electrons ($E > 25$ eV) can be estimated by integrating $f(E)$. The resulting quantity varies inversely

with the neutral gas pressure. When the oxygen gas pressure is 10 mtorr,

$$\int_{25}^{600} f(E)\, dE \simeq 2 \times 10^{8} cm^{-3}$$

Thus, the energetic electrons comprise only a small fraction of the total number of plasma electrons (.02% at 10 mtorr).

It is also of interest to compute the time dependence of the energy of the fast electrons. Since we already know the energy loss rate as a function of energy, $dE/dt = H(E)$, a relationship between time and energy is given by the expression

$$\tau(E) = \int_{E_o}^{E} \frac{dE'}{H(E')} \qquad (15)$$

Here, E_o is the initial energy of the fast electron and $H(E') = dE/dt$ is given by equation (8) and Figure 2.12. Numerical evaluation of the integral gives τ as a function of the electron energy E. The results of such a computation are presented in Figure 2.14, except that E is plotted as a function of τ to give $E(\tau)$. The insert shows the low energy region of the curve in greater detail. Note that the faster electrons ($E > 100$ eV) lose energy very rapidly, but that the rate of energy loss decreases markedly at low energy as expected.

Although the curve presented in Figure 2.14 corresponds to an oxygen gas pressure of 10 mtorr, the result is directly proportional to the inverse of the pressure.

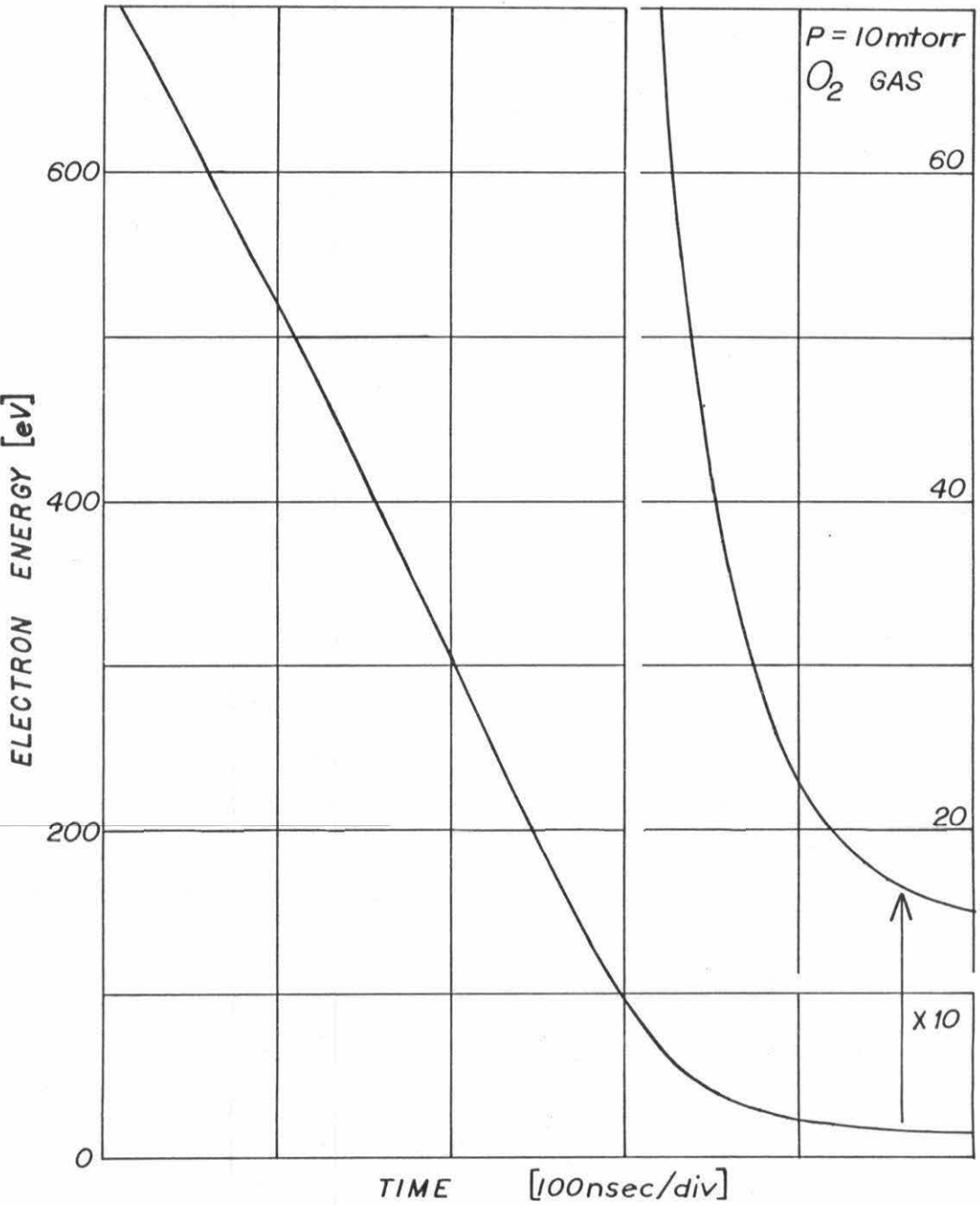

Figure 2.14 The Time Dependence of the Energy of a Fast Electron as Determined by the Computed Inelastic Energy Loss Rate

CHAPTER III

EXPERIMENTAL INVESTIGATION OF HARMONIC EMISSION

3.1 Introduction

This chapter presents the results of a systematic experimental investigation of microwave emission at the harmonics of the electron cyclotron frequency. The usual features of the harmonic emission spectrum are explored, with several notable exceptions. The Penning discharge is operated in both oxygen and argon. Harmonic emission is investigated in a grid-stabilized discharge in which low frequency instabilities and turbulence have been suppressed to produce a quiet plasma. Harmonic emission is also observed from a pyrex discharge tube as well as from a more conventional metal discharge chamber.

In Section 3.2 the basic features of the harmonic emission spectrum are presented. The dependences of the harmonic emission on the discharge current (plasma density) and the neutral gas pressure are indicated. Subsequently, three features of the harmonic emission spectrum are investigated in greater detail. The shape of the harmonic emission lines is examined in Section 3.3 and the emission line locations relative to the harmonics of the electron cyclotron frequency are measured in Section 3.4. The polarization of the emission is explored in Section 3.5.

In the remaining sections other specific aspects of harmonic emission are taken up. When the dimensions of the plasma column are altered or a stabilizing grid is inserted across the plasma column, the harmonic emission spectrum is affected. Therefore, the effects

of alterations to the plasma column and the surrounding environment are described in Section 3.6. In order to assess the importance of the receiver frequency, the harmonic emission is observed simultaneously at both 10 GHz and 50 GHz. This measurement is described in Section 3.7. The low power level absorption spectrum is investigated in Section 3.8 and compared with the emission spectrum. The plasma density dependence of the harmonic emission is examined in Section 3.9 with the aid of a microwave interferometer and the significance of the existence of a hybrid layer is discussed. Later, in Chapter IV, the experimental results presented in this chapter are compared with many of the possible theoretical models.

It should be kept in mind that one purpose of this chapter is to establish a basis for a general qualitative test whereby the relative merits of the various proposed or suggested theoretical models can be evaluated. Therefore much of the chapter is devoted to establishing a list of several of the basic features of the harmonic emission spectrum as observed in the Penning discharge. Because many of the harmonic emission theories involve extensive approximations, it is important that those features be very basic in nature and least sensitive to such approximations. For the same reason the comparison will, for the most part, be qualitative.

The following items have been chosen for comparison with the predictions of the various theories:

1. The location and symmetry of the harmonic emission lines. It is found that the harmonic emission lines, which are nearly symmetrical in shape, are located at the harmonics of the electron cyclotron frequency.

2. The role of low frequency instabilities and turbulence. It is found that the harmonic emission is not significantly affected by the radial electric field, the low frequency drift instabilities, or the plasma turbulence which are so characteristic of the nonstabilized Penning discharge.

3. The absolute value of the emission intensity. The power received by the microwave horn, which is only a small fraction of the total power radiated by the plasma column of the pyrex discharge tube, is approximately 1.6×10^{-18} watts/Hz ($T_R \simeq 10$ eV).

4. The relationship between the absorption spectrum and the emission spectrum. In the vicinity of the higher harmonics, there is no apparent relationship between the absorption spectrum of the plasma column and the emission spectrum.

5. The significance of the upper hybrid frequency. It is found that the existence of an upper hybrid layer on the plasma column is a necessary condition for the observation of harmonic emission. As the plasma density is increased, there is a sharp onset of harmonic emission when the hybrid layer condition is satisfied.

Although the process of establishing these features of the harmonic emission is an important part of this chapter, it is not the only function. The main purpose of this chapter is to present as much experimental information as possible. Included are additional features of the harmonic emission spectrum which could have been added to the above list but have not been for several reasons. Many features of the emission spectrum tend to be excessively quantitative or are features which are not dealt with by most of the theoretical models. Also, comparison with theory is simplified by keeping the list as short as is feasible.

3.2 The Harmonic Emission Spectrum

3.2.1 Harmonic Emission in Argon and Oxygen

A principal feature of the harmonic emission spectrum is the dependence of the emission intensity on the discharge current. This feature is displayed in Figures 3.1 and 3.3. These emission spectra were obtained using the microwave receiver diagrammed in Figure 2.1. The harmonic spectrum is recorded at a fixed receiver frequency by sweeping the magnetic field. The equivalent radiation temperature, T_R , of the plasma emission is calibrated in eV units using the standard noise source.

Figure 3.1 shows how the higher harmonics in the emission spectrum appear in the oxygen discharge as the discharge current is increased. When the discharge current is very low, the equivalent radiation temperature of the emission is also very low, only several hundred degrees Kelvin above room temperature. When the discharge current reaches a specific value, depending on the magnetic field strength, there is a sudden onset of the plasma emission.

For larger discharge currents, the harmonic emission spectrum is nearly independent of the discharge current. The bottom graph of Figure 3.1 shows the harmonic emission spectrum corresponding to this situation. An expansion of the same spectrum, which shows the higher harmonics more clearly, is presented in Figure 3.2. The emission intensity between the harmonics is typically 1 eV, whereas the emission intensity at the harmonics often reaches 45 eV. The sequence of spectra displayed in Figures 3.1 and 3.2 was obtained from the 2.6"

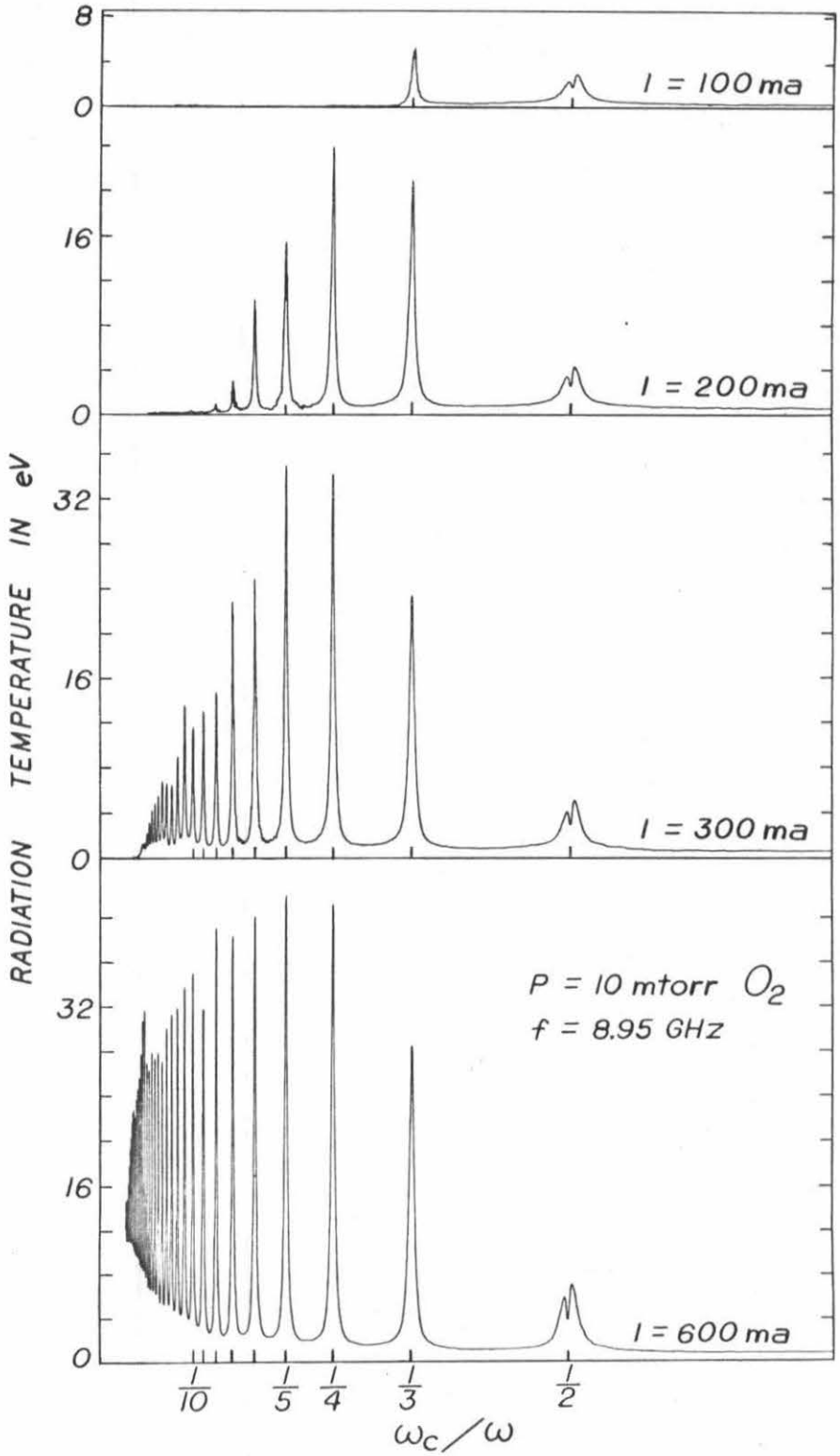

Figure 3.1 Radiation Temperature in eV as a Function of ω_c/ω for Several Values of Discharge Current when Using Oxygen Gas

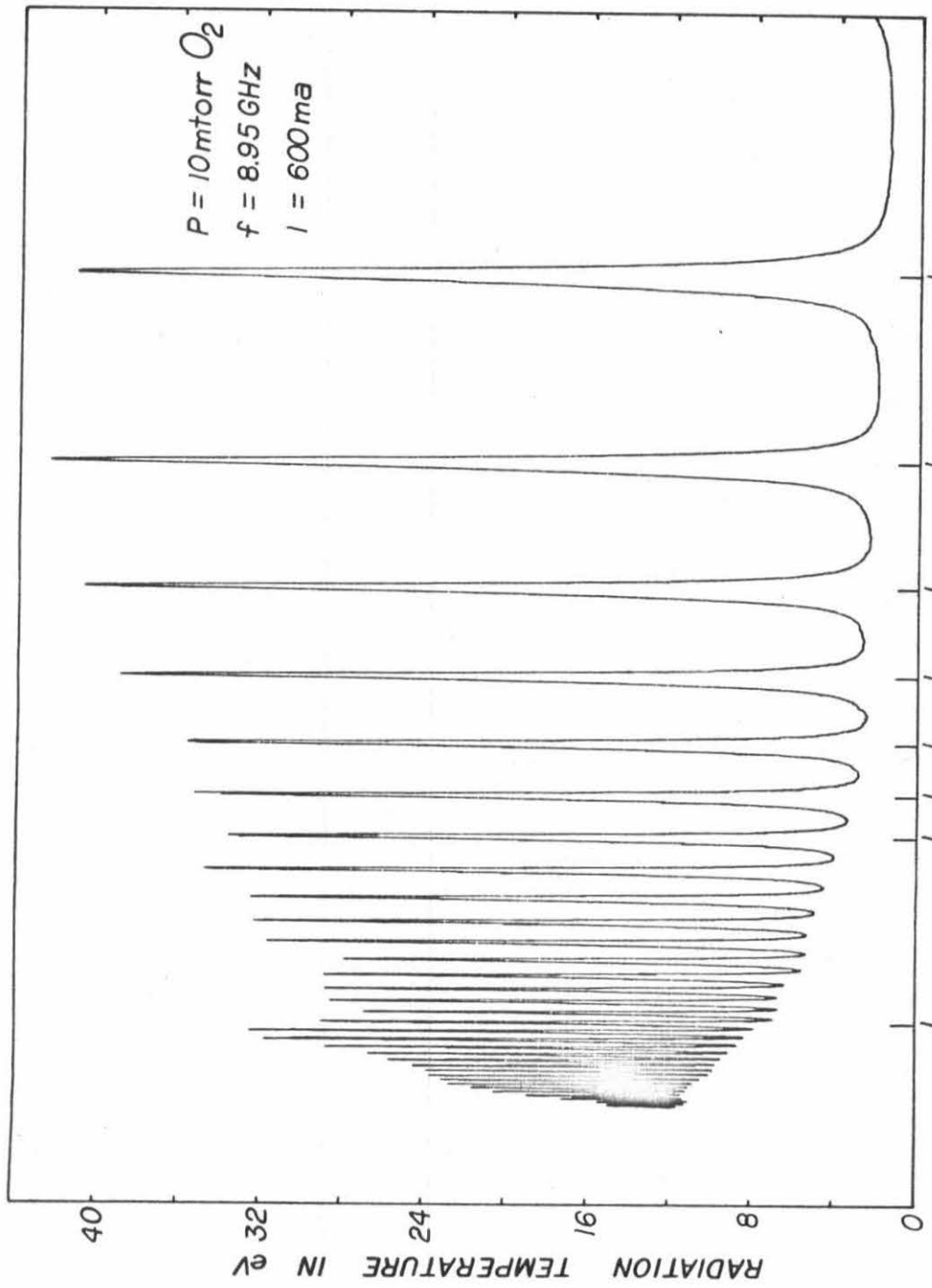

Figure 3.2 Radiation Temperature in eV as a Function of ω_c/ω Showing the Higher Harmonics of the Oxygen Gas Emission Spectrum in Greater Detail

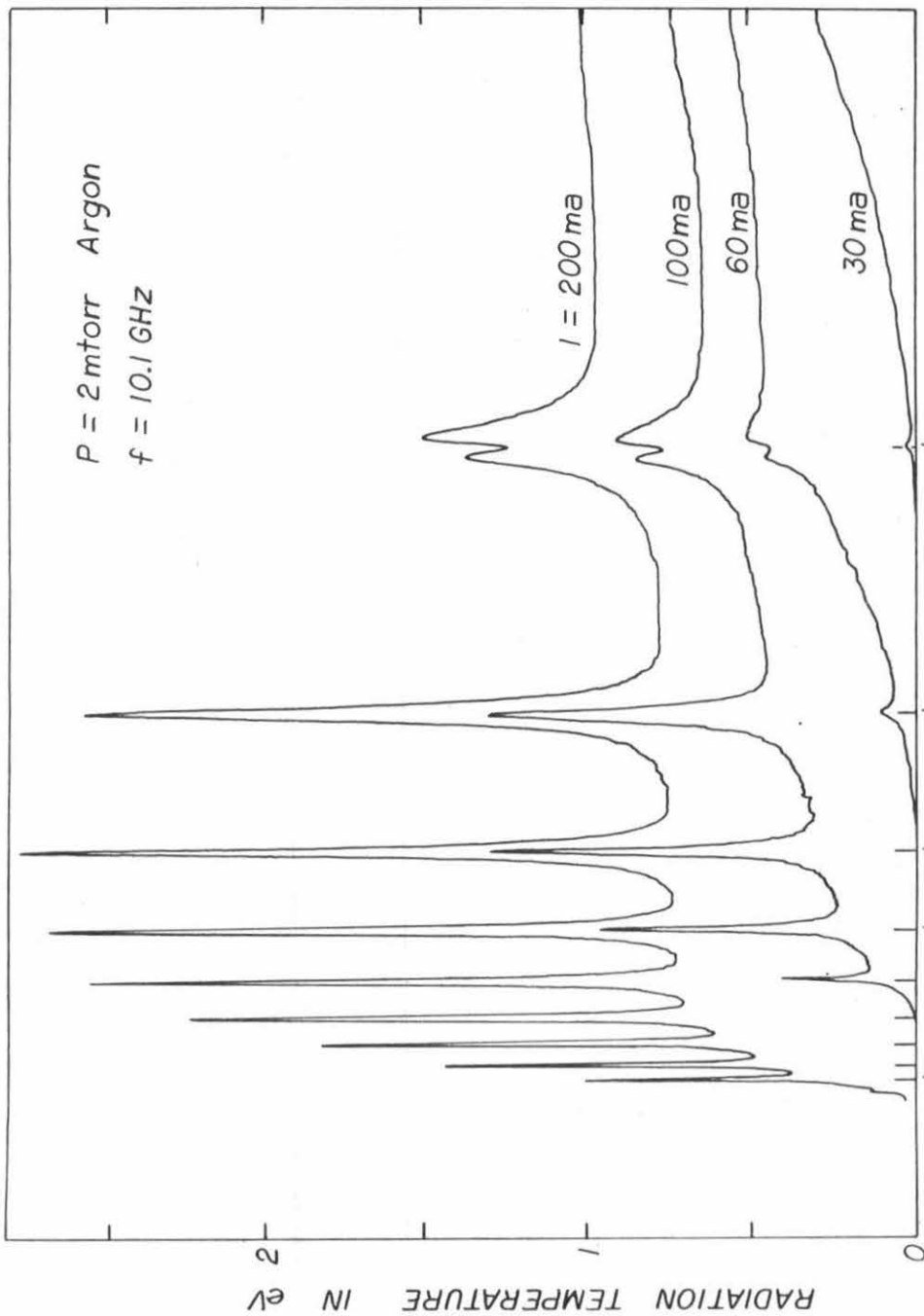

Figure 3.3 Radiation Temperature in eV as a Function of ω_c/ω for Several Values of the Discharge Current when Using Argon Gas

diameter nonstabilized plasma column of the modified discharge chamber sketched in Figure 5.2.

Similar behavior is also observed in the argon gas discharge. Figure 3.3 shows how the emission spectrum of the 4" diameter argon gas discharge evolves as the discharge current is increased. The intensity of the harmonic emission lines is not as great but the intensity between the harmonics is approximately the same as for the oxygen discharge. Note that harmonic emission is observed at a lower discharge current in the argon discharge in spite of the fact that the cathode diameter is significantly larger.

The argon plasma column was produced using the discharge chamber of Figure 2.7. Although this discharge chamber was used exclusively in the initial stages of the investigation, much of the data presented in this report were obtained using the 2.6" diameter plasma column of the nonstabilized discharge tube shown in Figure 5.2 .

3.2.2 Effect of Neutral Gas Pressure

When the neutral gas pressure is varied, the principal effect on the emission spectrum is a change in the emission intensity. Figure 3.4a shows how the amplitudes of several harmonics of the 2.6" diameter nonstabilized oxygen discharge depend on the neutral gas pressure. Figure 3.4b compares the harmonic emission intensities observed when using argon and oxygen in the 4" diameter brass discharge chamber. The indicated difference in emission intensities is noteworthy.

Dreicer observed that at low helium gas pressure, the higher harmonics disappear from the emission spectra [15]. Essentially the same behavior is observed in the present investigation. It is found

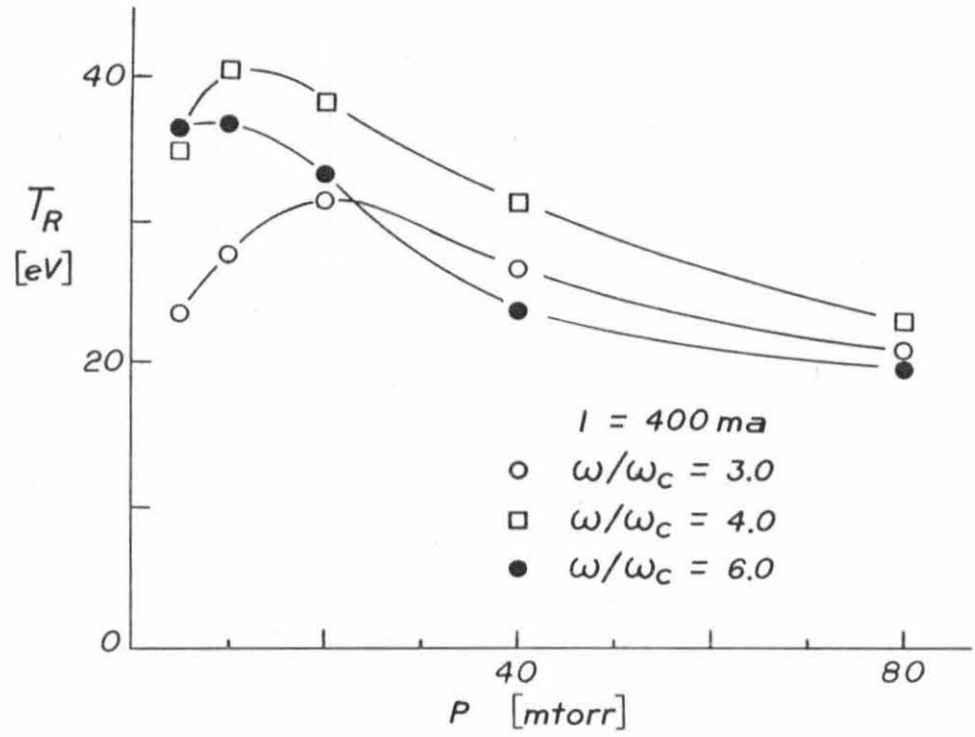

Figure 3.4a Radiation Temperature in eV as a Function of the Oxygen Gas Pressure for Several Different Harmonics

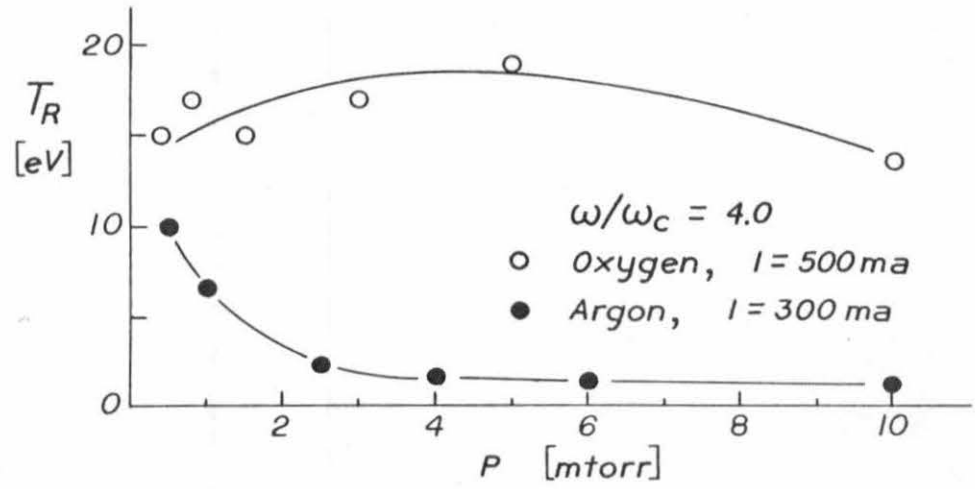

Figure 3.4b Radiation Temperature in eV as a Function of the Neutral Pressure for Both Oxygen and Argon Gas

that the higher harmonics appear in the oxygen discharge as the neutral gas pressure is increased, just as in the situation of increasing discharge current. However, in order to observe this effect, it is first necessary to set the discharge current at a sufficiently large value so that harmonic emission will be observed at high pressure.

In the case of the onset of harmonic emission with increasing discharge current, it is believed that the onset occurs at a critical plasma density. A similar explanation may hold for the observed pressure dependence if it can be shown that the plasma density increases with the neutral gas pressure.

To test this hypothesis, the pressure dependence of the electron density was monitored using the microwave interferometer. With the discharge current held fixed at 200 ma, the phase shift of the interferometer was recorded as a function of the neutral gas pressure. The results are shown in Figure 3.5. From the data, it is obvious that the electron density in the Penning discharge is indeed strongly dependent on the neutral gas pressure, at least in the low pressure range $P < 10$ mtorr. In addition, it can be seen from the data presented in Figure 3.16 that even at higher pressures, $P = 10\text{-}30$ mtorr, the plasma density continues to increase with the neutral gas pressure. In view of these results, it is not surprising that a similar effect can be observed by varying either the discharge current or the neutral gas pressure.

There is one notable feature of the lower harmonics of the spectrum which is especially evident at low pressure. At the lower harmonics ($m \leq 3$), the emission lines have a different shape. A

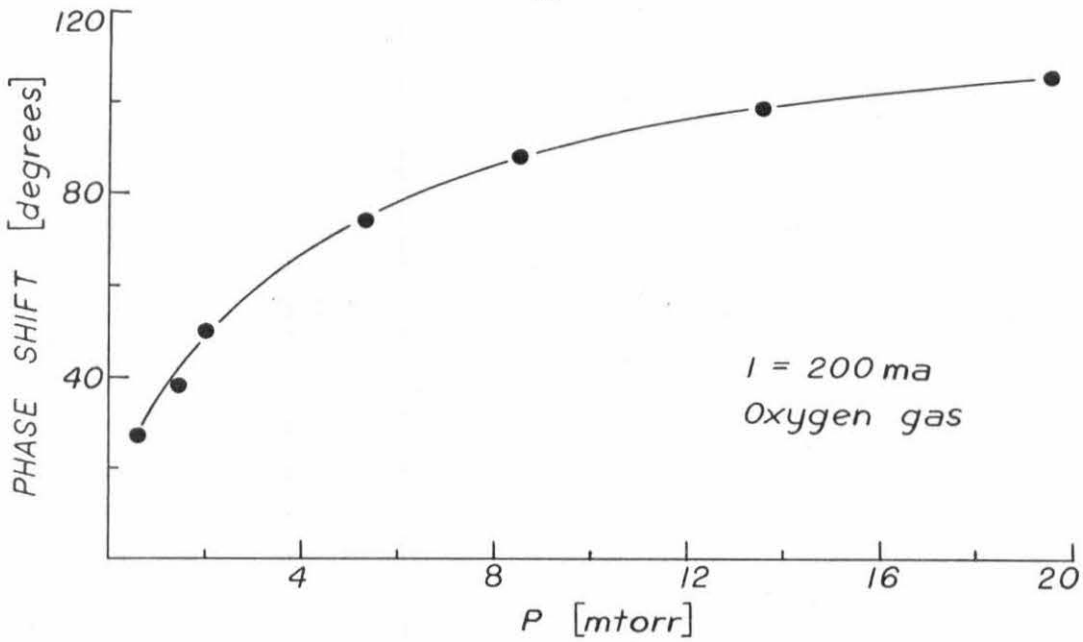

Figure 3.5 Interferometer Phase Shift as a Function of Pressure

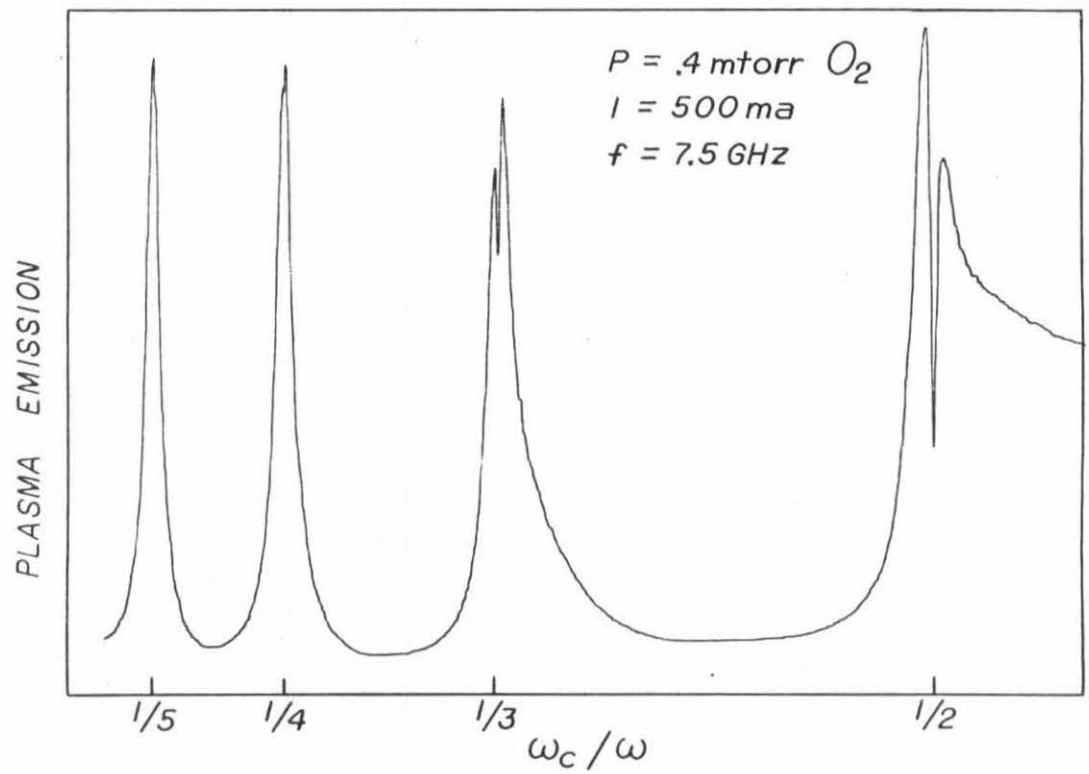

Figure 3.6 The Shape of the m = 2 and m = 3 Emission Lines when the Oxygen Gas Pressure is Low

narrow absorption resonance is almost always visible on the $m = 2$ emission line. However, when the neutral gas pressure is less than 1 mtorr, a similar resonance is also observed at the $m = 3$ harmonic. This feature is evident in the emission spectrum displayed in Figure 3.6. It is observed that when the neutral gas pressure is increased the absorption resonances broaden and become smaller in amplitude.

It might be noted that a significant amount of information can be obtained from the emission spectrum. For example, the emission spectrum indicates the location, width, shape, and amplitude of the harmonic emission lines and how each of these depends on the harmonic number. In addition, there are two principal independent experimental variables which influence the parameters listed above. They are the discharge current and the neutral gas pressure. A strong dependence of the harmonic emission amplitude on the discharge current has already been demonstrated. A weaker dependence on the neutral gas pressure is also observed. But what is remarkable is the observation that the location, shape, and width of the emission lines seem to be independent of both the discharge current and the neutral gas pressure. As a result, Figures 3.1 - 3.4 constitute a large portion of the experimental description of the cyclotron harmonic emission phenomenon.

3.2.3 Other Measurements

The shape, width, and location of the harmonic emission lines are three features of the emission spectrum which are difficult to determine accurately from the emission spectra as presented in Figures 3.1 and 3.3. Because of the narrowness of the emission lines, it is necessary to expand the frequency scale in the vicinity of the desired

harmonic before these parameters can accurately be determined. When this is done, it is found that all three features are seemingly independent of both the discharge current and the neutral gas pressure.

As an example, Figure 3.5 indicates how the width of the emission lines at the -3 db amplitude fluctuates when the neutral gas pressure is varied. Figure 3.5a was obtained from a grid-stabilized plasma column and Figure 3.5b was obtained from a turbulent plasma column.

The shape of the harmonic emission lines is examined more thoroughly in Section 3.3 and the emission line location is measured in Section 3.4 using NMR techniques. The polarization of the harmonic emission is explored in Section 3.5.

It is found that the harmonic emission spectrum is relatively static with respect to the experimental variables. Except for the hybrid layer condition, only limited changes in the emission spectrum are observed as the discharge current and the neutral gas pressure are varied. Therefore, it is of interest to investigate other circumstances which affect the harmonic emission spectrum.

Experimental results have already been presented which were obtained using different configurations of the Penning discharge. Plasma column diameters of 2.6" and 4" were used and the data presented in Figure 3.7b were obtained using a grid-stabilized discharge. Other modifications to the plasma column and the surrounding environment were carried out in an effort to determine what effect they have on the harmonic emission. The results of this investigation are discussed in Section 3.6 and provide a basis for comparison of the emission spectra obtained under various conditions.

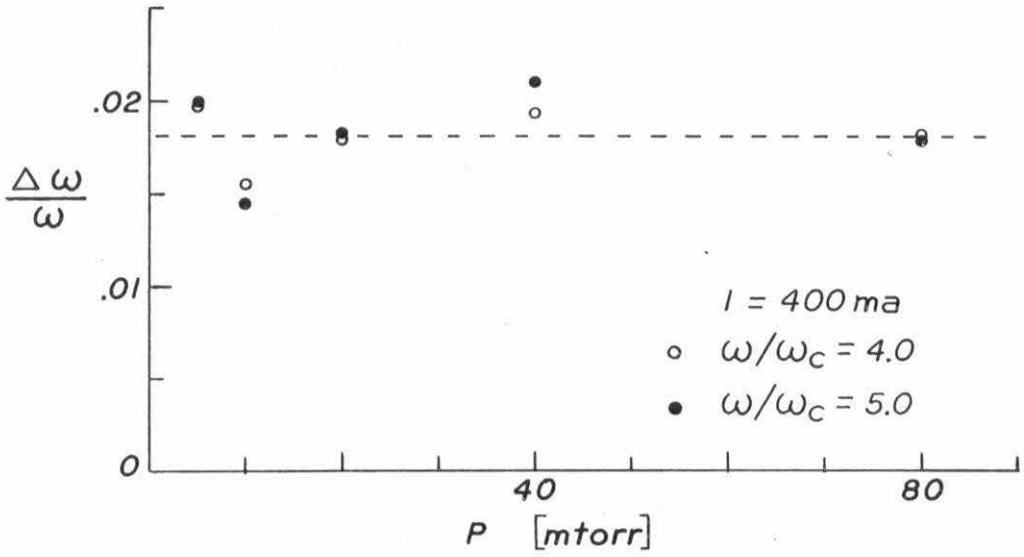

Figure 3.7a Linewidth $\Delta\omega/\omega$ as a Function of the Oxygen Gas Pressure for Several Harmonics of the Nonstabilized Discharge

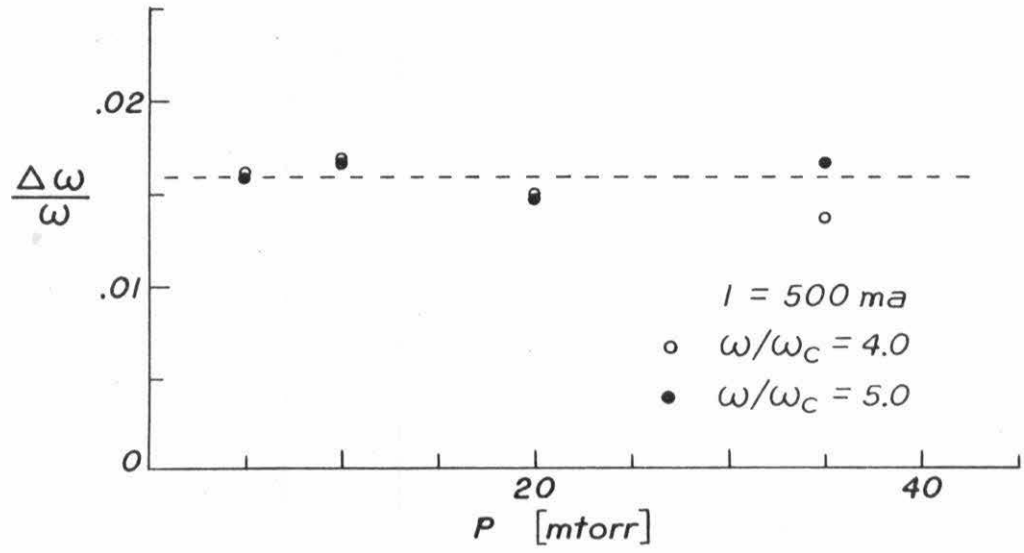

Figure 3.7b Linewidth $\Delta\omega/\omega$ as a Function of the Oxygen Gas Pressure for Several Harmonics of the Grid-Stabilized Discharge

In order to assess the importance of the receiver frequency, the harmonic emission is observed simultaneously at both 10 GHz and 50 GHz. The results of this investigation are reported in Section 3.7. It is found that the emission spectrum at 50 GHz contains a very large number of harmonics of the cyclotron frequency and that harmonic amplitude falls off slowly with harmonic number.

The low power level absorption spectrum is investigated in Section 3.8 and compared with the emission spectrum. The absorption spectrum is inferred from the transmission and reflection properties of the plasma column. No absorption resonances are detected in the vicinity of the higher harmonics ($m \geq 4$) of the electron cyclotron frequency. However, an absorption resonance is observed at the $m = 2$ harmonic. This effect appears to be related to the absorption dip which is observed in the emission spectrum at the $m = 2$ harmonic.

The plasma density dependence of the harmonic emission is examined in Section 3.9 with the aid of a microwave interferometer and the significance of the existence of a hybrid layer is discussed. The sudden onset of harmonic emission as the discharge current is increased indicates a strong dependence on the electron density. Dreicer concluded that the onset of the harmonic emission coincides with the existence of a hybrid layer on the plasma column [15]. The experimental evidence presented in Sections 3.7 and 3.8 lend support to this concept. However, microwave interferometer measurements of the electron density by Hanisch and Stetson indicate that the harmonic emission is present long before a hybrid layer is established on the plasma column [23]. In an attempt to clarify this point, a microwave

interferometer density measurement has been included in this investigation. The results verify the conclusions of Dreicer, that the existence of a hybrid layer is a necessary condition for the harmonic emission.

3.3 Emission Line Shape

Since the emission line shape did not appear to change significantly, it was analyzed in detail on only one occasion. The results are reported in this section. The shape of the emission lines should provide useful information concerning the nature of the harmonic emission mechanism.

The microwave superheterodyne receiver is set up to detect the extraordinary polarization of the emission and is operated as indicated in Figure 3.9. A tunable microwave filter is employed to reject the image frequency of the receiver. The receiver bandwidth is then determined by the 4 MHz bandwidth of the I-F amplifier. The line shape is recorded at several harmonics while sweeping the magnetic field at a very slow rate. The recorded line shape for the $m = 4$ harmonic is presented in Figure 3.8a.

The emission line is observed to be nearly symmetric with respect to the emission maximum. It is fairly evident that the shape of the emission line is not Gaussian and a more detailed examination revealed that it is not quite Lorentzian either. However, a very good fit to the line shape can be obtained using a more general expression of the form

$$f(\omega) = \frac{A}{1 + \left(\frac{\omega - m\omega_c}{\Delta}\right)^n} + B \qquad (16)$$

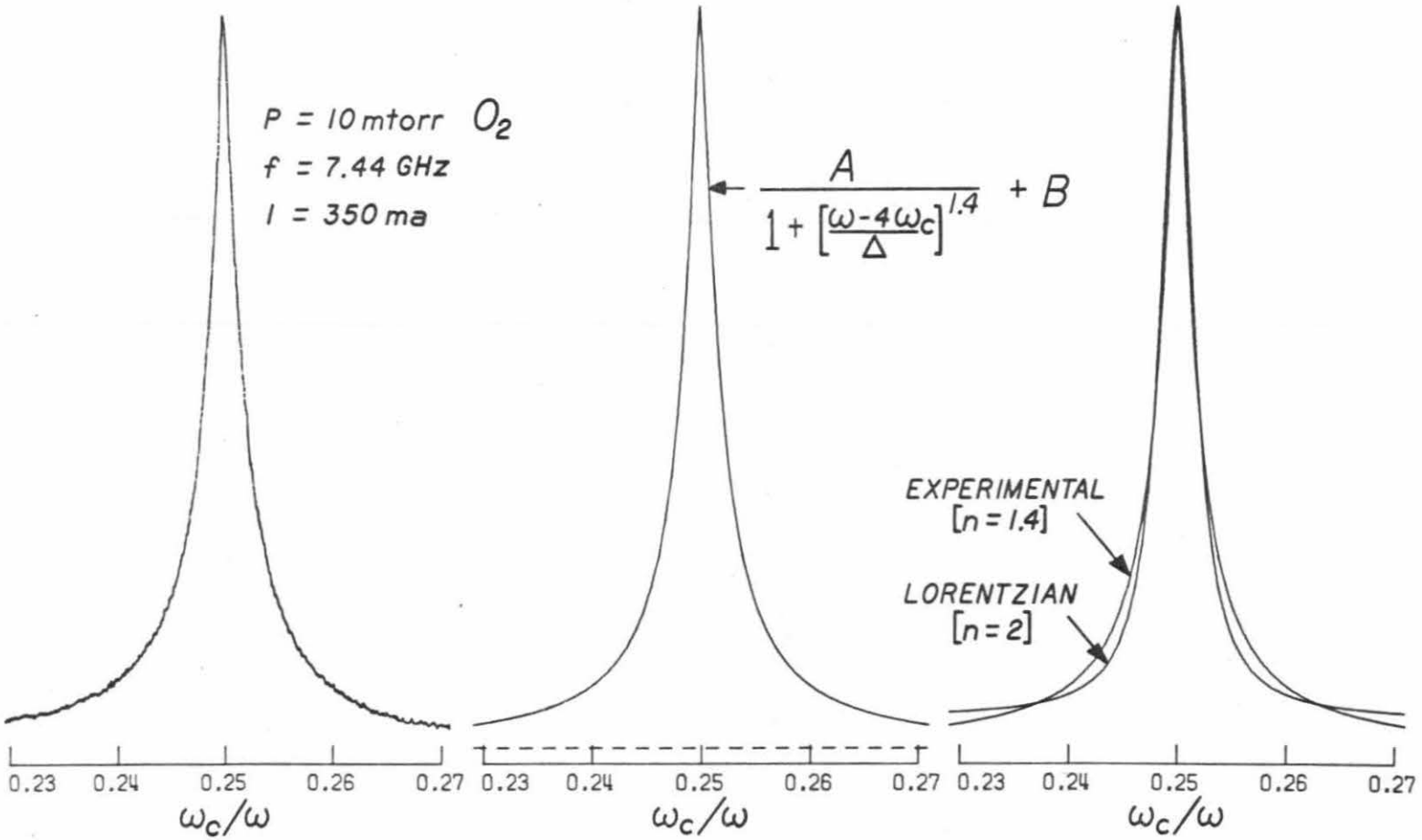

(a) Experimental Line Shape (b) Mathematical Fit [n=1.4] (c) Comparison with Lorentzian Shape

Figure 3.8 Shape of the m = 4 Harmonic Emission Line

where A and B are the relative amplitudes of the emission line and the background radiation, respectively, Δ is the emission line half-width, and n is a number which is adjusted to give the best fit.

For harmonics $m = 4$ and $m = 5$, n is found to lie between 1.3 and 1.4. Figure 3.8b shows the line shape given by equation (16) when $n = 1.4$. Note that the dashed line indicates the value of the constant B which must be added to the frequency dependent term in order to obtain the experimentally observed line shape. This suggests that even between the harmonics much of the emission may be nonthermal in origin.

In Figure 3.8c the experimental line shape, $n = 1.4$, is compared to a Lorentzian line shape, $n = 2.0$. This points out clearly how sharp the maximum of the observed line shape is, and also how slowly the emission amplitude falls off in the tails of the emission line. The sharpness of the emission maximum is very beneficial for accurate determination of the emission line location relative to the magnetic field (see Section 3.4).

Although the line shape at higher harmonics ($m > 5$) appears to be the same, it is difficult to carry out an accurate analysis because of the fact that the emission lines overlap extensively. However, the shapes of the $m = 3$ and $m = 2$ harmonics differ from those of the higher harmonics. The shape of the $m = 3$ harmonic is only slightly different and corresponds roughly to $n = 1.1$. However, the $m = 2$ harmonic has an entirely different shape and can not be described using equation (16).

In general, it is difficult to compare these results with the line shapes observed in other experiments. When the emission spectrum containing all of the harmonics is displayed on a single graph, the emission lines are so compressed that the line shape can not be accurately determined. The line shape can be evaluated accurately only when the emission spectrum is greatly expanded in the vicinity of an emission line.

For this reason, it is generally difficult to make comparisons with the compressed emission spectra presented by Landauer [4,6] and Dreicer [15]. In one instance, Dreicer [17] did investigate the line shape and found a definite asymmetry. However, such an asymmetry is not noticeable in the compressed emission spectra and is not found to be significant in the present investigation.

Tetenbaum [13] observed a line shape which is essentially identical with that described above by equation (16). However, he was observing emission from an r-f generated plasma.

The harmonic emission lines observed in this experiment have been found to be nearly symmetrical in shape. The fact that the line shape is similar to a Lorentzian might suggest collision broadening. However, the fact that the width of the emission lines is independent of the neutral gas pressure indicates that this is definitely not the case. The process which determines the shape of the emission lines is clearly more complicated.

3.4 Emission Line Location

3.4.1 Method of Measurement and Result

An experiment was undertaken to determine the exact location of the emission maxima relative to the harmonics of the electron cyclotron frequency, $\omega = m\omega_c$. A NMR gaussmeter is utilized for an accurate measurement of the magnetic field.

Using the proton resonance in water, the NMR frequency, ν , is related to the magnetic field by

$$\nu = \gamma B \quad \text{where} \quad \gamma = 4.25759 \times 10^{-3} \text{MHz/gauss} \ [48]$$

The cyclotron frequency, f_c , at the emission maximum is then

$$f_c(\text{GHz}) = \frac{1}{2\pi}\frac{e}{m} B = \frac{1}{2\pi}\frac{e}{m}\frac{\nu}{\gamma} = 0.657465\nu \ (\text{MHz})$$

When normalized to the microwave receiver frequency, the location of the emission maximum relative to the harmonic position is given by

$$\frac{mf_c}{f} = \frac{m\omega_c}{\omega} = 0.657465m \frac{\nu(\text{MHz})}{f(\text{GHz})}$$

where f is the microwave receiver frequency.

A block diagram of the experiment is given in Figure 3.9. The NMR frequency is displayed by the frequency counter and the microwave receiver frequency is measured using the cavity wavemeter. One sideband of the superheterodyne receiver is rejected by the tunable tee filter. The bandwidth of the receiver is then equal to the 4 MHz bandwidth of the I-F amplifier.

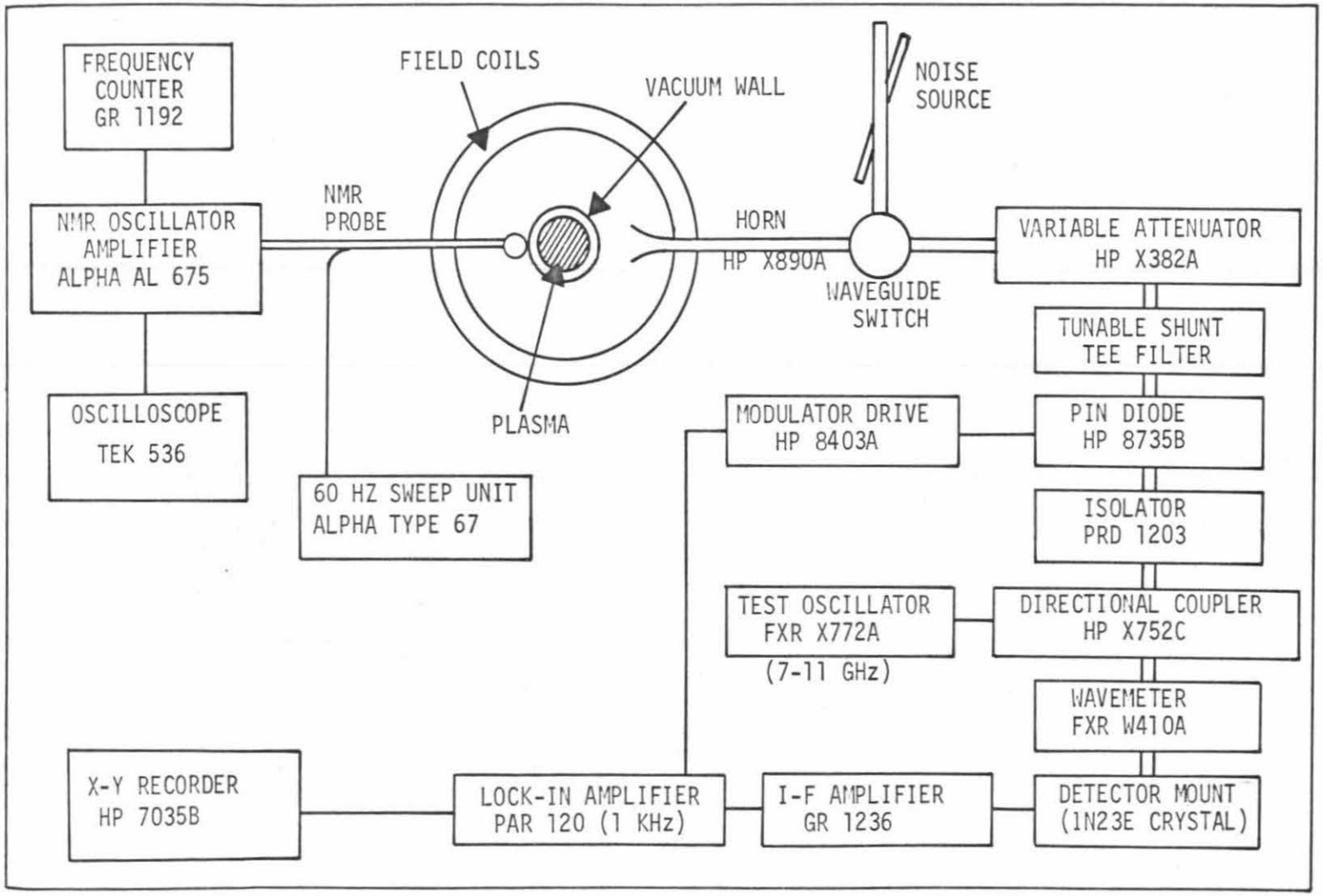

Figure 3.9 Block Diagram for NMR Determination of Emission Line Location

The location of each maximum is determined by repeatedly sweeping the magnetic field slowly through the emission maximum. The NMR frequency is repeatedly adjusted until the NMR resonance is exactly centered on the oscilloscope graticule at the time of maximum emission. The precision of this method is limited by the sharpness of the emission line. In the Penning discharge, the maxima are quite sharp, as indicated in Section 3.3. The results of the NMR measurement were reproducible on different days to 1 part in 3000. They are given in Table 3.1 and are plotted in Figure 3.10.

A measurement was carried out to determine if the emission lines shift position as the discharge current or the neutral gas pressure are varied. No detectable shift (> 0.1%) of the $m = 5$ harmonic is observed when the neutral gas pressure is varied over the range of 5-100 mtorr and the discharge current is varied from 250-600 ma.

3.4.2 Accuracy of Measurement

As indicated by the magnitude of the error bars in Figure 3.10, the accuracy of these results is not determined by the precision of the measurement. This is due to the presence of numerous sources of systematic error. These include spatial inhomogeneity of the magnetic field, wavemeter inaccuracy, and current ripple in the field coil.

The magnetic field variation over the volume occupied by the plasma ($r \leq 1.3$") is 0.25% from minimum to maximum. This value is obtained from NMR measurements and also from computer calculations which determine the proper spacing of the field coils. However, the NMR probe must be located at a radius of 3" during the measurements of

Table 3.1 Numerical Data for NMR Measurement of Emission Line Location

m	ν(MHz)	$\frac{m\omega_c}{\omega}$ ($\pm$ 0.1%)
3	3.7750	1.00050
4	2.8297	0.99995
5	2.2635	0.99985

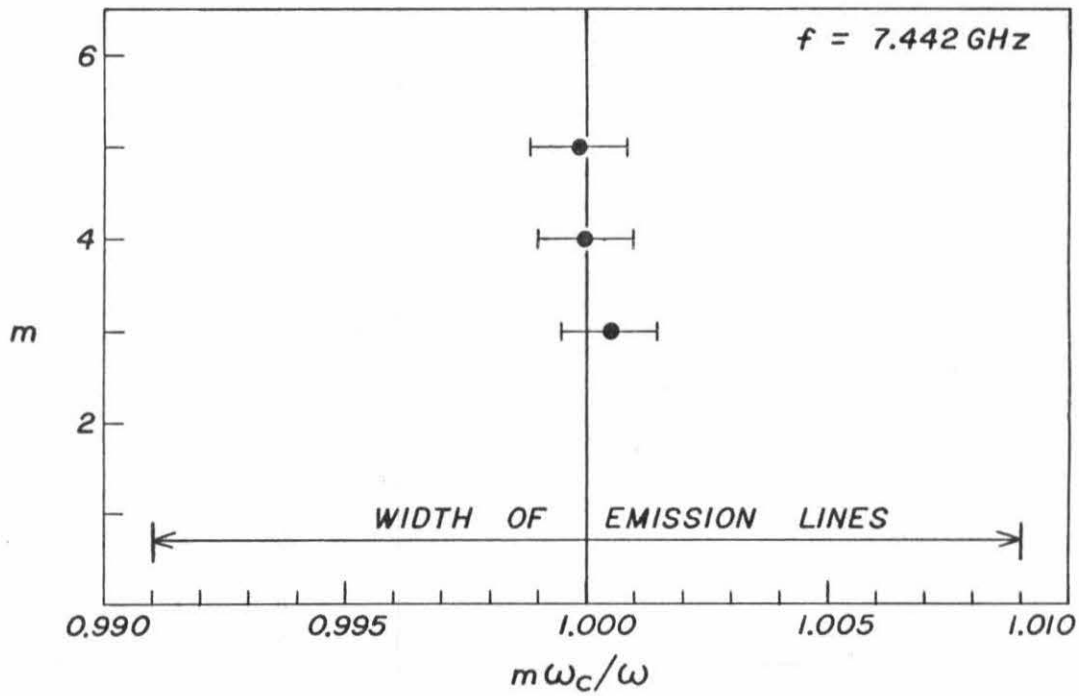

Figure 3.10 Location of the Emission Lines Relative to the Harmonics of the Electron Cyclotron Frequency

emission line location. At this radius, the axial field variation is 1.06% from minimum to maximum.

The NMR measurements of the magnetic field were performed at the axial positions of minimum and maximum field. It is necessary to predict from these measurements, the average value of the magnetic field in the region occupied by the plasma. To facilitate the determination of accurate adjustment factors, NMR probe measurements of the magnetic field profile of the empty solenoid were obtained. Any error in the adjustment factors so determined results in a systematic error in all of the emission line locations measurements.

The wavemeter manufacturer indicates that the accuracy of the wavemeter is 0.08%. To check the calibration of the wavemeter, it was compared with an HP X532B wavemeter in the overlapping frequency range of 8.2 - 9.0 GHz. The two wavemeters agreed to 1 part in 4000, indicating that the calibration is somewhat better than the manufacturer's specification.

The SCR power supply for the field coils is operated from the 240V three phase line. The resulting 180 Hz current ripple in the field coils is about .04% rms for the values of the magnetic field used in the measurements. In addition, 60 Hz and 120 Hz current ripple are also present. They can be generated by asymmetric triggering of the SCR's. Although the 60 Hz ripple is somewhat smaller at the power supply output, it can become important in the field coil because the filter is only 4% as effective at 60 Hz as it is at 180 Hz. The 60 Hz and 180 Hz time dependences of the magnetic field do not result in errors in the NMR measurement which employs a 60 Hz sweep.

The NMR measurement gives the time average value of the magnetic field when only these frequency components are present. Current ripple at 120 Hz, however, does result in a systematic error. The amplitude of such ripple is estimated to be relatively small, probably less than 0.01% rms.

Other sources of systematic error, such as the accuracy of the frequency counter, are negligible in comparison with the previously described errors. The net result of these independent systematic errors is a probable error of 0.1% in determining the location of the emission maxima relative to the harmonic positions, $\omega = m\omega_c$.

3.4.3 The Lower Harmonics

Although the determination of the absolute locations of the emission maxima is limited by the accuracy of the measurement , the determination of their relative positions is limited only by the precision of the measurement. Therefore the displacement of the $m = 3$ peak relative to the $m = 4,5$ peaks in Figure 3.10 is probably real.

Further evidence of this is found in the emission spectra at the $m = 2$ harmonic. As displayed in Figure 3.6, there is a dip offset to one side of the $m = 2$ emission line. NMR measurements indicate that this dip is located at the $m = 2$ harmonic of the electron cyclotron frequency. Therefore, the $m = 2$ emission line is displaced slightly in the direction $2\omega_c/\omega > 1$. At low neutral gas pressure, the dip becomes very narrow and a similar dip is also observed at the $m = 3$ harmonic. Again the dip location is such that the emission line is slightly displaced in the direction $3\omega_c/\omega > 1$ relative to the dip.

It appears that at the higher harmonics ($m \geq 4$), the emission lines are centered at the harmonic locations. However, for the $m = 2$ and possibly the $m = 3$ harmonic, there seems to be a real displacement from the harmonic location. It should be noted that even in the case of the $m = 2$ harmonic where the shift is greatest, the effect is still considerably less than 1%.

3.4.4 Summary

Measurements of the time and spatial averaged magnetic field indicate that within experimental accuracy, the $m \geq 4$ emission peaks are located at the harmonics of the electron cyclotron frequency. From the accuracy of the measurement, the emission line width is at least 20 times greater than any residual displacement from the harmonics locations. It can therefore be argued that unlike the situation encountered in other plasma configurations [8-10,12], displacement from the harmonics is not a significant feature of the $m \geq 4$ emission spectrum of the Penning discharge.

3.5 Polarization of Harmonic Emission

When observing emission from the pyrex discharge tube, the microwave receiver horn can be rotated to detect either the ordinary wave or extraordinary wave polarization of the plasma emission. Measurements indicate that the harmonic emission is polarized.

The superheterodyne receiver is operated as indicated in Figure 3.9 with the exception that the tunable microwave filter is not used to reject either image frequency. The local oscillator frequency is 7.2 GHz. The emission from the nonstabilized pyrex discharge tube is

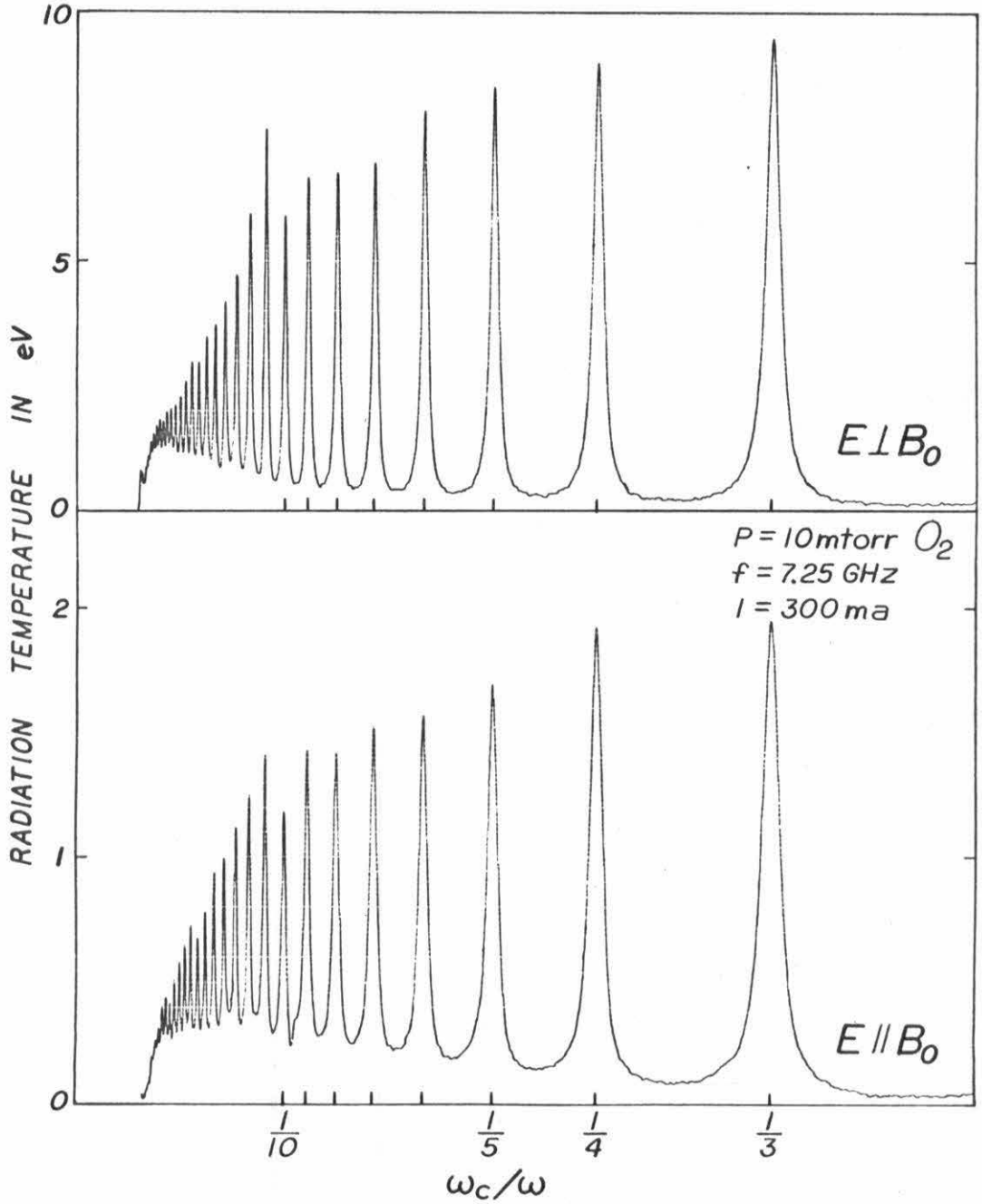

Figure 3.11 Radiation Temperature in eV as a Function of ω_c/ω for Both Orientations of the Microwave Receiving Antenna

observed with the microwave horn located 3 cm from the pyrex tube. Figure 3.11 presents the recorded emission spectra for the ordinary and extraordinary polarizations.

There are several noticeable features which distinguish the two polarizations. In comparison with the extraordinary wave polarization, the ordinary wave emission intensity is lower by about 7 db and the emission lines are wider by about 20%. The emission intensity between the harmonics experiences a lesser change in amplitude, partly associated with the broadening of the emission lines.

Landauer observed a similar reduction in the harmonic emission amplitude for the ordinary polarization [4]. With the exception of this section, only the extraordinary wave polarization is investigated in this report.

3.6 Importance of Discharge Configuration

From a theoretical standpoint it is of interest to know exactly how the harmonic emission depends on the discharge configuration. Before a realistic theoretical model can be developed, it is necessary to determine which aspects of the discharge need to be considered. As a prime example, it is of interest to know if the radial electric field, the low frequency drift instabilities, and the turbulence present in the nonstabilized plasma column play a role in the generation of harmonic emission. It is certainly easier to model the quiescent plasma of the grid-stabilized discharge than the turbulent plasma of the nonstabilized discharge. Therefore the plasma column and the surrounding environment were modified in several ways in order to determine which

aspects of the plasma configuration influence the harmonic emission and to what extent.

Modifications to the plasma include a change in the diameter of the plasma column and the insertion or removal of stabilizing grids. The principal modification to the environment surrounding the plasma column consists of enclosing the plasma column alternatively in either a microwave reflector (a microwave cavity) or a microwave absorber. The only feature of the emission spectrum which is observed to change as a result of the various modifications is the emission intensity. Other features of the emission spectrum such as the emission line shape and location do not appear to be affected by the alterations.

3.6.1 Changing the Diameter of the Plasma Column

When the diameter of the oxygen plasma column is decreased by reducing the anode diameter from 4" to 2.6", it is observed that the harmonic emission intensity is increased from approximately 25 eV to 45 eV. At the same time there is a significant increase in the operating voltage of the discharge. It is believed that these two effects are strongly interrelated. The relationship between the harmonic emission intensity and the discharge voltage is clearly demonstrated in Chapter V. For this reason, it is concluded that the harmonic emission intensity is only indirectly related to the diameter of the plasma column. The column diameter is just one of the many parameters which determine the discharge voltage and the harmonic emission intensity is strongly dependent on the discharge voltage.

3.6.2 Effect of Metal Discharge Chamber

When the environment surrounding the plasma column is changed from a microwave absorber to a microwave reflector, it is found that the harmonic emission intensity is increased by approximately 3 db. The fact that the emission intensity is not greatly enhanced by the reflector means that the plasma is a relatively good absorber. Most of the harmonic emission produced by the plasma is also re-absorbed by the plasma column after it is reflected. The experimental results indicate that the absorptivity of the plasma column is roughly half that of a blackbody, when a hybrid layer is present.

Experimentally, a good reflector is obtained by using the brass discharge chamber of Figure 2.7. The chamber is an excellent reflector of the microwave radiation produced by the plasma column. When the chamber is lined with a microwave absorber, the opposite situation is realized. Also, when the pyrex discharge tube of Figure 2.8 is used, a good absorbing environment is achieved by lining the inside of the magnetic field solenoid with a microwave absorber. In the final analysis, harmonic emission from the 4" diameter plasma column of the reflecting brass discharge chamber is essentially identical with that from the 2.6" diameter column of the pyrex discharge tube.

Previous investigations of harmonic emission in the Penning discharge have used a metal discharge chamber. Because of the complication of re-absorption of emission by the plasma column, it is difficult to estimate the total power radiated by the column. If instead, the plasma is surrounded by an absorber, then the total radiated power can

readily be inferred from the observed radiation intensity.

3.6.3 Effect of Grid Stabilization

When stabilizing grids are placed across the plasma column, the harmonic emission intensity is sometimes found to be unchanged but in some instances is reduced by as much as 3 db. The effect of the grids on the harmonic emission is confusing but appears to be explainable. The most noticeable changes in the plasma column which result from the presence of the stabilizing grids are the reduction of the radial electric field and the elimination of low frequency instabilities and turbulence. However, additional changes result from the presence of the grids.

The grids collect a significant number of the energetic electrons present in the plasma column. This results in a drop in the plasma production rate and a compensating rise in the operating voltage of the discharge. The energetic electrons are believed to be responsible for the harmonic emission. Therefore, ignoring the increased operating voltage of the discharge, a reduction in the number density of energetic electrons should lead to a reduction of the harmonic emission intensity.

An additional complication results from the build-up of an oxide layer on the stabilizing grid. This causes the transparency of the grids to change slowly with time and leads to confusion about what is happening. As a result, on some occasions it is found that the emission intensity is unchanged by the stabilizing grids but in other circumstances the emission intensity is decreased by as much as 3 db. Although the experimental observations seem reasonable, this matter is not fully understood.

Nevertheless, it is significant that the observed changes in the emission intensity are as small as they are. Recall that the stabilizing grids reduce fluctuations in the ion saturation current and the floating probe potential by several orders of magnitude. The radial electric field is reduced by an order of magnitude and low frequency instabilities are virtually eliminated from the plasma column. The fact that correspondingly large changes in the intensity of the harmonic emission are not observed indicates that the harmonic emission mechanism is not attributable to these aspects of the Penning discharge.

There is additional evidence to support the supposition that the radial electric field, the low frequency drift instabilities, and the turbulence of the nonstabilized plasma column are not important in the harmonic emission process. In Chapter II it is noted that there is a critical magnetic field associated with the operation of the nonstabilized Penning discharge. At the critical magnetic field there is a sudden change in the nature of the plasma. At lower values of the magnetic field the plasma is quiescent and at high fields the plasma is highly turbulent. Yet, when the harmonic emission spectrum is recorded by sweeping the magnetic field, no significant change is detected in the emission spectrum at the critical magnetic field. There is no indication that the harmonic emission process is influenced by the radial electric field, the low frequency drift instabilities, or the plasma turbulence.

It is found that the location of the stabilizing grid along the axis of the plasma column is not an important parameter. Usually a pair

of stabilizing grids is used, one at each end of the plasma column. However, in one instance a single stabilizing grid was located near the midplane of the discharge column. Essentially the same results are obtained in each case.

Although the axial location of the stabilizing grids is not found to be an important parameter with respect to the harmonic emission, it is a critical parameter for the high intensity nonharmonic radiation which is also observed in the discharge. This subject is covered in detail in Chapter V.

3.6.4 Summary of the Configurations Used for Various Measurements

In order to eliminate confusion concerning the many discharge configurations which were investigated during the experiments, a summary of the configurations is in order. Basically, there are two discharge tubes. Two modifications of the brass chamber discharge tube are shown in Figures 2.7 and 5.2. The pyrex discharge tube is shown in Figure 2.8. The usage of each of these discharge tubes and various modifications will be summarized below. The pyrex discharge tube will be treated first because it is less complicated.

There is only one feature of the pyrex discharge tube which can easily be changed. It can be operated either with or without the stabilizing grids. The parallel wire grids can be attached to the anode rings at each end of the plasma column. The diameter of the plasma column is fixed at 6.6 cm. In order to prevent the deposition of sputtered metallic aluminum onto the pyrex tube, only oxygen gas is used. When the inside surface of the magnetic field solenoid is lined with a microwave absorber, the environment surrounding the plasma column

constitutes a good absorber. Thus, there is only one option in the operation of the pyrex tube discharge, the plasma column can be either grid stabilized or nonstabilized.

The pyrex discharge tube is utilized mainly for the investigation of the hybrid layer condition described in Section 3.9. Microwave interferometer measurements of the electron density, as well as harmonic emission measurements, are carried out using both the turbulent and the grid-stabilized plasma. The same experimental data is also used to determine the effect of the stabilizing grid on the harmonic emission.

The pyrex discharge tube is particularly well suited for two other measurements. In the measurement of the emission line location (Section 3.4) it was necessary to have the NMR probe as close as possible to the center of the magnetic field solenoid where the field is nearly uniform. The small outside diameter of the pyrex tube, 4 inches, is very beneficial in this respect. The pyrex discharge tube is also particularly suited to measurements of the polarization of the harmonic emission (Section 3.5). The receiver horn is easily rotated to detect either polarization, and the surrounding microwave absorber prevents scattered radiation from reaching the receiver horn. In addition, the emission line shape data of Section 3.3 were obtained using the pyrex discharge tube.

The brass chamber discharge tube is used in a large variety of modifications. The brass chamber effectively surrounds the plasma with an excellent reflector, unless the chamber is lined with microwave absorber. These two situations are compared to determine how much the

harmonic emission intensity is enhanced by surrounding the plasma column with a reflector.

When the chamber was operated in the configuration of Figure 2.7, only a 4" diameter plasma column was used. However, after the discharge configuration was modified to that of Figure 5.2, column diameters of both 4" and 2.6" were used. Therefore the latter configuration was used to investigate the significance of the diameter of the plasma column.

The brass discharge chamber is also used extensively to investigate grid stabilization of the plasma column. For the 4" diameter column, only a single movable grid is used. It is usually located near the midplane of the plasma column. When the column diameter is reduced to 2.6", a pair of grids is used. In fact, these are the same parallel wire grids that are used in the pyrex discharge tube. The grids are mounted on the anode structures at opposite ends of the plasma column. Since the harmonic emission spectrum was investigated using each of the indicated modifications, there are several instances where the effects of the stabilizing grids can be checked. Therefore, the brass discharge tube was very useful in determining the role of the plasma configuration and the surrounding environment in the harmonic emission process.

The brass discharge tube is also used exclusively for several measurements. They include the microwave absorption experiment of Section 3.8 and the pulsed experiments of Section 3.7 and Chapter V. Both argon and oxygen are used in the brass discharge tube as the neutral gas.

3.7 Harmonic Emission at 50 GHz

An experiment was undertaken to simultaneously observe the harmonic emission at both 10 GHz and 50 GHz. The microwave hardware available at 50 GHz is quite limited. It consists of a single crystal mixer mount, a 10 db directional coupler, a variable attenuator, a standard gain horn (to make a transition to the X-band waveguide), and a 50-60 GHz klystron. However, this proved to be sufficient.

A notable feature of this experiment was the initial difficulty in detecting any 50 GHz emission at all in the dc operated discharge. Since Dreicer had previously concluded that the existence of a hybrid layer on the density profile was a necessary condition for the harmonic emission, it was decided that the density obtained in the dc discharge was not sufficient to satisfy the hybrid layer condition at 50 GHz. The discharge was then operated on a pulsed basis with discharge currents reaching values as large as 40 amps. In this case, harmonic emission was observed at 50 GHz.

Except for the fact that the 50 GHz microwave components are limited to those listed above, the microwave receiver is essentially the same as the pulsed plasma set-up of Figure 2.1. The 4" plasma column is produced using argon gas in the discharge chamber sketched in Figure 2.7. This is the only experiment which was not repeated later using oxygen gas.

In Figure 3.12, the harmonic emission observed at 10 GHz (5th harmonic) is compared with the harmonic emission observed at 50 GHz (19th harmonic). In each case the cathode voltage and the discharge

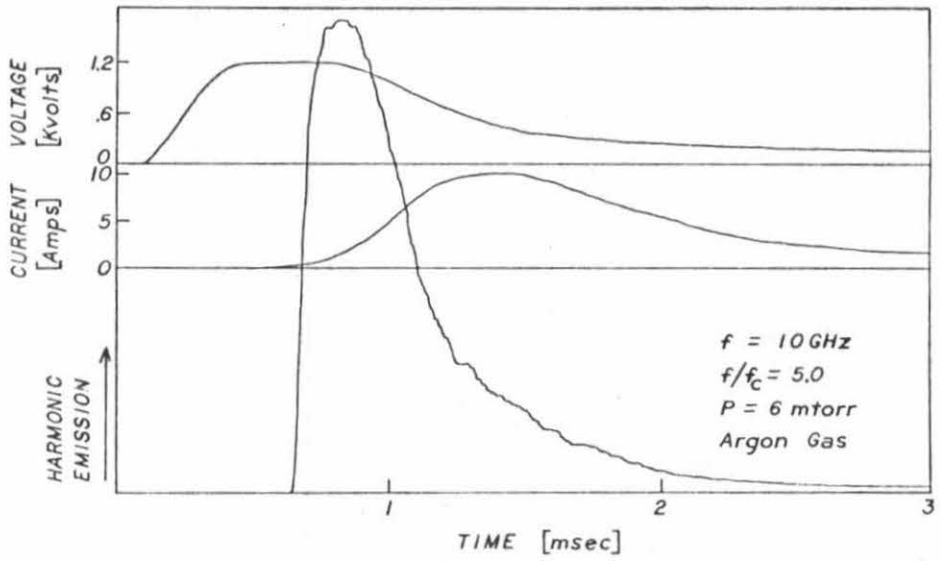

Figure 3.12a Emission at the 5th Harmonic as a Function of Time during the Pulsed Discharge when Using a Receiver Frequency of 10 GHz.

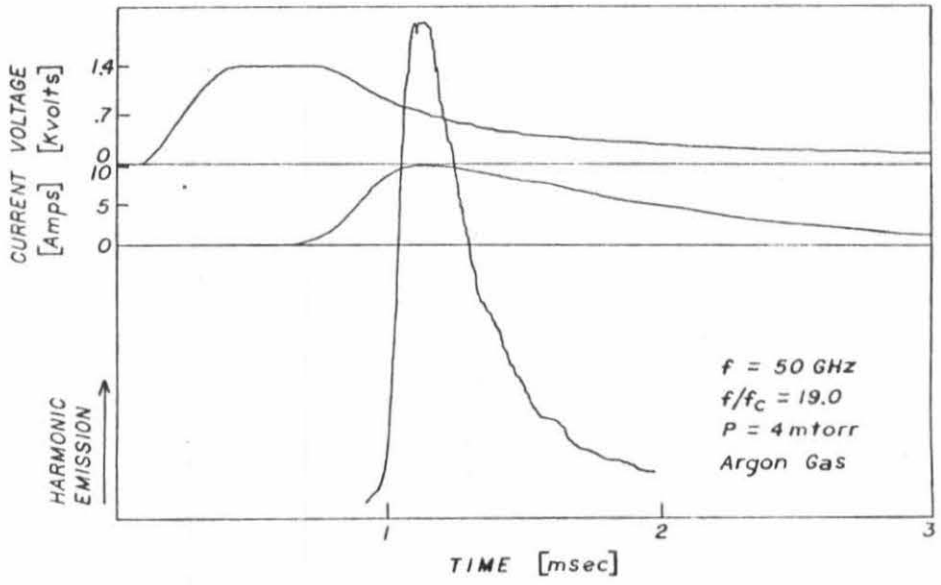

Figure 3.12b Emission at the 19th Harmonic as a Function of Time during the Pulsed Discharge when Using a Receiver Frequency of 50 GHz. The voltage and current waveforms of the pulsed discharge are also presented.

current are also displayed. All of the waveforms are recorded using the boxcar integrator.

The waveforms reflect the manner in which the discharge is pulsed. A capacitor bank in parallel with the discharge is pulse charged. This process determines the rise time of the voltage waveform. Breakdown of the argon plasma takes place in about 0.5 milliseconds after which the current increases rapidly, discharging the capacitor.

Because the 50 GHz receiver experienced a transient pickup problem associated with the pulse charging of the capacitor, the entire 50 GHz emission waveform is not accurately known.

It is interesting to compare the point in time at which the harmonic emission appears in each case. At 10 GHz, the emission rises very rapidly at a well-defined time early in the pulse. The discharge current is still relatively low, approximately 300 ma. At 50 GHz the high intensity radiation does not appear until later in the pulse when the discharge current is roughly 10 amps, and therefore the electron density is much higher.

This observation supports the conclusions of Dreicer that the existence of a hybrid layer is a necessary condition for the harmonic emission. The plasma density is roughly proportional to the discharge current, $I \propto N$. At high harmonic numbers, the upper hybrid and plasma frequencies are nearly equal and $f_H \simeq f_p \propto \sqrt{N}$. The observations at 10 GHz indicate that $f_H \simeq f_p \geq 10$ GHz when $I \simeq 0.3$ A. Therefore, the hybrid layer condition will be satisfied at 50 GHz when

$f'_H \simeq f'_p \geq 50$ GHz. This requires that $f'_p/f_p \geq 5$ and therefore that $I'/I = (f'_p/f_p)^2 \geq 25$. Thus, the hybrid layer condition indicates that emission will not be observed at 50 GHz unless $I \geq 25(0.3A) = 7.5$ A. This agrees very well with the experimental results.

What is puzzling about the harmonic emission displayed in Figure 3.12 is the rapid decrease of the harmonic emission amplitude later in the pulse , even when the discharge current is still large. This behavior proved to be fascinating. In Chapter V the pulse modulation experiments finally revealed that the emission amplitude is also strongly dependent on the cathode voltage.

The 50 GHz emission spectrum is displayed in Figure 3.13. The sampling time of the boxcar integrator is set for the time during the pulse when the emission amplitude is near maximum and the spectrum is recorded by slowly sweeping the magnetic field. The insert shows the higher harmonics in greater detail. It was obtained by increasing the gain of the X-Y recorder and repeating the measurement.

It might be observed that the harmonic amplitude falls off very uniformly with harmonic number. However, there is a danger in interpreting this feature of emission spectrum too literally. It must be remembered that the spectrum is obtained by sweeping the magnetic field and the nature of the discharge depends strongly on this parameter. The magnetic field affects everything from the radial density profile and the discharge voltage to the electron cyclotron radius. In addition, the overlapping of adjacent emission lines must be considered.

Due to the overlap of the emission lines, it is difficult to observe the very high numbered harmonics. The emission line width is

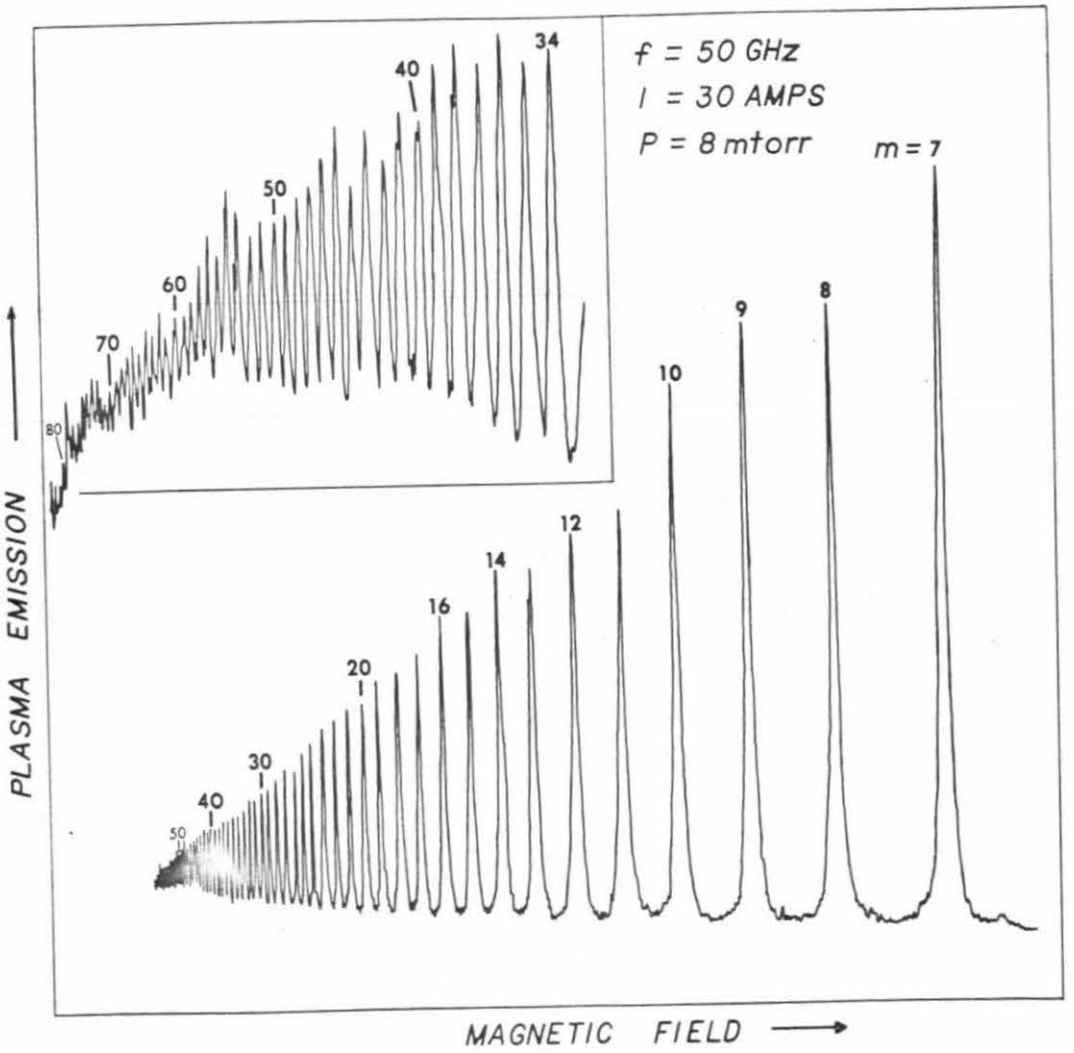

Figure 3.13 The Harmonic Emission Spectrum Obtained with a 50 GHz Receiver

nearly independent of the harmonic number and at 50 GHz is typically given by $\Delta f/f \simeq 80$. As a result, harmonics $m = 80$ and $m = 81$ overlap at their half power points. Because of the broad tails of the emission lines, each emission line overlaps many other emission lines. Therefore, the higher harmonics tend to merge into a continuum in which only the tips of the emission lines can be distinguished.

The emission intensity at 50 GHz is not known very accurately. It is difficult to determine how well the 50 GHz receiver is coupled to the discharge cavity via the X-band waveguide, vacuum iris, and horn. Although the receiver was not calibrated when the spectrum of Figure 3.13 was obtained, later measurements (which were calibrated) indicate that the emission intensity at 50 GHz is somewhat less than at 10 GHz. However, the difference is less than 2 db.

3.8 Harmonic Absorption Spectrum

This experiment was initiated to determine the relationship between the absorption spectrum and emission spectrum of the plasma column. In at least one previous absorption measurement [13], observed harmonic effects were found to be dependent on the power level of the incident wave and did not exist at less than milliwatt power levels. In this investigation of harmonic emission, it is the low power level absorption spectrum which is of interest and has been measured.

A block diagram of the experiment is given in Figure 3.14. The absorption spectrum is obtained by sending a microwave signal into the discharge chamber through one horn and detecting how much of that signal comes out of the other horn. A TWT amplifier provides an incident signal which consists of broadband noise. The TWT is located

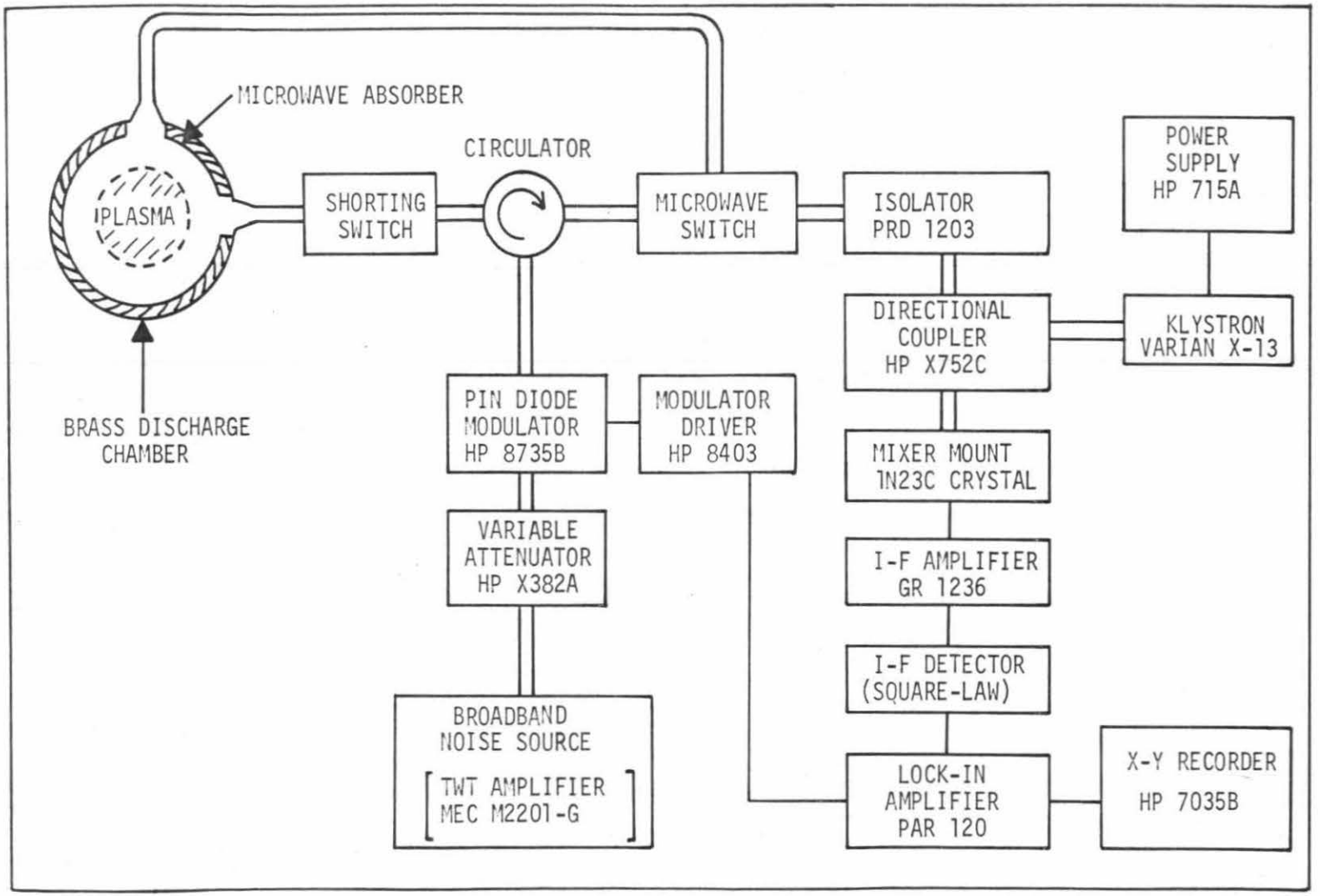

Figure 3.14 Block Diagram for Transmission and Reflection Measurement

4 meters from the solenoid to avoid effects of the magnetic field. The incident signal is square wave modulated so that it can be distinguished from the harmonic noise emission which is produced by the plasma. The incident power level is limited to an intensity no more than 10 db greater than the intensity of the harmonic emission maxima. Care is taken to ascertain that the I-F detector is very nearly square law. If this is not done, extraneous effects are observed which result from the manner in which the TWT noise combines with the harmonic noise emission of the plasma.

Both the signal transmitted through the discharge chamber and the signal reflected back out the input horn can be observed. The position of the microwave switch determines which is observed. A shorting switch allows a direct amplitude comparison to be made between the incident signal and the transmitted and reflected signals.

A typical experimental result is presented in Figure 3.15. The top curve depicts the transmission loss of the signal transmitted through the discharge chamber. This curve is closely related to the absorption spectrum of the plasma column and should reveal any harmonic structure which exists in that spectrum. The bottom curve is a harmonic emission spectrum which is presented for comparison and also to indicate the locations of the cyclotron harmonics.

The noise level for the measurement is sufficiently low that resonances as small as 0.1 db can easily be detected. Yet, absolutely nothing is observed at the harmonics, except at the $m = 2$ harmonic, where a 0.5 db resonance is easily detected.

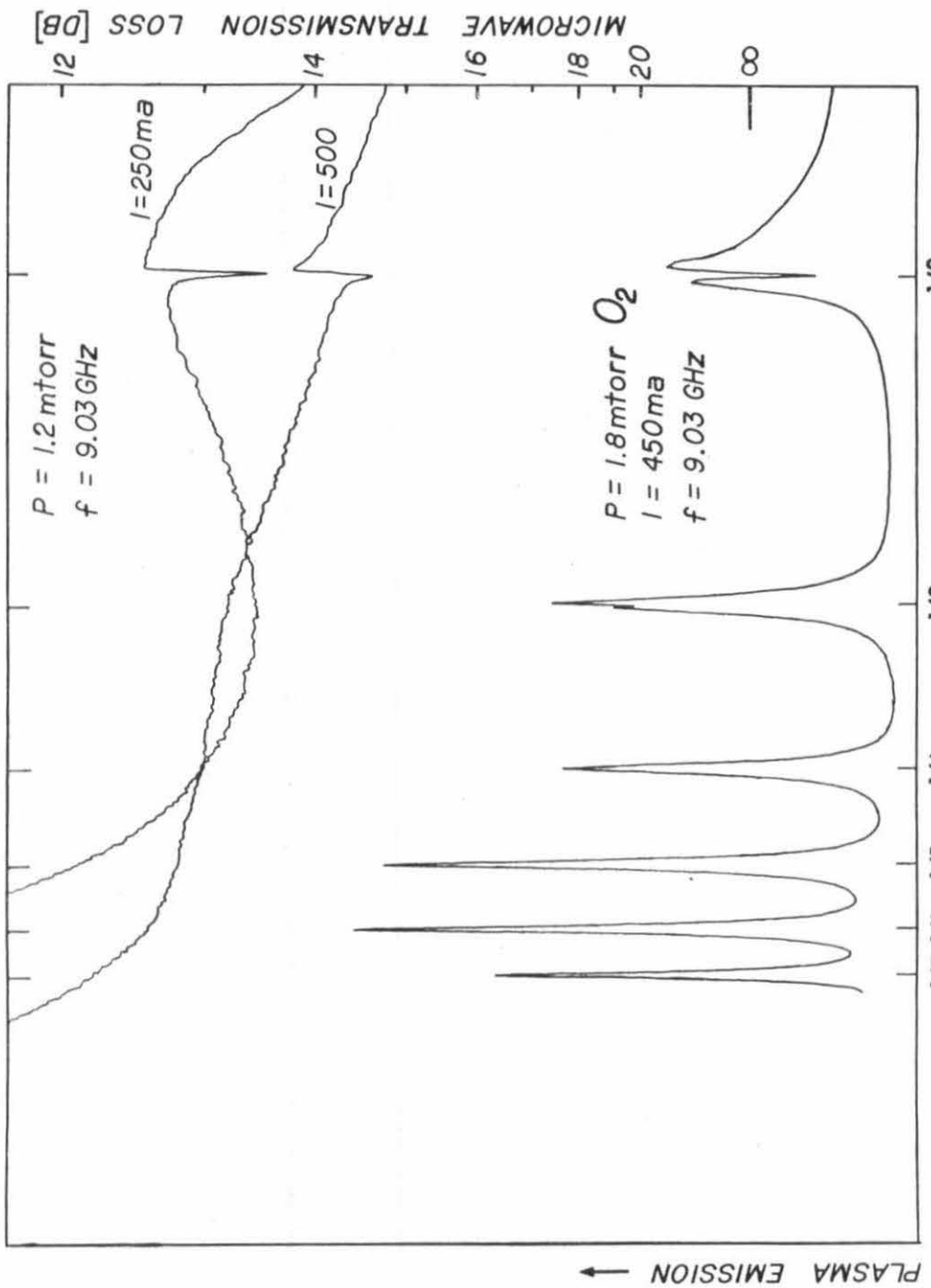

Figure 3.15 The Microwave Transmission Loss in db Relative to the Incident Signal Level. The emission spectrum is included to indicate the locations of the harmonics.

The transmission and reflection measurements were repeated in many variations. On one occasion the discharge cavity was lined with a microwave absorber as indicated in Figure 3.14. Thus, plasma absorption was investigated with the plasma column surrounded by either an absorber or a reflector. Different power levels were tried and many measurements were made using a standard microwave signal generator for the incident signal in place of the TWT. However, the same result was obtained on each occasion. No harmonic absorption effects were observed at harmonics other than the $m = 2$ harmonic. Note that this same behavior has been observed previously by Dreicer in a helium gas discharge [15].

It is concluded that in the vicinity of the higher harmonics, there is no direct relationship between the emission and absorption spectra of the plasma column. Since the plasma is not in thermal equilibrium, this result is not unexpected. It is a significant point, however, because several of the theories of harmonic emission predict a definite similarity between the absorption and emission spectra.

Returning for a moment to the resonance at the $m = 2$ harmonic, it appears to be related to the absorption dip which is observed in the emission spectrum exactly at the location of the $m = 2$ harmonic. When the neutral gas pressure is increased, both of these resonances broaden and disappear at the same rate. In fact when the pressure is very low, a similar resonance is observed in the emission spectrum at the $m = 3$ harmonic. However, the effect is quite small and the corresponding resonance is not detected in the transmission and reflection measurements. Dreicer has suggested that the resonance at the $m = 2$

harmonic of the emission spectrum might be due to either cyclotron damping or the excitation of Bernstein-like modes [15].

When the discharge current is increased slowly from a low value, it is observed that the transmission and reflection properties are virtually unchanged from the empty cavity until a critical discharge current is reached. Then absorption by the plasma increases enormously. It is believed that the onset of absorption is due to the appearance of a hybrid layer on the density profile of the plasma column. Thus, plasma absorption can be used as an indication of the plasma density. Dreicer observed that the plasma generated harmonic emission only when the plasma acted as a good absorber and concluded that the existence of a hybrid layer was a necessary condition for the emission [15].

It is found that the critical current for the onset of plasma absorption depends on the magnetic field. Therefore, if the magnetic field is swept while the discharge current is held fixed, the plasma changes from a good to a poor absorber. At high magnetic field the plasma is a good absorber. However, as the magnetic field is decreased, at some point the absorption starts to fall off rapidly and eventually becomes negligible. This behavior is partially illustrated in Figure 3.15.

It is observed that the harmonic emission disappears at the same time that the plasma absorption falls off rapidly. Therefore the sudden disappearance of the harmonic emission above a certain harmonic number is attributed to the disappearance of the hybrid layer from the plasma column as the magnetic field is decreased.

Figure 3.15 indicates that the ratio of the incident power to the transmitted power is typically 12-14 db. The reflected signal is comparable but is usually slightly larger than the transmitted signal. It is of interest to compare with the situation which exists when there is no plasma present in the discharge chamber. In that case, it is expected that roughly half of the microwave power will leave the discharge chamber through each horn and as a result both the transmitted and reflected signal levels will be reduced 3 db below the incident signal.

The experimental results indicate that when an absorbing plasma is present, most of the incident microwave signal is absorbed by the plasma. Usually more than 90% of the incident signal is absorbed and much of the remaining power is reflected because of a mismatch at the input horn. Therefore one can conclude that the combination of the plasma and the reflecting discharge chamber is a good microwave absorber.

Up to this point the discussion has been oriented toward the harmonic emission which is nonthermal in origin. In addition, there is emission present which is thermal in origin. Consider, for example, the emission which is observed well into the afterglow of the pulsed discharge. At such time, very few energetic nonthermal electrons are present in the plasma and the electron velocity distribution is approximately maxwellian. In the present experiment such thermal emission is relatively low in intensity but conveys valuable information.

The strong absorption property of the plasma column indicates that the electron temperature can be inferred from the thermal plasma

emission. The transmission and reflection measurements indicate that the plasma surrounded by a reflector is a good absorber when a hybrid layer is present on the column. Therefore, the plasma reflector system is necessarily also a good emitter of thermal radiation. The radiation temperature observed in the afterglow of the pulsed discharge should then be a good indicator of the electron temperature, provided that a good match exists between the microwave transmission line and the plasma-reflector system.

An indication of the electron temperature in the dc operated discharge can be obtained in a similar fashion if proper care is taken to eliminate the nonthermal harmonic emission from the measurement. If most of the nonthermal radiation is suppressed in some way, then the remaining emission provides an indication of the electron temperature. Such a measurement is most accurate when done between the harmonics where the nonthermal harmonic emission is minimum. In Appendix C, the electron temperature is measured using this method and the technique used to suppress the nonthermal harmonic emission is described.

3.9 Upper Hybrid Layer

3.9.1 Interferometer Measurement of Electron Density

A polar microwave interferometer is used in conjunction with profiles of the ion saturation current to determine the absolute plasma density. The pyrex discharge tube described in Section 2.3.5 was constructed to allow microwave interferometer density measurements using horns located outside of the vacuum wall. A description of the polar interferometer is given in Section 2.2.4, together with a discussion of the accuracy of the density measurement.

The microwave interferometer horns are oriented for ordinary wave propagation across the plasma column. The index of refraction of the wave is given by $N = \sqrt{\epsilon} = \sqrt{1 - \omega_p^2/\omega^2}$. Therefore, the difference in the microwave path length attributable to the presence of the plasma is given by

$$\Delta\phi = = \frac{\omega}{c} \int_{-R}^{R} [1 - \sqrt{1 - \omega_p^2(r)/\omega^2}\,]\, dr \qquad (17)$$

In a more convenient form,

$$\Delta\phi = -12.01 f \int_{-R}^{R} [1 - \sqrt{1 - 80.61\ N_e(r)/f^2}\,]\, dr \qquad (18)$$

where $\Delta\phi$ is the observed phase shift in degrees, f is the interferometer frequency in GHz, and $N_e(r)$ is the electron density profile normalized to $10^{12}/cm^3$. Note that a low density approximation for equation (18) is not valid for the parameters of the present experiment.

The plasma density is determined from the interferometer phase shift and the ion saturation current profile. The shape of the electron density profile, $N_e(r)$, is assumed to be identical to the ion saturation current profile. Computer computations using equation (18) determine the density scaling factor for which the computed phase shift, $\Delta\phi$, is equal to the observed phase shift.

Figure 3.16 shows how the phase shift of the polar interferometer increases with discharge current for several situations. At small discharge current, the phase shift increases very rapidly with increasing current. For large current the phase shift is less sensitive to the discharge current and there is a noticeable difference in behavior

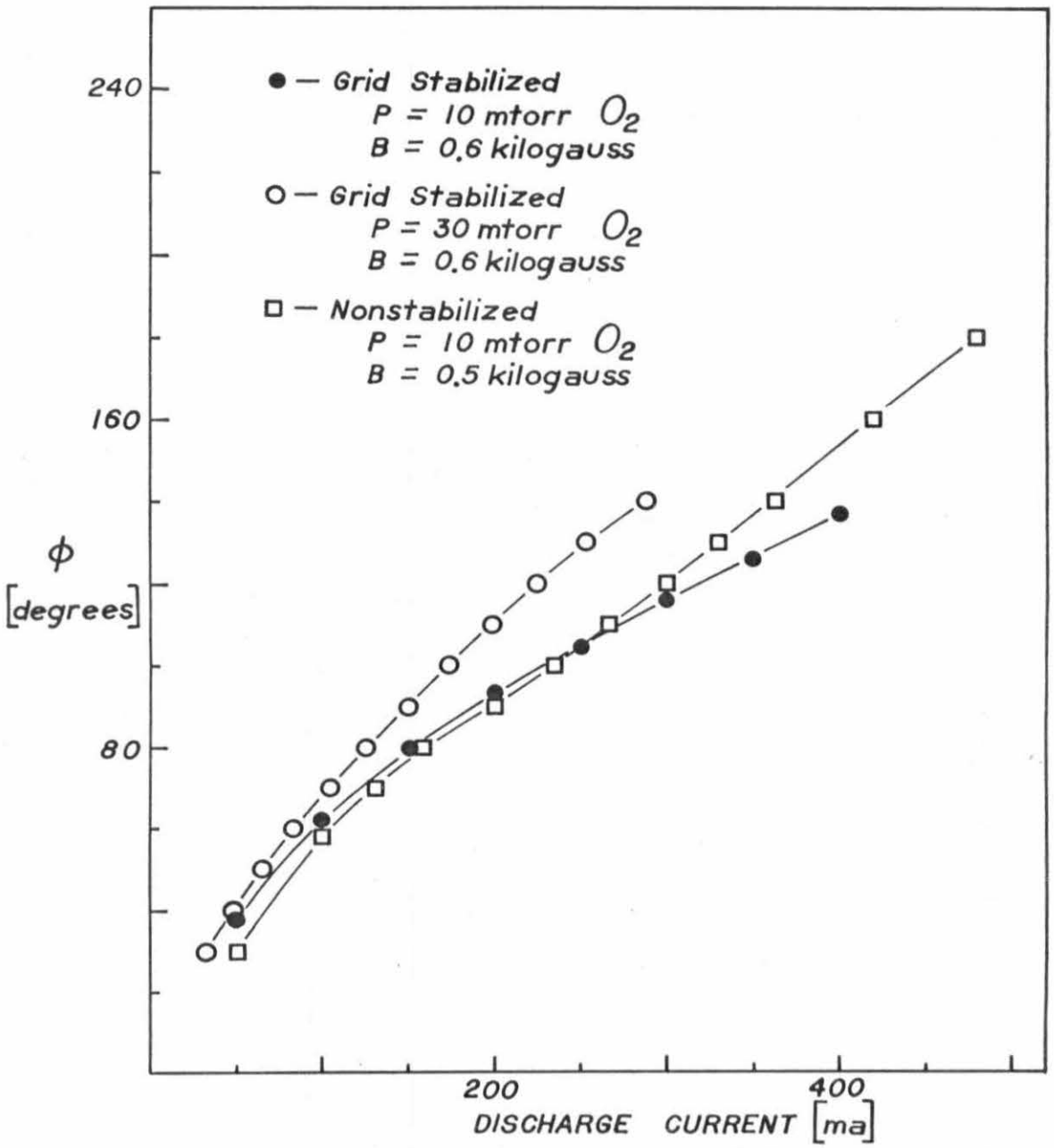

Figure 3.16 The Phase Shift Indicated by the Polar Interferometer as a Function of the Discharge Current for Several Different Situations

between the grid-stabilized and the nonstabilized discharge.

In the investigation of the onset of cyclotron harmonic noise emission, it is the maximum electron density on the density profile that is important. Although there are instances where the maximum electron density has the same current dependence as the average electron density, this is not usually the case. The shape of the density profile usually changes somewhat with the discharge current. In general, for each phase shift recorded there is a corresponding ion saturation current profile from which the maximum electron density is computed.

3.9.2 Onset of Harmonic Emission

The X-band radiometer is oriented to receive the extraordinary mode. For very low plasma densities, the radiometer indicates a radiation level slightly above room temperature. This radiation level does not change much with magnetic field or discharge current provided that the current remains small.

When the discharge current reaches the onset value, I_{ons}, the noise emission rises sharply by more than two orders of magnitude, finally reaching a saturation level at large discharge current. N_{ons} is the onset electron density. This behavior is shown in Figure 3.17 for the $m = 6$ harmonic. The same general behavior is observed at the other harmonics and also between the harmonics, with the obvious change in the saturation level.

Thus, the only dependence of the noise emission on the plasma density appears to be contained in the transition region, $N_{ons} < N_e < N_{sat}$, where N_{sat} is the plasma density at which the noise emission saturates. Outside of this region, the noise emission appears to be

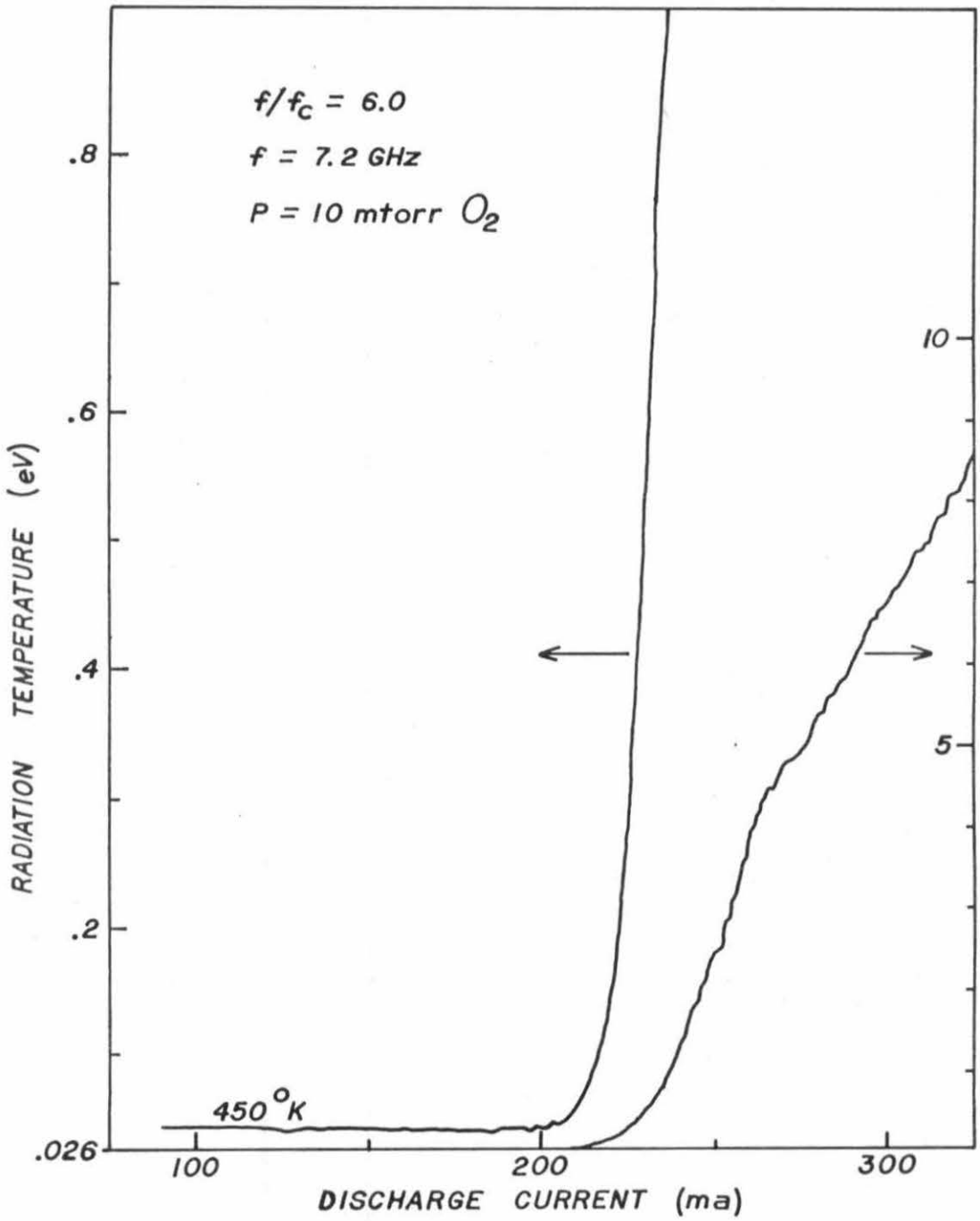

Figure 3.17 Noise Emission at the m=6 Harmonic as a Function of the Discharge Current. The detected radiation temperature increases abruptly by several orders of magnitude from a level slightly above room temperature (.04 eV) to a value close to 10 eV.

independent of the density. Therefore, the significance of the transition region will be explored in greater detail.

3.9.3 Existence of Upper Hybrid Layer

In order to investigate the dependence of cyclotron harmonic emission on the plasma density, it is necessary to record the interferometer phase shift, the ion saturation current profile, and the harmonic emission from the plasma. Figure 3.18 illustrates the axial positions at which these three measurements are carried out. The ion saturation current probe is located midway between the cathodes of the discharge, with the interferometer and radiometer microwave horns located on opposite sides. The discharge tube is accessible through the spaces between the field coils.

The microwave interferometer density measurement indicates that at the onset of harmonic emission, the maximum plasma density is typically given by $N_{ons} \cong .84\ N_H$, where N_H is the electron density which satisfies the hybrid frequency condition ($\omega^2 = \omega_H^2 = \omega_p^2 + \omega_c^2$). Since the accuracy of the interferometer density measurement is believed to be better than 10%, this result might be interpreted as an indication that the onset of harmonic emission occurs slightly before the hybrid layer appears on the plasma column. However, the onset density, N_{ons}, changes with harmonic number in just the way it should if the hybrid layer were involved. Therefore, it is necessary to consider several additional observations.

Figure 3.19 illustrates the onset of harmonic emission for the nonstabilized discharge. Graphs (a) and (b) give the maximal electron density and the harmonic emission intensity as a function of the

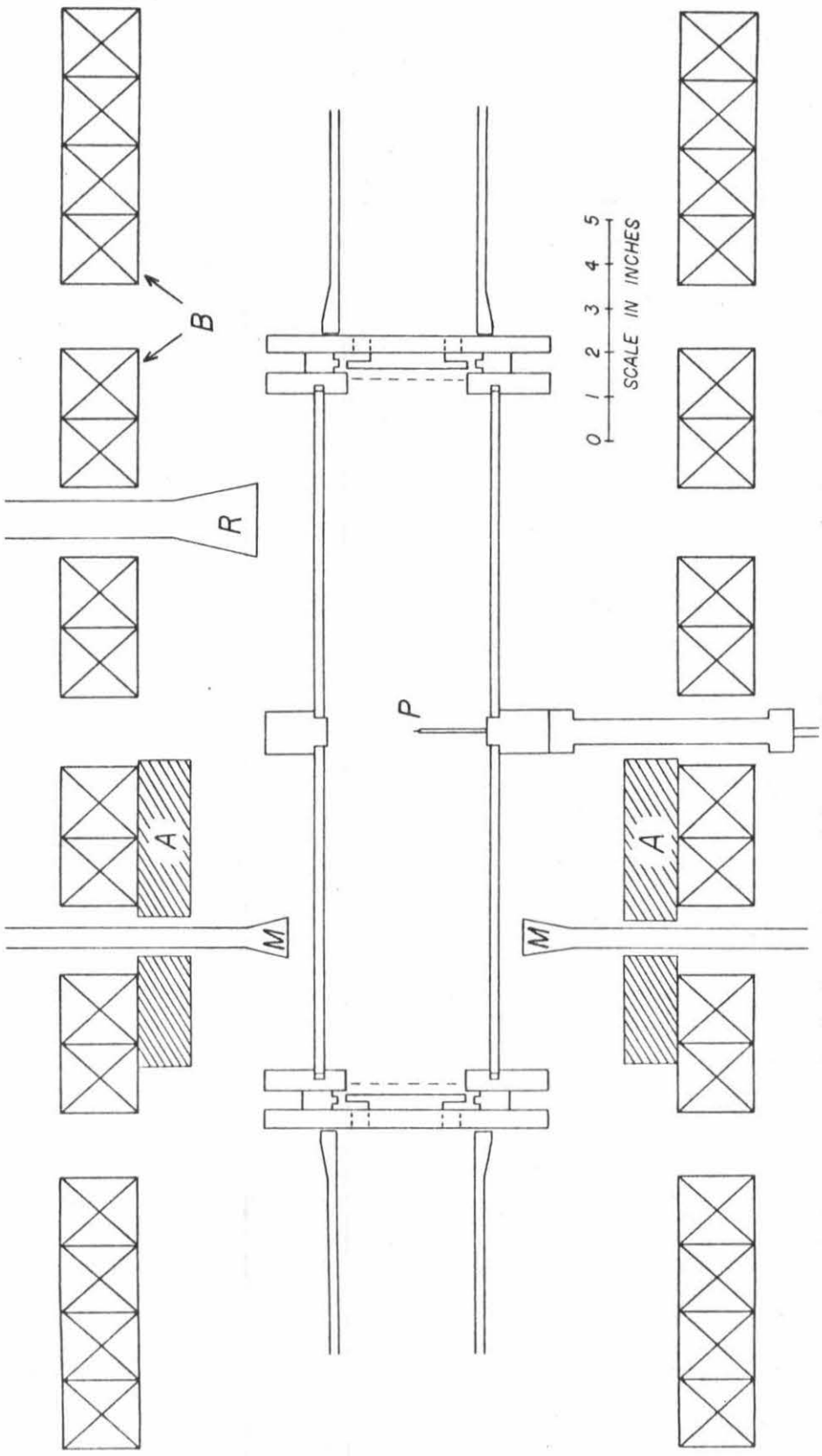

Figure 3.18 Scale Drawing of the Experimental Setup which Was Used to Investigate the Onset of Harmonic Emission. A - Microwave absorber, B - Magnetic field coils, M - Microwave interferometer horns, P = Insulated probe, R = Microwave receiver horn

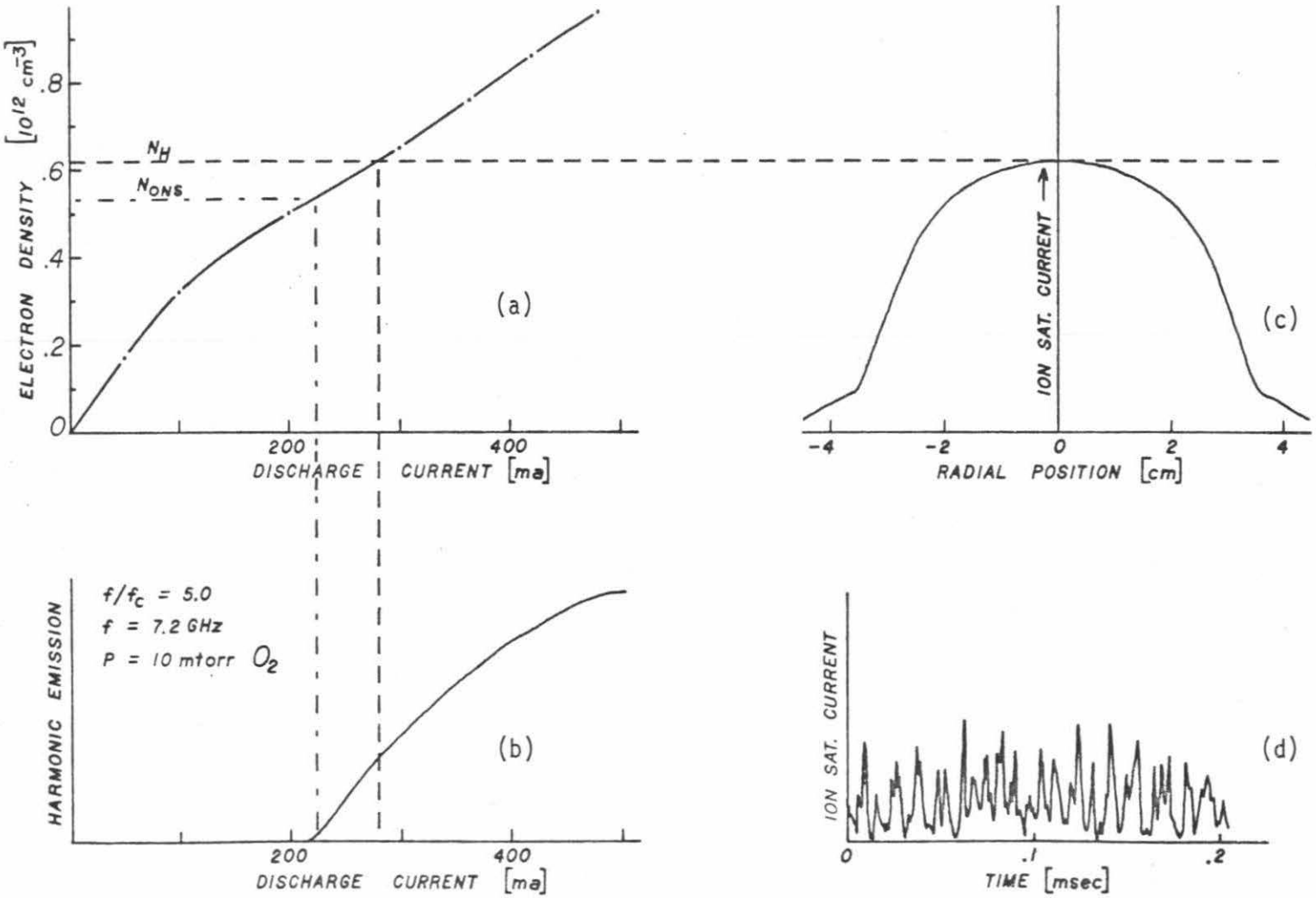

Figure 3.19 The Onset of Harmonic Emission in the Nonstabilized Discharge. The electron density, the density profile, and fluctuations in the ion saturation current are also presented.

discharge current. The radial electron density profile is presented in Figure 3.19c, and an oscillogram of fluctuations in the ion saturation probe current is given in Figure 3.19d.

The ion saturation current oscillogram, Figure 3.19d shows that the ion density undergoes large amplitude fluctuations. These fluctuations are present everywhere in the nonstabilized plasma column. The ion saturation current profile, Figure 3.19c, gives the time average density at each radial position. Similarly, the microwave interferometer density measurement gives a spatial average over the density fluctuations. Even though the time average onset density is such that $N_{ons} \cong .84\ N_H$, the magnitude of the ion density fluctuations indicates that the condition $N_{ons} > N_H$ is frequently satisfied locally. Thus, the hybrid frequency condition may be satisfied locally for a significant fraction of the time, even though it is not satisfied on an average basis.

The grid-stabilized discharge produced similar results. A typical case is shown in Figure 3.20. Noise emission onset occurs when the maximum density indicated by the microwave interferometer is such that $N_{ons} \cong 0.90\ N_H$. The ion saturation current oscillogram indicates that density fluctuations are less than 1% throughout the body of the plasma column ($R < 3$ cm), but that fluctuations are present on the surface ($R > 3$ cm). It is important to note the spatial variation of the density. This variation is due to the presence of the stabilizing grid.

Thermal expansion of the plasma heated tungsten grid wires causes them to distort, resulting in a nonuniform spacing of the grid wires. The magnitude of the resultant spatial density variation is a function of the axial distance from the location of the grids. The ion

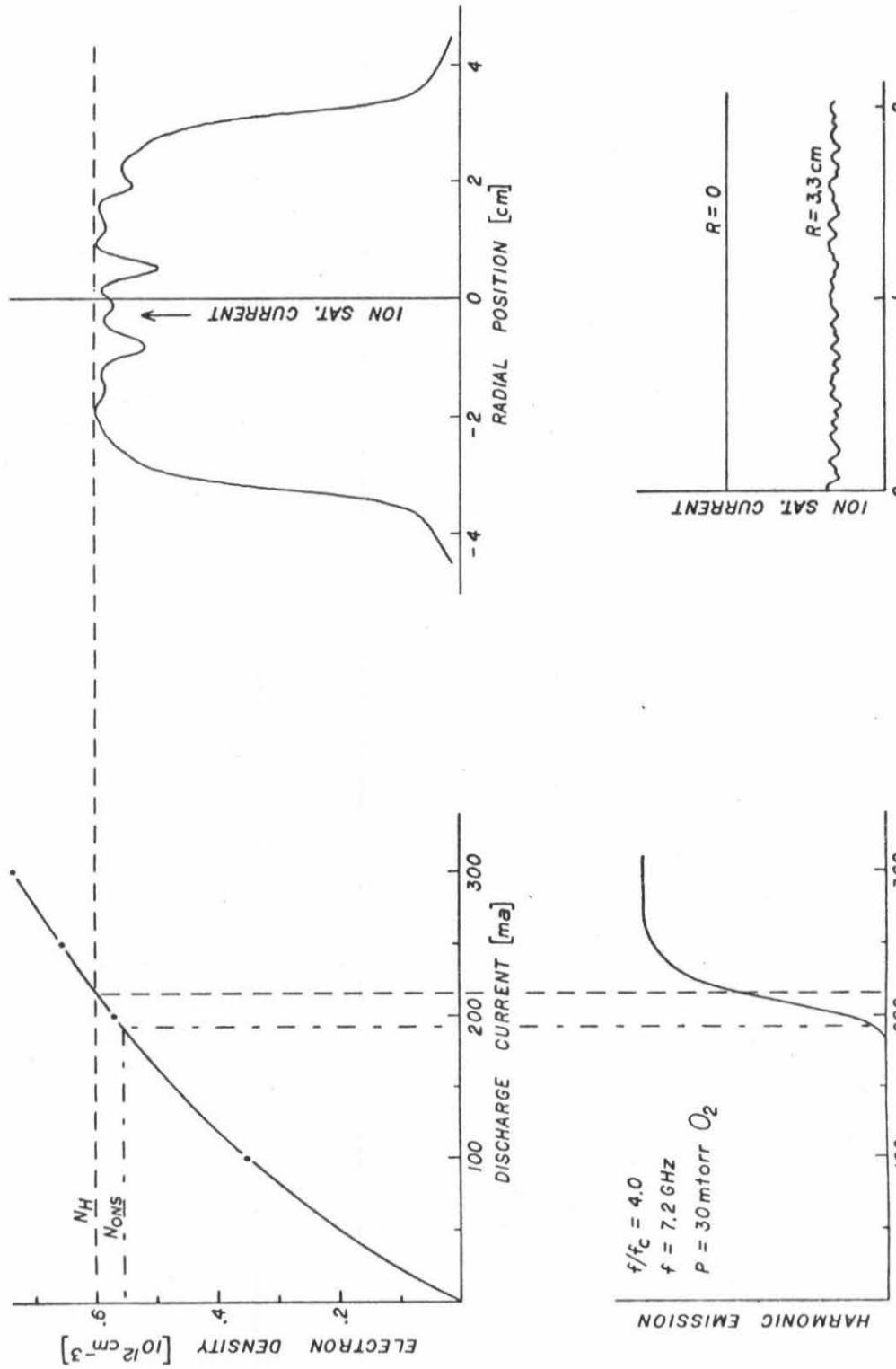

Figure 3.20 The Onset of Harmonic Emission in the Grid-Stabilized Discharge. The electron density, the density profile, and fluctuations in the ion saturation current are also presented.

saturation probe is located midway between the stabilizing grids where the spatial variation is minimal. Also, the probe tip has a finite length ($\sim$ 2 mm) which tends to average out some of the spatial variation. But most importantly, the probe has a fixed angular position, and therefore can not sample the entire cross section of the plasma column. The position of maximum density on the column cross section is probably not accessible to the probe. Although the profile obtained using the probe gives $N_{ons} \cong 0.9\ N_H$, it is very likely that there is a plasma density maximum elsewhere on the column such that $N_{max} \geq N_H$.

This hypothesis is supported by the pressure dependence of the onset condition. The magnitude of the spatial density variation is related to the pressure dependent diffusion coefficient. When the oxygen gas pressure is 10 mtorr, the spatial variation is quite large and $N_{ons} \cong .83\ N_H$. When the neutral pressure is increased by a factor of three to 30 mtorr, the spatial variation at the location of the probe is reduced by roughly 40% and $N_{ons} \cong .90\ N_H$. Thus the onset condition apparently depends on the magnitude of the spatial density variation.

It is concluded that when the existing time and spatial variations of the plasma density are taken into account, the onset of harmonic emission coincides within experimental accuracy with the appearance of the upper hybrid layer on the plasma column. Thus, the results of the microwave interferometer density measurement support the findings of Dreicer, that the existence of the upper hybrid layer is a necessary condition for the harmonic emission [15].

In addition to the hybrid layer onset criterion, the plasma density measurement provides further information about the transition region following the onset of the harmonic emission. The bulk of the measurements indicate that the harmonic emission saturates when the hybrid layer reaches a radial position of 2.5-3.0 cm. The emission intensity appears to increase roughly with the surface area of the hybrid layer until the dimension of the layer approaches that of the plasma column.

This may explain why the transition region for the stabilized discharge is much smaller than that for the nonstabilized discharge. The density profile of the stabilized discharge is very flat. Once the onset condition is satisfied, $N_{ons} \cong 0.9\ N_H$, only a 20% density increase is sufficient to locate the hybrid layer at a large radial position and cause the noise emission to saturate.

The nonstabilized discharge presents a somewhat different situation. The density profile is peaked at the center of the column and density fluctuations are important in the onset condition. A large increase in plasma density is required in going from a situation where a hybrid layer exists only part of the time because of density fluctuations to a situation where the hybrid layer exists on a time average basis at a radial location of $R \cong 2.5 - 3.0$ cm.

Similarly, this approach can be used to explain an observed increase in the size of the transition region with harmonic number. Figure 2.11 indicates how the plasma density profile changes with magnetic field. When the shape of the plasma density profile changes, the size of the transition region should change accordingly. A flat

profile at high magnetic field will result in a very rapid transition. On the other hand, a center peaked profile at low field will result in a prolonged transition. Since high harmonic numbers correspond to low magnetic fields, the higher harmonics should have a larger transition region. This expectation is consistent with experimental results.

Finally, it is noted that the transition from emission onset to saturation can be traversed by relatively small changes in the plasma density. In the grid-stabilized plasma column of the brass discharge chamber, it is found that under certain conditions the entire transition takes place during only a 10% change in the discharge current.

CHAPTER IV

THEORY OF HARMONIC EMISSION

4.1 Introduction

In order that a comparison can be made between theory and experiment, it is necessary to review briefly the theoretical work which has been done. A summary of the many harmonic emission theories is presented in Section 4.2. Then in Section 4.3, theory and experiment are compared on a very qualitative basis. The experimental evidence presented earlier in Chapter III is used to evaluate the various theories and determine which are relevant to the Penning discharge. The major conclusions are summarized in Section 4.4, and in Section 4.5 the motivation for further experimental work is given in terms of questions which can not be answered on the basis of existing experimental results.

4.2 Summary of Harmonic Emission Theories

As a result of many independent efforts to explain the harmonic emission observed in the experiments, a remarkable number of distinctly different theoretical models have been developed, all of which feature radiation maxima near the harmonics of the electron cyclotron frequency. Many of the theories are discussed in the reviews by Crawford [1,3] and Bekefi [2]. The common starting ground for most of the analyses is the assumption that a tenuous group of the nonthermal electrons prominent in the Penning discharge supply the energy for the nonthermal harmonic radiation. The majority of the plasma electrons constitute a dielectric medium supporting characteristic electrostatic plasma waves.

Basically, the nonthermal electrons can generate harmonic radiation in the form of either electromagnetic waves or electrostatic plasma waves. In the latter case a coupling mechanism between the electrostatic wave and the observed electromagnetic radiation is needed. The theories can also be divided into those in which the nonthermal electrons act as independent sources and those in which they act coherently. The former are single particle radiation theories and the latter include wave instabilities which result from nonmaxwellian velocity distributions and beam-plasma interactions. This review will begin with single particle radiation of electrostatic waves and will cover each of the other cases in turn.

Canobbio and Croci [49] proposed single particle excitation of electrostatic waves as a possible mechanism for the harmonic radiation observed by Landauer. They evaluated the spectral distribution of the radiation produced by a fast test electron spiralling in a uniform warm plasma in a magnetic field. Most of the radiation appears as quasi-electrostatic waves propagating nearly perpendicular to the magnetic field with frequencies near the cyclotron harmonics. The propagation characteristics of these waves in the direction nearly perpendicular to the magnetic field have been treated by many authors [50-56]. Using approximate solutions to the dispersion relation for these waves, Canobbio and Croci obtained an expression for the emission radiated by a single test electron and indicated that the width of the emission line is determined by Landau damping.

In this model the energy which sets up the propagating electrostatic waves in the plasma comes from the slowing down of energetic

electrons through the interaction of the electrons with the dielectric plasma medium. Basically, the polarization cloud of an energetic test electron exerts a drag force which slows down the electron.

For a plasma in thermal equilibrium, all of the plasma electrons contribute toward a thermal spectrum of electrostatic waves. However, when nonthermal electrons are present, the radiation at the harmonics is enhanced principally by those nonthermal electrons whose velocity component perpendicular to the magnetic field $V_\perp$ exceeds the phase velocity of the electrostatic wave, $V_\perp \geq V_{ph}$. Note that the phase velocities of the electrostatic waves are comparable to the electron thermal velocity.

Stone and Auer [57] extended the calculations of Canobbio and Croci to obtain the shape of the emission line. However, they limited their investigation to the weakly damped solutions of the dispersion relation which are excited when $V_{||}^2 >> V_{th}^2$, where $V_{||}$ is the velocity component of the test electron parallel to the magnetic field, and V_{th} is the thermal velocity. It is well known that undamped electrostatic waves do not exist exactly at the cyclotron harmonic frequencies. As a result, Stone and Auer obtain emission lines which are displaced from the harmonic positions and find that the emission intensity for a single electron vanishes exactly at the harmonics.

Shimomura [58] carried out a similar computation but integrated over the electron velocity distribution to obtain contributions from all of the plasma electrons.

In a subsequent publication, Croci and Canobbio [59] emphasize the importance of collisionless damping in the solutions of the

dispersion relation. They calculate contributions to the emission from all waves existing in the plasma and conclude that the emission observed in the very neighborhood of the harmonics can only result from the excitation of collisionless damped waves by electrons with $|V_{\parallel}| \lesssim \sqrt{2}\, V_{th}$. The strongest emission results from such electrons spiralling in a plasma region where $\omega = m\omega_c \simeq \sqrt{\omega_p^2 + \omega_c^2}$.

Sugihara [60] has also done calculations of the radiation loss by a single electron whose velocity is much greater than the electron thermal velocity. His theory predicts that enhancement of the harmonic radiation can only result from electrons with $V_{\perp} >> V_{\parallel}$. The harmonic radiation is found to be localized to the plasma region where $\omega_p < \omega < \sqrt{\omega_p^2 + \omega_c^2}$ and the radiation maxima are located exactly at the cyclotron harmonics, $\omega = m\omega_c$.

Except for the initial investigation by Canobbio and Croci, conversion of the excited electrostatic wave energy to the electromagnetic radiation which is detected in the experiments has not been considered in the theoretical investigations referred to above. Stix [61] and others [62-65] have considered the mode conversion which takes place in a nonuniform plasma near the upper hybrid layer, $\omega_H = \sqrt{\omega_p^2 + \omega_c^2}$. A different conversion mechanism has been treated by Boyd [66] who considered mode conversion of propagating electrostatic waves via scattering from ion density fluctuations.

Up to this point, only single particle radiation theories have been considered. In each of the above calculations, the total electrostatic radiation can be estimated by assuming complete incoherence

between the radiating electrons. Instabilities have been neglected.

Crawford [67] and Bers [68] have pointed out that the emission may be due to electrostatic wave instabilities excited by the energetic electrons present in the Penning discharge. Crawford [1,3] has reviewed much of the early theoretical work which has been done on a wide variety of instabilities that result from anisotropic velocity distributions and particle beams. A more recent bibliography is to be found in the publication by Seidl [69].

Most of the relevant theory of wave instabilities has been developed in terms of a dispersion relation which is based on the quasistatic approximation. As a result, mode conversion of the unstable modes is again involved.

In the Penning discharge the group of electrons which is most likely to excite a plasma-wave instability is the secondary electron beam which originates from the cathodes. The beam has a finite temperature. Other groups of nonthermal electrons present in the discharge are characterized by a very substantial velocity spread, as indicated in Chapter II. Since the relative number density of energetic electrons in the Penning discharge is small, the theoretical results which are most applicable are those which consider a diffuse group of energetic electrons in an otherwise maxwellian plasma. It is important to consider the velocity spread of the energetic electrons.

In this respect, the theoretical analysis of Seidl is very useful [69]. He characterizes his publication as an "Experimentor's Guide". The theory predicts the frequency, wavelength, and growth rate of the most unstable quasistatic wave that results from the interaction of

either a parallel or a helical beam with a maxwellian plasma. Effects of the plasma temperature and the large velocity spread of the beams are investigated in detail. The theoretical results obtained by Seidl will be discussed in greater detail in Chapter V.

Recently, Kaladze and Stepanov [70] analyzed an instability in a plasma containing a low density group of energetic electrons with a humped isotropic velocity distribution. The theoretical results have been used to explain the experiments of Vasiliyev et al. [21].

Moving on to a different class of theories, Neufeld and Wiginton [71] do not invoke the electrostatic approximation in their theoretical investigation. They present a treatment of the interaction of a helical electron beam with a stationary plasma and find that electromagnetic waves propagating nearly perpendicular to the magnetic field can be excited at the electron cyclotron harmonics. The radiation easily escapes from the plasma since mode conversion is not necessary. Further work in this area has been done by Zayed and Kitsenko [72].

Johnston and Moore [73] postulate that a ring of electrons is trapped at the midplane of the plasma column by cusp-like electric fields. They find that an annular ring of trapped electrons rotates collectively at the cyclotron frequency and exhibits free modes of vibration at all harmonics of the electron cyclotron frequency. If the uniform current of the rotating ring is turbulence modulated, electromagnetic radiation results.

Several single particle radiation mechanisms have been proposed which result in electromagnetic radiation predominantly at the harmonics of the electron cyclotron frequency.

Kuckes and Dawson [74] evaluated the radiation which results when a high energy electron repeatedly crosses the hybrid layer region in a non-uniform plasma. The hybrid resonance region can be much thinner than the cyclotron radius of a thermal electron. When fast electrons repeatedly pass through the resonance region, important perturbations of the electron trajectory occur leading to excitation of plasma oscillations. These oscillations couple through the evanescent region immediately outside the hybrid layer to the vacuum radiation field. The resulting emission exhibits peaks at the harmonics of the electron cyclotron frequency.

Simon and Rosenbluth [75] find that when a particle with a velocity component perpendicular to the magnetic field experiences periodic elastic collisions with a rigid wall, the resulting radiation has a large harmonic content. Similar radiation results when periodic changes in the electron trajectory occur due to collision with a plasma sheath instead of a wall.

Another possible explanation by Rauchle [76] considers the electromagnetic radiation which results from the interaction of spiralling electrons with the shielded ions in the plasma. This radiation was called magnetic bremsstrahlung.

Persson, Johnson, and Uhlenbrock [77] calculated the electromagnetic radiation which results from the interaction of the space charge wake attached to the high velocity electrons with fluctuations in the ion density. Nonuniformities in the ion positions resulting from thermal fluctuations are found to be sufficient to allow electromagnetic

radiation. It is expected that the emission will be enhanced by turbulent fluctuations in the ion density, a condition which is characteristic of the nonstabilized Penning discharge.

There are some indications that the harmonic emission might be related to the low frequency macroscopic instabilities which are prominent in the Penning discharge. Klan [24] has experimentally demonstrated a correlation between the harmonic radiation and a rotational instability. Datlov [78] has suggested that the harmonic radiation might be related to the inverted ion magnetron spiral drift wave instability.

4.3 Comparison of Theoretical and Experimental Results

There are many conceivable explanations for the emission which is observed in the Penning discharge at the harmonics of the electron cyclotron frequency. Keep in mind that throughout this report we are only seeking to identify the dominant harmonic emission mechanism in the Penning discharge. It is very possible that others are present to a lesser extent, but they are not of major interest here. Fortunately there is a sufficient variety of experimental evidence available to conclude that most of the theories reviewed in Section 4.2 are not relevant to the Penning discharge.

This section begins with a list that summarizes several of the basic features of the harmonic emission which is observed in the Penning discharge. In the discussion which follows, it is demonstrated that many of the theories are basically incompatible with the considered experimental evidence and therefore can not account for the bulk of the harmonic emission. Several promising theoretical possibilities

emerge from the analysis.

The following basic features of the harmonic emission of the Penning discharge have been established by the experiments:

1. In the vicinity of the higher harmonics, there is no apparent relationship between the absorption spectrum of the plasma column and the emission spectrum. Since harmonic absorption effects are not observed at the higher harmonics of the electron cyclotron frequency, the theory should not predict any.
2. The existence of an upper hybrid layer on the plasma column is a necessary condition for the observation of harmonic emission. As the plasma density is increased, there is a sharp onset of harmonic emission when the hybrid layer condition is satisfied. Therefore, the hybrid frequency should be a characteristic frequency in the theory.
3. The harmonic emission is not significantly affected by either the radial electric field, the low frequency drift instabilities, or the plasma turbulence which are so characteristic of the nonstabilized Penning discharge. Therefore these aspects of the plasma need not be included in the theory and certainly the theory should not be based on them.
4. The harmonic emission lines, which are nearly symmetrical in shape, are located at the harmonics of the electron cyclotron frequency. The theory should predict the same.
5. The power received by the microwave horn, which is only a small fraction of the total power radiated by the plasma column of the pyrex discharge tube, amounts to approximately 1.6×10^{-18} watts/Hz ($T_r \simeq 10$ eV). The theory must be capable of generating at least as much emission from a relatively small number of energetic electrons.

In order to properly evaluate the theories, it is essential to recognize that many of them involve extensive approximations. Those

characteristics of the harmonic emission which have been included in the list were chosen because they are very basic and are least sensitive to such approximations. Although the last feature in the list is quantitative, it is only used as an order of magnitude guide.

The discussion which follows concentrates on the discrepancies which exist between the experimental evidence and the various theories. This process is essentially an elimination procedure. For this reason the theories which are basically compatible with the evidence will not be discussed here except in the summary at the end.

A number of theories predict that the absorption and emission spectra should be closely related. These include the theories of Simon and Rosenbluth [75] and of Kuckes and Dawson [74]. In fact, it is the absorption spectrum which is calculated by Kuckes and Dawson. They then apply Kirchhoff's law to obtain the emission spectrum. Several additional theories, including those of Johnston and Moore [73] and of Rauchle [76], also expect absorption at the harmonics of the electron cyclotron frequency. However, absorption resonances at the higher harmonics of the electron cyclotron frequency are not observed in the Penning discharge.

In general, it is difficult to reconcile the strong plasma density dependence of the harmonic emission with the electromagnetic radiation theories. The experimental evidence strongly favors the concept of excitation of quasi-electrostatic waves by nonthermal electrons, followed by mode conversion at the hybrid layer. The hybrid layer is then a necessary condition for the harmonic radiation, a feature which is in good agreement with the experimental evidence.

The hybrid frequency does not emerge as a characteristic frequency in most of the electromagnetic theories. The existence of a hybrid layer is not essential in the theories of Simon and Rosenbluth [75], Johnston and Moore [73], Rauchle [76], or Boyd [66]. In fact, the existence of a hybrid layer is detrimental to these radiation processes. Electromagnetic radiation can not escape from the plasma volume inside of the hybrid layer where the propagation of electromagnetic waves is severely restricted. Although the plasma density is a parameter in these theories, the complete absence of harmonic emission even when the plasma density is only slightly below the onset density is not predicted by the theories.

Similarly, in the theory of Neufeld and Wiginton [71] emission in the vicinity of the higher harmonics can only occur when $\omega > \omega_p$. The existence of a hybrid layer again appears to be detrimental. When there is no hybrid layer present on the plasma column, the emission process can be operative throughout the plasma volume. However, when a hybrid layer is present, emission is confined to the thin plasma region outside of the hybrid layer. The emission process is then a surface effect and the applicability of uniform plasma electromagnetic theory is questionable.

According to the theories of Persson [77], Boyd [66], and Johnston and Moore [73], the harmonic emission intensity should be sensitive to ion density fluctuations and turbulence. Boyd expects considerable enhancement of the harmonic emission intensity in the Penning discharge because of strongly nonequilibrium fluctuations of the ion density. Experimentally, ion density fluctuations and

turbulence are reduced by several orders of magnitude through grid stabilization of the plasma column. However, only a minor change in the amplitude of the harmonic emission is observed.

That grid stabilization of the plasma column does not greatly affect the harmonic emission is significant for other reasons as well. Since grid stabilization of the plasma column nearly eliminates low frequency drift instabilities, it appears that such instabilities are not involved in the emission process. Also, turbulence is likely to have a much greater disruptive effect on electrostatic wave instabilities than on single particle radiation mechanisms.

In addition, grid stabilization of the plasma column results in major changes in the radial electric field and the density profile. The amplitude of the radial electric field is important in the theory of Simon and Rosenbluth [75] and the nature of the density profile in the vicinity of the hybrid layer is important to the theory of Kuckes and Dawson [74]. However, grid stabilization has only a minor effect on the harmonic emission spectrum.

In the theories of Stone and Auer [57], and Shimomura [58], the harmonic emission lines can not be located exactly at the harmonic positions but must be displaced by an amount which depends on the plasma density. The expression for the emission intensity obtained by Stone and Auer vanishes exactly at the cyclotron harmonic frequencies. A similar shifting of the location of the emission lines is predicted by the theory of Simon and Rosenbluth [75]. In contrast, the harmonic emission lines observed in the Penning discharge are located exactly at the cyclotron harmonics and do not shift position when the plasma

density is varied.

Many of the single particle radiation theories have been developed to the extent that an expression for the emission intensity is available. In the case of a collective wave instability, it is much more difficult to predict the emission intensity, since only the linear growth rate is known. In most cases, however, such instabilities can easily account for the intensity of the observed emission, which seldom exceeds the thermal emission level by more than 20 db. Nevertheless, it is of interest to compare the emission intensities predicted by the various independent particle theories because many fall orders of magnitude short of the experimentally observed emission intensities.

For the purpose of comparison, it is necessary to use the experimental results which were obtained using the pyrex discharge tube. It is difficult to interpret the emission intensity observed in the metal discharge chamber because the plasma column reabsorbs much of the emission and it is therefore impossible to determine the total emission from the plasma column. In the case of the pyrex discharge tube, it is assumed that the plasma column radiates uniformly in all directions and it is surrounded by a perfect microwave absorber so that none of the emitted signal is reflected back onto the plasma column. The microwave horn is located 9 cm from the axis of the plasma column.

For the pyrex discharge tube, the observed equivalent radiation temperature or antenna temperature is typically given by T_A = 10 eV, where T_A is the antenna temperature at the cyclotron harmonics. The antenna temperature can be expressed in terms of the "brightness

temperature" of the plasma,

$$T_A = \frac{\int T_B(\theta,\phi)\, G(\theta,\phi)\, d\Omega}{\int G(\theta,\phi)\, d\Omega} (1 - \Gamma)$$

where $G(\theta,\phi)$ is the gain function of the microwave antenna, $T_B(\theta,\phi)$ is the "brightness temperature" of the source, and Γ is a reflection coefficient which accounts for the mismatch between the antenna and the line [79].

In the present situation, the plasma column does not entirely fill the radiation pattern of the antenna. In addition, there is a slight mismatch between the antenna and the microwave transmission line. As a result the observed antenna temperature, which is an average temperature, is less than the brightness temperature of the plasma column. The power flowing in in the waveguide is related to the brightness temperature of the plasma column by the relationship $P = kT_A = skT_B$ where s is a fractional number given by

$$s = \frac{\int T_B(\theta,\phi)\, G(\theta,\phi)\, d\Omega}{T_B \int G(\theta,\phi)\, d\Omega} (\Gamma - 1)$$

In the present experimental configuration, s is estimated to be roughly 0.5.

Thus, the radiation produced by the plasma column at the harmonics of the electron cyclotron frequency has the same intensity as that from a blackbody column of the same dimensions but at a temperature which is approximately twice the observed antenna temperature of 10 eV.

The power flux for a single polarization from a blackbody surface is given by

$$\pi I_B = \pi \frac{\nu^2}{c^2} kT_B = \frac{\pi}{\lambda^2} kT_B \ (\text{watts/M}^2\text{Hz})$$

Therefore a brightness temperature of 20 eV corresponds to an intensity of 10^{-18} watt/cm^2 Hz at the plasma surface, assuming a wavelength of 3.3 cm.

Note that the volume to surface ratio of the plasma column is given by R/2 = 1.5 cm. Therefore, if the harmonic generation mechanism is a volume effect instead of a surface effect, the mechanism must be capable of producing 0.7×10^{-18} watt/cm^{3}Hz at the harmonics of the electron cyclotron frequency.

Many of the single particle radiation theories can not account for this emission intensity, which is observed experimentally in the Penning discharge. The theories of Kuckes and Dawson [74] and Simon and Rosenbluth [75] predict emission intensities which are too low by two or three orders of magnitude. Both Rauchle [76] and Persson [77] predict even lower emission intensities. The mode conversion mechanism of Boyd [66] gives an emission intensity approximately five orders of magnitude below the observed level. Again, several of these theories are based on a thermal level of ion density fluctuations and it is expected that the emission intensity would be greatly enhanced by the turbulent fluctuations of the Penning discharge. However, this prediction has not been substantiated by the experiments which used the grid-stabilized plasma column.

Even the theory of Stone and Auer [57] does not appear to be able to account for the observed emission intensity if the neutral gas pressure is high. Since this case is marginal, it will be examined in greater detail.

From the analysis of Section 2.4 in Chapter II, the number density of energetic electrons in the energy range of 15-200 eV can be estimated to be $5 \times 10^7/cm^3$ when the oxygen gas pressure is 30 mtorr. Stone and Auer found that the emission intensity for a single test electron is given by the equation

$$\left(\frac{dW}{dtd\omega}\right)_{\omega \simeq m\omega_c} = \frac{e^2}{8\pi^2} \frac{\omega}{V_{||}} J_m^2 \left(\frac{k_\perp V_\perp}{\omega_c}\right)$$

subject to the condition $V_{||}^2 >> 2V_{th}^2$. Assume that all of the emission originates from a 1 cm thick plasma layer in the vicinity of the hybrid resonance. In order to account for the experimental results, the above equation should predict an emission intensity of at least 10^{-18} watts/cm^2 Hz from only 5×10^7 energetic electrons.

A rough estimate of the emission intensity near the $m = 4$ harmonic can be obtained by setting $\frac{1}{2} mV_{||}^2 = 10$ eV and $\omega = 9$ GHz. The maximum emission occurs at the first maximum of the J_4 Bessel function, where $k_\perp V_\perp/\omega_c = 5.3$. The emission intensity is then

$$\frac{dW}{dtdf} \simeq 8 \times 10^{-19} \text{ergs/sec Hz} = 8 \times 10^{-26} \text{watts/Hz}$$

Therefore 5×10^7 "similar" electrons would result in an emission intensity of 4×10^{-18} watts/Hz.

Although this might at first appear to be sufficient to account for the experimentally observed intensity, it is clear that the calculation is a significant overestimate. First of all, most of the energetic electrons do not have the same velocity components as the first test electron and therefore do not maximize the expression for the emission intensity. The emission intensity falls off rapidly when $V_\perp$ departs significantly from the value which maximizes the Bessel function, $V_\perp = 5.3\ \omega_c/k_\perp$. The emission intensity is also inversely proportional to $V_{||}$, and many of the indicated energetic electrons possess a much larger value of $V_{||}$ $(\frac{1}{2} mV_{||}^2 >> 10$ eV) .

In addition, only a fraction of the excited electrostatic wave energy is converted to electromagnetic radiation. Since only a small part of the cubic centimeter plasma volume is immediately adjacent to the hybrid layer, electrostatic wave energy will be reabsorbed in the plasma through collisional damping of the propagating electrostatic waves. Also, mode conversion losses have been ignored. A more realistic estimate of the emission intensity would fall short of the experimental value by an order of magnitude. Therefore it is difficult to account for the emission intensity observed at high pressures by using the theory of Stone and Auer.

It might be argued that electrons with energies less than 15 eV are also important in the above calculation. However, the results of Chapter V indicate that this is not the case.

4.4 Summary of the Comparison

In summary, it is found that many of the theories are incompatible with the experimental evidence in several ways. The preceding discussion helps to establish the relative importance of the various harmonic radiation theories with respect to the Penning discharge by indicating which theories can not account for the greater part of the observed radiation. This analysis does not rule out the possibility that these same theories might in fact account for smaller amounts of radiation. It is also interesting to note that several of the theories which are not found to be relevant in the Penning discharge have been useful in explaining harmonic emission which is observed in other types of plasma sources [9,12,80-83].

Although the preceding analysis rules out many of the possible harmonic radiation mechanisms, several promising theoretical possibilities still remain. They include single particle radiation of electrostatic waves as described by Canobbio and Croci [59] and Sugihara [60]. In particular, these approaches are in agreement with the observed emission intensities and the fact that the emission lines are located at the harmonics of the cyclotron frequency. They are also compatible with the hybrid layer condition and the differences between the absorption and emission spectra.

Electrostatic wave instabilities are also a likely possibility. They can certainly account for the observed emission intensity and the observed differences between the absorption spectrum and emission spectrum. Several such theories, for example the helical beam model of

Seidl [69], predict emission exactly at the harmonics of the electron cyclotron frequency. And regardless of how the electrostatic waves might be excited, the necessity of an upper hybrid layer in the mode conversion process is compatible with the experimental evidence.

The theories which have been ruled out by the preceding analysis are principally the electromagnetic radiation theories. The sharp onset of the harmonic emission at a critical plasma density, corresponding to the existence of a hybrid layer on the plasma column, is not generally compatible with the electromagnetic radiation theories, but instead indicates that electrostatic waves play an important role in the emission process. In addition, most of the single particle electromagnetic radiation theories predict insignificantly low emission intensities and several predict a direct relationship between the absorption and emission spectra.

Several single particle electrostatic radiation theories also seem to be ruled out by the analysis. The theories of Stone and Auer[57] and of Shimomura [58] do not predict emission exactly at the harmonics and have some difficulty in accounting for the observed emission levels. In addition, the possibility that the harmonic emission is associated with the radial electric field, the low frequency drift instabilities, or the turbulence of the Penning discharge seems to be ruled out by the experimental work which was carried out on the grid-stabilized discharge.

4.5 The Role of Additional Experimental Work

Before the harmonic radiation mechanism can be positively identified, much additional experimental work is needed. The choice

between excitation of electrostatic waves by single independent electrons as in the theory of Canobbio and Croci [59], or by a wave instability as in the helical beam theory of Seidl [69] appears to be one of the principal unresolved questions. From a theoretical viewpoint, it would also be useful to know which particular group of nonthermal electrons in the Penning discharge is responsible for the harmonic emission. Unfortunately the experimental evidence presented up to this point is not very useful in providing conclusive answers to these questions. Therefore it is of interest to develop new experiments, such as the pulse modulation experiment to be described in Chapter V, which can resolve such questions.

It would also be hoped that a new experimental approach might uncover an additional strong parameter dependence which can contribute toward identification of the radiation mechanism. Up to this point, only one parameter has been identified on which the harmonic emission has a strong dependence: the plasma density. The sharp onset of the harmonic emission at the critical density has been invaluable in the consideration of the many possible theoretical models.

In this respect, it is interesting that in the pulsed experiments described in Section 3.7, the harmonic emission intensity appears to be strongly influenced by the discharge voltage. This effect will be examined in detail in Chapter V where it is found that the harmonic emission can be switched on or off by manipulating the cathode voltage. Also, when the emission is turned on or off, the corresponding rise and fall times on the harmonic emission can be measured. The response time of the harmonic emission provides valuable additional clues about

the generation mechanism.

The pulse modulation experiment of Chapter V provides a new experimental approach which may lead to positive identification of the source of the harmonic emission in the Penning discharge. The experimental results which are obtained provide some answers to the questions which could not be answered on the basis of the experiments described in Chapter III.

CHAPTER V

THE PULSE MODULATION EXPERIMENT

5.1 Introduction

The experimental results which have been presented up to this point are not sufficient to positively identify the harmonic emission mechanism. It appears that the harmonic emission process involves the excitation of electrostatic waves followed by mode conversion at the hybrid layer as described by Stix [61]. However, it is not clear whether the electrostatic waves are excited by independent electrons as in the single particle radiation theory of Canobbio and Croci [59] or through a wave instability such as that described by the helical beam theory of Seidl [69]. In addition, it is not clear which group of energetic electrons in the Penning discharge is responsible for the harmonic emission.

The pulse modulation experiment described in this chapter will seek to clarify these points. The principal topics which are investigated in the experiment include the relaxation time of the harmonic emission, the dependence of the harmonic emission amplitude on the discharge voltage, and the source of a different kind of high intensity nonharmonic radiation which can be excited by pulse modulation.

Originally, the pulse modulation experiment was undertaken to investigate the time response of the harmonic emission as observed in a pulsed plasma. The relaxation time of the harmonic emission is a new type of information which has not been available in previous investigations of harmonic emission. Yet, it appears to be the kind of

experimental information which is needed if the harmonic emission mechanism is to be identified. For example, the relaxation time seems to indicate which electrons are responsible for the harmonic emission.

In the pulse modulation experiment it is demonstrated that the harmonic emission intensity depends strongly on the operating voltage of the Penning discharge. This effect has not been documented in previous investigations. Although the proper interpretation of this result is not entirely certain, it is nevertheless a very important result.

Unexpected observations of a different type of high intensity microwave radiation proved to be very useful. The high intensity radiation is identified as resulting from a beam-plasma induced wave instability, thereby eliminating the same instability as a possible source of the harmonic emission.

Before a pulse modulation experiment could be assembled it was necessary to do some preliminary experimental work to ascertain the relaxation time of the harmonic emission so that instrumentation could be designed accordingly. This preliminary experimental work is discussed in Section 5.2.

Then, the experimental details of the pulse modulation experiment are given in Section 5.3. Pulse modulation is explained and the instrumentation and apparatus are described.

Two types of microwave radiation are observed in the pulse modulation experiment: the usual harmonic emission and a different type of higher intensity radiation. The high intensity radiation is quite unlike the harmonic emission. The radiation amplitude is several orders of magnitude greater, the radiation is well localized to the vicinity

of the cathodes of the discharge, and the frequency spectrum has minima at the harmonics of the electron cyclotron frequency. The experimental investigation of this high intensity radiation is described in Section 5.4 and the results are interpreted in Section 5.5.

Then, in Section 5.6, pulse modulation of the harmonic emission is described in detail. The relaxation time of the harmonic emission is investigated and it is found that the relaxation time decreases with increasing neutral gas pressure. It is found that the harmonic emission amplitude is strongly dependent on the cathode voltage and also that the width of the emission lines increases with the cathode voltage. These results are interpreted in Section 5.7.

The chapter ends with a discussion of the significance of the results of the pulse modulation experiment, Section 5.8.

5.2 Preliminary Experimental Work

The pulse modulation experiment evolved as a result of exploratory work carried out in the pulsed discharge. Interesting effects had always been observed whenever the Penning discharge was operated on a pulsed basis. For example, in the pulsed experiment described in Section 3.7, the harmonic emission intensity appears to be strongly influenced by the discharge voltage. After the discharge voltage has dropped, the plasma column does not produce very much harmonic emission, even though the discharge current and the plasma density are still near maximum.

The principal objective of the pulse modulation experiment is to investigate the time response of the harmonic emission. It is expected

that the decay time for the harmonic emission will provide valuable clues about the nature of the harmonic emission process and might give some indication as to which group of energetic electrons is responsible for the emission.

This anticipation led to exploratory experimental work which established the parameters and requirements of such an experiment. In the preliminary experiment, the plasma was produced using a 1 kilovolt, 10 amp pulse generator. The breakdown pulse is typically 150 microseconds in length (2.5 milliseconds for argon) and has a risetime of 1 microsecond. A second pulse of variable length, which can be applied to the discharge at any time during the afterglow, is also available from the pulse generator. The discharge chamber is essentially that shown in Figure 2.7 and the microwave receiver for pulsed operation is diagrammed in Figure 2.1.

The exploratory work revealed that the harmonic emission disappears very rapidly in the afterglow of the discharge. The decay time for the harmonic emission is found to be much shorter than the time scales associated with changes in the electron temperature and density. In fact, the decay time could not be measured because it was found to be identical with the 1 microsecond decay time of the applied pulse. Because the decay time of the voltage waveform appearing at the cathodes of the discharge is affected by the cathode-anode capacitance ($\sim$2000 pf), an improvement of the decay time of the applied pulse would not by itself eliminate the problem.

In an effort to observe the decay time of the harmonic emission, a thyratron was used to clip the end of the applied pulse and discharge

the anode-cathode capacitance. Under these conditions, the falltime of the cathode voltage is observed to be approximately 60 nanoseconds and the decay time of the harmonic emission is found to be roughly 300 nanoseconds. In this case the emission decay time is governed largely by the response time (~180 nsec) of the 4 MHz bandwidth I-F amplifier. Therefore, it is not possible to accurately determine the response time of the harmonic emission using this experimental system.

The exploratory work was very useful in defining the requirements of the experimental system. It was these observations which led to the development of a wideband I-F system, modification of the discharge chamber to allow fast risetime pulsing and the design of a floating pulse generator.

5.3 Experimental Details of the Pulse Modulation Experiment

5.3.1 Experimental Set-Up

The experimental set-up is diagrammed in Figure 5.1. The microwave receiver, including the wideband I-F system, has already been described in detail in Chapter II and requires no further description here. The brass discharge chamber has been modified to meet the pulse risetime requirements of the pulse modulation experiment. Details of the discharge chamber are given in Section 5.3.2.

The Penning discharge is powered by a DC power supply during the pulse modulation experiment, but the voltages which appear at the cathodes of the discharge are pulse modulated using a floating pulse generator. The pulse repetition rate (typically 5 KHz) is controlled by the HP 214A pulse generator which triggers both the boxcar integrator

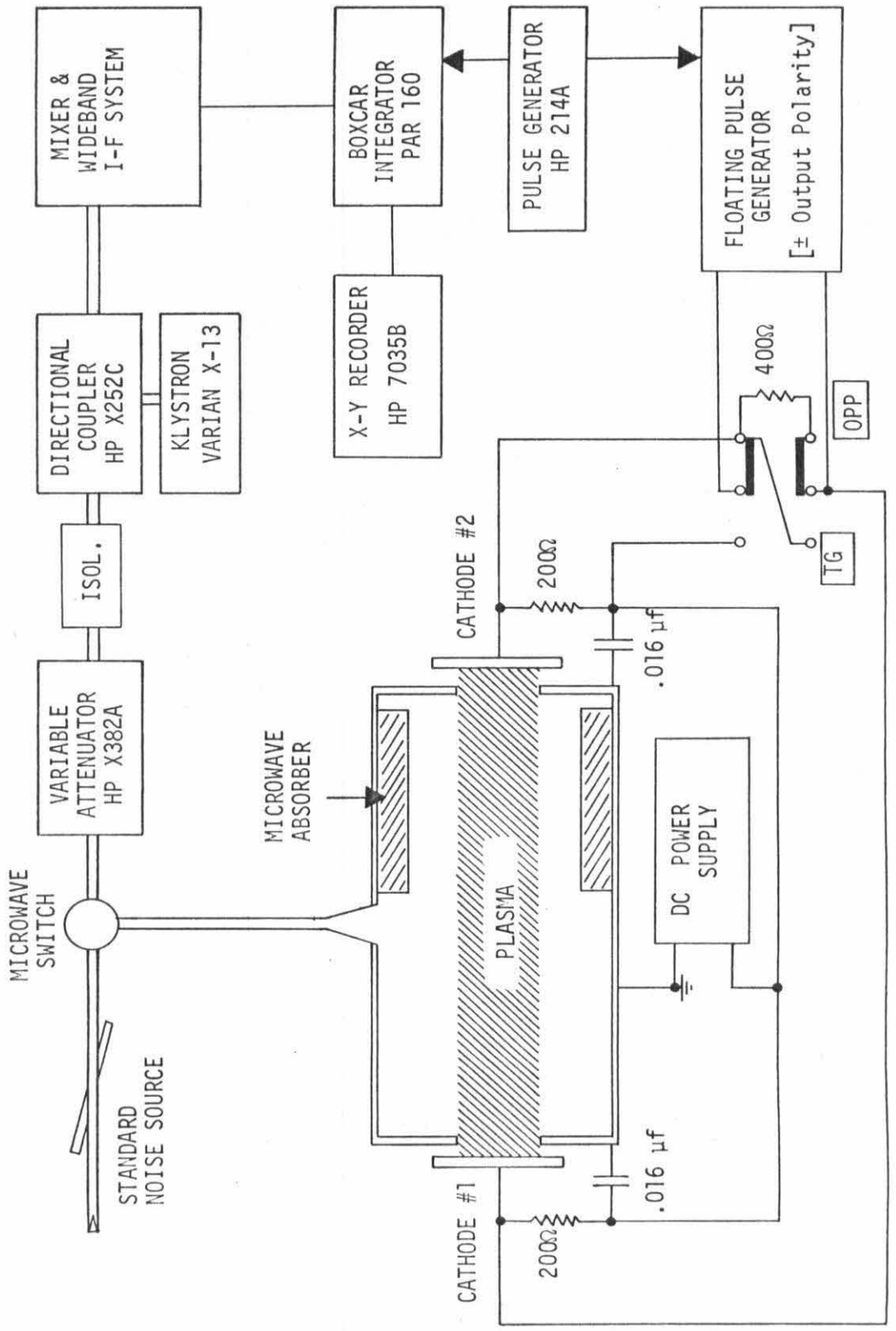

Figure 5.1 Block Diagram of the Pulse Modulation Experiment

and the floating pulse generator. The floating pulse generator, which was assembled solely for use in this experiment, is described in greater detail in Section 5.3.3. The pulse generator floats at the operating voltage of the Penning discharge and has a polarity switch which allows output pulses of either positive or negative polarity to be applied to the cathode of the discharge. The pulses are superimposed on the DC operating voltages of the cathodes of the discharge.

Some of the advantages of using the pulse modulation technique are discussed in Section 5.3.4. Then, Section 5.3.5 indicates how the plasma emission is affected by the two different modes of pulse modulation.

For simplicity, the cathodes of the discharge are only pulsed in two ways. When the mode switch is in the OPP position, the cathodes are isolated from each other and are pulsed with opposite polarity. When the same switch is in the TG position, the cathodes are connected together and as a result are pulsed together with the same polarity. In both cases the polarity switch on the floating pulse generator has a major effect. For the OPP mode, the polarity switch interchanges the waveform appearing at cathode #1 with that of cathode #2. For the TG mode of operation in which both cathodes are pulsed identically, the polarity switch changes a positive-going pulse into a negative-going pulse. Other methods of pulsing the cathodes were tried but did not result in any new plasma emission phenomena. However, for the measurement of the coefficient of secondary emission by electron bombardment described in Appendix B, only one cathode of the discharge is pulsed.

5.3.2 Modified Discharge Chamber

A sketch of the modified discharge chamber is given in Figure 5.2. The principal modification consists of the addition of the teflon O-ring spacers. They increase the separation between the anode and cathode flanges to 1/2 inch, thereby reducing the anode-cathode capacitance by an order of magnitude. The reduced capacitance facilitates fast risetime pulsing of the cathodes. The teflon surface which is exposed to the plasma is contoured to inhibit the uniform deposition of sputtered aluminum. This design proved to be quite successful in reducing the arcing problem caused by sputtering.

Also shown in Figure 5.2 is a cylinder of microwave absorbing material. This absorber was inserted into the discharge chamber during the course of the experiment for the purpose of investigating the localization of the observed microwave radiation. It is reasonably effective in preventing radiation which is generated in the vicinity of cathode #2 from reaching the microwave receiver. This same absorber was also used in the microwave absorption experiment of Chapter III. The absorber is made from a Sauereisen mixture similar to that described by Heald and Wharton [84]. Structural strength is obtained by interleaving layers of fiberglass gauze throughout the absorber.

The grid used to stabilize the 4" diameter plasma column is sketched in Figure 5.2. It can be located anywhere in that part of the discharge chamber not occupied by the microwave absorber. When the grid is located next to the absorber, it greatly improves the effectiveness of the absorber in isolating the microwave receiver from the plasma region enclosed by the microwave absorber.

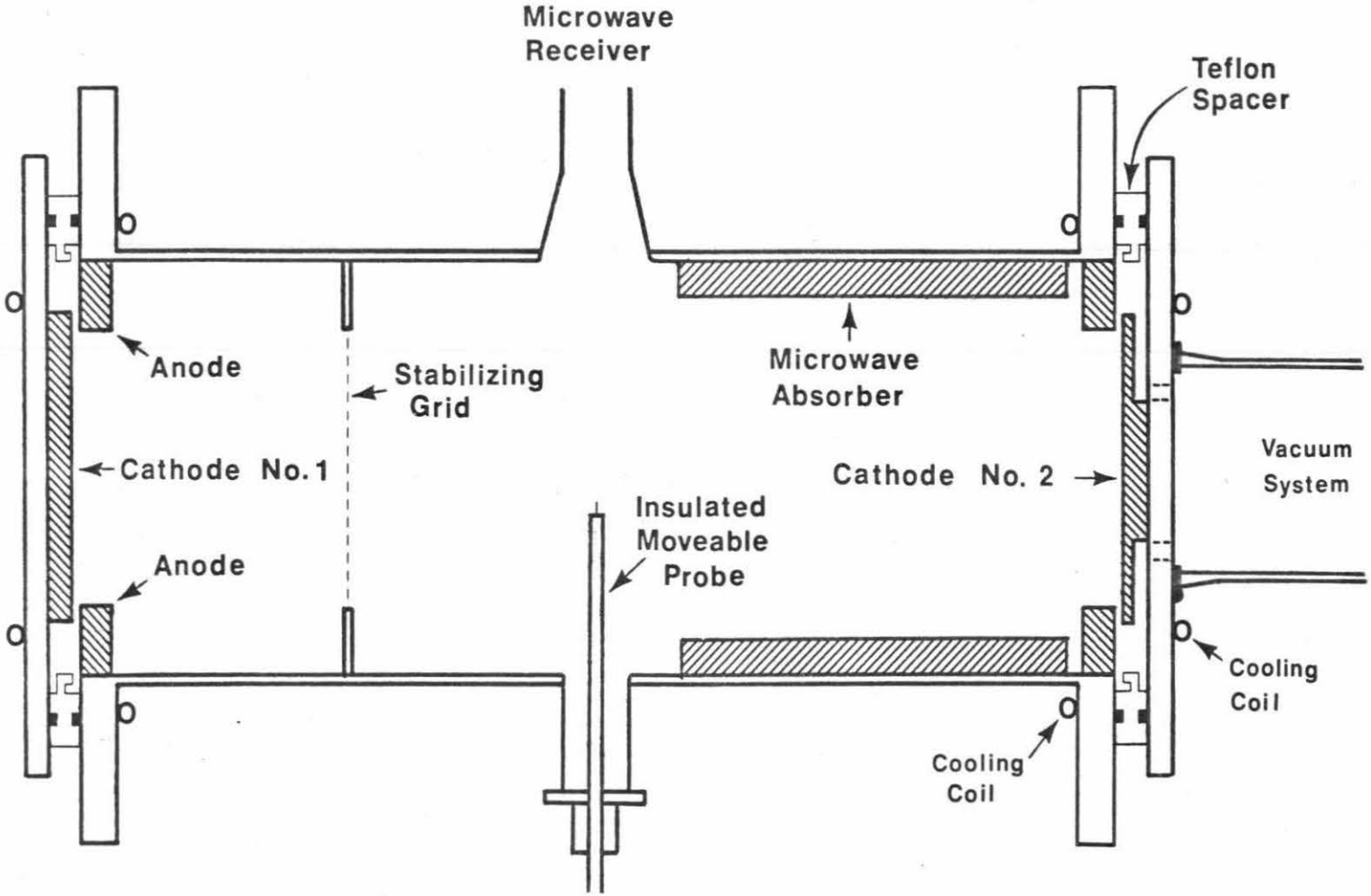

Figure 5.2 Sketch of the Modified Discharge Chamber

The pulse modulation experiment also used a plasma column with a 2.6" diameter. Such a column is obtained by reducing the inside diameter of the anode rings from 4" to 2.6". The 2.6" plasma column is stabilized using the same grids which were used to stabilize the pyrex discharge tube. The parallel wire grids are mounted on the anode rings at both ends of the discharge chamber.

Note that only the brass discharge tube is used in the pulse modulation experiment. The pyrex discharge tube is not set up for fast risetime pulsing. Oxygen is the standard working gas, but argon is used occasionally.

5.3.3 Floating Pulse Generator

The floating pulse generator consists of a pair of 6KD6 beam pentodes together with the necessary floating filament, screen, grid bias, and anode power supplies. It is controlled by the HP 214A pulse generator which supplies a gate pulse through an isolation transformer. During the pulse, the tubes deliver a fixed current to the load resistors which are shown in Figure 5.1. When the discharge is pulsed in the OPP mode the load resistance is 200 ohms and when the discharge is pulsed in the TG mode the load resistance is 100Ω. This choice of load resistors allows the same range of cathode voltages to be covered when using either pulse mode.

The voltage of the pulse is determined by how much current is driven through the load resistors by the floating pulse generator. The pulse current is controlled by adjusting the screen voltage of the pentodes. The maximum current of the pulse generator is 4 amperes.

Because the transmission line between the floating pulse generator and the discharge chamber is less than 20 centimeters in length, it is not a major consideration. The capacitances which are shown in Figure 5.1 shunt the discharge power supply and help to maintain a constant power supply voltage throughout the modulation pulse.

It should be noted that the 200 ohm resistors and .016 μf capacitors were originally added to the discharge circuit for a reason which is completely unrelated to the requirements of pulse modulation. When the discharge chamber, as modified for low anode-cathode capacitance, was operated in oxygen gas at low pressure, large amplitude oscillations appeared on the cathodes (∿800 volts p-p). The two cathodes oscillate 180 degrees out of phase and the frequency of the oscillation is found to be determined jointly by the anode-cathode capacitance and the inductance of the strap which connects the cathodes. When the connecting strap is replaced by inductors of different sizes, the frequency changes accordingly. In this way the frequency of oscillation was varied throughout the frequency range of 0.1-20 MHz.

The oscillation is attributed to a negative resistance effect associated with secondary electron emission by electron bombardment. When a large potential difference exists between the two cathodes, secondary emission by electron bombardment occurs at the most positive cathode. If δ_e, the coefficient of secondary emission by electron bombardment, is greater than unity, then the most positive cathode experiences a negative resistance. The magnitude of δ_e for the oxide covered cathodes is examined in Appendix B. The R-C network of Figure 5.1 effectively adds a positive resistance at each cathode which causes

the oscillations to be overdamped. Note that this effect has only been observed in the oxygen gas discharge.

5.3.4 Advantages of Pulse Modulation

During the pulse modulation experiment, the plasma is operated continuously using a DC power supply. The time response of the plasma emission is observed while pulse modulating the cathodes of the Penning discharge at a 2-10 KHz repetition rate. The applied pulse is typically 1 microsecond in length and has a risetime of 25 nanoseconds. The technique of using a floating pulse generator to observe the relaxation time of the harmonic emission has several advantages.

In order to maintain a reasonable data acquisition rate when using an averaging instrument such as the boxcar integrator, it is essential to have a high repetition rate. The 5 KHz repetition rate typically used in the pulse modulation experiment is very satisfactory in this respect.

The pulse modulation technique provides considerable flexibility and continuous control of the cathode voltages during the modulation pulse. It is this last feature which made it possible to carry out a detailed investigation of the dependence of the harmonic emission amplitude on the cathode voltage.

Since the power requirements for the floating pulse generator are moderate, the fast pulse rise times which are needed for the experiment are easily achieved. In comparison, the power requirements for the pulse generator which is used to operate the discharge on a pulsed basis are ten times greater and the pulse risetime is considerably longer.

Because the modulation pulse is only 1 microsecond in length it is possible to avoid the complications of time dependent plasma density and electron temperature. The relaxation times for the temperature and density are both expected to be two orders of magnitude longer than the observed response times of the harmonic emission. Experimentally, the decay time for thermal radiation in the afterglow of the argon discharge is found to be nearly 100 μsec, and the density decay time is found to be considerably longer. Therefore both the electron temperature and density are essentially constant for the duration of the applied pulse (1 μsec).

5.3.5 Effects of Pulse Modulation on the Plasma Emission

The microwave emission from the plasma column is observed while pulse modulating the cathodes. It is found that the two modes of pulse modulation produce very different results. When the cathodes are pulse modulated with opposite polarity (OPP mode), a new type of high intensity radiation is observed. However, only minor changes are observed in the intensity of the harmonic emission. If instead the cathodes are pulse modulated together with the same polarity (TG mode), the harmonic emission undergoes strong amplitude modulation. However, in this case the high intensity radiation is less prominent and is only observed under certain conditions wherein the radiation intensity is reduced from the previous case.

In the initial stages of the investigation, the behavior of the plasma emission was explored qualitatively by displaying the detected I-F output on an oscilloscope. In this way the role of each of the

many experimental variables including the pulse amplitude, time during the pulse, discharge current, neutral gas pressure, and magnetic field intensity could be explored thoroughly in an expeditious way. After all of the major effects had been observed in this manner, the plasma emission was recorded systematically using the boxcar integrator and the X-Y recorder.

The plasma emission can be recorded in two ways. It can be recorded as a function of time during the modulation pulse, or the time during the pulse can be held fixed and the emission spectrum can be obtained by sweeping the magnetic field. In both cases, the plasma emission is influenced by the many experimental parameters listed above.

It is found that the major experimental effects can be separated into two types of plasma radiation phenomena, each predominently associated with one mode of pulse modulation. Therefore, the discussion is separated accordingly. First, the high intensity radiation excited by the OPP pulse modulation mode is described in Section 5.4. A description of the effects of TG pulse modulation on the harmonic emission follows in Section 5.6.

5.4 Investigation of High Intensity Radiation

5.4.1 The High Intensity Radiation and Its Significance

Although the purpose of the experiment is to investigate the harmonic emission, it is also of interest to explore the high intensity radiation which is observed in the discharge. Basically, it is difficult to study the harmonic emission when the high intensity radiation is present in greater amounts. It is essential to explore

thoroughly the parameter dependences of the high intensity radiation so that the high intensity radiation can be avoided during investigations of the harmonic emission through proper choice of the experimental parameters.

There is an additional reason for studying the high intensity radiation. We have been examining the possible sources of harmonic emission in the Penning discharge. The high intensity radiation eliminates one of those possibilities, because the radiation mechanism which is responsible for the high intensity radiation is obviously not also the source of the harmonic emission. Specifically, the high intensity radiation is identified as resulting from a wave instability induced by the interaction of the secondary electron beam with the plasma.

The wave instability which is responsible for the high intensity radiation is interesting in itself. It is the result of a fascinating beam-plasma system. The secondary electron beam in the Penning discharge is diffuse and relatively large in dimension. Because the electron beam is diffuse, the growth rate of the instability is moderate. The diameter of the beam is identical with the diameter of the plasma column, 2.6" or 4". Everywhere on the density profile of the plasma column, the electron beam density is a constant fraction of the plasma density. In contrast, beam-plasma experiments frequently employ a high density electron beam whose diameter is much less than that of the plasma column, or else the plasma diameter is very small.

The high intensity radiation is observed principally when the cathodes are pulsed with opposite polarity (OPP mode). The nature of

the radiation depends on the magnetic field. Although high intensity radiation is easily observed at both large and small values of the magnetic field, very little such radiation is observed for intermediate values in the range of 0.7 to 1.8 kilogauss. The radiation observed at low fields differs noticeably from that observed at higher fields. At low magnetic field ($B < 0.7$ Kg) the radiation is well localized to the cathode regions, depends strongly on both the discharge current and the amplitude of the applied pulse, exhibits emission minima at the cyclotron harmonics, and occurs only in the pressure range $p \lesssim 40$ mtorr. At high magnetic field, the radiation is only weakly localized to the cathode regions and is confined to a limited frequency range between the cyclotron frequency and the $m = 2$ harmonic.

5.4.2 Radiation at Low Magnetic Field

The high intensity radiation observed at low magnetic field was investigated most thoroughly because this magnetic field range coincides with the location of the $m > 3$ harmonic emission lines. Most of the results described in this section were obtained using the 4" diameter nonstabilized plasma column with the microwave absorber in place. Other configurations will be mentioned briefly.

Figure 5.3 indicates the time response of the high intensity radiation which is excited when the cathodes are pulse modulated with opposite polarity. The top half of the figure displays the voltage waveforms of the two cathodes. In the OPP pulse modulation mode, one cathode is driven positive and the other cathode is driven negative.

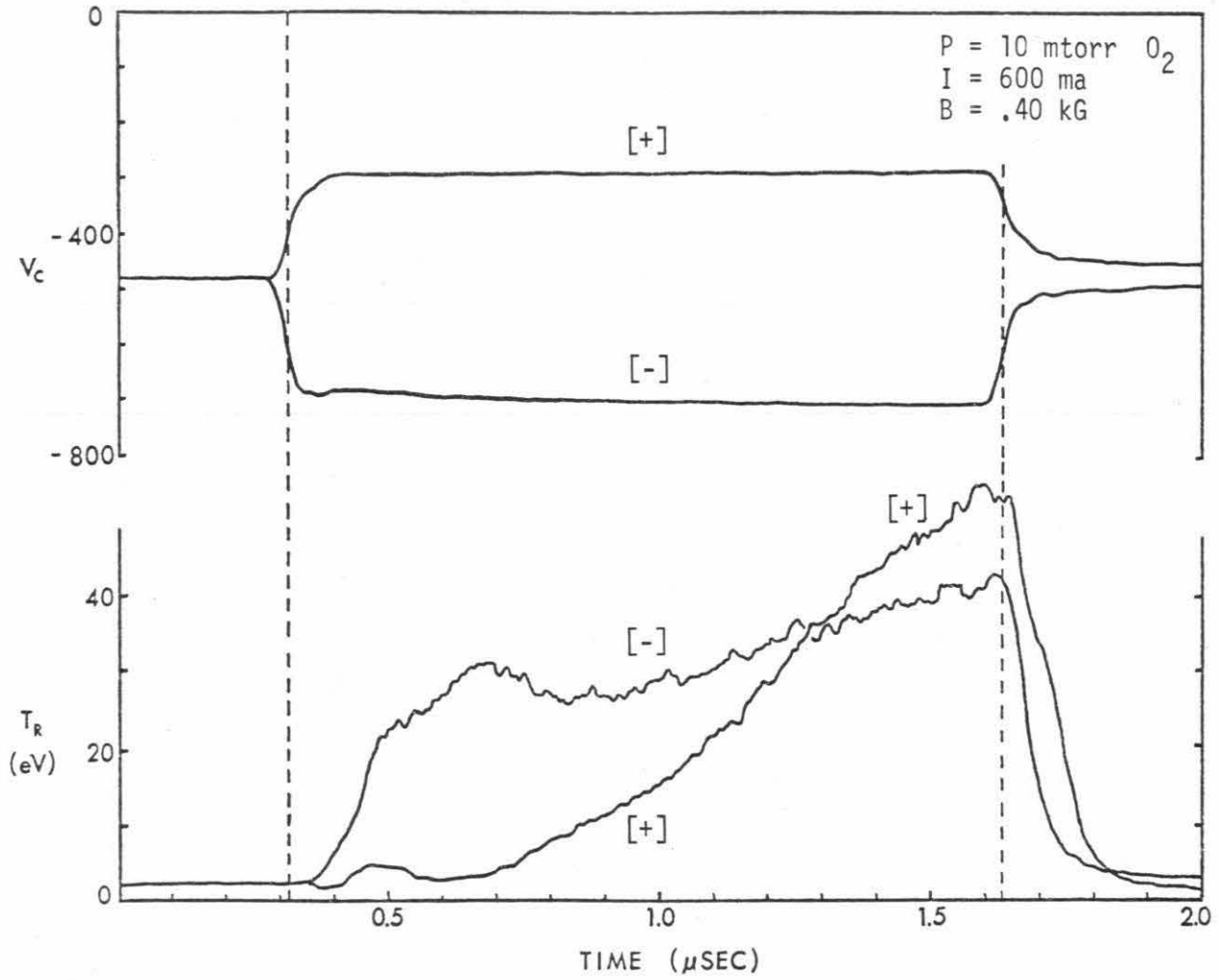

Figure 5.3 Average Radiation Temperature in eV as a Function of Time During the OPP Modulation Pulse. The cathode voltage waveforms are included at the top of the graph.

The bottom half of Figure 5.3 displays the resulting plasma radiation waveforms. Because the microwave absorber is located between cathode #2 and the microwave antenna, microwave radiation generated in the vicinity of cathode #2 is attenuated, whereas microwave radiation generated in the vicinity of cathode #1 is not. Therefore the detected radiation comes predominantly from the unattenuated portion of the plasma column including the region close to cathode #1.

When the pulse polarity is such that cathode #1 is driven positive with respect to cathode #2, then the plasma radiation waveform labeled [+] is obtained. This denotes that the detected radiation comes mainly from the positive cathode end of the discharge chamber. When the pulse polarity is reversed, the voltage waveforms of the two cathodes are interchanged. In this case cathode #1 is driven negative and the radiation waveform is labeled [-].

In all of the data recorded in the manner of Figure 5.3, the plasma radiation waveforms are delayed approximately 40 nanoseconds with respect to the voltage waveforms. This effect results from the propagation delay of the I-F system. To compensate for the delay, all figures have been corrected graphically by shifting the voltage waveforms 40 nanoseconds to the right. As a result, the waveforms in each of the figures can be compared directly in real time.

The main features of the high intensity radiation observed at low magnetic field are as follows:

1. The time behavior of the [+] radiation differs significantly from that of the [-] radiation.
2. The radiation amplitude increases rapidly with the voltage of the applied pulse.

3. For large pulse amplitudes, the radiation from the [-] cathode is much stronger than that from the [+] cathode. Peak radiation temperatures exceed 10^5eV.

4. The radiation is very sporadic. There is considerable variation from pulse to pulse and some pulses produce little radiation.

5. The radiation is localized to the cathode regions and becomes more localized as the neutral gas pressure is increased.

6. The radiation amplitude is sharply peaked when $\omega \simeq \omega_p$ as the discharge current is increased.

7. The frequency spectrum has minima at the harmonics of the electron cyclotron frequency.

8. The radiation intensity is quite sensitive to the presence and the location of the stabilizing grids. The radiation is enhanced in the grid stabilized discharge except when the grids are located close to the cathodes.

9. The radiation intensity is maximal for a particular combination of the magnetic field, discharge current, and gas pressure, and can be suppressed if desired by adjusting these same parameters.

10. The high intensity radiation does not occur when the neutral gas pressure is high, $p > 50$ mtorr.

The [+] and [-] plasma radiation waveforms exhibit substantially different time response. The [-] waveform rises rapidly after an initial delay and thereafter remains nearly constant. In contrast, the [+] waveform exhibits a long delay during which only minor transient effects are observed. Then the radiation rises steadily. When a longer pulse is used, the [+] radiation amplitude is observed to reach a steady state value after about one microsecond has elapsed. The time

response of the [+] waveform is found to be essentially the same whenever this radiation is observed. However, the [-] waveform exhibits some variations. Under various conditions the [-] radiation waveform might attain a maximum value at the beginning, middle, or end of the pulse. However, no significant changes are observed in the short delay and rapid rise at the beginning of the pulse. For both types of radiation, the behavior at the end of the pulse remains basically the same.

The amplitudes of the [+] and [-] radiation waveforms are not usually as nearly equal in amplitude as is indicated in Figure 5.3. The dependence of the amplitude of the [+] and [-] radiation on the voltage of the modulation pulse is indicated in Figure 5.5. The amplitude of the radiation is plotted versus the voltage difference developed between the cathodes by the modulation pulse. When the amplitude of the modulation pulse is small, the [+] radiation dominates. And when the amplitude of the modulation pulse is large, only the [-] radiation is important. The latter situation is displayed in Figure 5.4.

The data of Figure 5.4 were obtained in the same manner as those of Figure 5.3. In Figure 5.4, both radiation waveforms are found to be identical except for the obvious change in the radiation intensity. This indicates that very little radiation is being generated in the vicinity of the positive cathode. Instead, all of the radiation is localized to the negative cathode. The [+] radiation waveform is simply the [-] waveform attenuated 8 db by the microwave absorber.

Keep in mind that the radiation waveforms of Figures 5.3 and 5.4 are the result of many waveforms which have been averaged by the boxcar

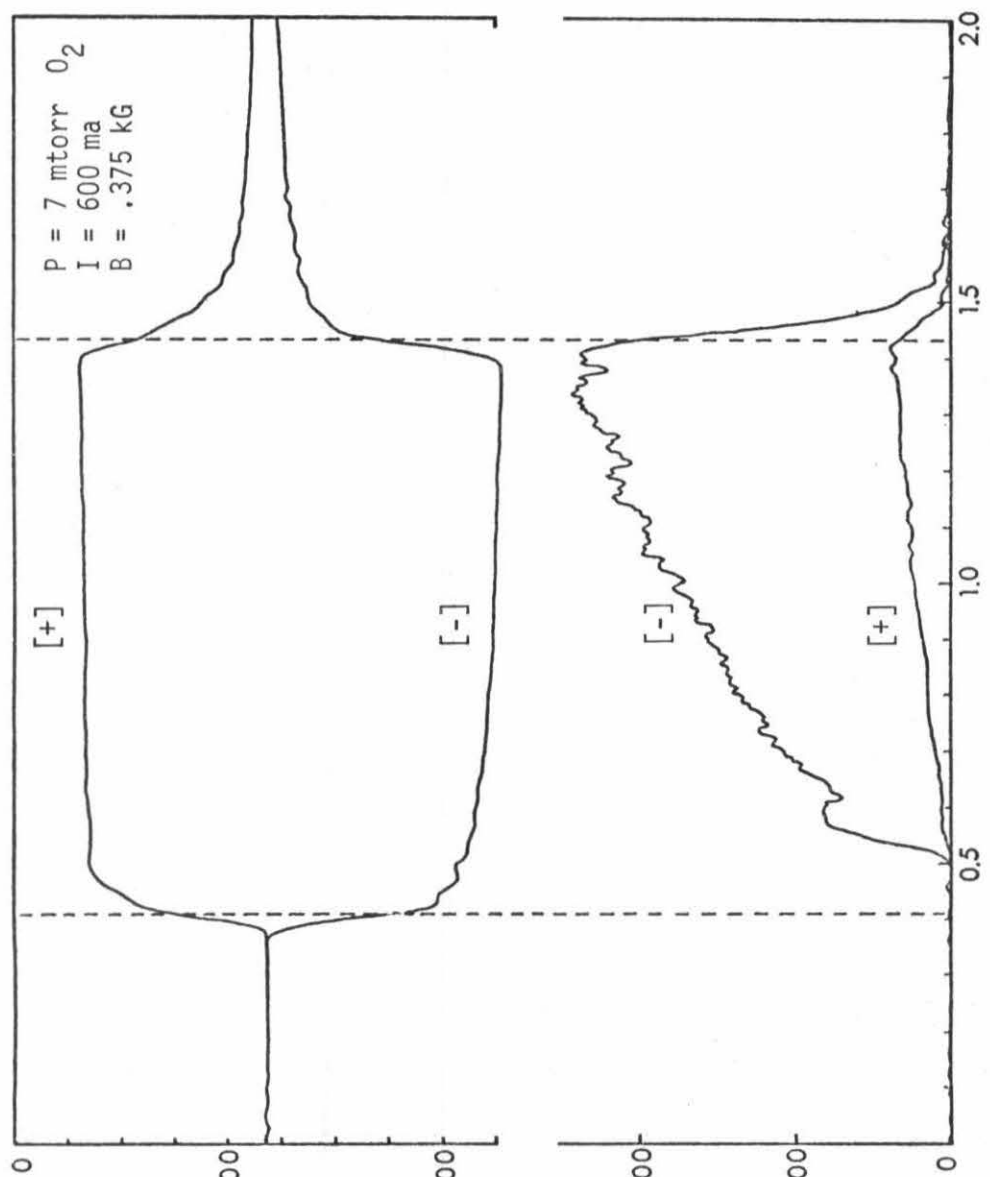

Figure 5.4 Average Radiation Temperature in eV as a Function of Time during the OPP Modulation Pulse, Showing that the High Intensity Radiation is Localized to the [-] Cathode. The cathode voltage waveforms are included at the top of the graph.

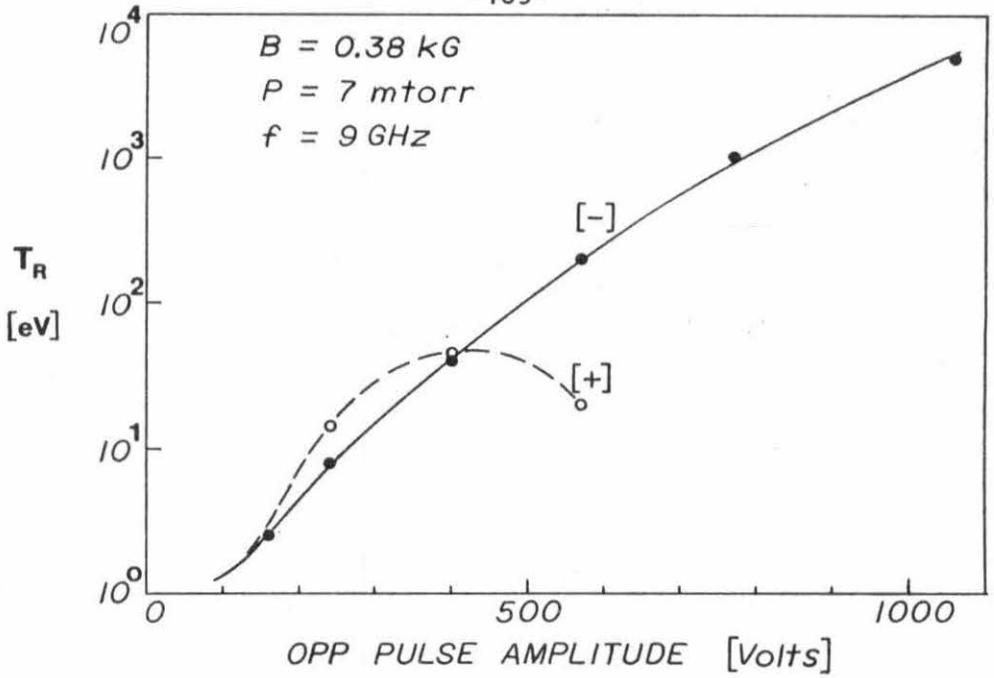

Figure 5.5 Average Radiation Temperature of the High Intensity Radiation in eV as a Function of the Amplitude of the Modulation Pulse

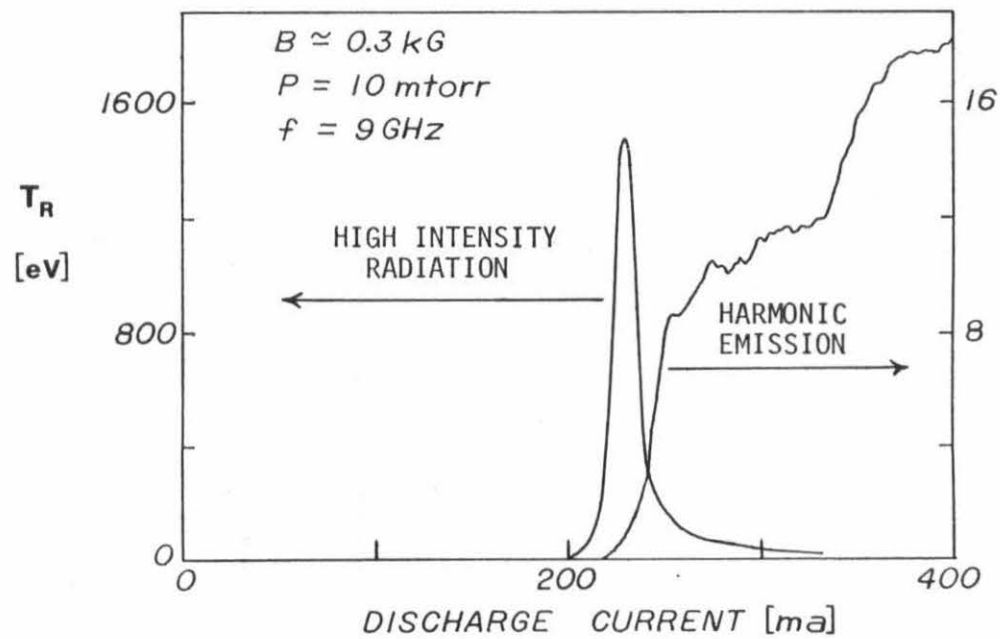

Figure 5.6 Comparison of Harmonic Emission and High Intensity Radiation as a Function of the Discharge Current in the 2.6" Nonstabilized Plasma Column

integrator. Unlike the harmonic emission which is nearly continuous with time, this new type of radiation is very sporadic. The radiation waveform for an individual pulse is, in general, quite different from the "average" behavior displayed here. Quite often the modulation pulse results in no radiation at all. When radiation is produced, it appears in bursts, the amplitudes of which are usually at least an order of magnitude larger than the "average" of Figures 5.3 and 5.4.

The highest observed radiation intensity is obtained using a special pulse which results in voltages of -100 volts and -1200 volts at cathodes #2 and #1 respectively. Under these conditions the peak radiation intensity frequently exceeds 10^5eV. At the same time, the "average" radiation level exceeds 10^4eV. More typical radiation levels are somewhat lower but are still 20 to 30 db above the intensity of the harmonic emission.

It is found that the degree of localization of the high intensity radiation increases with the neutral gas pressure. The localization of the [+] radiation is investigated by using a small amplitude pulse and the [-] radiation is investigated using the maximum pulse amplitude. The [-] radiation is found to be the most strongly localized. It is observed that the high intensity radiation is localized to the cathode regions and the extent of localization increases with the neutral gas pressure.

To further explore this concept, the measurements were repeated with the stabilizing grid located between the microwave absorber and the receiving horn. This modification greatly increases the isolation between the microwave receiver and that part of the plasma column

which is in the vicinity of cathode #2. In this case the [+] and [-] waveforms are found to differ in amplitude by more than 18 db, reflecting the increased isolation and the high degree of localization of the radiation.

The balance between the [+] and [-] radiation is also found to depend on how long the Penning discharge had been operated previous to the observation. Shortly after the discharge is turned on, the [+] radiation dominates even when the pulse amplitude is very large. However, after several hours of operation the [-] radiation dominates under most circumstances. Apparently cathode surface conditions are important.

The strong dependence of the high intensity radiation on the discharge current is indicated in Figure 5.6. As nearly as can be determined, the high intensity radiation is maximum just at the onset of the harmonic emission. Since ω_c is small for the high harmonics, this indicates that $\omega \simeq \omega_p$ is a condition for the high intensity radiation. Note that the data displayed in Figure 5.6 were obtained using the 2.6" nonstabilized plasma column. For the 4" column the harmonic onset is more gradual and the peak of the high intensity radiation is broader.

The unusual frequency spectrum of the high intensity radiation is fascinating. The spectrum is shown in Figure 5.7. The top graph is a spectrum of the high intensity radiation excited by OPP pulse modulation. The bottom graph is a harmonic emission spectrum obtained without pulse modulation. It is presented for reference to indicate the harmonic locations.

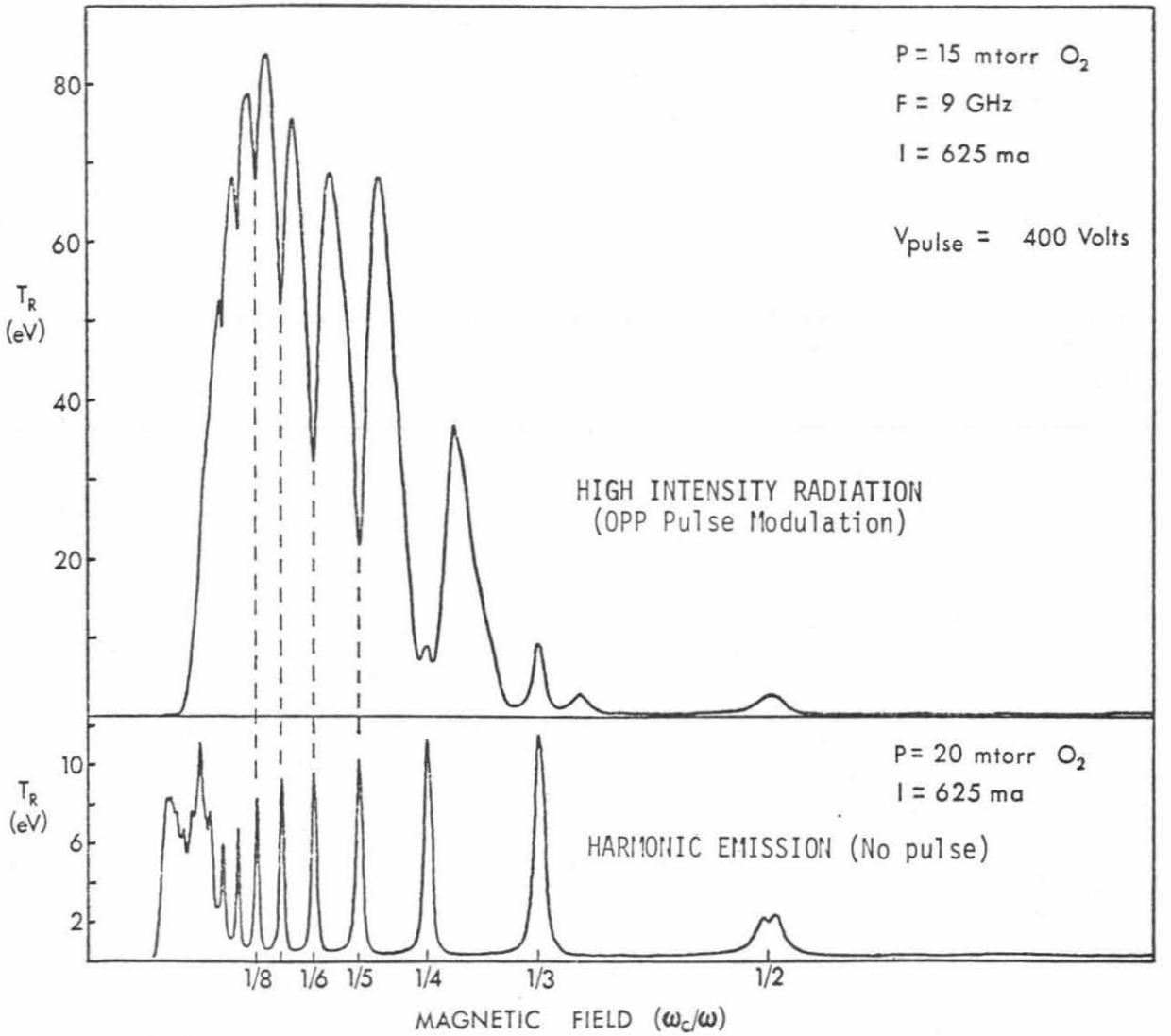

Figure 5.7 Average Radiation Temperature in eV as a Function of ω_c/ω Showing the Minima in the Frequency Spectrum of the High Intensity Radiation at the Cyclotron Harmonics. The harmonic emission spectrum is shown on the bottom graph.

The frequency spectrum of the high intensity radiation exhibits minima at the locations of harmonics of the electron cyclotron frequency. This unusual feature is observed consistently for both the [+] and [-] radiation. Admittedly, the minima at the harmonics are not always as pronounced as they are in Figure 5.7, but nevertheless they are always present.

In a sense, the high intensity radiation spectrum of Figure 5.7 is not very typical. It is presented because it shows the harmonic minima clearly and covers a broad portion of the spectrum. Usually the radiation intensity changes more rapidly as a function of B and only a narrow portion of the spectrum dominates. The resulting spectrum consists of a relatively narrow maximum which is not especially interesting when displayed using a linear scale.

Note that the lower graph of Figure 5.7 displays some extra radiation in the harmonic emission spectrum at low magnetic field which is obviously not harmonic emission. Landauer also observed relatively high intensity nonharmonic radiation in the range of low magnetic field [4]. This effect is frequently observed while investigating the harmonic emission of the dc operated discharge, and proved to be very frustrating when attempting to obtain a clean harmonic spectrum. It is found that this radiation is very similar to the high intensity radiation excited by pulse modulation. It has a much greater intensity than the harmonic emission, but is only present for a small percentage of the time, appearing in short bursts.

The similarity between the radiation excited by pulse modulation and that present in the dc discharge is especially evident when

the 4" column is operated with the stabilizing grid in place. Apparently, this configuration is particularly suitable for the generation of high intensity radiation. The high intensity radiation is present at relatively high levels even before the pulse modulation is turned on. And the modulation pulse itself turns out to have an unusual effect. The [-] radiation waveform still shows that the radiation in the vicinity of the negative cathode is enhanced. However, the [+] waveform is unusual; it reveals that the radiation level is actually suppressed in the vicinity of the positive cathode.

The location of the stabilizing grid is very important with respect to the generation mechanism of the high intensity radiation. When the stabilizing grid is placed near the center of the 4" plasma column, the high intensity radiation is enhanced significantly. It appears that the quiescent plasma is more suitable for the generation mechanism. In contrast, when the stabilizing grid is placed near the cathode, as in the case of the 2.6"column, the high intensity radiation is reduced by nearly two orders of magnitude. The principal difference in this case is that two grids are involved, one mounted immediately in front of each cathode. Apparently the presence of the grids in the vicinity of the cathodes severely disrupts the generation mechanism of the high intensity radiation. This is plausible because such radiation was previously found to be localized to the immediate vicinity of the cathodes. Thus the quiescent plasma of the grid-stabilized discharge is most suitable for the production of the high intensity radiation provided that the stabilizing grids are not located near the cathodes.

It should be noted that although the high intensity radiation observed in the 4" diameter grid-stabilized plasma column has a much greater amplitude than that observed in the 2.6" diameter column, when the stabilizing grids are removed both columns exhibit similar behavior. The radiation spectra of the 4" column have better defined minima at the harmonics of the electron cyclotron frequency, but the radiation intensities are essentially the same. Therefore, the only important difference between the 4" and 2.6" diameter columns is the location of the stabilizing grids.

As previously noted, there are several parameters which can be varied in the experiment, and all of them are found to have a major influence on the high intensity radiation. The high intensity radiation can be enhanced or suppressed by proper choice of these parameters. Although the following remarks are intended to describe the [-] radiation which is localized to the negative cathode, the behavior of the [+] radiation is similar.

It is found that the amplitude of the high intensity radiation depends jointly on the magnetic field (B), the discharge current (I), and the neutral gas pressure (P). Figures 5.6 and 5.7 indicate how the high intensity radiation depends on B and I separately. These graphs were obtained by varying only one parameter at a time. More generally, it is found that there is one particular combination of the parameters B and I which yields the maximum radiation intensity. If the magnetic field is then increased, it is found that the radiation maximum occurs at a lower value of the discharge current. Or if I is increased, B

must then be decreased to again maximize the radiation intensity.

Changing the pressure parameter P only results in a minor modification. If P is increased, then the radiation maximum requires a combination of higher B and lower I. And if P is decreased, the maximum shifts to lower B and higher I. Thus the high intensity radiation at low magnetic field occurs mainly for a particular combination of parameter values.

It is found that the high intensity radiation can easily be avoided during investigations of the harmonic emission. Such investigations normally require larger values of the discharge current, in which case the high intensity radiation is greatly reduced.

Finally, it is found that the high intensity radiation disappears when the neutral gas pressure exceeds 50 mtorr. This behavior is indicated in Figure 5.8. At low pressure, $P < 20$ mtorr, the amplitude of the [-] radiation is found to be nearly independent of the neutral gas pressure.

5.4.3 Radiation at High Magnetic Field

Up to this point the only high intensity radiation which has been described is that which is observed at low magnetic fields corresponding to the location of the higher harmonics of the electron cyclotron frequency. At the beginning of Section 5.4 it was mentioned that high intensity radiation is also observed at higher magnetic fields, $B > 1.8$ kG, corresponding to the frequency range $1 < \omega/\omega_c < 2$. The high intensity radiation observed at high magnetic fields behaves very differently than the low field radiation.

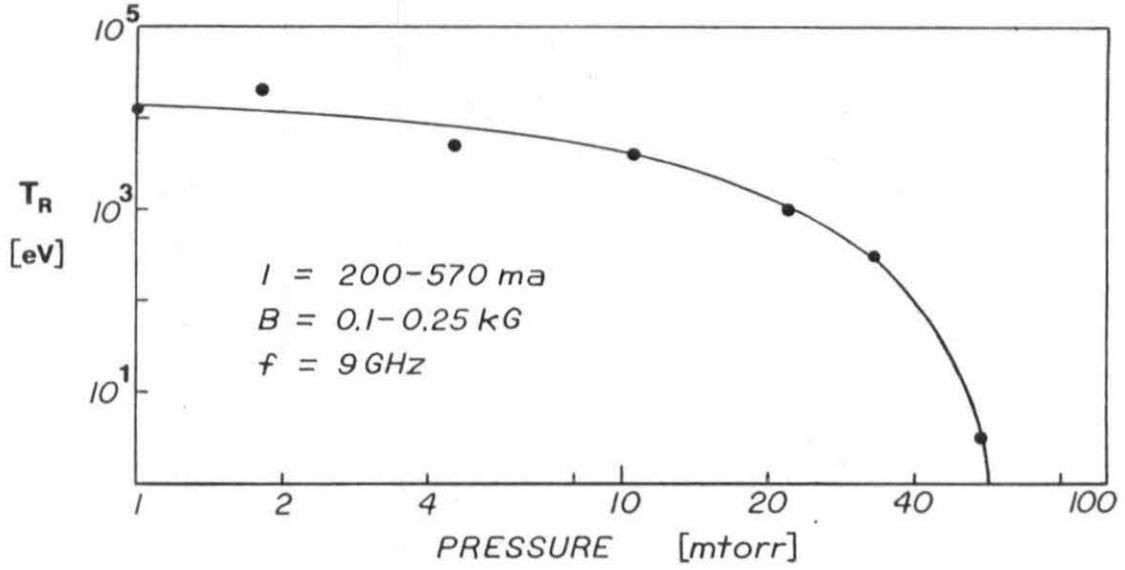

Figure 5.8 Average Radiation Temperature in eV as a Function of the Neutral Gas Pressure when the Amplitude of the OPP Modulation Pulse is Maximal. The discharge current and the magnetic field are adjusted to maximize the high intensity radiation.

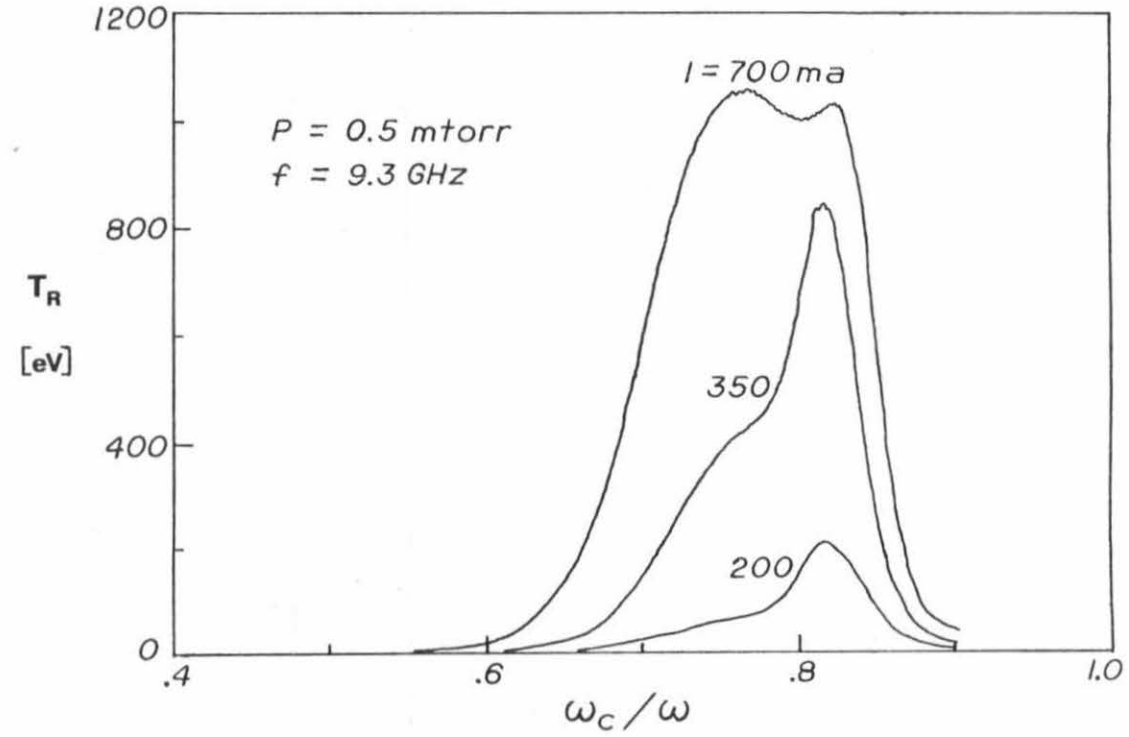

Figure 5.9 The Frequency Spectrum of the High Intensity Radiation Observed at High Magnetic Field.

The emission spectra shown in Figure 5.9 are typical of the radiation at high magnetic field. When the receiver frequency is changed, the radiation spectrum shifts accordingly to a new value of the magnetic field such that ω/ω_c = constant. The parameter dependences differ noticeably from the low field radiation. As indicated by the data in Figure 5.9, the shape and amplitude of the emission spectra change with the discharge current. The radiation exists over a large range of the discharge current parameter. In some cases the radiation is found to be localized to the cathode regions, but the extent of localization is not as great as was previously found for the low field radiation. In the dc discharge, the radiation intensity is found to be maximum at low pressures (P < 5 mtorr). However, when the discharge is pulse modulated, the radiation is most intense at higher pressures (P > 20 mtorr). Pulse modulation of the cathodes results in strong amplitude modulation of the radiation and, under the right conditions, the radiation intensity is comparable to that of the high intensity radiation observed at low magnetic field.

The high magnetic field radiation is not investigated as thoroughly as the low field radiation because it is more complicated and does not occur in the frequency range of interest to this investigation, $\omega_c/\omega \gtrsim .33$. In addition, this type of radiation has apparently been observed previously by Vasiliyev [21] in a dc operated discharge (his Figure 12). Note that he also indicates the presence of a continuum of high intensity radiation at low magnetic field in the vicinity of the higher harmonics (his Figure 11). However, he does not observe the existence of minima in the radiation spectrum at the location of

the harmonics of the electron cyclotron frequency. The very high intensity radiation ($\sim 10^8$eV) which he observed at the harmonics is not observed here.

5.4.4 Other Effects of OPP Pulse Modulation

In addition to the high intensity radiation and the harmonic emission, transient radiation is also observed. When the discharge is pulse modulated, transient radiation is frequently observed at the beginning and end of the pulse. The transient radiation consists of a short burst of radiation which lasts from 50 to 100 nanoseconds. However, since this effect only occurs at low pressure, it can be avoided by operating in the pressure range $P > 10$ mtorr.

Finally, the OPP modulation pulse has only a minor effect on the harmonic emission. If the amplitude of the modulation pulse is very large, the intensity of the harmonic emission is slightly reduced. But for smaller pulse amplitudes, the intensity of the harmonic emission is increased slightly. In both cases the change is usually less than 0.5 db. Also, no localization effects are detected for the harmonic emission. Therefore OPP pulse modulation is used principally to investigate the high intensity radiation at low magnetic field.

5.5 Interpretation of the High Intensity Radiation

5.5.1 The Radiation Mechanism

The amplitude of the high intensity radiation is sufficiently great that it can not be accounted for on the basis of radiation from independent electrons, but must instead involve a coherent collective phenomenon. As indicated, the radiation intensity frequently exceeds 10^5eV. A beam-plasma or velocity space instability is undoubtedly involved. The localization of the high intensity radiation to the vicinity of the cathodes and the observation that the high intensity radiation is severely disrupted when grids are placed close to the cathodes suggests that secondary electrons are responsible for the radiation. The secondary electrons result in a beam-plasma wave instability. This same interaction has previously been considered to be a possible source of the harmonic emission. However, it is found that the high intensity radiation from both the dc discharge and the pulse modulated discharge can be understood in terms of just such an instability.

The secondary electron beam produced as a result of ion bombardment of the cathode has already been described in Chapter II. The beam density is determined by the ion current J_i and the coefficient of secondary electron emission by ion bombardment γ_i. The secondary electrons are accelerated into the plasma column by the cathode sheath, acquiring an energy, E_o, corresponding to the difference between the cathode potential and the plasma potential. The secondary electrons have nearly identical energies and constitute a diffuse, low temperature electron beam ($T_b \simeq 3$ eV). The electron beam is injected into the

plasma in the direction parallel to the magnetic field.

This situation is very similar to that treated theoretically by Seidl [69]. He solved the quasistatic dispersion equation corresponding to the interaction of a diffuse electron beam moving parallel to the magnetic field with a maxwellian plasma. The resulting high frequency beam-plasma wave instabilities are described. It is assumed that the electron beam has an isotropic velocity spread, meaning that in the velocity frame of the beam the electrons have the same velocity spread in the directions parallel and perpendicular to the magnetic field. Although his treatment assumed infinite geometry, it is nevertheless of interest to compare his theoretical results with the high intensity radiation observed experimentally.

5.5.2 Radiation in the DC Discharge

As the secondary electron beam moves away from the cathode sheath, two processes occur simultaneously. The beam electrons lose energy via inelastic electron neutral collisions and simultaneously acquire a velocity spread or "temperature". Therefore, the characteristics of the secondary beam are a function of both the distance from the originating cathode and the neutral gas pressure. Seidl found that the growth rate of the unstable wave is suppressed when the velocity spread of the beam is increased. Therefore the growth rate of the instability can be expected to be a function of position.

First consider the case of the dc operated discharge where both cathodes are at the same potential. For high neutral gas pressures the energy distribution function of the beam changes rapidly as a function of distance from the cathode. Moreover, there is very little overlap

in energy space of the beams injected on successive transits of the discharge column. In this case a strong beam-plasma interaction can exist but only in the immediate vicinity of the cathode.

At low pressures such that the ionization length is comparable with the cathode separation, the energy distribution function of the secondary electron beam changes slowly as a function of position and the electron beams injected on successive transits of the discharge column overlap extensively in energy space. Therefore the secondary electron beam is imbedded in almost a continuum of energetic electrons and the beam plasma description is no longer accurate. This situation is shown in Figure 2.13 where the neutral gas pressure is 1 mtorr.

This suggests that the high intensity radiation observed in the dc operated discharge will occur at high pressure but not at low pressure. Of course, at sufficiently high pressures the instability will be damped out by electron-neutral collisions. The net growth rate of the instability is equal to the growth rate due to the beam minus the damping due to the plasma. Roughly, this is what is observed experimentally.

Figure 5.10 displays the harmonic emission spectra obtained from the dc discharge for two values of the neutral gas pressure. The presence of high intensity nonharmonic radiation in the emission spectrum is found to be maximal when $P \simeq 15$ mtorr. Such radiation is observed in the dc discharge only when the pressure is in the range of 5-40 mtorr.

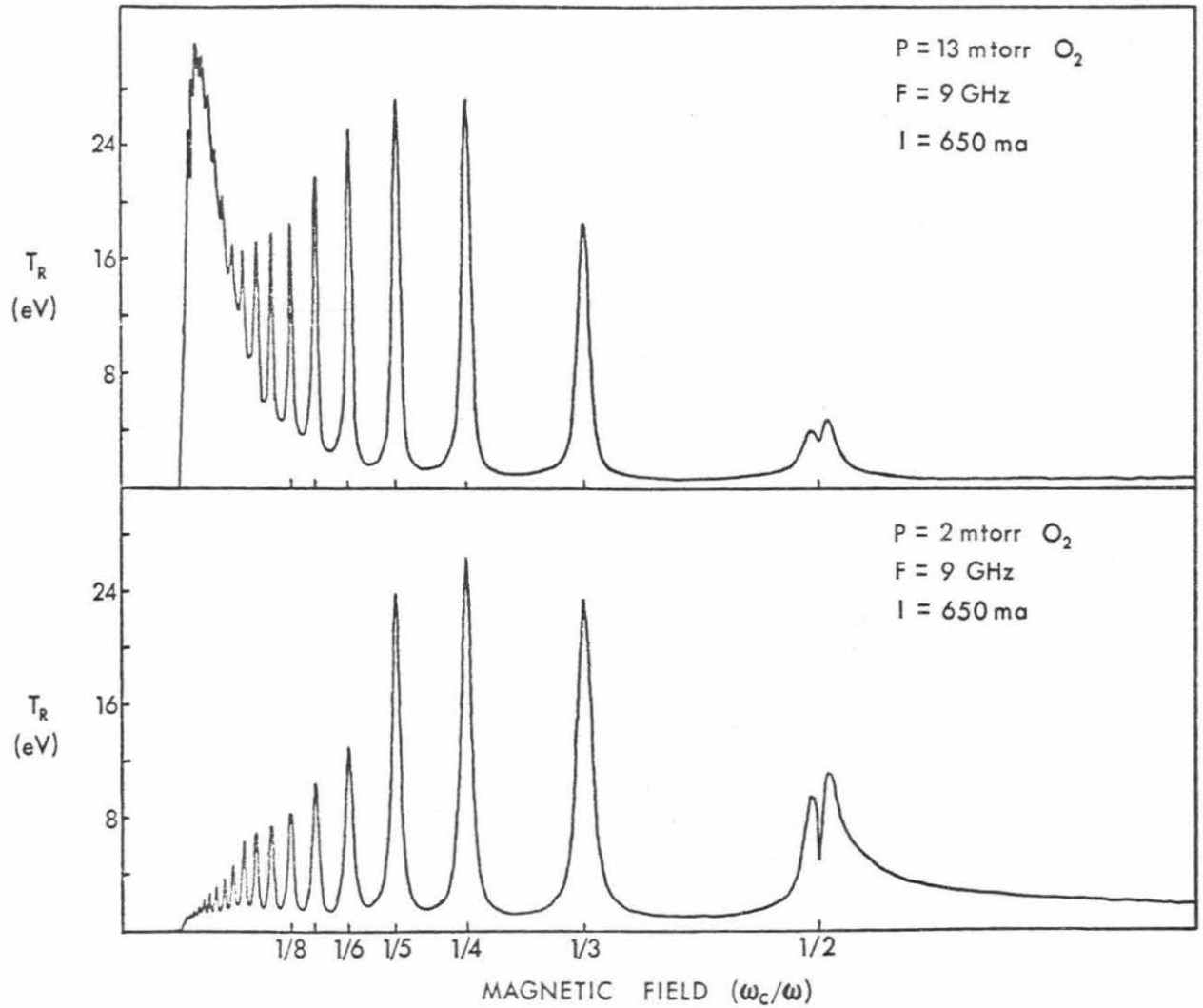

Figure 5.10 Radiation Temperature in eV as a Function of ω_c/ω Displaying the Presence of High Intensity Nonharmonic Radiation in the Harmonic Emission Spectrum of the DC Discharge when P ≈ 15 mtorr.

5.5.3 Radiation in the Pulse Modulated Discharge

The situation changes considerably when the discharge is pulse modulated. If the cathodes are pulsed together in the TG mode, the situation is very similar to that described for the dc discharge. However, if the cathodes are pulsed with opposite polarity (OPP mode), a significant change occurs. When a voltage difference exists between the cathodes during the pulse, the secondary electrons from the negative cathode are collected by the positive cathode. Thus, the secondary electron beam of the positive cathode results from a combination of electron and ion bombardment. As a result the temperature and density of that beam are modified somewhat. Still, the qualitative behavior of the [+] high intensity radiation should be similar to that of the high intensity radiation observed in the dc operated discharge.

The situation in the vicinity of the negative cathode, however, is quite different. The [-] radiation is expected to change significantly, most notably at low pressure. Previously it was noted that beam-plasma effects disappear at low pressure in the dc discharge because the secondary electron beam becomes immersed in a continuum of energetic electrons. However, the OPP modulation pulse separates the secondary electron beam from the continuum of electrons. This occurs because the most energetic electrons in the continuum are no longer reflected by the positive cathode. Basically, all energetic electrons whose parallel energy component is given by $E_{\parallel} > E_o - V$ are collected by the positive cathode, where E_o is the injection energy of secondary electrons at the negative cathode and V is the voltage difference

between the cathodes. The only electrons with energy $E_{\parallel} > E_o - V$ are the secondary electrons ($E_{\parallel} = E_o$) in transit from the negative cathode to the positive cathode. Thus, during the OPP modulation pulse there is a well defined beam-plasma interaction in the vicinity of the negative cathode. And as the amplitude of the OPP pulse increases, the validity of the beam-plasma description improves.

When the amplitude of the OPP pulse is large, a well defined beam-plasma situation exists for all values of the neutral gas pressure. If the potential of the positive cathode is comparable to the plasma potential, then the only high energy electrons present in the discharge are the secondary beam electrons in transit from the negative to the positive cathode. Under these conditions, the amplitude of the [-] radiation is experimentally found to be nearly independent of the neutral gas pressure for $P < 10$ mtorr. This is indicated in Figure 5.8. Again, high intensity radiation is not observed when $P \gtrsim 50$ mtorr, presumably because the wave instability is overdamped by electron-neutral collisions.

Thus, in both the dc discharge and the pulse modulated discharge, the pressure dependence of the amplitude of the high intensity radiation can be understood in terms of a beam-plasma wave instability.

5.5.4 Comparison with the Theory

There are several features of Seidl's theory, in particular, which fit the behavior of the high intensity radiation quite well. The theory predicts that the growth rate is maximum when $\omega \simeq \omega_p$, in excellent agreement with the experimentally observed dependence on the discharge current. Also, Seidl's theory predicts that the growth rate

of the instability is greatest when $\omega = (m+\frac{1}{2})\omega_c$. As a result, radiation is most likely to be observed between the harmonics of the electron cyclotron frequency. This describes the high intensity radiation spectrum presented earlier in Figure 5.7 quite well.

Also, the localization of the high intensity radiation to the cathode regions is understandable since the degree of localization depends on the neutral gas pressure in the expected way. The effects of plasma turbulence on the high intensity radiation and the importance of the location of the stabilizing grid are also understandable. When the stabilizing grids are located near the midplane of the plasma column, the high intensity radiation is enhanced considerably. The increased radiation intensity is attributed to the reduction in turbulence associated with the presence of the grid. The radiation mechanism appears to be adversely affected by turbulence. And when the stabilizing grids are located immediately in front of the cathodes, the high intensity radiation is severely disrupted as might be expected if a wave instability were localized there.

Note that no attempt has been made here to understand how the growing quasistatic wave is coupled to the electromagnetic signal which is detected by the microwave receiver. Although one can not be certain, it is not expected that the mode conversion will greatly alter the basic parameter dependences of the radiation.

In conclusion, the high intensity radiation is identified with a wave instability excited by the interaction of the parallel secondary electron beam with the plasma column. The striking similarities

between the experimental observations and the parallel beam theory of Seidl, in particular, are impressive.

5.5.5 Comparing Harmonic Emission and High Intensity Radiation

We have seen that the parameters which describe the high intensity radiation are quite unlike those which characterize the harmonic emission. There are several notable differences between the two types of radiation which are worth pointing out. They involve the parameter dependences and the amplitudes of the two types of radiation.

The high intensity radiation exhibits a strong dependence on the plasma density and the neutral gas pressure. The experimental results indicate that the growth rate of the instability is sharply peaked at a single plasma density ($\omega \simeq \omega_p$) and that the growth rate decreases rapidly when $P > 50$ mtorr. In contrast, the amplitude of the harmonic emission is only weakly dependent on the neutral gas pressure.

It has also been noted that the high intensity radiation is strongly influenced by the presence of the grids, yet the harmonic emission is not. The high intensity radiation in the nonstabilized discharge is received in bursts whereas the harmonic emission is very continuous in time. This indicates that the necessary conditions for the high intensity radiation are only satisfied part of the time.

It is also instructive to consider the large difference in the peak radiation intensities of the two types of radiation. The radiation level of the high intensity radiation is determined by the linear growth rate and the saturation conditions of the unstable wave. The

high intensity radiation level frequently exceeds the thermal radiation level by more than four orders of magnitude. In contrast, the harmonic emission level seldom exceeds the thermal level by more than two orders of magnitude.

As a result of this investigation, we conclude that the harmonic emission does not result from the parallel secondary electron beam. Instead, this beam-plasma interaction is found to be the source of a new type of high intensity radiation which seems to correspond with the theory of Seidl. The predominant features of the radiation are grossly different from those of the harmonic emission. Therefore, it is concluded that the harmonic emission is not generated by this same process. The principal features of the harmonic emission are so distinctly different from those of the high intensity radiation that the generation mechanism of the harmonic emission must be of a markedly different nature--very likely not a wave instability at all.

5.6 Pulse Modulated Harmonic Emission

In the two previous sections of this chapter, the high intensity radiation excited by pulsing the cathodes with opposite polarity has been investigated. It was noted that such a pulse has very little effect on the harmonic emission. This section will describe what happens when the cathodes are pulsed together with the same polarity (TG mode). In this case it is found that pulse modulation has a major effect on the harmonic emission. As a result of this investigation, several characteristics of the harmonic emission have been documented for the first time. It is found that the amplitude of the harmonic emission depends strongly on the cathode voltage, that the response time of the harmonic emission decreases with increasing neutral gas pressure, and that the linewidth of the harmonic emission lines increases with the cathode voltage. Since high intensity radiation is also observed, we will begin with a brief summary of the behavior of the high intensity radiation and indicate how it is avoided during the harmonic emission experiment. Then the harmonic emission effects will be described in detail.

5.6.1 Suppression of High Intensity Radiation

The harmonic emission can not be studied effectively unless it can be distinguished from the high intensity radiation. Such radiation presents a potential problem, since it is much more intense than the harmonic emission which is of interest here. In the TG pulse modulation mode, the cathodes are connected in parallel and are pulsed identically. The modulation pulse merely alters the cathode voltage for a short time corresponding to the duration of the pulse. As a result, the high

intensity radiation associated with the TG pulse behaves very much like the high intensity radiation of the dc discharge. Such radiation has been discussed in the previous sections of this chapter.

It is found that the amplitude of the high intensity radiation depends strongly on the amplitude and the polarity of the applied TG pulse. The high intensity radiation of the dc discharge is suppressed when the polarity of the TG pulse is positive. For very large positive pulse amplitudes, all high intensity radiation is eliminated during the pulse. On the other hand, if the pulse polarity is negative the radiation is greatly enhanced. The radiation amplitude is proportional to the pulse amplitude as is the duty cycle of the radiation bursts. However, even for the largest pulse amplitudes the intensity is somewhat less than that observed previously using the OPP pulse mode.

Fortunately this high intensity radiation can be avoided by proper choice of the experimental parameters, even when the pulse polarity is negative and the pulse amplitude is large. The high intensity radiation is minimized during the investigation of harmonic emission by keeping both the magnetic field and the discharge current large.

The high intensity radiation exhibits a strong dependence on the discharge current. It is maximum for the discharge current which corresponds to onset of the harmonic emission. Ordinarily the harmonic emission is studied at significantly larger discharge currents in which case the high intensity radiation is greatly reduced.

The high intensity radiation also depends on the magnetic field. As noted previously in Section 5.4, the magnetic field and discharge

current dependences of the radiation are interrelated. Since relatively large discharge currents are used, the high intensity radiation occurs principally at low magnetic fields where $\omega/\omega_c \simeq 20$. Therefore, the high intensity radiation can be avoided by restricting the investigation to the lower harmonics ($\omega/\omega_c \simeq 3$-6) which are located at higher fields. The high intensity radiation is never very pronounced at the lower harmonics even when the discharge current is more favorable. Recall that high intensity radiation is seldom observed for $B \gtrsim 0.7$ kilogauss ($\omega/\omega_c \gtrsim 3$). Also, the fact that the high intensity radiation spectrum exhibits deep minima at the lower harmonics of the electron cyclotron frequency is beneficial.

Because the behavior of the high intensity radiation has been carefully investigated, it can usually be avoided. It is relatively simple to determine how well the high intensity radiation has been suppressed: when the cathodes are modulated with a large amplitude negative polarity pulse, the high intensity radiation should be negligible between the harmonics.

Although the problem caused by the high intensity radiation is solvable, there is an additional complication which can not be overcome. Unavoidable transient effects are observed when the neutral gas pressure is low. These effects will be pointed out in the data and will be described in greater detail at that time.

5.6.2 The Time and Voltage Response of the Harmonic Emission

The time and voltage response of the harmonic emission were explored using TG pulse modulation. The investigation was carried out in both the nonstabilized and grid-stabilized columns of the 2.6" and 4"

discharges. Although the emission amplitude experienced minor variations in the different configurations, the major effects of pulse modulation were essentially the same in each case. The data described below were obtained using the 2.6" unstabilized plasma column.

The time response of the harmonic emission during the modulation pulse is indicated in the lower waveform of Figure 5.11. The upper waveform shows the cathode voltage corresponding to a -200 volt TG modulation pulse. The modulation pulse is approximately one microsecond in length and has a 5 KHz repetition rate. The upper waveform provides an accurate indication of the beginning and end of the pulse. However, since it was obtained by using a 100X probe on the input of the boxcar integrator, the waveform does not accurately reproduce the shape of the modulation pulse. When this same waveform is displayed on an oscilloscope using the same 100X probe, the oscillations at the beginning and end of the pulse are reduced and the risetime is found to be less than 25 nanoseconds.

The lower waveform of Figure 5.11 displays the time response of the harmonic emission. The emission amplitude is indicated in terms of the equivalent radiation temperature in electron volts. It is readily seen that the harmonic emission amplitude is enhanced by the negative polarity TG pulse. The harmonic emission amplitude increases to a new level shortly after the application of the pulse and then returns to the original level following the end of the pulse.

Observe that the harmonic emission does not respond immediately to the change in the cathode voltage. Rather, there is a brief delay at both the beginning and end of the pulse. The delay time at the

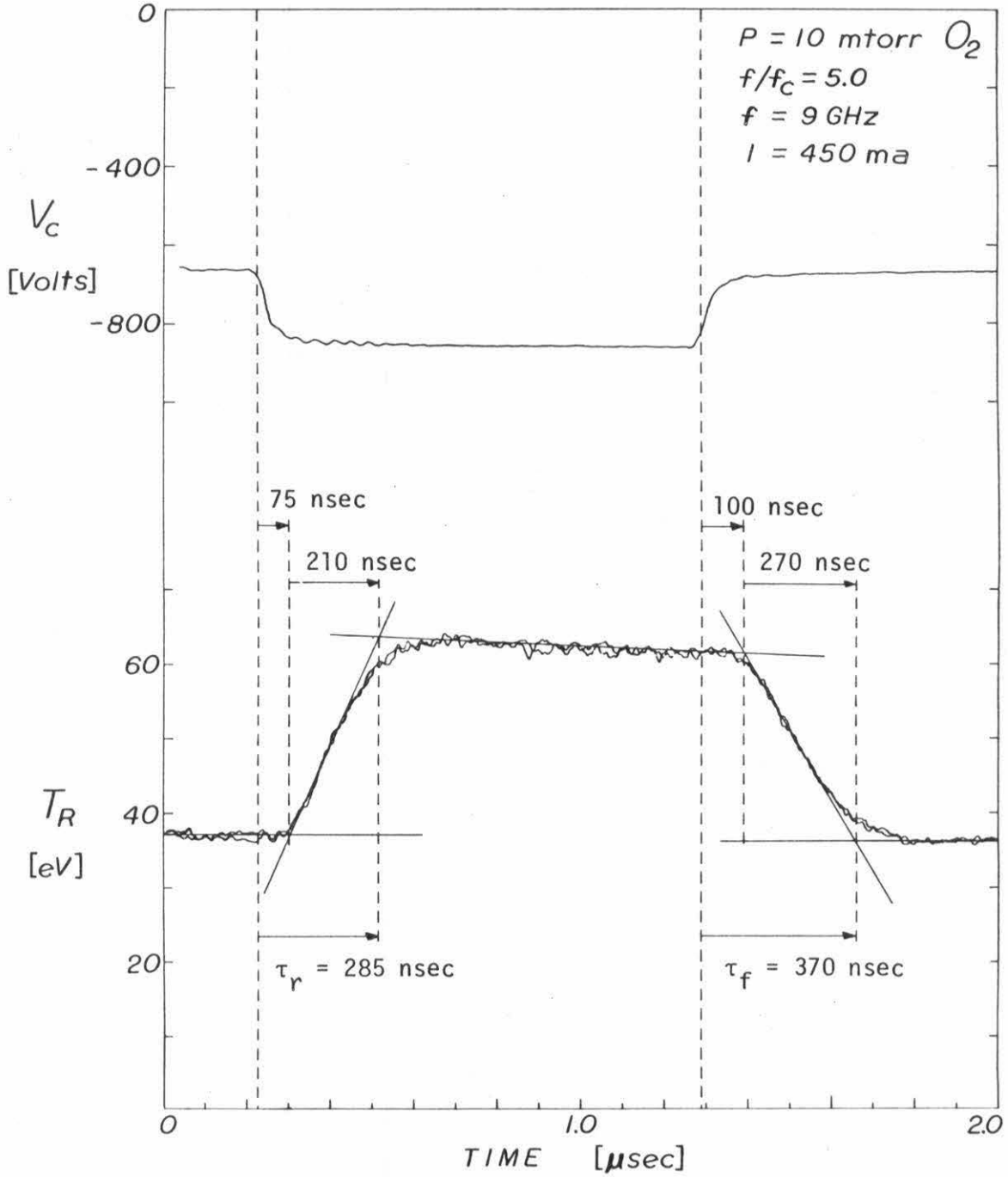

Figure 5.11 Radiation Temperature of the Harmonic Emission (m=5) in eV as a Function of Time During the TG Modulation Pulse. The upper waveform shows the cathode voltage during the pulse.

beginning of the emission waveform shown in Figure 5.11 is 75 nanoseconds. Note that a correction has already been made for the 40 nanosecond propagation delay of the I-F system.

Following the initial delay, there is a transition time during which the emission changes from the original level to a new level. This transition time is estimated by drawing a line through the waveform which matches the slope of the emission during the first half of the transition. For the emission waveform shown in Figure 5.11, the transition time at the beginning of the pulse is 210 nanoseconds.

The sum of the delay time and transition time will be referred to as the emission response time, τ_R . If the emission level increases during the transition, the response time will be referred to as a rise time, τ_r . And if the emission level decreases during the transition, the response time will be referred to as a fall time, τ_f . The reason for this choice of terminology will become clear later. However, for clarity it is necessary to point out that the rise and fall times as used here include both the transition time and the initial delay time. For the emission waveform of Figure 5.11, the emission risetime, τ_r, is 285 nanoseconds and the emission falltime, τ_f , is 370 nanoseconds.

Thus the response of the harmonic emission to TG pulse modulation consists of a change in the emission level for the duration of the pulse together with the associated rise and fall times. These parameters were investigated in a systematic fashion. But before presenting additional results, there are two considerations which should be mentioned. The first is that the emission waveform of Figure 5.11 was recorded at the

$m = 5$ harmonic of the electron cyclotron frequency. All subsequent graphs which indicate the time response of the harmonic emission were also obtained at the $m = 5$ harmonic. The second consideration concerns the fact that the emission waveform obtained using the boxcar integrator is an average of many individual waveforms. The waveform obtained from a single pulse was examined using the oscilloscope and it was determined that the envelopes of the individual waveforms are nearly identical. As a result the boxcar averaged waveform gives an accurate indication of the waveform obtained for a single pulse.

Figure 5.12 shows the time response of the harmonic emission for a variety of pulse amplitudes and polarities. The corresponding harmonic emission and cathode voltage waveforms are identified with capital letters. Recall that both cathodes are pulsed together in the TG pulse modulation mode. It is evident that the harmonic emission is enhanced by a negative polarity TG pulse which increases the magnitude of the cathode voltage and is diminished by a positive pulse.

The data of Figure 5.12 were obtained at a significantly higher pressure than that of Figure 5.11. Observe the corresponding decrease in the response time of the harmonic emission. Both the rise time and the fall time of the harmonic emission are considerably shorter. The decreased response time results principally from a shorter transition time although there is also a minor decrease in the delay time.

Figure 5.13 shows how the time response of the harmonic emission is modified when the neutral gas pressure is reduced to a low value. Observe that the rise time and falltime are considerably longer than they were at higher pressure. The response time of the harmonic emission is

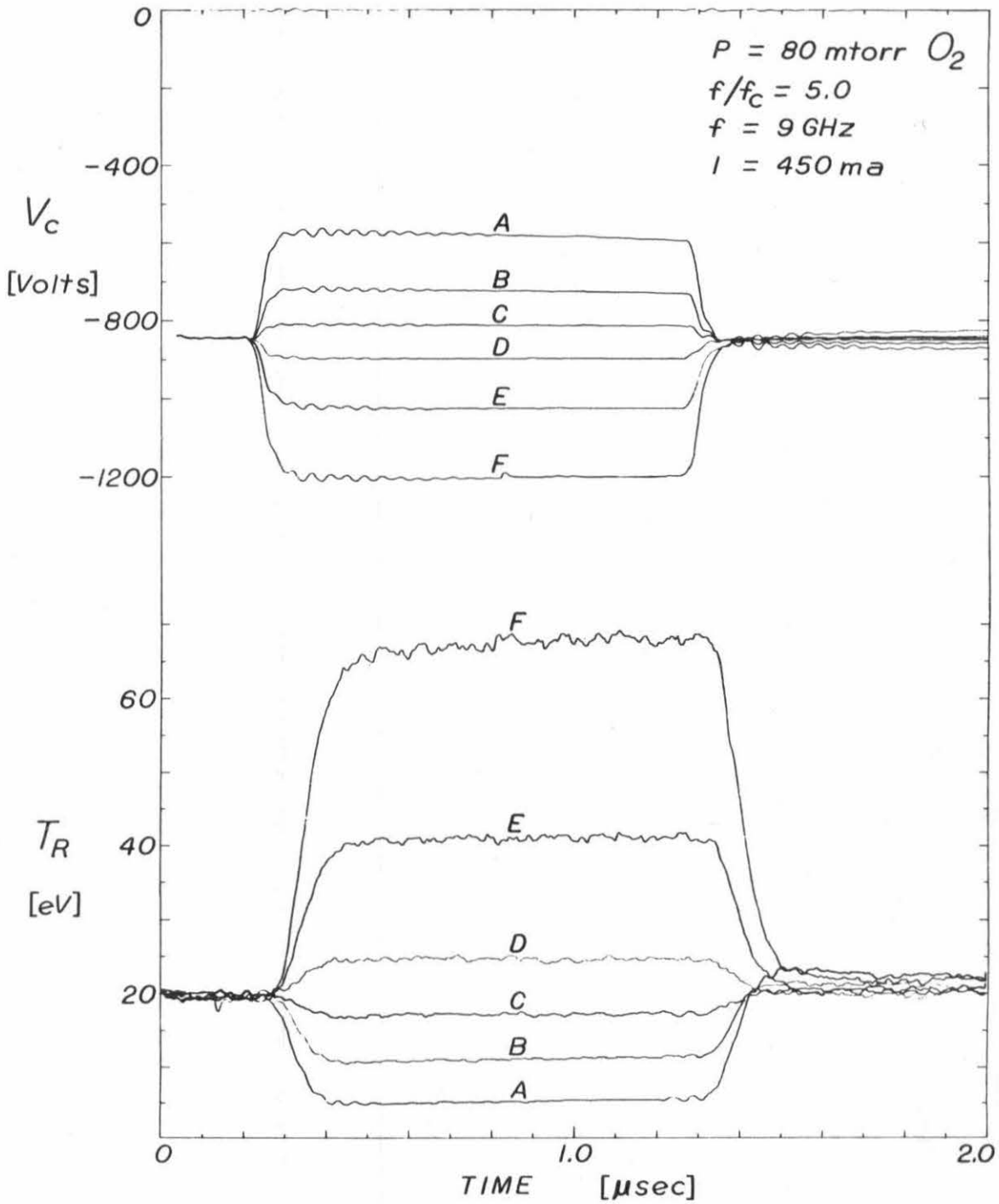

Figure 5.12 Radiation Temperature of the Harmonic Emission (m=5) in eV as a Function of Time During the TG Modulation Pulse for Several Pulse Amplitudes of Each Polarity. The corresponding cathode voltage waveforms are shown at the top of the graph.

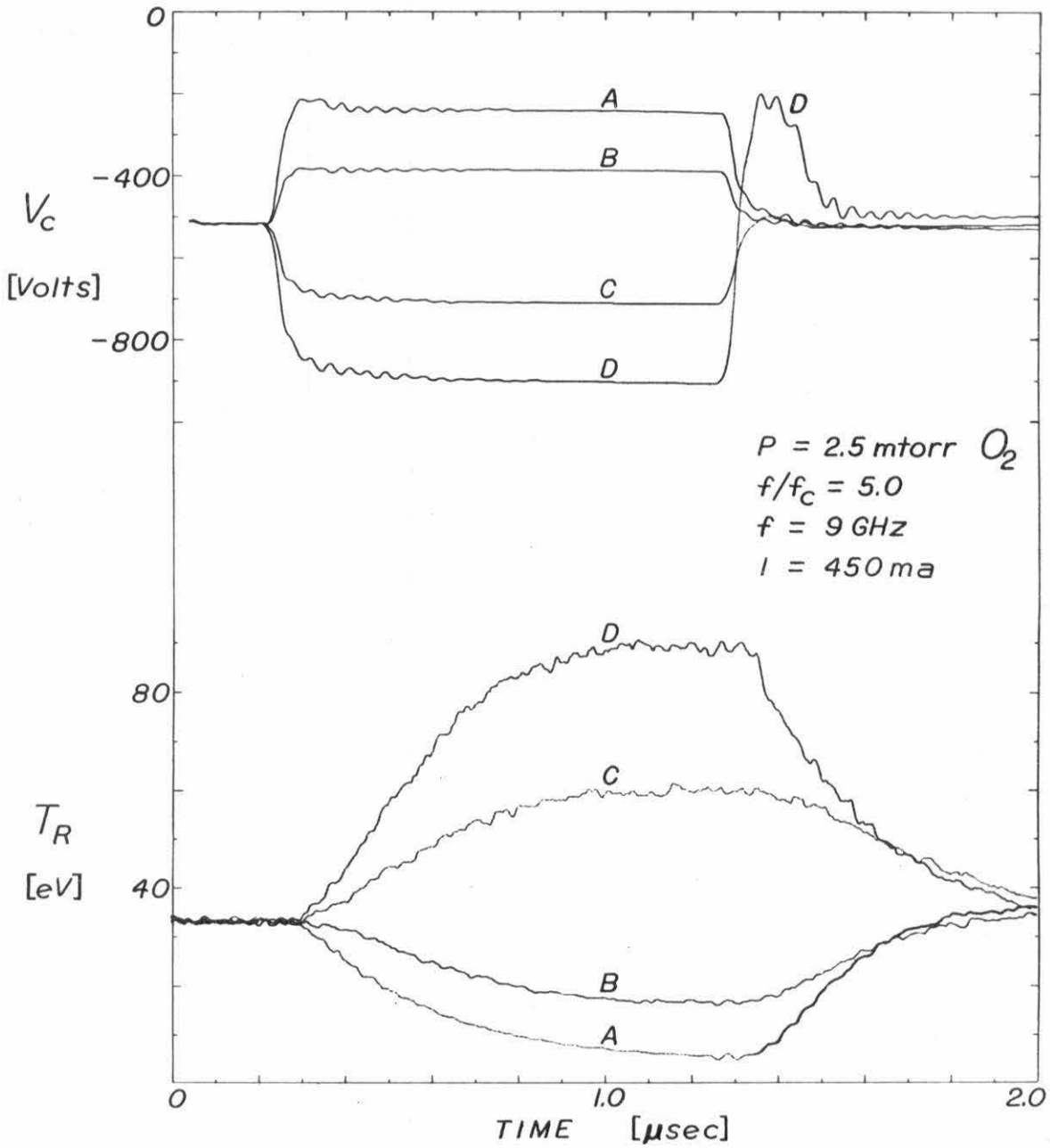

Figure 5.13 Radiation Temperature of the Harmonic Emission (m=5) in eV as a Function of Time During the TG Modulation Pulse for Several Pulse Amplitudes of Each Polarity. The corresponding cathode voltage waveforms are shown at the top of the graph.

comparable to the length of the pulse. When the neutral gas pressure is further reduced, it is necessary to increase the pulse length in order to obtain accurate indications of the rise and fall times and the emission level during the pulse.

A more serious problem is displayed by waveform D of Figure 5.13. The voltage waveform (D) behaves strangely at the end of the pulse. This complication is attributed to a negative resistance effect associated with electron bombardment of the cathodes. At low pressures this effect is observed at the beginning of positive TG pulses and at the end of negative TG pulses. The effect is strongest when the pulse amplitude is large. It occurs whenever the discharge voltage is changing very rapidly in the positive direction in which case many of the energetic electrons in the discharge are collected by the cathodes with a significant amount of excess energy. If the coefficient of secondary emission for these electrons is greater than unity, then the cathodes experience a dynamic negative resistance.

The unfortunate aspect of this effect is the influence which it has on the response time of the harmonic emission. As indicated by emission waveform D, the harmonic emission experiences a sudden drop at the end of the pulse. Therefore, the emission response time obtained under these circumstances reflects a different process and can not be compared directly with the other response times.

After the pulse response of the harmonic emission was investigated over a large pressure range, two features of the emission were quantified. They include the dependence of the harmonic emission intensity on the cathode voltage and the pressure dependence of the rise and fall

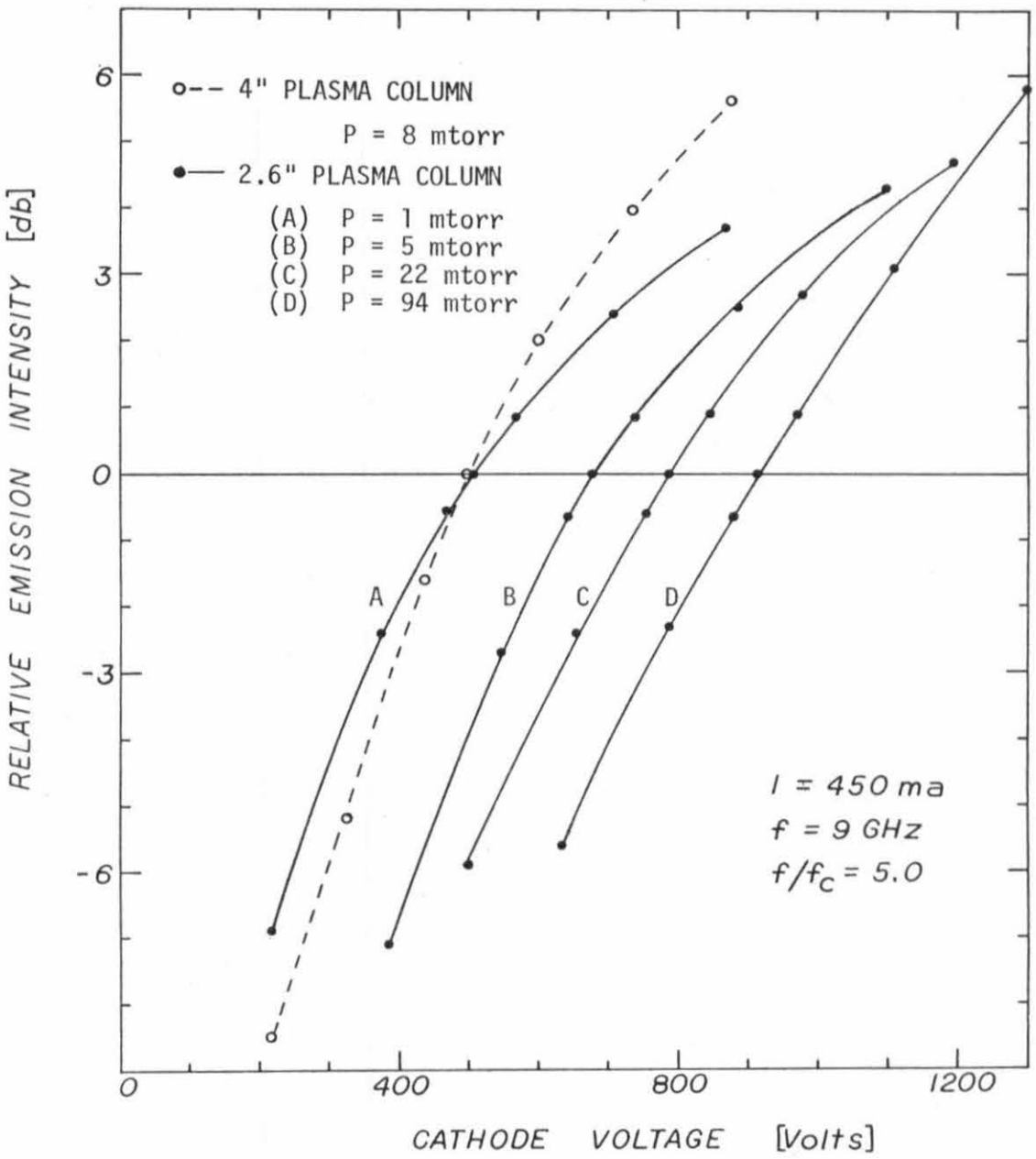

Figure 5.14 Relative Harmonic Emission Intensity in db as a Function of the Pulsed Cathode Voltage. At Each Value of the Neutral Gas Pressure the 0 db Level Corresponds to Emission from the DC Discharge with No Pulse Modulation.

times of the emission.

The first of these results is presented in Figure 5.14. The voltage dependence of the harmonic emission intensity is plotted at each pressure. The emission level relative to the level observed both before and after the modulation pulse is plotted in db versus the cathode voltage. The data were obtained using three different pulse amplitudes for each pulse polarity. Although most of the data were obtained from the 2.6" nonstabilized column, the dashed line indicates a similar curve obtained in the 4" column. The displacement of the curves from one another reflects the fact that the DC voltage of the discharge changes with pressure. The voltage of the dc discharge corresponds to the 0 db emission level. Because the emission intensities are relative, they do not reflect the fact that the harmonic emission intensity changes with pressure.

In Figure 5.15 the voltage dependence of the harmonic emission intensity is plotted on a linear scale. The data are from the same series plotted in Figure 5.14, but include different values of the neutral gas pressure. The linear graph illustrates the strong cathode voltage dependence of the harmonic emission intensity more clearly

The rise and fall times of the harmonic emission are plotted as a function of the neutral gas pressure in Figure 5.16. In each case, the response time decreases with increasing neutral gas pressure. Note that the rise time characterizes the response of the harmonic emission intensity at the beginning of a negative modulation pulse and at the end of a positive modulation pulse. Accordingly, the fall time characterizes the emission response at the end of a negative pulse and at the

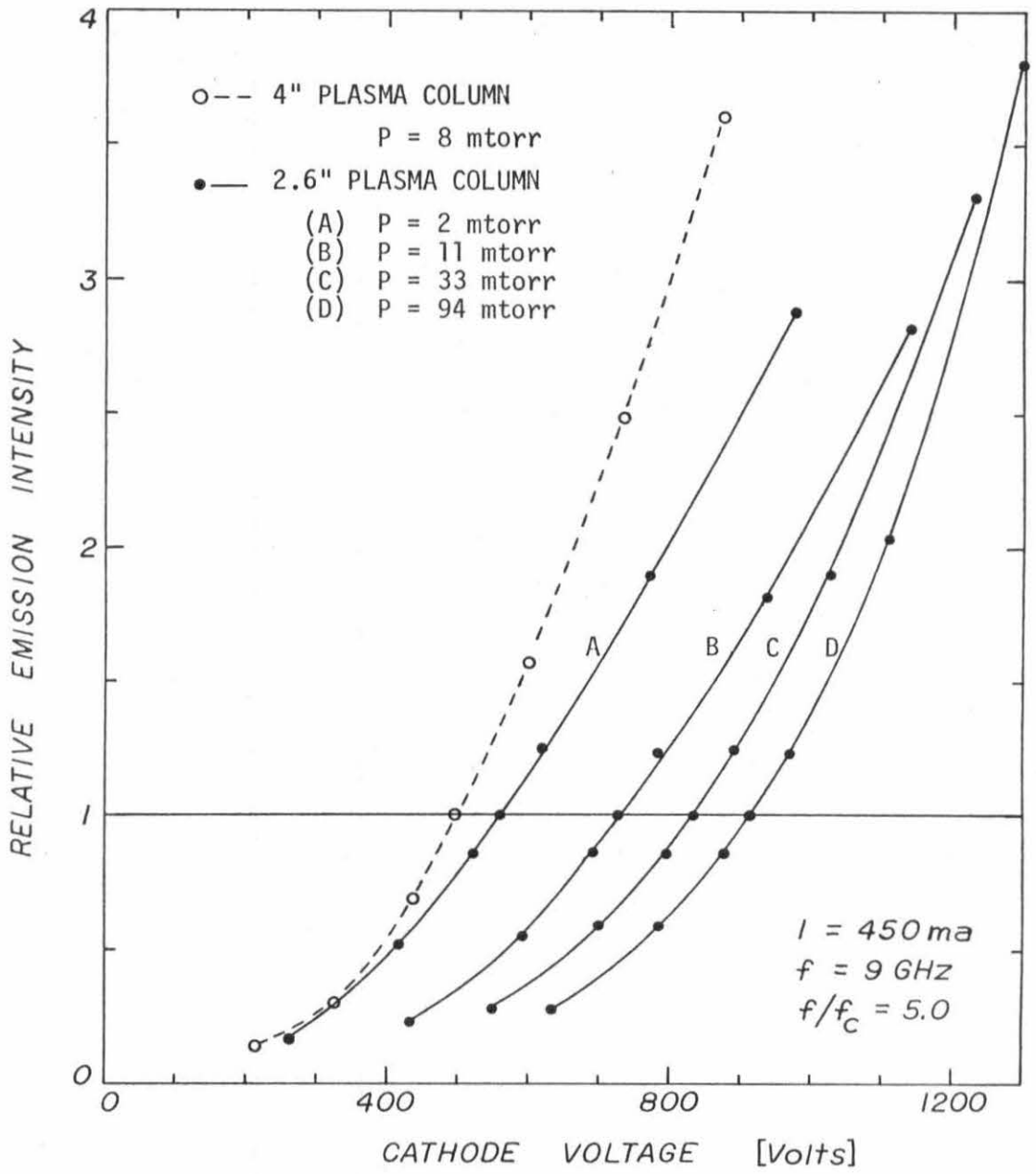

Figure 5.15 Harmonic Emission Intensity Relative to the Level Observed in the DC Operated Discharge as a Function of the Pulsed Cathode Voltage.

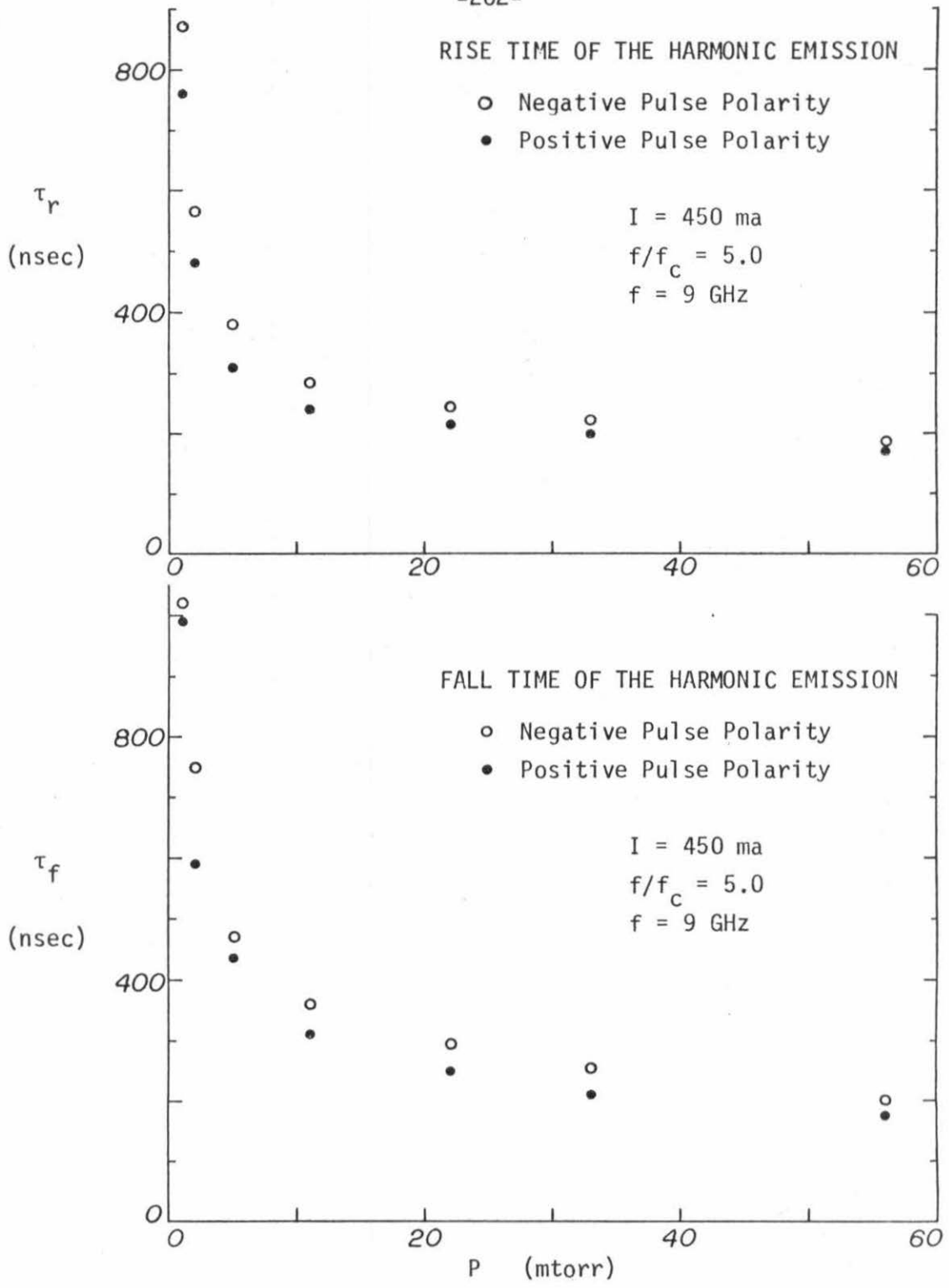

Figure 5.16 The Rise Time τ_r and the Fall Time τ_f of the Pulse Modulated Harmonic Emission as a Function of the Neutral Gas Pressure.

beginning of the positive pulse. Observe that the response times for the negative modulation pulse are consistently longer than the corresponding response times for the positive pulse. Also the rise times for a given polarity pulse are consistently shorter than the fall times.

It has already been noted that the change in the response time of the harmonic emission results principally from a change in the transition time, although there is also a minor change in the delay time. At high pressure the delay time is typically 50 nanoseconds. The delay time exhibits the same general behavior as the rise and fall times. The rising delay time is consistently shorter than the falling delay time and the delay observed for a negative pulse is consistently longer than that observed for a positive pulse.

The time response of the harmonic emission was also investigated for several different values of ω_c/ω in the vicinity of the $m = 5$ harmonic of the electron cyclotron frequency. When the time response at the peak of the emission line ($\omega/\omega_c = 5.0$) is compared with the time response at the -3 db and -10 db points on the emission line, no changes are detected. Both the delay and transition of the harmonic emission are apparently independent of the frequency. The time response of the harmonic emission was also investigated at several different harmonics.

Thus, two features of the harmonic emission have been documented using TG pulse modulation. It is found that the harmonic emission intensity increases rapidly with the magnitude of the cathode voltage and that the response time of the harmonic emission decreases with increasing pressure.

5.6.3 The Frequency Spectrum of the Pulse Modulated Harmonic Emission

Up to this point, the harmonic emission has only been displayed as a function of time during the modulation pulse. If instead the boxcar sampling time is held fixed at a certain time during the pulse, then the emission spectrum can be obtained by sweeping the magnetic field. Typical spectra are shown in Figure 5.17. The upper graph was obtained using a negative TG modulation pulse and the lower graph was obtained using a positive TG modulation pulse. Observe that the emission intensity for the upper spectrum is 11-12 db greater than that of the lower spectrum. During these measurements, the image frequency of the heterodyne receiver was rejected using the tunable microwave filter.

An interesting feature of the harmonic emission spectra shown in Figure 5.17 is the change in the width of the emission lines. It is found that the emission linewidth increases with the cathode voltage. This behavior is documented more quantitatively in Figure 5.18, where the width of the emission line, 100 $(\Delta\omega/\omega)$, is plotted as a function of the cathode voltage. This is the only situation throughout the entire investigation in which the emission linewidth was found to change in a systematic fashion when an experimental parameter was varied. As indicated earlier in Figure 3.7, the emission linewidth fluctuates when the neutral gas pressure is varied but does not change in a systematic fashion.

Note that the background radiation observed between the harmonics in Figure 5.17 constitutes a greater fraction of the plasma emission when the positive pulse is used. This result is reasonable since some of the background radiation is thermal radiation and therefore would

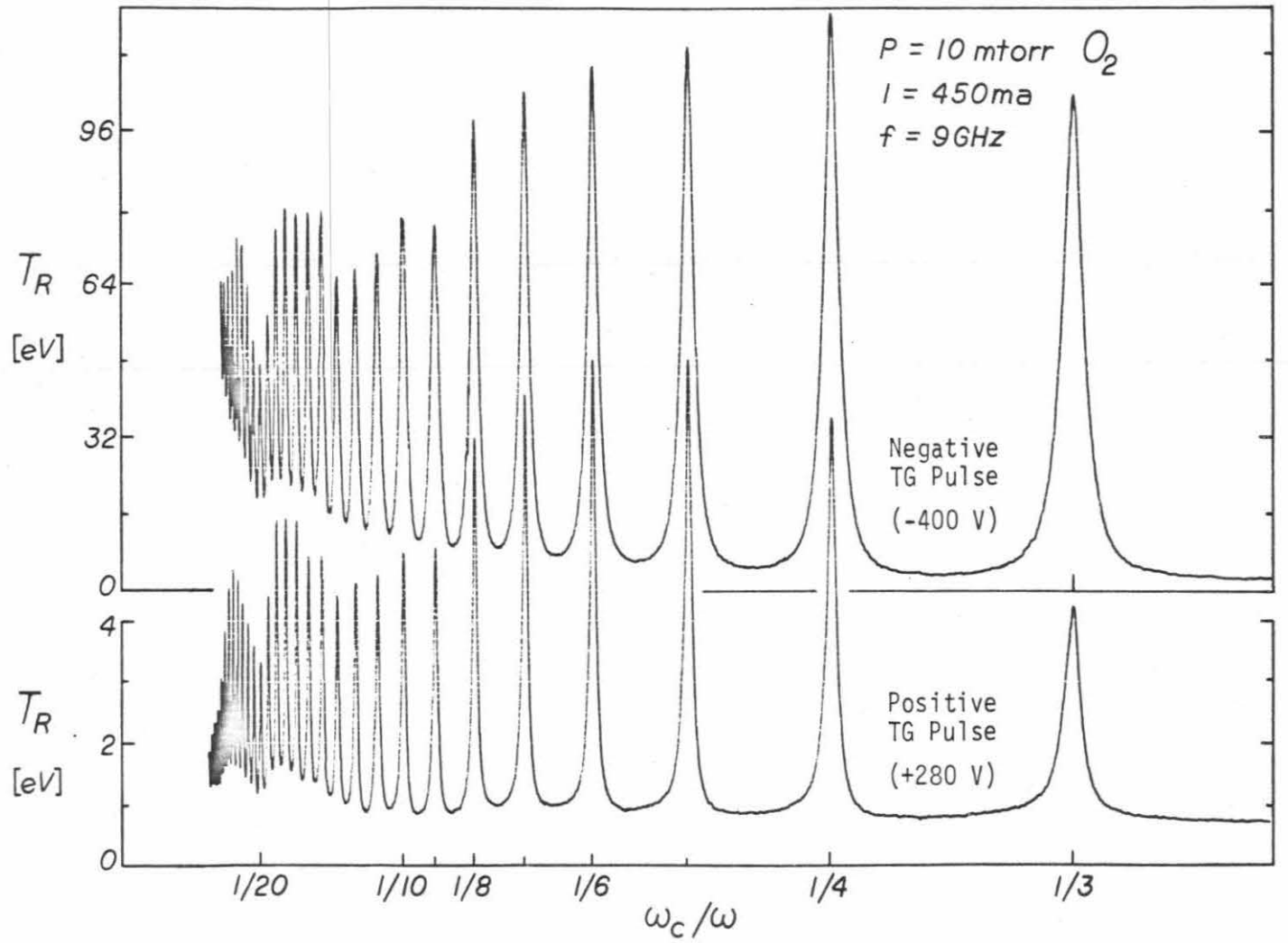

Figure 5.17 Harmonic Emission Spectra Obtained During Both a Positive and a Negative TG Modulation Pulse

still be present even if all of the nonthermal radiation were suppressed.

This concludes the presentation of the harmonic emission effects observed using TG pulse modulation. These results provide information which could not be obtained in the dc operated discharge. The approach developed here extends the scope of the experimental investigation of electron cyclotron harmonic emission and should be quite helpful in clarifying the mechanism of that radiation.

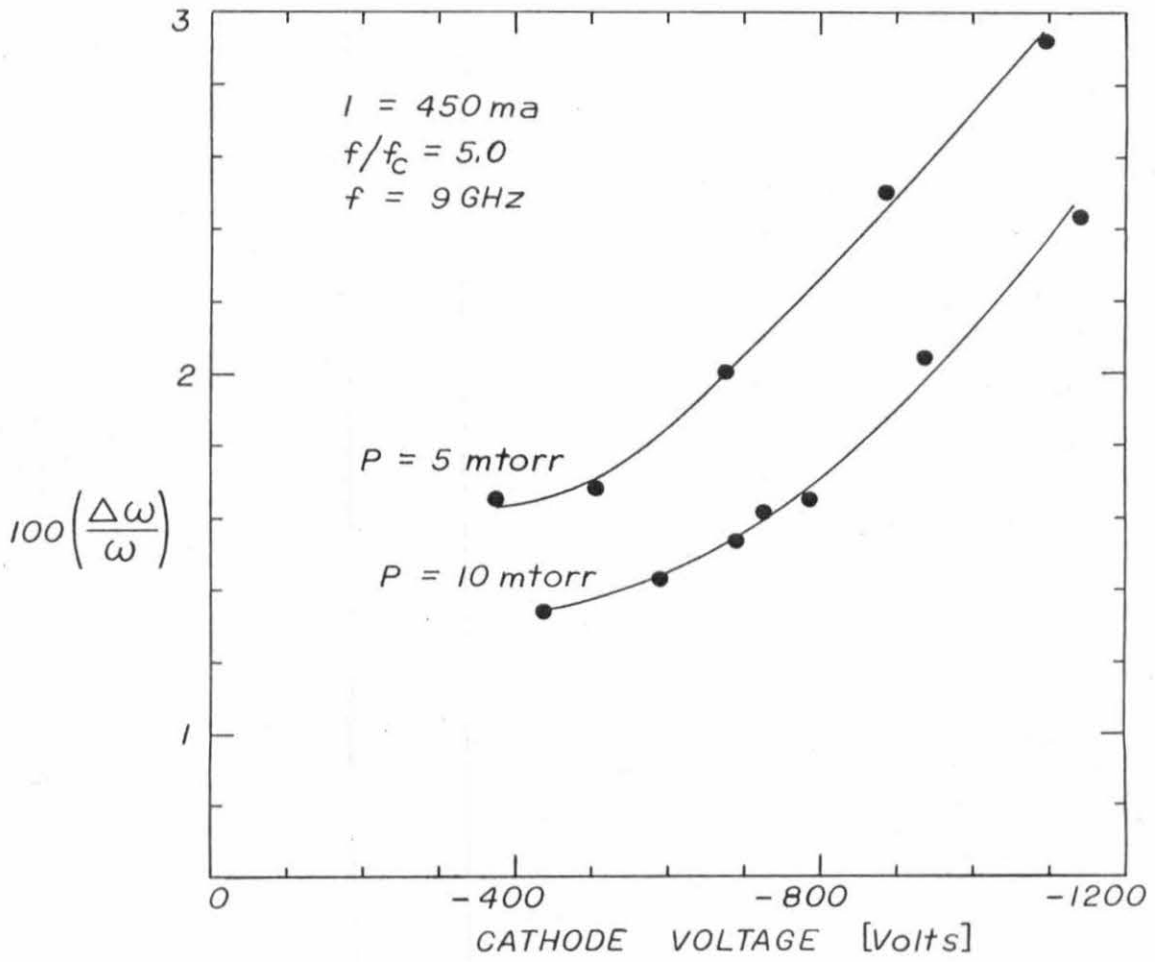

Figure 5.18 Linewidth of the m=5 Harmonic Emission Line as a Function of the Pulsed Cathode Voltage.

5.7 Interpretation of Harmonic Emission Effects

The harmonic emission of the Penning discharge has been explored using a pulse modulation technique. As a result of this investigation the following three features of Landauer emission have been documented for the first time:

1. It is found that the response time of the harmonic emission decreases with increasing neutral gas pressure.

2. The harmonic emission intensity increases rapidly with the magnitude of the cathode voltage.

3. The width of the harmonic emission lines increases with the magnitude of the cathode voltage.

In this section, plausible explanations are presented for the observed behavior. It is found that the experimental results provide important clues concerning the mechanism of the harmonic emission. For example, the response time of the harmonic emission suggests that the emission is produced by electrons of intermediate energy $15\ eV < E < 100\ eV$. Also, the voltage dependence of the intensity of the harmonic emission suggests that the radiating electrons have a large velocity component perpendicular to the magnetic field. The following discussion will concentrate mainly on the first two items in the above list, the third being a smaller effect which is also more difficult to explain.

5.7.1 Time Response of the Harmonic Emission

The pressure dependence of the response time of the harmonic emission is evident from figure 5-16. The fact that the response time, τ_R, decreases with increasing pressure suggests that τ_R is related to the lifetime of the energetic secondary electrons. When the cathode voltage is suddenly changed, the distribution function of the energetic electrons (E > 15 eV) is replaced by a new distribution in a time interval corresponding to the lifetime of the energetic secondary electrons. That lifetime is determined by the energy loss rate via inelastic electron-neutral collisions.

The energy loss time, τ_E, of the energetic secondary electrons is given by equation (15) of chapter II. Note that the time dependence of the energy of a fast electron has already been computed and is plotted in figure 2.14. If E_o is taken to be the energy of a secondary emission electron, then

$$\tau(25\ \text{eV}) = \int_{E_o}^{25} \frac{dE'}{H(E')}$$

gives the time required for the secondary electron energy to fall to 25 eV. τ(25 eV) was computed for several values of the neutral gas pressure taking into account the fact that the secondary electron energy E_o is the difference between the cathode potential and the plasma potential, both of which are pressure dependent. The results of this calculation are indicated by the dashed curve in figure 5.19. The remainder of the figure is the same as figure 5.16. The extent of agreement between the computed energy loss time τ_E and the

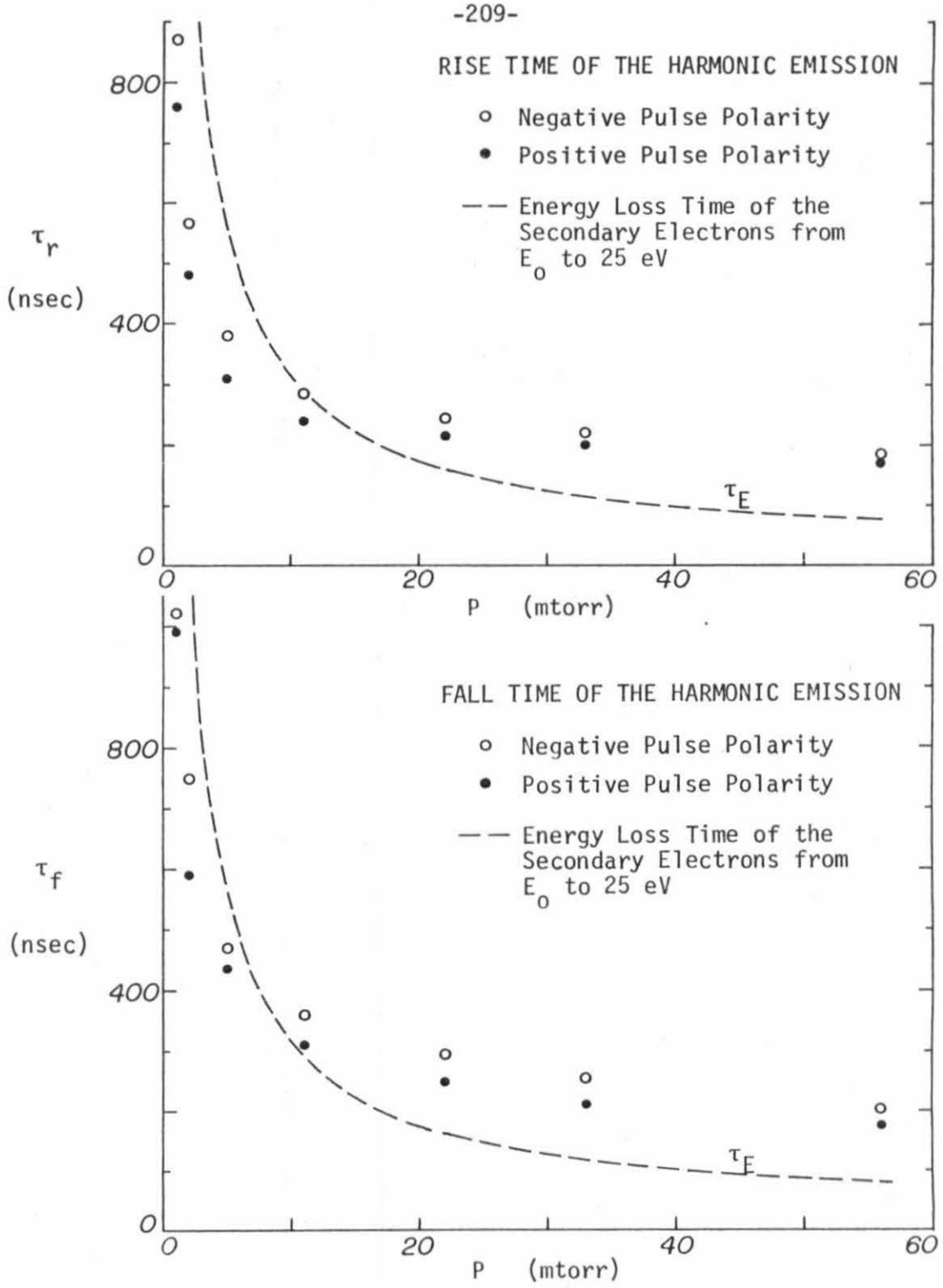

Figure 5.19 Comparison of the Computed Energy Loss Time τ_E with the Observed Rise and Fall Times, τ_r and τ_f, as a Function of the Neutral Gas Pressure

experimentally observed response times, τ_r and τ_f, is significant. The differences which are evident can be accounted for.

As indicated by figure 5.19, the experimentally observed harmonic emission response time remains nearly constant at high pressure. This behavior can be explained. Observe that the plasma is capacitively coupled to the cathodes of the discharge tube. The cathodes are separated from the plasma by relatively thin boundary sheaths. Since the surface area of the cathode is large, the capacitance involved is significant. When a pulse is applied to the cathode, capacitive coupling causes the plasma potential to follow the cathode potential. Therefore the potential drop across the cathode sheath doesn't change as rapidly as might be inferred by simply observing the cathode voltage waveform. Instead, the potential difference changes with an R-C time constant which is determined by the cathode sheath capacitance and the plasma impedance. Attempts to observe the time response of the plasma potential by using a probe were not satisfactory due to the lack of shielding of the probe and the limited bandwidth capability. Nevertheless, it appears that the response time of the harmonic emission at high pressure is limited not by the energy loss time of the injected electrons, τ_E, but rather by the time response of the potential difference across the cathode sheath.

Figure 5.19 also indicates that the response times, τ_r and τ_f, depart from the expected pressure dependence when the neutral gas pressure is low. When the oxygen gas pressure is 10^{-3} torr, a secondary electron injected into the plasma column with an energy of

500 eV transits the length of the column more than 50 times during the energy loss time τ_E . During this time the electron can be lost, for example, by turbulent diffusion across the plasma column. Therefore, particle losses can contribute to the energy loss rate. This is particularly true when the stabilizing grids are used. Many energetic electrons are collected by the grids. Therefore when the neutral gas pressure is low the energy loss time, τ_E , is not entirely determined by inelastic collisions. In addition, the pressure measurement is not very accurate at 10^{-3} torr and may be in error by a factor of two.

The above interpretation of the emission response time as an energy loss time provides an indication of the energy of the electrons involved in the emission process. The magnitude of the response time indicates that the relevant electrons have energies roughly in the range defined by 15 eV < E < 100 eV. If the emission producing electrons had energies much greater than 100 eV, then the emission response time would be significantly shorter. Also, it would be difficult to account for the initial delay which is observed in the time response of the emission during which the emission level does not change.

A similar statement holds for the lower bound of 15 eV. If the emission producing electrons had energies much less than 15 eV, then the expected response time would be much longer. Observe that the energy loss rate decreases by several orders of magnitude when the electron energy falls below 15 eV. This occurs because the

cross section for inelastic electron-neutral collisions vanishes at low energies. These electrons lose energy principally through collisions with thermal electrons. As a result, the energy loss time for $E < 15$ eV electrons is very long and nearly independent of the neutral gas pressure. Therefore, emission produced by $E < 15$ eV electrons would exhibit only a weak dependence on the neutral gas pressure. The emission response time would be much longer than is observed to be the case and would be nearly independent of the neutral gas pressure. Thus, both the magnitude of the response time and pressure dependence indicate that the harmonic emission is generated by electrons roughly in the intermediate energy range $15 \text{ eV} < E < 100 \text{ eV}$.

The association of the response time of the harmonic emission with the electron energy loss time is useful in explaining the fact that the emission rise time is consistently shorter than the fall time. As an illustration, assume that the harmonic emission is produced equally by all of the electrons in the energy range $15 \text{ eV} < E < 100$ eV and that the potential drop across the cathode sheath is 500 Volts. The energetic electrons present in the plasma column before the application of the cathode pulse will be referred to as "old" electrons and the secondary electrons injected into the plasma column after the application of the cathode pulse will be referred to as "new" electrons.

When a -100 volt pulse is applied to the cathodes, the harmonic emission increases to a higher level. The transition takes place during a response time which corresponds to the time required

for "new" beam electrons to lose energy and fall into the emission producing energy range of 15-100 eV. If the oxygen gas pressure is 10^{-2} torr, a 600 eV electron can lose 570 eV and become a 30 eV electron in 310 nsec. This is the characteristic time associated with adding "new" emission electrons.

When a +100 volt pulse is applied to the cathodes, the harmonic emission decreases to a lower level. In this case the transition time corresponds to the time required for all "old" electrons to be removed from the energy range $E > 15$ eV. First, note that when the cathodes are pulsed positively, all "old" electrons with energies greater than 400 eV are no longer reflected by the cathodes but are instead collected in one transit time. The remainder of the "old" electrons are then removed in the time required for a 400 eV electron to lose 385 eV of energy. If the oxygen gas pressure is 10^{-2} torr, this process takes 350 nsec. This is the characteristic time for the removal of the "old" emission electrons. That this later characteristic time is longer results from the rapid fall off of the inelastic energy loss rate at low energy, $E < 50$ eV.

It is important to point out that the expression derived in Chapter II for the inelastic energy loss rate, dE/dt, is oversimplified. Actually, dE/dt is somewhat greater at high energy and somewhat smaller at low energy. As a result, the asymmetry between the rise and fall times will be accentuated.

Thus, an analysis of the response time of the harmonic emission and the pressure dependence thereof reveals that the response time of the harmonic emission can be associated with the energy loss

time of the energetic secondary electrons. The experimental results are compatible with the view that the emission results from electrons of intermediate energy.

The asymmetry of the rise and fall times of the harmonic emission is attributed solely to the energy dependence of the inelastic energy loss rate. As a result, "new" electrons can be added in the energy range 15 eV < E < 100 eV more quickly than "old" electrons can be removed. One might inquire what distinguishes the "new" and "old" electrons such that each results in a different harmonic emission intensity in spite of the fact that both have the same energy and are present in roughly the same number density. That distinction will be taken up in the next section.

5.7.2 Cathode Voltage Dependence of the Harmonic Emission Intensity

The dependence of the harmonic emission intensity on the cathode voltage is evident from Figures 5.14 and 5.15. It is possible to interpret this dependence in several ways, only one of which is very satisfying. The cathode voltage dependence of the emission intensity cannot be attributed to a change in the number density of energetic electrons because the secondary electron current density is determined only by γ_i and J_i, both of which are nearly independent of the cathode voltage. Instead it is concluded that the amplitude of the emission is related to the perpendicular velocity component, $v_\perp$, of the source electrons.

Consider how the energetic electrons in the Penning discharge are affected by a change in the cathode voltage. The energy distribution of the energetic electrons computed in chapter II is based on the assumption that the energy distribution is determined by the inelastic electron-neutral energy loss rate (see Figure 2.13). This description predicts only a minor change in the distribution function when the energy of the secondary electron beam is temporarily altered by a cathode pulse. The only change consists of a temporary displacement of the location of the electron source in energy space by an amount determined by the amplitude of the applied pulse. Note that any dependence of either J_i or γ_i on the cathode voltage is ignored at this point. The distribution function is not appreciably altered except at high energies comparable to the energy at the secondary electron beam. However, in section 5.7.1 it was concluded

that such high energy electrons are not involved in the emission process. Therefore the indicated change in the energy distribution cannot account for the cathode voltage dependence of the harmonic emission.

It is important to note that up to this point the discussion has been based on a one dimensional energy space. A more useful description results if the electron energy is separated into components parallel and perpendicular to the magnetic field. The secondary emission electrons are injected into the plasma with only a parallel velocity component. As these energetic electrons move through the plasma, two processes occur simultaneously. The parallel velocity component is reduced very rapidly by the high inelastic energy loss rate. But in addition, the energetic electrons diffuse in velocity space acquiring a perpendicular velocity component at a rate characterized by the deflection time τ_D .

Observe that the deflection process and the energy loss process involve movement in orthogonal directions in the two dimensional energy space. Utilizing a polar coordinate system, energy loss involves movement in the $-\vec{r}$ direction and deflection involves movement in the $\pm\ \vec{\theta}$ directions.

It is essential to note that the deflection time is much longer than the collision time of the energetic electrons. This occurs because both elastic and inelastic scattering of high energy electrons by neutral gas atoms is principally forward scattering.

Born's approximation can be used to accurately describe the scattering of the high energy electrons in the neutral gas. The

differential scattering cross section, $I(\theta)$, is very large at small angles and falls off very rapidly as θ increases. Although the total collision cross section is given by

$$Q_T = \int I(\theta) d\Omega ,$$

the cross section which describes deflection in velocity space is given by

$$Q_D = \int I(\theta)(1 - \cos^2\theta) d\Omega .$$

The factor $1 - \cos^2\theta = \sin^2\theta$ characterizes the mean square increment in the transverse velocity of the electron.

It is evident that whenever strong forward scattering is involved, $Q_D << Q_T$. When Q_D and Q_T are computed for a 600 eV electron in O_2 gas using the approximate expressions for $I(\theta)$ given by Massey and Burhop [85], it is found that the ratio Q_T/Q_D ranges between 10 and 30 depending on which approximation is used and the nature of the collision, elastic or inelastic. Thus, the deflection time of the energetic secondary electrons is comparable to the energy loss time and the electron velocity remains directed nearly parallel to the magnetic field.

Losses of high energy electrons by diffusion across the plasma column helps to maintain a parallel directed velocity distribution. The diffusion rate is proportional to $v_\perp^2$. Therefore those electrons which experience a large deflection are lost most rapidly by diffusion across the magnetic field and the velocity distribution remains concentrated in the parallel direction.

For low energy electrons, the situation is very different. The differential scattering cross section $I(\theta)$ is much more isotropic. In this case $Q_D \simeq Q_T$ and isotropy of the velocity distribution is achieved after several collisions. At the same time, the energy loss rate of these electrons is greatly reduced from that at high energies. As a result the velocity distribution becomes isotropic in a time interval which is short in comparison with the energy loss time. Therefore the velocity distribution of $E < 15$ eV electrons is expected to be highly isotropic under all conditions.

The above considerations indicate that the velocity distribution is concentrated in the parallel direction at high energies but is always isotropic for $E < 15$ eV. For intermediate values of the electron energy in the range of 15-100 eV, the velocity distribution reflects various degrees of isotropy. It was concluded from the time response that these electrons are responsible for the harmonic emission. It seems apparent that the isotropy of this group of electrons depends on the cathode voltage. When the cathode voltage is increased, the secondary electrons have more time in which to acquire a perpendicular velocity component before falling into the indicated energy range. Therefore, the perpendicular energy content of the energetic emission producing electrons depends strongly on the cathode voltage. Since this appears to describe a major effect of the cathode pulse, it suggests that the emission amplitude is related to the perpendicular velocity component of the emission electrons.

This point of view gives further evidence that low energy electrons ($E < 15$ eV) are not involved in the emission process and

predicts saturation of the emission amplitude at high cathode voltages. When the cathode voltage is very low, the distribution function is only isotropic for E < 15 eV electrons. When the cathode voltage is increased, the isotropy and perpendicular energy content of the E < 15 eV electrons is not expected to change significantly. Therefore, electrons in this energy range cannot account for the cathode voltage dependence of the harmonic emission. However, as the cathode voltage is increased, the isotropy of the energy distribution at energies greater than 15 eV does in fact change.

Now consider what happens when the cathode voltage is very large. As the cathode voltage is increased, so is the perpendicular energy content of the electrons in the energy range of 15-100 eV. The perpendicular energy content of these electrons reaches a maximum when the energy distribution becomes isotropic in this energy range. This occurs when the cathode voltage reaches a value such that the time required for secondary electrons to fall to 100 eV exceeds the deflection time τ_D. At this point further increases in the cathode voltage will not increase the perpendicular energy content of the E < 100 eV electrons. Thus, the harmonic emission should saturate at high cathode voltages.

Of course this is an oversimplification because the harmonic emission is not produced equally by all of the indicated electrons. Also, electrons of higher and lower energies might produce smaller amounts of emission. As a result, saturation should occur more

gradually. In any case, this concept is in agreement with the data of Figure 5.14 and 5.15 which shows that the emission amplitude does not increase as rapidly at high voltages as it does at lower voltages.

There is additional experimental evidence which indicates the importance of the perpendicular velocity component $v_\perp$. On one occasion the discharge was operated with special conical cathodes. The cathodes were shaped so that the normal to the cathode surface is at a 30° angle with respect to the magnetic field. In this case the cathode sheath has an electric field component in the direction perpendicular to the magnetic field. Therefore secondary electrons acquire a perpendicular velocity component when they are injected into the plasma. The observed harmonic emission intensity was found to be consistently higher by 1-2 db when using this cathode configuration. Unfortunately, it is not known how much of this change is due to changes in the cathode voltage and floating potential. Nevertheless, the increase seems to be attributable to a change in the initial angular position of the secondary electrons in velocity space.

Consider briefly another possible interpretation of the observed dependence of the harmonic emission amplitude on the cathode voltage. The interpretation presented earlier assumed that both the incident ion saturation current, J_i, and the coefficient of secondary emission by ion bombardment, γ_i, were independent of the cathode voltage. Observe that the production rate of energetic electrons is directly proportional to the second emission current, $J_e = \gamma_i J_i$. It is apparent that if this product is voltage dependent, then a change in the cathode voltage will result in a change in the number

density of energetic electrons and the emission amplitude will be altered accordingly.

Adopting this explanation, the interpretation of the time response of the harmonic emission would undergo only a minor change of meaning. The response time would indicate the time required to increase or decrease the number density of energetic electrons in the relevant energy range.

Assume, for a moment, that the voltage dependence of the parameter $\gamma_i J_i$ is solely responsible for the dependence of the harmonic emission amplitude on the cathode voltage. Then it must be able to account for a 10 db change in the emission amplitude when the potential drop across the cathode sheath changes from 300 volts to 800 volts. It is difficult to perceive how the quantity $\gamma_i J_i$ (and therefore the energetic electron density) could change by a factor of ten. The ion saturation current is not expected to change by more than 20% under these conditions. Similarly, in the absence of an oxide layer on the cathode surface γ_i should be independent of the energy of the incident ions. Although the oxide layer might result in a stronger voltage dependence, an order of magnitude change in γ_i is not expected for the indicated conditions. While it is true that the cathode voltage dependence of the parameter $\gamma_i J_i$ can account for minor changes in the emission amplitude, a factor of ten is difficult to believe.

In addition, it is observed that the width of the emission lines is dependent on the cathode voltage. It is difficult to associate the line width with the number density of energetic

electrons. However, when the perpendicular velocity component of the energetic electrons becomes involved, such an effect does not seem so unlikely.

In summary, we have presented an interpretation of the behavior of the pulse modulated harmonic emission. From the response time of the harmonic emission it is concluded that the emission results from electrons of intermediate energy, roughly 15 eV < E < 100 eV. From the cathode voltage dependence of the harmonic emission it is concluded that the emission intensity is related to the perpendicular velocity component of the source electrons. In both cases, the behavior of the harmonic emission indicates that the low energy electrons (E < 15 eV) are not of major importance.

5.8 Discussion of the Results

It is appropriate at this point to examine how the results of the pulse modulation experiment fit in with the theories of harmonic emission. At the beginning of this chapter it was stated that the harmonic emission apparently results from excitation of electrostatic waves followed by mode conversion at the hybrid layer. At that point, it was not clear whether the electrostatic waves were excited by independent electrons as in the single particle radiation theory of Canobbio and Croci [59] or through a wave instability such as that described by the helical beam theory of Seidl [69]. Both of these possibilities will be examined in light of the results of the pulse modulation experiment.

5.8.1 Comparison with the Theory of Canobbio and Croci

The experimental results are in good agreement with the suggestion by Canobbio and Croci [49] that electrons with velocity $v \sim 7v_{th}$ are responsible for the harmonic emission. In the present experiment ($T_e \sim .5$-1.0 eV) such electrons have energies of roughly 25-50 eV. This agrees quite well with the conclusion developed in section 5.7.1, that the harmonic emission results from electrons in the energy range of 15-100 eV.

According to Canobbio and Croci [53], the harmonic emission results mainly from nonthermal electrons whose perpendicular velocity component exceeds the phase velocity of the quasi-electrostatic wave, $v_\perp > v_{phase}$. In addition they conclude that the emission in the immediate vicinity of the harmonics can only be due to electrons whose

parallel velocity component is less than the thermal velocity, $v_{\parallel} \gtrsim \sqrt{2}\, v_{th}$ [59]. These theoretical predictions are in good agreement with the experimental results which indicate that the perpendicular velocity component is important and that electrons with a very large parallel velocity component are not involved in the emission process.

Recall that the secondary emission electrons are injected into the plasma column with a very large $v_{\parallel}$ velocity. According to the theory, these energetic electrons cannot excite harmonic emission until they lose their $v_{\parallel}$ velocity component. However they must retain a sizeable $v_{\perp}$ velocity component. Hence, the response time of the harmonic emission corresponds to the deflection time in velocity space, the large parallel velocity component is transformed into a lesser perpendicular component. Since the deflection process proceeds very slowly at high energies, the deflection time is comparable to the energy loss time. The experimental results indicate that even after a response time, the secondary electrons still retain roughly 15 eV of energy. Apparently this is the $E_{\perp}$ energy component of the emitting electrons.

With a single exception, the radiation mechanism described by Canobbio and Croci is in good agreement with the experimental evidence presented in chapters III and V. However, the theory cannot account for the weak dependence of the emission intensity on the neutral gas pressure shown in figure 3.4. If the harmonic emission is indeed the result of incoherent emission from independent source electrons, then the emission intensity should be directly proportional to the

number density of the energetic radiating electrons. In chapter II it was found that the number density of energetic electrons is inversely proportional to the neutral gas pressure. Therefore it is expected that the emission intensity should also be inversely proportional to the neutral gas pressure. This was not found to be the case in chapter III where we did not consider the fact that the discharge voltage changes with the neutral gas pressure. Now we have observed that both the amplitude and the width of the harmonic emission lines increase with the magnitude of the cathode voltage. Therefore it is important to correct the harmonic emission amplitude for the cathode voltage dependence on the neutral gas pressure.

In order to obtain the pressure dependence of the total harmonic emission power, it is necessary to consider both the amplitude and the width of the harmonic emission line. In performing this correction, it is not the cathode potential itself but rather the difference between the cathode potential and the plasma potential which is relevant. Since the plasma potential changes with the neutral gas pressure, care must be taken to properly determine the potential drop across the cathode sheath.

Figure 5.20 shows how the total harmonic emission power varies as a function of the potential drop across the cathode sheath. The total harmonic emission power is a product of the amplitude and the width of the harmonic emission line. Figure 5.21 shows how the total harmonic emission power varies as a function of the neutral gas pressure. The data has been corrected (using Figure 5.20) to compensate for the fact that the potential drop across the cathode

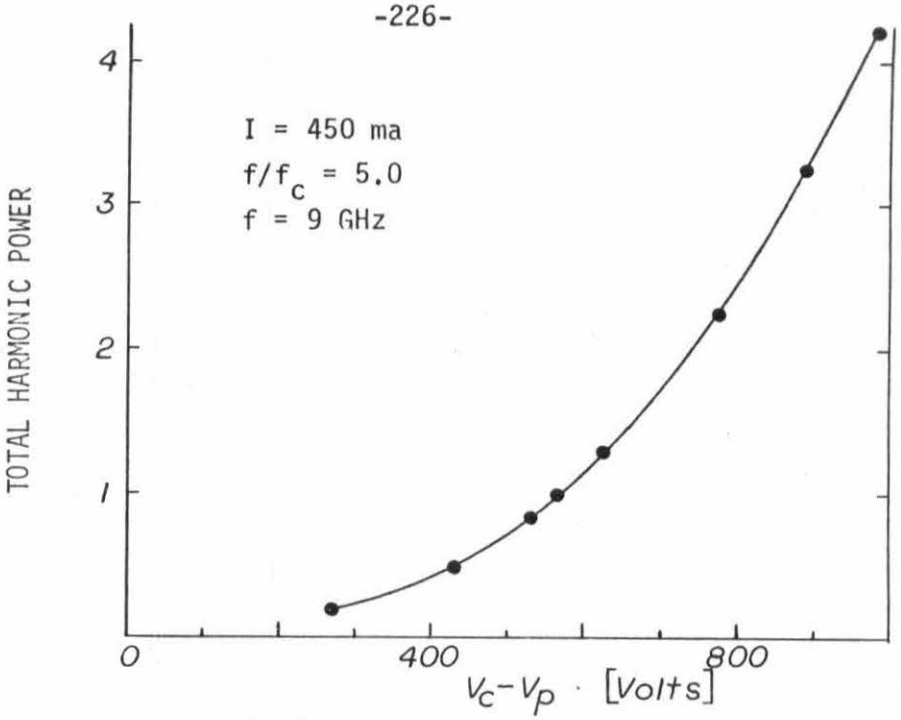

Figure 5.20 Total Harmonic Power as a Function of the Potential Drop across the Cathode Sheath, $V_c - V_p$

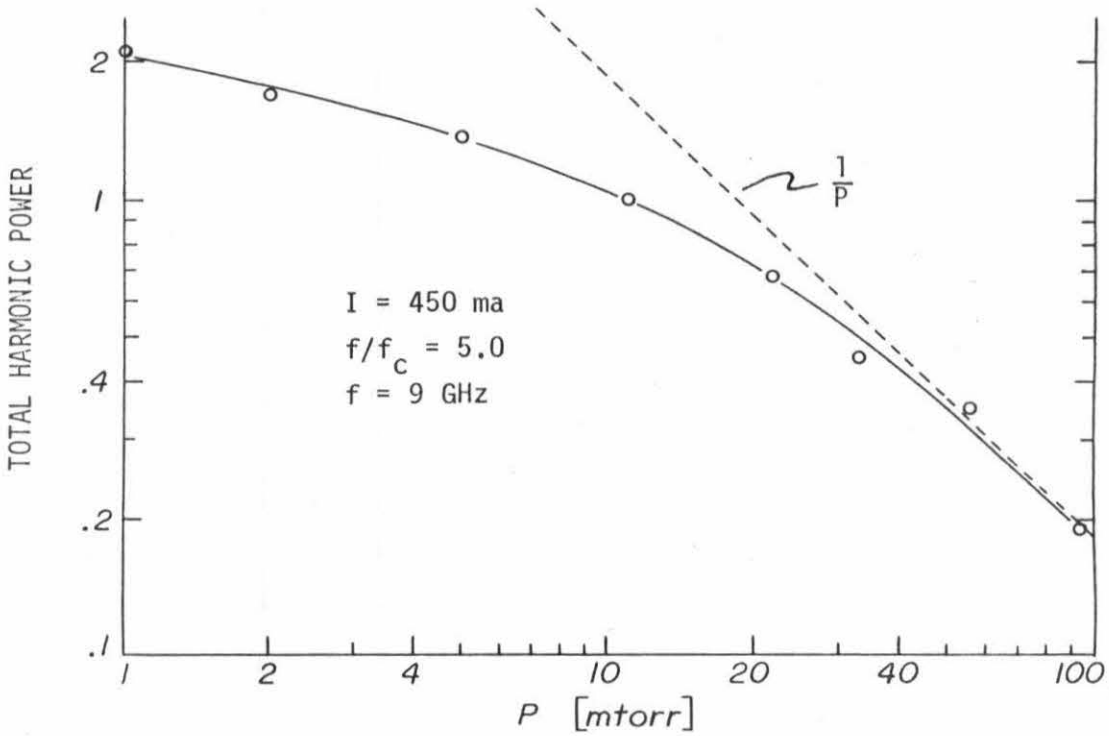

Figure 5.21 Total Harmonic Power Normalized to the Value at P = 10 mtorr as a Function of the Neutral Gas Pressure

sheath is a function of the neutral gas pressure. The graph indicates that at least at high pressure (P > 10 mtorr) the total harmonic emission power is nearly proportional to the reciprocal of the neutral gas pressure. This result is very encouraging.

Observe that the total emission power departs from the expected behavior at low pressure. There are several considerations which may explain why this occurs. For example, the electron temperature is pressure dependent (see Appendix C). Exactly how the electron temperature influences the harmonic emission is unknown, but it is not expected to be negligible.

However, the most important factor is quite simple. Recall that the emission intensity depends strongly on the electron density, saturating when the electron density reaches a value heretofore labeled N_{sat}. This electron density corresponds to a particular value of the discharge current. During the experiment the data were obtained using the same discharge current at each value of the neutral gas pressure. But figure 3.5 demonstrates that when discharge is operated at constant current, the electron density is much lower at low pressures. Although the electron density may have been sufficient to cause the harmonic emission to saturate when the neutral gas pressure was high, it is doubtful that saturation was achieved at low pressure. Therefore the departure of the emission amplitude from the expected reciprocal pressure dependence is believed to be due principally to the fact that the data is influenced by a pressure dependent electron density. This factor could be eliminated by taking precautions to assure saturation of the harmonic emission at

each setting of the neutral gas pressure.

In addition, the harmonic emission amplitude will not scale inversely with the pressure if the number density of the energetic electrons doesn't. At low pressure, the energy loss time of the energetic electrons corresponds to many transit times of the plasma column. Therefore diffusion losses become more important. In addition, in the electron energy range $E < 30$ eV energy losses by electron-electron collisions become comparable to the inelastic energy loss rate. As a result, the lifetime of these energetic electrons does not scale exactly inversely with the pressure. Both of these complicating factors probably contribute toward the observed pressure dependence.

Note that the pressure dependence of the total harmonic emission power (Figure 5.21) gives further evidence that electrons in the energy range $E < 15$ eV are not important to the emission process. The number density of these electrons is expected to be only weakly dependent on the neutral gas pressure. As a result, radiation produced by these electrons would not be expected to fall off as the reciprocal of the neutral gas pressure.

In summary, a comparison of the experimental results with the single particle radiation theory of Canobbio and Croci has resulted in good agreement. It is found that the harmonic emission can be explained on the basis of independent source electrons in the energy range of 15-100 eV. The amplitude of the emission is associated with the $v_\perp$ velocity component of the source electrons, that velocity component being determined by the potential drop across the cathode

sheath (the initial energy of the secondary emission electrons).

Although the comparison has indicated some departure from the behavior expected on the basis of the theory, at the same time no direct conflicts have appeared. Some of the discrepancies may be due to unknown factors such as the temperature dependence of the harmonic emission and other discrepancies can be attributed to real anticipatible effect such as capacitive coupling between the plasma and cathodes. Still, an interpretation has been presented which is consistent with all of the experimental results.

5.8.2 Possible Wave Instabilities

It is of interest to explore briefly the possibility that the experimental results might also be explainable on the basis of a collective effect in which the source electrons radiate coherently. It was concluded in section 5.5 that the harmonic emission does not result from a parallel beam-plasma interaction where the beam consists of the secondary emission electrons.

Thus, only one situation involving the collective interaction of energetic electrons has been ruled out, that being the beam-plasma excited wave instability which is responsible for the high intensity radiation. That similar effects involving a different group of energetic electrons might occur has not been ruled out. In this regard, the theoretical treatment by Seidl is very useful.

Seidl [69] investigated the effects of the interaction of a diffuse helical beam with a Maxwellian plasma. The velocity distribution of the helical beam is taken to be of the form

$$f_b(v_\perp, v_\parallel) = n_b\left(\frac{1}{\pi v_b^2}\right)^{1/2} \frac{1}{\pi V_\perp^2}\left(\frac{v_\perp}{V_\perp}\right)^2 \exp\left[-\left(\frac{v_\perp}{V_\perp}\right)^2 - \left(\frac{v_\parallel - V_\parallel}{v_b}\right)^2\right]$$

where the beam density n_b is assumed to be much less than the plasma density. In his calculations Seidl chose $V_\parallel = \sqrt{2}\, V_\perp$. Therefore the helical beam electrons have comparable parallel and perpendicular velocity components. The perpendicular velocity spread is very large and comparable to $V_\perp$. Thus, if the beam also has a very large parallel velocity spread, $v_b/V_\parallel \tilde{=} 1$, then the helical beam is a reasonably good description of the velocity distribution of intermediate energy electrons in the Penning discharge and the theoretical results should be reasonably applicable.

Seidl initially assumed that both the plasma electrons and the helical beam electrons were cold, $v_{th} = v_b = 0$. In this case he found that the helical beam can excite quasistatic waves propagating nearly perpendicular to the magnetic field. When the helical beam is given a finite parallel velocity spread, $v_b > 0$, the instability growth rate is suppressed everywhere except in the vicinity of the cyclotron harmonics where the growth rate is unaffected by the beam temperature, even when the beam temperature is very large. As a result, a helical beam with large parallel velocity spread, $v_b/V \simeq 1$ will only excite waves in the vicinity of the cyclotron harmonics. Seidl indicates that this result is in good agreement with the earlier experimental investigations of cyclotron harmonic emission in the Penning discharge.

Seidl gives an expression for the growth rate of the instability in the vicinity of the cyclotron harmonics (his equation 35). It is informative to compute the growth rate for the situation where the oxygen gas pressure is 100 mtorr, and the resulting helical electron beam density is only $10^7/cm^3$. If the mode of interest is the $m = 5$ mode, then his equation gives a normalized growth rate of $\omega_i/\omega_r \simeq 10^{-4}$ where ω_r and ω_i are the real and imaginary components of the complex frequency.

Note that the computed growth rate is the linear growth rate. One might expect that a wave instability with such a slow linear growth rate would be severely disrupted by the fluctuations of a turbulent plasma. Also, it is doubtful that the computed growth rate can account for the rise time of the harmonic emission. Since the microwave receiver frequency is 9 GHz ($\omega_r \simeq 5.7 \times 10^{10}$ rad/sec), Seidl's growth rate gives a minimum rise time of $\tau = 1/\omega_i \simeq 180$ nsec. Although the observed rise time at $P = 100$ mtorr is comparable, it should be noted that only the linear growth rate is available from the theory. Also, it is very difficult to describe the pressure dependence of the rise time in this way. Because of collisional damping due to electron neutral collisions it is expected that the rise time should decrease with increasing pressure, contrary to the experimental results.

In fact, calculations of the collision frequency indicate that collisional damping is severe at high pressure. When the oxygen gas pressure is 100 mtorr, the electron neutral collision frequency of the plasma electrons is approximately $\nu/\omega_r \gtrsim .01$. Since Seidl did not

include collisions in his model, the computed growth rate should be compared with the collision frequency. This suggests that if the instability is to be observed, the linear growth rate must exceed the collision frequency, $\omega_i/\omega_r \simeq .01$.

The possibility that a group of electrons with a large velocity spread and a fractional density of 10^{-5} can excite an instability with a growth rate on the order of $\omega_i/\omega_r \simeq .01$ is doubtful. Note that when the neutral gas pressure is 100 mtorr, the energetic electrons are so diffuse that their average spacing is approximately three Debye lengths ($\lambda_b \simeq 1.5 \times 10^{-3}$cm). Of course, since the electron velocity is much greater than the thermal velocity, the screening of these electrons is less effective. In view of the slow growth rate predicted by the theory of Seidl, strong collective interaction among such a diffuse group of energetic electrons seems unlikely.

Instead, the comparison with the theory of Canobbio and Croci presented in Section 5.8.1 is far more encouraging in terms of being able to account for the sum total of the experimental results.

CHAPTER VI

SUMMARY AND SUGGESTIONS FOR FURTHER WORK

6.1 Summary and Conclusions

This report presents a detailed experimental investigation of the harmonic emission produced by the magnetized plasma column of an oxygen gas Penning discharge. This investigation was undertaken to develop additional experimental data and to explore areas of agreement between the qualitative predictions of the theoretical models and the experimental results.

The harmonic emission is observed at 9 GHz while operating the Penning discharge in a large variety of configurations. When the usually turbulent plasma column of the Penning discharge is transformed into a quiescent plasma by grid stabilization, it is found that the harmonic emission is not significantly affected. Replacement of the reflecting metal vacuum wall with a transparent pyrex tube allows an accurate estimate of the total power radiated by the plasma column to be made.

The experimental results include a number of detailed quantitative measurements. On the basis of a microwave interferometer measurement of the electron density, it is concluded that the existence of a hybrid layer somewhere on the plasma column is a necessary condition for the observation of the harmonic emission. It is found that the individual emission lines are nearly symmetrical in shape and are located at the harmonics of the electron cyclotron frequency. It is found that the absorption spectrum of the plasma column is very different from the

emission spectrum, there are no detectable absorption resonances at the higher harmonics of the electron cyclotron frequency. Although the discharge is usually operated continuously at low current, the harmonic emission is also investigated during a high current pulsed discharge using receiver frequencies of 10 GHz and 50 GHz.

When these initial experimental results are compared with the various theories of harmonic emission, it is concluded that most are not important in the Penning discharge. However, several theoretical models look promising and it is concluded that additional experimental data of a basically different nature are needed before these theories can be distinguished.

A new experimental approach has been developed which utilizes a pulse modulation technique to investigate the cathode voltage dependence and the relaxation time of the harmonic emission. It is found that the intensity of the harmonic emission increases rapidly with the magnitude of the cathode voltage. Since pulse modulation of the cathode voltage results in amplitude modulation of the harmonic emission, the rise time and relaxation time of the harmonic emission are readily obtained. It is found that the response time of the harmonic emission decreases with increasing neutral gas pressure. In addition, it is found that the harmonic emission lines undergo broadening as the magnitude of the cathode voltage is increased.

High intensity nonharmonic radiation is observed and identified as resulting from a beam-plasma induced wave instability, thereby

eliminating the same instability as a possible source of the harmonic emission.

Plausible explanations are presented for the results of the pulse modulation experiment. From the relaxation time of the harmonic emission it is concluded that the emission results from electrons in the energy range of roughly 15-100 eV. The cathode voltage dependence of the emission intensity is attributed to the perpendicular velocity component of the emission electrons, as is the broadening of the emission lines. It is found that this picture, as well as the sum total of the experimental results, is in agreement with the single particle radiation theory of Canobbio and Croci.

6.2 Suggestions for Further Work

Although much progress has been made, it can not be said that the harmonic emission is completely understood. There is much to be gained by repeating the pulse modulation measurements described in this report, and there are several ways in which the investigation of harmonic emission can be extended.

Because much of the experimental pulse modulation work described in this report is exploratory in nature, in many ways it is not as detailed and accurate as might be desired. This situation exists because a consistent interpretation of the data did not emerge immediately, and as a result existing deficiencies did not become apparent until after the measurements had been completed. Therefore it would be valuable to repeat the pulse modulation measurements paying careful attention to those specific details which the analysis has revealed to be important.

For example, although the cathode voltage is an important parameter, it is actually the potential drop across the cathode sheath and the time response of that potential which are most relevant to the analysis. In addition, care should be taken to achieve saturation of the harmonic emission intensity at each setting of the neutral gas pressure.

A better understanding of the pulse modulation measurements might be achieved by repeating the experiment using a different working gas. If the measurements were repeated in helium, for example, one might expect a slower relaxation time for the harmonic emission because the cross sections for inelastic electron-neutral collisions are considerably smaller. Although it is realized that difficulties may be encountered when operating the Penning discharge in other gases, note that the operation of the argon gas discharge is found to be greatly improved without affecting the harmonic emission spectrum by leaking small amounts of oxygen into the discharge tube ($\lesssim$ 1% mixture).

It would also be of interest to see if the emission intensity continues to decrease as the reciprocal of the neutral gas density when the oxygen gas pressure is greater than 100 mtorr. Unfortunately, the discharge tubes used in the present experiment failed to operate as a Penning discharge when the oxygen gas pressure exceeded 100 mtorr. Instead, a glow discharge developed between the anode and cathode at one end of the discharge tube.

It would be interesting to measure the axial distribution of the harmonic emission intensity along a plasma column operating at high pressure. Such a measurement would give an indication of the energy of the radiating electrons. In the high pressure discharge, the secondary

electrons lose energy very rapidly, and the energy distribution function is a strong function of distance from the cathode. If the harmonic emission is indeed produced by electrons in the energy range of 15-100eV then the emission intensity should be localized along the plasma column at the appropriate distance from the cathode. Note that such an experiment would not necessarily have to be done in a Penning discharge. A better controlled experiment might be achieved by producing a long plasma column by some other means, using a cathode at one end of the column only for the purpose of injecting high energy electrons ($\sim$500 eV).

It seems likely that the harmonic emission can be utilized as a diagnostic of superthermal electrons in nonequilibrium plasmas. The fact that the width of the harmonic emission line changes with the cathode voltage suggests that the line shape is related to the velocity distribution of the radiating electrons. In this case the intensity and the line shape of the harmonics reveal the number density and the velocity distribution of the radiating superthermal electrons.

Before such a diagnostic can be realized, it is first necessary to extend the theory (presumably that of Canobbio and Croci) to obtain a description of the line shape near the harmonics and to determine how the line shape is related to the velocity distribution of the radiating electrons. In addition, it is not known if the line shape is affected by mode conversion.

APPENDIX A

Measurement of γ_i

The coefficient of secondary electron emission by ion bombardment, γ_i , was measured calorimetrically, a technique used by Backus [86]. The method utilizes the fact that the cathodes are heated by ion bombardment. Positive ions strike the cathode with the energy obtained by falling through the potential difference of the cathode sheath. The power delivered to the cathodes, H , is given by

$$H = I_i(V_c - V_p)$$

where I_i is the positive ion current and $V_c - V_p$ is the difference between the cathode potential V_c and the plasma potential V_p . If I_T is the total discharge current, then $I_i = I_T/(1+\gamma_i)$, and it follows that

$$H = \frac{I_T}{1+\gamma_i}(V_c - V_p)$$

This power flow to the cathode can easily be determined calorimetrically by measuring the flow rate and temperature change of the cathode cooling water. Solving for γ_i ,

$$\gamma_i = \frac{I_T}{H}(V_c - V_p) - 1$$

The parameters V_c and I_T can be read directly from the power supply meters and V_p can be estimated by observing the potential of a floating plasma probe. Therefore a value can be computed for γ_i based on a calorimetric measurement of H .

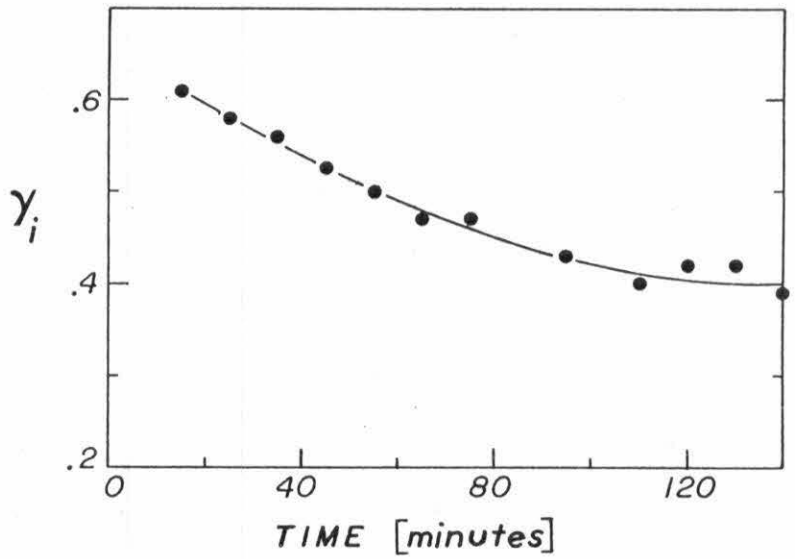

Figure A-1 Coefficient of Secondary Emission by Ion Bombardment γ_i as a Function of Time after the Initiation of the Discharge

The values obtained in this way are found to change with time. When the discharge is initially turned on, large values are measured for γ_i . This is indicated in Figure A-1. The value of γ_i decreases slowly, finally stabilizing at a value of $\gamma_i = 0.4$ after two hours of operation. At the same time, the operating voltage of the discharge increases in a similar fashion, just as expected if the plasma generation rate is to remain constant. Measurements of γ_i using argon gas give a similar result.

If $\gamma_i = 0.4$, then the incident ions constitute 71% of the cathode current and secondary electrons account for the remaining 29%. This result is similar to those obtained by Backus. Note that these results can not be compared with other determinations of γ_i which are

based on the use of a clean metal surface.

In conclusion, the values measured for γ_i are relatively large and they are observed to change with time. Cathode surface conditions, including the presence of an oxide layer, are no doubt involved. After several hours of operation, γ_i can be estimated to be 0.4. However, it is probable that γ_i varies with those parameters which affect cathode surface conditions such as the neutral gas pressure and the operating voltage of the discharge.

APPENDIX B

Measurement of δ_e

Two different methods were used to obtain an estimate for δ_e, the coefficient of secondary electron emission by electron bombardment. For the oxide covered aluminum cathodes of the oxygen discharge δ_e is found to be large. In fact, sufficiently large to account for the negative resistance effects which are observed in the low pressure ($\lesssim$ 10 mtorr) oxygen gas discharge. It is doubtful that the values measured for δ_e, like those for γ_i, can be compared directly with any previous measurements. The exact nature of the cathode surface layer which these values reflect cannot easily be duplicated except in another oxygen gas Penning discharge.

DC Measurement

The first method of measuring δ_e involves operating the discharge with a potential difference between the cathodes. While operating the two cathodes from separate power supplies it was accidently discovered that the lowest voltage cathode draws the most current, accounting for as much as 60% of the total discharge current. The discharge tends to operate with the cathodes at the same potential. However, if a potential difference of more than 50 volts is created between the cathodes, the I-V characteristic for the cathode whose potential is most positive exhibits a negative slope. In short, the most positive cathode experiences a negative resistance. This effect

is not surprising when it is realized that secondary emission by electron bombardment (with $\delta_e > 1$) is involved.

Figure B-1 shows the composition of the currents at each cathode, assuming that the potential of cathode #2 is significantly negative with respect to that of cathode #1. At both cathodes, the dominant contribution comes from the ion saturation current J_i. As a result of ion bombardment, both cathodes emit a secondary electron current J_e. Because of the potential difference between the cathodes, the secondary electrons emitted by cathode #2 are collected by cathode #1. This process results in secondary emission by electron bombardment. Therefore the cathode currents are

$$I_1 = A[J_{i1} + J_{e1} - J_{e2} + \delta_e J_{e2}]$$

and

$$I_2 = A[J_{i2} + J_{e2}]$$

where A is the surface area of the cathode.

Using the relationship $J_e = \gamma_i J_i$ and taking the ratio of the cathode currents, one finds that

$$T = \frac{I_1}{I_2} = \frac{J_{i1}(1+\gamma_{i1}) + \gamma_{i2}J_{i2}(\delta_e - 1)}{J_{i2}(1+\gamma_{i2})}$$

Observe that since $J_{i1} \approx J_{i2}$ and $\gamma_{i1} \approx \gamma_{i2}$, it is reasonable to expect that $T > 1$ when $\delta_e > 1$ and that $T < 1$ when $\delta_e < 1$. Also note that the expression is not valid when $V_1 = V_2$. In that case a limited number of secondary electrons is collected by both cathodes in equal numbers and $T = 1$.

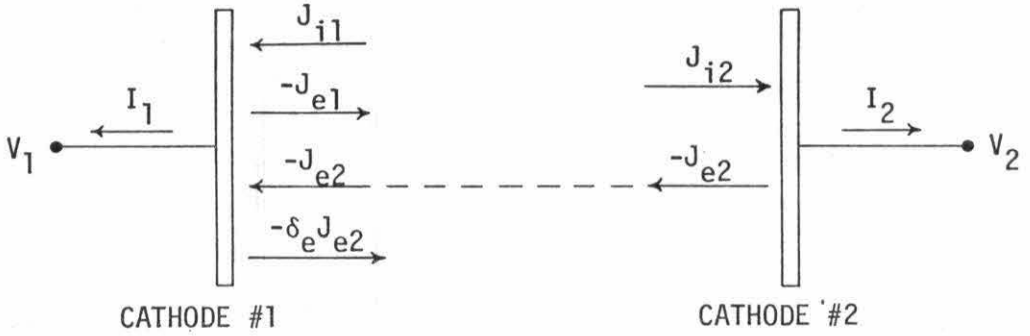

Figure B-1 Composition of the Cathode Currents when $|V_2| > |V_1|$

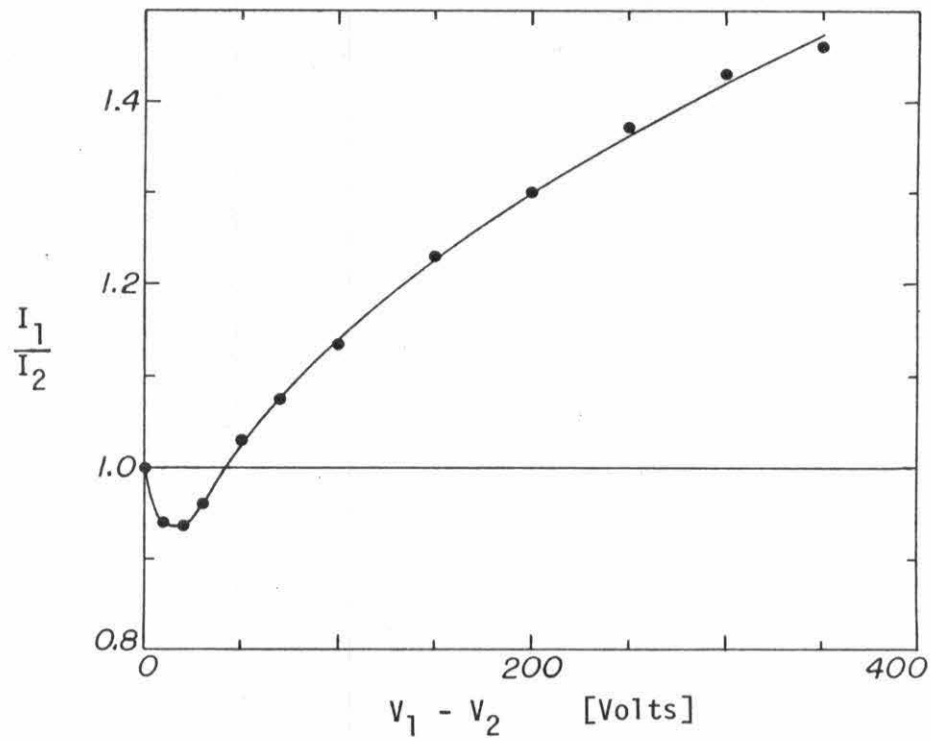

Figure B-2 Cathode Current Ratio I_1/I_2 as a Function of the Voltage Difference Between the Cathodes V_1-V_2

Solving the above expression for δ_e gives

$$\delta_e = 1 + \frac{T\, J_{i2}(1+\gamma_{i2}) - J_{i1}(1+\gamma_{i1})}{\gamma_{i2} J_{i2}}$$

The ratio, T, is observed experimentally and is shown in Figure B-2. The graph indicates that $T \simeq 1.4$ when $V_1 - V_2 \simeq 300$ volts. For this value of T, the expression for δ_e is only weakly dependent on γ_i and J_i. And since γ_i and J_i are both nearly independent of the cathode voltage, it is accurate to take $J_{i1} = J_{i2}$ and $\gamma_{i1} = \gamma_{i2}$. Using the result of Appendix A, $\gamma_i = 0.4$, the expression for δ_e reduces to

$$\delta_e = 3.5T - 2.5$$

Note that T is measured at low pressure so that the secondary electrons lose very little energy during a single transit of the discharge column. Thus, when $V_1 - V_2 = 300$ eV and the incident electron energy is roughly 300 eV we find that $T = 1.4$ and therefore $\delta_e(300 \text{ eV}) \approx 2.4$.

Pulsed Measurement

The second method of measuring δ_e involves pulse modulation of the cathode voltage. Figure B-3 shows how cathode #2 of the discharge is pulse modulated using a floating pulse generator. The current at cathode #1 is monitored by observing the voltage drop across the 200 ohm series resistor. By recording the DC power supply voltage

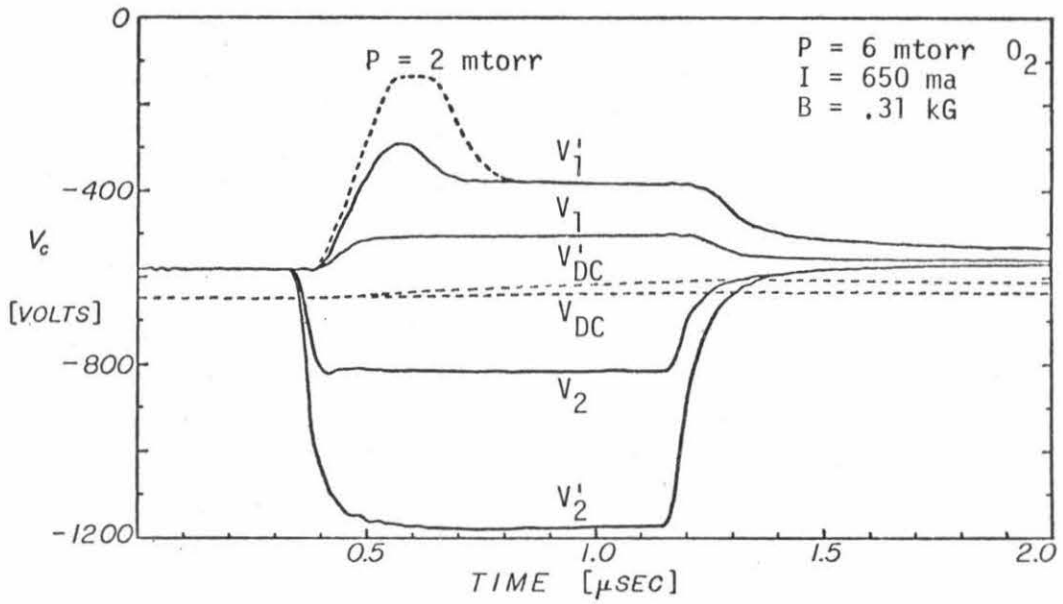

(a) The Voltage Waveforms Obtained when Pulsing One Cathode of the Discharge

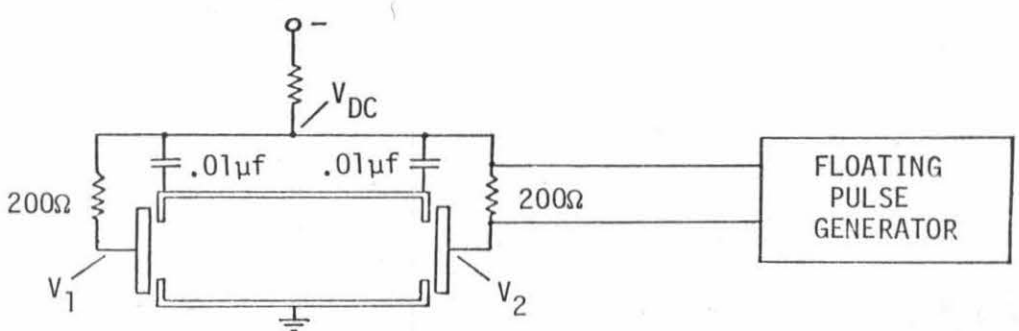

(b) System for Pulsing One Cathode of the Discharge

Figure B-3 Pulsed Measurement of δ_e

and the voltage waveforms at the cathodes (labeled V_{DC}, V_1, and V_2 respectively) it is possible to estimate δ_e as a function of time during the modulation pulse. Also, by varying the amplitude of the applied pulse the energy dependence of δ_e can be determined.

The indicated voltage waveforms are shown in Figure B-3 for both a large and small amplitude pulse. The oxygen gas pressure is 6 mtorr. Ignore for the moment the behavior of the dashed V_1 voltage waveform corresponding to a pressure of 2 mtorr. This effect will be explained later.

In the DC discharge the current of cathode #1 is given by $I_1(DC) = J_{iDC} + J_{eDC}$. This treatment ignores the fact that in the DC discharge the cathodes collect some secondary electrons which do not experience a reduction in their $E_{||}$ energy component on the first transit of the plasma column.

During the pulse, the secondary electrons from cathode #2 strike cathode #1 with excess energy $e(V_1-V_2)$ producing additional secondary electrons. The current at cathode #1 during the pulse is given by

$$I_1(\text{Pulse}) = J_{i1} + J_{e1} - J_{e2} + \delta_e J_{e2}$$

Again, the current at cathode #1 is measured experimentally by observing the voltage drop across the series resistor, $I_1 = (V_{DC}-V_1)/200\Omega$.

The ratio of the cathode current during the pulse to the DC cathode current is given by

$$R = \frac{I_1(\text{Pulse})}{I_1(\text{DC})} = \frac{J_{i1} + J_{e1} - J_{e2} + \delta_e J_{e2}}{J_{iDC} + J_{eDC}} = \frac{(V_{DC}-V_1)_{\text{Pulse}}}{(V_{DC}-V_1)_{DC}}$$

Using the relationship $J_e = \gamma_i J_i$ and solving for δ_e results in the expression

$$\delta_e = 1 + \frac{R\, J_{iDC}(1+\gamma_{iDC}) - J_{i1}(1+\gamma_{i1})}{\gamma_{i2}\ J_{i2}}$$

If it is assumed that γ_i and J_i are both independent of the cathode voltage so that $\gamma_{iDC} = \gamma_{i1} = \gamma_{i2} = 0.4$ and $J_{iDC} \simeq J_{i1} = J_{i2}$, then the expression for δ_e again reduces to $\delta_e = 3.5R - 2.5$. For the small amplitude pulse, $R \simeq 2$ and $V_2 - V_1 \simeq 300$ volts leading to $\delta_e(300\text{ eV}) \simeq 4.5$. For the large amplitude pulse, $R \simeq 3.5$ and $V_2 - V_1 \simeq 800$ volts. In this case $\delta_e(800\text{ eV}) \simeq 9.8$. A careful evaluation of the approximations made indicates that the values computed in this way are probably overestimates.

It is found that the values of δ_e are time dependent. This is especially noticeable for longer pulses ($\sim$10 μsec) where R is observed to decrease markedly during the pulse. It appears that the oxide covered cathode surface can give a very large value for δ_e for a short period of time.

It is observed that even for long pulses, $I_1(\text{DC})$ is nearly the same after the pulse as it was previous to the pulse. This indicates that the plasma density and electron temperature do not change significantly during the pulse.

In conclusion, both methods of measurement indicate that δ_e is large but the values obtained using the pulse modulation technique are significantly greater. Measurements of δ_e by other investigators also yield values in the range of 2.0 - 9.0 for an aluminum oxide layer [87]. In any case, δ_e is large enough to explain a number of effects which are observed in the low pressure oxygen gas discharge.

Negative Resistance Effects

One such effect is evident in figure B-3. The dashed waveform indicates the time variation of the V_1 voltage waveform when a large amplitude pulse is applied to cathode #2. This effect is always noticeable whenever the oxygen gas pressure is less than 10 mtorr. It can be understood in terms of an electron multiplication process which occurs at cathode #1.

When a negative pulse is first applied to cathode #2, nothing happens at cathode #1 until approximately 30 nanoseconds later. The delay corresponds to the transit time of the secondary electrons between the cathodes. Following the delay, the voltage at cathode #1 begins to change in the positive direction. Thus, after 30 nanoseconds, the current at cathode #1 suddenly increases to a larger value (assuming $\delta_e > 1$) determined by δ_e. Note that δ_e depends on the amplitude of the applied pulse and if the potential difference between the cathodes changes during the pulse, δ_e will change accordingly.

Now, consider what happens to the secondary electrons which are

produced at cathode #1 by the first energetic electrons which arrive from cathode #2. The secondary electrons which originate from cathode #1 transit the length of the discharge and are reflected by the larger cathode sheath of cathode #2. By the time that they return to cathode #1, approximately 60 nanoseconds later, V_1 has changed significantly becoming more positive. As a result the electrons strike the cathode surface with excess energy, producing new secondary electrons. Let δ_e' be the coefficient of secondary emission for this process. If V_1 changes by 150 volts in 60 nanoseconds as indicated in figure B-3, then δ_e' can be considerably greater than unity. But $\delta_e' > 1$ means electron multiplication. Therefore cathode #1 emits more electrons than it collects.

As a result of the increased current at cathode #1, the cathode potential is driven even more positive. As the cathode potential becomes more positive, the cathode current becomes more negative. Thus, the slope of the I-V characteristic of cathode #1 is negative, implying a negative resistance.

The electron multiplication process continues until the cathode potential approaches the plasma potential. The cathode voltage is clamped when the cathode begins to collect thermal plasma electrons. Observe that at this point the voltage drop across the 200 ohm resistor is 500 volts, implying a cathode current of 2.5 amps. This current is considerably greater than the original DC value of 0.32 amps. The voltage remains at this value until all of the secondary electrons in transit along the discharge column are collected

($\sim$ 100 nsec). Then the cathode potential falls to a steady state value.

Another similar effect involving oscillation of the cathode voltages was described briefly in section 5.3.3. In short, unusual behavior is to be expected whenever conditions favorable for strong secondary emission by electron bombardment exist. There are two such situations in the oxygen gas Penning discharge. Whenever a large DC or low frequency potential difference exists between the cathodes, the most positive cathode can experience a negative resistance provided that δ_e is large and increasing rapidly with the energy of the primary electrons. In this case the cathode current increases as the cathode voltage decreases. The large amplitude oscillations which were described in section 5.3.3 can be explained in this way, particularly the fact that the two cathodes oscillate 180 degrees out of phase.

In addition, an electron multiplication process has been described which occurs at low neutral gas pressure whenever the potential of one or both cathodes are driven positive rapidly. If the increase in the cathode potential during the time required for a secondary electron to traverse the length of the discharge tube ($\sim$ 30 nsec) is sufficient to give $\delta_e > 1$ when the secondary electrons are collected, then electron multiplication will occur. When $\delta_e >> 1$, the electron multiplication results in a strong dynamic negative resistance which continues to drive the cathode potential positive until it reaches the plasma potential. Such an effect is indicated by the cathode voltage waveforms of figure 5.13 in section 5.6.

APPENDIX C

The Electron Temperature

This appendix indicates how the electron temperature is derived from microwave noise emission measurements.

The radiation temperature of the plasma gives a meaningful measure of the kinetic energy of the plasma electrons only when the radiating electrons have an equilibrium velocity distribution. This condition certainly does not exist in the DC operated Penning discharge where the emission is dominated by nonthermal harmonic emission and high intensity radiation. The afterglow of the pulsed discharge, however, presents an entirely different situation. Measurements in the pulsed discharge indicate that the nonthermal radiation decays very quickly in the afterglow ($\tau < 1$ μsec). Therefore a radiation measurement can be used to infer the electron temperature of the afterglow plasma. However this is not exactly the method which is used here. Instead, a very similar technique is used in the DC operated discharge.

When the discharge voltage is pulse modulated with a large amplitude positive pulse, it is found that the nonthermal radiation is strongly suppressed. See, for example, the discussion of TG pulse modulation in section 5.6. A very large positive TG pulse, in effect, turns off the discharge for the duration of the pulse. Unfortunately the largest pulse amplitude available in the experiment only partially turns off the discharge so that some nonthermal radiation remains. However, most of the remaining nonthermal radiation (harmonic emission)

is concentrated in the vicinity of the cyclotron harmonics. It is believed that the remaining background radiation observed between the harmonics is predominantly thermal in origin and gives a good indication of the electron temperature.

Before the electron temperature can be inferred from measurements of thermal plasma emission, it is first necessary to determine the emissivity of the plasma column. The emissivity is certainly less than unity. However, in chapter III it was found that when the plasma is enclosed in a reflecting cavity, the plasma-reflector system is a very good absorber. Conversely, the emissivity of the plasma-reflector system with respect to thermal radiation should also be very good. Therefore it is expected that the equivalent radiation temperature of the thermal emission will be roughly the same as the temperature of the thermal plasma electrons.

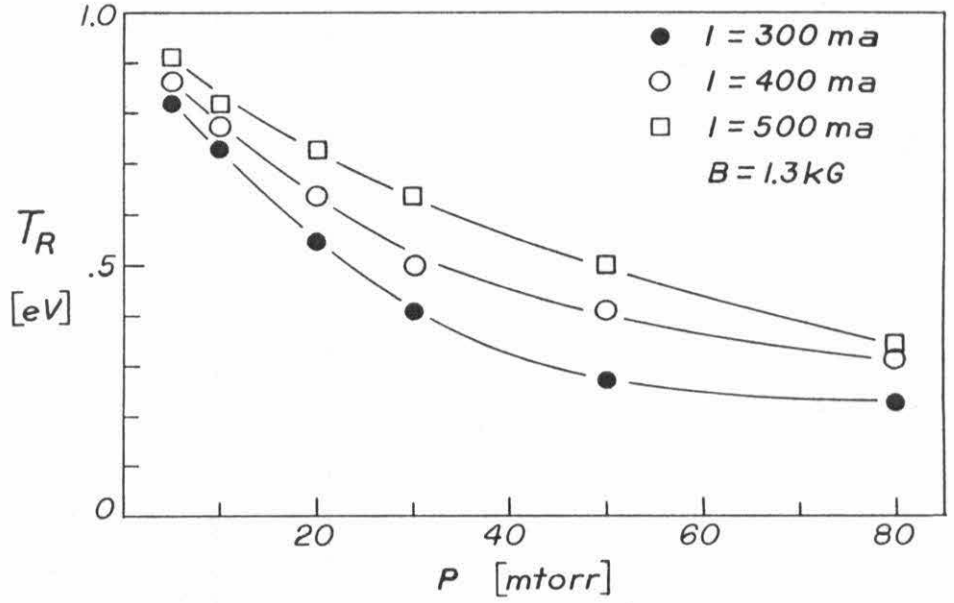

Figure C-1 Background Radiation Temperature in eV as a Function of the Oxygen Gas Pressure

To obtain an indication of the electron temperature, the background radiation between the cyclotron harmonics is monitored during a large amplitude positive TG modulation pulse. The results of the measurement are shown in Figure C-1 for several values of the discharge current and the neutral gas pressure.

The equivalent radiation temperature is found to vary between 0.3 and 1.0 eV, depending on the discharge parameters. The temperature increases with increasing discharge current and decreases with increasing neutral gas pressure. Based on energy balance considerations, the electron temperature is expected to behave in this way.

Klan has considered the energy balance of the thermal electrons in the Penning discharge [88]. There are two groups of electrons in the Penning discharge which are relevant to this discussion. One group of electrons having a low temperature and a high density is supposed to have Maxwellian velocity distribution. The other group is more energetic (1-20 eV) but has a much lower density. Because of electron-electron collisions between these two groups of electrons, the colder thermal electrons are heated by energy transfer from the hot electrons.

This heating rate has to be balanced by a cooling rate which describes energy transfer by elastic collisions to the colder ions and neutrals which are at room temperature. The plasma electron temperature is determined by equilibrium between the heating and cooling rates. When the heating and cooling rates for the indicated processes are estimated and compared, the inferred electron

temperature has essentially the same magnitude and the same pressure and current dependence as is indicated by Figure C-1.

It is interesting that the electron temperatures obtained by this method are in sharp disagreement with the values obtained from probe measurements. In the present experiment, probe measurements indicate electron temperatures in the range of 2 to 5 eV. When Brand and Cohen measured the electron temperature in a similar discharge using a double probe, they obtained values between 2 and 6 eV [89]. Essentially the same values were also obtained by Brifford [90] and Thomassen [91]. However, Brand and Cohen performed two additional measurements to check the accuracy of the probe measurement. They obtained the electron temperature from the propagation of cyclotron harmonic waves and from a spectroscopic measurement. The spectroscopic measurement gave a value of roughly 0.2 eV and the cyclotron harmonic wave measurement indicated an electron temperature of 0.3 to 0.6 eV. They concluded that the probe measurements are grossly misleading. The probe measurement is very sensitive to the presence of relatively small numbers of nonthermal electrons whereas the propagation of cyclotron harmonic waves is determined principally by the thermal electrons.

In conclusion, it is believed that the low electron temperatures indicated by the radiation temperature measurement are accurate. It is essential, however, to be certain that the hybrid layer is well established in the plasma column during the measurement so that the plasma-reflector system is a good absorber. Also,

if some of the plasma emission is nonthermal in origin, the measurement will overestimate the electron temperature.

References

1. F. W. Crawford, Nuclear Fusion 5 (1965) 73.

2. G. Bekefi, Radiation Processes in Plasmas, John Wiley & Sons, Inc. (1966), 246-253.

3. F. W. Crawford, Stanford University Institute for Plasma Research Report No. 189, July 1967.

4. G. Landauer, Plasma Physics 4 (1962) 395.

5. C. B. Wharton, Proc. 4th Inter. Conf. on Ion. Phen. in Gases, Uppsala, 1959, Vol. 2 (1964) 737.

6. G. Landauer, Proc. 5th Inter. Conf. on Ion. Phen. in Gases, Munich, 1961, Vol. 1 (1962) 389.

7. G. Bekefi, J. D. Coccoli, E. B. Hooper, and S. J. Buchsbaum, Phys. Rev. Letters 9 (1962) 6.

8. K. Mitani, H. Kubo, and S. Tanaka, J. Phys. Soc. Japan 19 (1964) 211.

9. C. D. Lustig, Phys. Rev. 139 (1965) A63.

10. S. Gruber, W. D. McBee, and L. T. Shepard, Appl. Phys. Letters 4 (1964) 137.

11. G. Bekefi and E. B. Hooper, Appl. Phys. Letters 4 (1964) 135.

12. H. Ikegami and F. W. Crawford, Proc. 7th Inter. Conf. on Ion. Phen. in Gases, Belgrade, Yugoslavia, 1965, Vol. 2 (1966) 503.

13. S. J. Tetenbaum, Phys. Fluids 10 (1967) 1577.

14. G. Landauer, Bull. Am. Phys. Soc. 9 (1964) 312.

15. H. Dreicer, Plasma Waves in Space and in the Laboratory, Edinburgh Univ. Press (1969) Ch. VI.

16. H. Dreicer, Bull. Am. Phys. Soc. 9 (1964) 312.

17. H. Dreicer, Proc. 7th Inter. Conf. on Ion. Phen. in Gases, Belgrade, Yugoslavia, 1965, Vol. 2 (1966) 491.

18. O. S. Pavlichenko, L. A. Dushin, Yu. K. Kuznetsov, and I. Yu. Adamov, Sov. Phys. Tech. Phys. 10 (1966) 1082.

19. L. A. Dushin, Yu. K. Kuznetsov, and O. S. Pavlichenko, Proc. 8th Inter. Conf. on Ion. Phen. in Gases, Vienna, 1967 (1968) 427.

20. Yu. K. Kuznetsov, O. S. Pavlichenko and V. N. Starikov, Sov. Phys. Tech. Phys. 14 (1970) 1184.

21. M. P. Vasiliyev, Yu. K. Kuznetsov, and O. S. Pavlichenko, Plasma Physics 15 (1973) 807.

22. L. A. Dushin, Y. K. Kuznetsov, and O. S. Pavlichenko, Sov. Phys. Tech. Phys. 13 (1969) 1030.

23. J. L. Hanisch and R. F. Stetson, Plasma Physics 13 (1971) 1059.

24. F. Klan, Proc. 8th Inter. Conf. on Ion. Phen. in Gases, Vienna, Austria, 1967, Vol. 1 (1968) 190.

25. Y. Beers, in Microwave Receivers, ed. by S. N. Van Voorhis, Dover Publications, Inc., New York (1966) Ch. 4, p. 105.

26. H. Wallman, in Microwave Receivers, ed. by S. N. Van Voorhis, Dover Publications, Inc., New York (1966) Ch. 6, p. 169.

27. M. A. Heald and C. B. Wharton, Plasma Diagnostics with Microwaves, John Wiley & Sons, Inc., New York (1965) Ch. 4.

28. H. Leaderman, W. Ellis, and L. A. Turner, in Radar Scanners and Radomes, ed. by W. M. Cady, M. B. Karelitz, and L. A. Turner, McGraw-Hill Book Company, Inc., New York (1948) Ch. 11.

29. Corning, Pyrex Brand Labware Catalog (Corning Glass Works, Corning, New York 14830), Table: "Properties of Other Selected Corning Glasses", pp 10-11.

30. F. M. Penning, Physica 4 (1937) 71.

31. J. Backus, Gaseous Electrical Discharges in Magnetic Fields, ed. by A. Guthrie and R. K. Wakerling, McGraw-Hill Book Company, Inc., New York (1949) Ch. 11, p. 346.

32. E. C. Evans and K. E. Burmaster, Proc. IRE 38 (1950) 651.

33. F. M. Penning, Philips Tech. Rev. 2 (1937) 201.

34. F. M. Penning and K. Nienhuis, Philips Tech. Rev. 11 (1949) 116.

35. E. B. Hooper, Jr., in Advances in Electronics and Electron Physics, Vol. 27, ed. by L. Marton, Academic Press, New York (1969) 295.

36. F. Klan, Z. Naturforsch 25a (1970) 263.

37. B. Lehnert, Plasma Physics 9 (1967) 301.

38. E. B. Hooper, Jr., Plasma Physics 12 (1970) 855.

39. A. Simon, Phys. Fluids 6 (1963) 382.

40. F. C. Hoh, Phys. Fluids 6 (1963) 1184.

41. M. A. Allen, P. Chorney, and H. S. Maddix, Appl. Phys. Letters 3 (1963) 30.

42. K. I. Thomassen, Phys. Fluids 9 (1966) 1836.

43. L. V. Dubovoi and P. G. Popov, Soviet Phys. JETP 22 (1966) 19.

44. J. Backus, Gaseous Electrical Discharges in Magnetic Fields, ed. by A. Guthrie and R. K. Wakerling, McGraw-Hill Book Company, Inc., New York (1949) Ch. 11, p. 367.

45. D. J. Rose and M. Clark, Jr., Plasmas and Controlled Fusion, MIT Press, Massachusetts Institute of Technology, Cambridge, Massachusetts (1965) 46.

46. S. C. Brown, Basic Data of Plasma Physics, John Wiley & Sons, Inc., New York (1959) 3.

47. Ibid., p. 116.

48. Handbook of Chemistry and Physics, 51st Edition, The Chemical Rubber Co., Cleveland, Ohio (1970), p. E-75.

49. E. Canobbio and R. Croci, Proc. 6th Int. Conf. on Ion Phen. in Gases, Paris, France, 1963, Vol. 3 (1964) 269.

50. I. B. Bernstein, Phys. Rev. 109 (1958) 10.

51. Yu. N. Dnestrovski and D. P. Kostomarov, Soviet Phys. JETP 14 (1962) 1089.

52. Y. Furutani and G. Kalman, Plasma Phys. 7 (1965) 381.

53. E. Canobbio and R. Croci, Phys. Fluids 9 (1966) 549.

54. I. P. Shkarofsky, Phys. Fluids 9 (1966) 561,570.

55. M. K. Andrews and M.T.C. Fang, J. Plasma 6 (1971) 579.

56. S. Puri, F. Leuterer, and M. Tutter, J. Plasma Phys. 9 (1973) 89.

57. P. M. Stone and P. L. Auer, Phys. Rev. 138 (1965) 695.

58. N. Shimomura, J. Phys. Soc. Japan 29 (1970) 759.

59. R. Croci and E. Canobbio, Proc. 7th Int. Conf. on Ion Phen. in Gases, Belgrade, Yugoslavia, 1965, Vol. 2 (1966) 496.

60. R. Sugihara, J. Phys. Soc. Japan 20 (1965) 591.

61. T. H. Stix, Phys. Rev. Letters 15 (1965) 878.

62. C. W. Horton, Phys. Fluids 9 (1966) 815.

63. T. Tang, Phys. Fluids 13 (1970) 121.

64. H. H. Kuehl, B. B. O'Brien, and G. E. Stewart, Phys. Fluids 13 (1970) 1595.

65. H. Oya, Radio Sc. 6 (1971) 1131.

66. T. J. M. Boyd, Proc. 7th Int. Conf. on Ion Phen. in Gases, Belgrade, Yugoslavia, 1965, Vol. 2 (1966) 512.

67. F. W. Crawford, G. S. Kino, H. H. Weiss, Phys. Rev. Letters 13 (1964) 229.

68. A. Bers and S. Gruber, Appl. Phys. Letters 6 (1965) 27.

69. M. Seidl, Phys. Fluids 13 (1970) 966.

70. T. D. Kaladze and K. N. Stepanov, Ukr. Fiz. Zh. 13 (1969) 1786.

71. J. Neufeld and C. L. Wiginton, Phys. Rev. 148 (1966) 97.

72. K. E. Zayed and A. B. Kitsenko, Plasma Physics 10 (1968) 673.

73. J. R. Johnston and R. L. Moore, Nuclear Fusion 5 (1965) 1.

74. A. F. Kuckes and J. M. Dawson, Phys. Fluids 8 (1965) 1007.

75. A. Simon and M. N. Rosenbluth, Phys. Fluids 6 (1963) 1566.

76. E. Rauchle, Proc. 7th Int. Conf. on Ion Phen. in Gases, Belgrade, Yugoslavia, 1965, Vol. 2 (1966) 500.

77. K. B. Persson, E. Q. Johnson, and D. A. Uhlenbrock, Phys. Fluids 11 (1968) 619.

78. J. Datlov, Czech. J. Phys. 15 (1965) 858.

79. G. Bekefi, Radiation Processes in Plasmas, John Wiley & Sons, Inc., New York (1966) Sect. 10.2.

80. S. J. Buchsbaum, Bull. Am. Phys. Soc. 9 (1964) 317.

81. J. W. Wassink, Phys. Fluids 11 (1968) 629.

82. W. Hess and E. Rauchle, Proc. 7th Int. Conf. on Ion Phen. in Gases, Belgrade, Yugoslavia, 1965, Vol. 2 (1966) 521.

83. P. Bocchieri, E. Crosignani, and G. Siragusa, Nuovo Cimento 56 (1968) 173.

84. M. A. Heald and C. B. Wharton, Plasma Diagnostics with Microwaves, John Wiley & Sons, Inc., New York (1965), p. 362.

85. H.S.W. Massey and E.H.S. Burhop, Electronic and Ionic Impact Phenomena, Oxford University Press, London (1956), Ch. III.

86. J. Backus, J. Appl. Phys. 30 (1959) 1866.

87. Handbook of Chemistry and Physics, 51st Edition, The Chemical Rubber Co., Cleveland, Ohio (1970), p. E-224.

88. F. Klan, Z. Naturforsch 25a (1970) 707.

89. G. F. Brand and D. D. Cohen, J. Appl. Phys. 44 (1973) 2172.

90. G. Brifford, M. Gregoire, and S. Gruber, Plasma Physics 6 (1964) 329.

91. K. I. Thomassen, J. Appl. Phys. 39 (1968) 5017.

"The last thing one discovers in doing a task is to know what ought to have been done first."

--Enivel